Wissenschaftszentrum Weihenstephan für

Ernährung, Landnutzung und Umwelt

Lehrstuhl für Botanik

Coordination between membrane and microtubule dynamics during cytokinesis in *Arabidopsis thaliana*

Alexander Steiner

Vollständiger Abdruck der von der Fakultät Wissenschaftszentrum Weihenstephan für Ernährung, Landnutzung und Umwelt der Technischen Universität München zur Erlangung des akademischen Grades eines

Doktors der Naturwissenschaften

genehmigten Dissertation.

Vorsitzender:		Prof. Dr. Ralph Hückelhoven
Prüfer der Dissertation:	1.	Priv.-Doz. Dr. Farhah Assaad-Gerbert
	2.	Prof. Dr. Jörg Durner
	3.	apl. Prof. Dr. Ramon Torrez-Ruiz

Die Dissertation wurde am 02.08.2016 bei der Technischen Universität München eingereicht und durch die Fakultät Wissenschaftszentrum Weihenstephan für Ernährung, Landnutzung und Umwelt am 02.10.2016 angenommen.

Abstract

During plant cytokinesis, the division of the cytoplasm following nuclear division, a cell wall emerges in between two newly formed daughter cells. Vesicles are delivered via the phragmoplast, a plant-specific microtubule array, to a transient membrane compartment called the cell plate. The cell plate loses its distinct juvenile traits and matures into a cross wall. A number of questions regarding cell plate development remain open. Furthermore, the coordination between membrane trafficking and microtubule dynamics and their regulation via cell cycle cues during cytokinesis is poorly understood.

To learn more about cell plate development, two tethering complexes, the transport protein particle II (TRAPPII) and the exocyst, were monitored throughout cytokinesis. Both tethering complexes localise sequentially to the cell plate with a brief overlap at the onset and towards the end of cytokinesis. The TRAPPII complex is required for biogenesis and the exocyst for maturation of the cell plate. In addition, TRAPPII mediates the sorting of plasma membrane proteins, including the exocyst, at the cell plate. Both complexes show a transient physical interaction.

To shed light on the coordination between membrane trafficking and microtubule dynamics, membrane- and microtubule-related proteins were tracked throughout cytokinesis. Our data support the general consensus that microtubule dynamics precede membrane dynamics during cell plate development. A quantitative analysis of cytokinesis-defective mutants was performed. Of four analysed microtubule-related mutants, only *Microtubule Organization 1* (*mor1-1*) mutants show severe impairment in cell plate formation. Conversely, the membrane-related *keule* mutant exhibits the strongest defect in phragmoplast microtubule reorganisation during telophase. In addition, the appearance and localisation dynamics of the Sec1/Munc18 (SM) protein KEULE and its known interaction partner, the syntaxin KNOLLE, differs throughout cytokinesis.

A proteomic screen and binary interaction assays revealed the microtubule-associated protein 65 family (MAP65) as an interaction partner of the TRAPPII tethering complex. The interaction does not alter the recruitment or localisation of either TRAPPII or MAP65 to or at the cell plate. The double mutants compared to single mutants have a synthetically enhanced number of cells in which four or more nuclei are clumped together in the apparent absence of even vestigial cross walls. We postulate that this interaction might coordinate cell cycle progression with the completion of cytokinesis.

Taken together, we show how the identity of the cell plate changes as this compartment matures and highlight the importance of the coordination between membranes and microtubules. In addition, we outline a conceptual framework for the integration of cell cycle cues with membrane and microtubule dynamics during plant cytokinesis.

Zusammenfassung

Bei der pflanzlichen Zellteilung, der Teilung des Zytoplasmas im Anschluss an die Kernteilung, entsteht eine Zellwand zwischen zwei neu gebildeten Tochterzellen. Der Phragmoplast, eine pflanzenspezifische Mikrotubuli-Anordnung, transportiert Vesikel zu einem transienten Zellkompartiment, der Zellplatte. Diese verliert ihre juvenilen Merkmale und reift zu einer Querwand. Viele Fragen bezüglich der Zellplattenentwicklung bleiben noch offen. Des Weiteren ist das Wissen über die Abstimmung des Membrantransfers mit den Mikrotubulidynamiken und deren Steuerung durch den Zellzyklus noch sehr gering.

Um mehr über die Mechanismen der Zellplattenentwicklung zu erfahren wurden zwei Tethering-Komplexe, Transport Protein Partikel II (TRAPPII) und exocyst, im Verlauf der Zellteilung untersucht. Beide Tethering-Komplexe sind sequentiell auf der Zellplatte lokalisiert und überschneiden sich in ihrer Lokalisation nur kurz zu Beginn und am Ende der Zellteilung. Der TRAPPII Komplex ist für die Biogenese, exocyst für die Reifung der Zellplatte verantwortlich. Des Weiteren ist TRAPPII für die Verteilung von Plasmamembran Proteinen, inklusive exocyst, an der Zellplatte verantwortlich. Beide Komplexe interagieren transient miteinander.
Die Koordination des Membrantransfers mit der Mikrotubulidynamik wurde durch die Nachverfolgung von membran- und mikrotubuliassoziierten Proteinen während des gesamten Verlaufes der Zellteilung untersucht. Unsere Ergebnisse stimmen mit dem aktuellen Wissensstand überein, dass bei der Zellplattenentwicklung die Mikrotubulidynamik der Membrandynamik vorausgeht. Eine quantitative Untersuchung von zellteilungsdefekten Mutanten wurde durchgeführt. Von vier untersuchten mikrotubuliassoziierten Mutanten, zeigen die *Microtubule Organization I* (*mor1-1*) Mutanten die stärkste Zellplattenbildungsstörung. Während der Telophase zeigen *keule* Mutanten wiederum, als membranassoziierte Mutanten, die größte Beeinträchtigung in der Reorganisation von Mikrotubuli. Außerdem unterscheidet sich das Sec1/Munc18 (SM) Protein KEULE von seinem bekannten Interaktionspartner, dem Syntaxin KNOLLE, im Erscheinungsbild und den Dynamiken im Verlauf der gesamten Zellteilung.
Durch eine biochemische Untersuchung und binäre Interaktionsanalysen konnte die Interaktion zwischen der mikrotubuliassoziierten Protein Familie 65 (MAP65) und TRAPPII gezeigt werden. Diese Interaktion hat jedoch keinen Einfluss auf die Rekrutierung von TRAPPII zu oder der Lokalisation von MAP65 an der Zellplatte. Doppelmutanten im Vergleich zu Einzelmutanten zeigen ein synthetisch vermehrtes Auftreten an Zellen, in denen vier oder mehr Zellkerne, ohne sichtbare Anzeichen von rudimentären Querwänden, miteinander fusioniert sind. Dies führt uns zu der Annahme, dass diese Interaktion das Voranschreiten des Zellzyklus mit der Beendigung der Zellteilung koordinieren könnte.

Zusammengefasst zeigen wir wie sich die Identität der Zellplatte während des Reifungsprozesses verändert und heben außerdem die Bedeutung der Koordination zwischen Membranen und Mikrotubuli hervor. Des Weiteren schlagen wir ein konzeptionelles Gerüst für die Verflechtung des Zellzyklus mit den Dynamiken der Membranen und Mikrotubuli während der Zellteilung vor.

List of Publications

2016 **Cell cycle-regulated PLEIADE/AtMAP65-3 links membrane and microtubule dynamics during plant cytokinesis.**

Accepted in *The Plant Journal*, June 2016

Steiner, A., Rybak, K., Altmann, M., McFarlane, H. E., Klaeger, S., Nguyen, N., Facher, E., Ivakov, A., Wanner, G., Kuster, B., Persson, S., Falter-Braun, P., Hauser, M.-T. and Assaad, F.F.

2016 **The Membrane-Associated Sec1/Munc18 KEULE is required for phragmoplast microtubule reorganization during cytokinesis in Arabidopsis.**

Molecular Plant 9, 528–540.

Steiner, A., Müller, L., Rybak, K., Vodermaier, V., Facher, E., Thellmann, M., Ravikumar, R., Wanner, G., Hauser, M.-T., and Assaad, F.F.

2014 **Plant cytokinesis is orchestrated by the sequential action of the TRAPPII and exocyst tethering complexes.**

Developmental Cell 29, 607–620.

Rybak, K., **Steiner, A.**, Synek, L., Klaeger, S., Kulich, I., Facher, E., Wanner, G., Kuster, B., Zarsky, V., Persson, S. and Assaad, F.F

Abbreviations

At	*Arabidopsis thaliana*
Arf	ADP-Ribosylation Factors
App	APPendix
Bet3/Bet5	Blocked Early in Transport 3/5
BY2	Bright Yellow-2 (tobacco cell line)
C1/C2/C3	(truncations of CLUB/AtTRS130)
CDK	Cyclin-Dependent Kinases
CDS	Cortical Division Site
CLASP	CLip-ASsociated Protein
COG	Conserved Oligomeric Golgi
CORVET	endosomal class C cORe Vacuole/Endosome Tethering
CP	Cell Plate
Dsl1	Dependence on SLy1
ER	Endoplasmic Reticulum
G2/M	Gap2-phase/M-phase (mitosis/cytokinesis)
GARP	Golgi-Associated Retrograde Protein
GFP/YFP/RFP	Green/Yellow/Red Fluorescent Protein
GEF	Guanine nucleotide Exchange Factor
GDP	Guanosine DiPhosphate
GTP	Guanosine TriPhosphate
HA	HemAgglutinin
HOPS	HOmotypic fusion and Protein Sorting
EB1	End Binding1
EE	Early Endosome
EARP	Endosome-Associated Recycling Protein
ESCRT	Endosomal Sorting Complexes Required for Transport
FIB/SEM	Focused Ion Beam/Scanning Electron Microscope
KEU	KEUle

MAP	Microtubule-Associated Proteins
MAP	Mitogen-Activated Protein
MAPK	Mitogen-Activated Protein Kinase
MAP65	Microtubule-Associated Protein 65
MOR1	Microtubule ORganization 1
Munc18	Mammalian UNCoordinated-18
NACK	Npk1-ACtivating Kinesin 1
NSF	N-ethylmaleimide-Sensitive Factor
Nt	*Nicotiana tabacum*
PLE	PLEiade
PVC	Pre-Vacuolar Compartment
Rab	RAs-related in Brain
SAC	Spindle Assembly Checkpoint
SCF	Skp, Cullin, F-box containing complex
SM	Sec1/Munc18
SEC1	SECretory 1
SNAP	Soluble Nsf Attachment Protein
SNARE	SNAp (Soluble Nsf Attachment Protein) REceptor
SYP61/SYP121	SYntaxin of Plants 61/121
T1/T2/T3	(truncations of AtTRS120)
TGN/EE	Trans-Golgi-network/Early Endosome
TRAPP	TRAnsport Protein Particle
TRS	TRapp Subunit
TUA	TUbulin Alpha-5
UBQ	UBiQuitin
UTR	UnTranslated Region
VAMP	Vesicle-Associated Membrane Proteins
VHAa1	Vacuolar H^+ ATPase a1 subunit

Table of contents

List of figures

List of tables

1. Introduction

1.1. Cytokinesis

The most frequently studied type of cytokinesis in plants is that of somatic cells (Figure 1). During the G2/M transition of the cell cycle, a belt-like cytoskeletal array of microtubules and actin filaments, the preprophase band (Mineyuki, 1999), frames the future division plane (Figure 2A; Lipka et al., 2015). Throughout cytokinesis, a distinct microtubule array, the phragmoplast, delivers vesicles to the division plane and thus helps build the cell plate (Samuels et al., 1995). The cell plate centrifugally expands towards the previously marked cortical division site (CDS) (Figure 1A-D, Figure 3). Following nuclear division, the chromosomal content and the cytoplasm are divided into two daughter cells (Figure 1E; Staehelin and Hepler, 1996). In contrast to plants, in animal cells a contractile ring, consisting of the motor protein myosin II, actin filaments and additional proteins forms a cleavage furrow, which leads to a centripetal constriction of the cell (Neto and Gould, 2011). Cytokinesis can occur in diverse ways not just across kingdoms, but also between different plant tissues. For instance, the preprophase band is not present in male meiosis or during the cell division of nuclear endosperm (Peirson et al., 1997; Olsen, 2007). Cell plate formation in male meiotic cells resembles either the mitotic division or occurs after two meiotic divisions with an inward-oriented growth of new cross walls (De Storme and Geelen, 2013). In nuclear endosperm, a single cell undergoes multiple synchronous nuclear divisions before multiple cell plates are initiated between sister and non-sister nuclei (Olsen, 2007). Taken together, cytokinesis is a very complex and not yet fully understood process that successfully leverages a variety of different approaches to divide cells. The first detailed model of plant cytokinesis results from experiments with synchronised tobacco BY2 cells and tobacco root tips. Due to the quality of the electron micrographs of cryofixed, freeze substituted cells, somatic cytokinesis has become the prime model for cytokinesis in plants (Figure 1; Samuels et al., 1995; Seguí-Simarro et al., 2004).

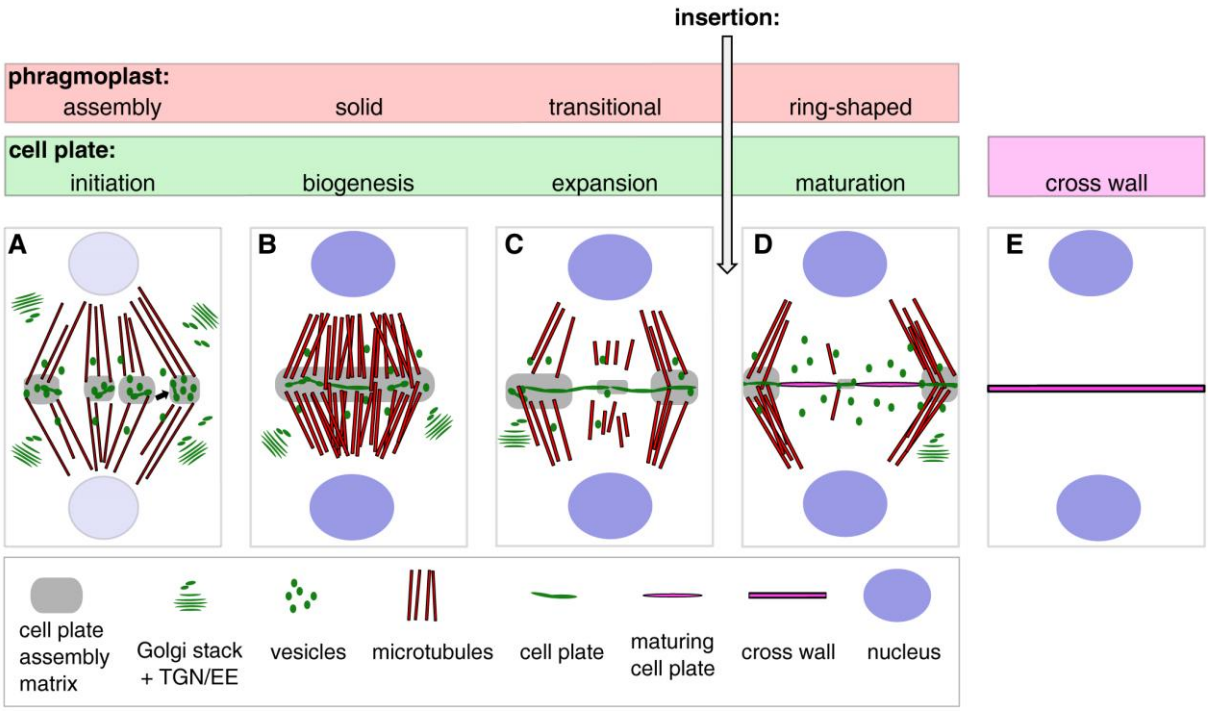

Figure 1. Somatic cytokinesis in plants.
(A) Two opposing sets of phragmoplast microtubules arise from former spindle microtubules. A 'Golgi-belt', consisting of Golgi apparatus and trans-Golgi network/early endosomes (TGN/EE) surrounds the division plane. Right after arrival, vesicles fuse to dumbbell-shaped cell plate initials (black arrow).
(B) The microtubules arrange into a barrel-like structure at the solid phragmoplast stage and further rounds of fusion initiates cell plate biogenesis within a cell plate assembly matrix.
(C) The cell plate expands centrifugally towards the lateral cell walls. The phragmoplast microtubules reorganise into a ring-shaped pattern surrounding the expanding cell plate.
(D) Cell plate maturation is triggered by insertion into the parental cell walls.
(E) The cell plate has fully matured into a cross wall, which divides the cell into two daughter cells, flanked on either side by plasma membranes. Adapted from (Seguí-Simarro et al., 2004) with permission from the American Society of Plant Biologists.

1.1.1. Mutants required for the establishment of the division plane and for the execution of cytokinesis

The establishment of the division plane and cytokinesis in somatic plant cells can be broken down into four consecutive steps. First, the division plane needs to be determined; thereafter, in a second step, a new cell plate is formed. Subsequently, in a third step, the cell plate is inserted into the lateral walls and finally, in the fourth step, the cell plate has to mature into a new cross wall. A genetic dissection of cytokinesis identifies mutants characteristic for each of the four steps (Söllner et al., 2002; Gillmor et al., 2016). In this thesis, a subset of cytokinesis-specific mutants was analysed (Table 1). Mutants of the first step such as *clasp-1* and *mor1-1* are impaired in either the formation or the positioning of the preprophase band. Incorrect positioning leads to an abnormal orientation of the cell plate (Kawamura et al., 2006; Ambrose et al., 2007). Mutants impaired in the second step are characterised by

multinucleate cells with gapped or incomplete cross walls (Söllner et al., 2002). *TRAPPII*, *knolle*, *keule*, *hinkel* and *pleiade* belong to this mutant class and are impaired in either cell plate or phragmoplast formation (Lukowitz et al., 1996; Assaad et al., 2001; Strompen et al., 2002; Müller et al., 2004; Jaber et al., 2010; Thellmann et al., 2010). Mutants in the third class such as *massue* are not able to insert the cell plate properly into the lateral wall (Thiele et al., 2009). In the final step of cytokinesis, *exo84b-2*, among other mutants, may play a role in the maturation of the cell plate into a cross wall (Fendrych et al., 2010; Rybak et al., 2014).

The interdependence between membranes and microtubules is crucial for the proper execution of cytokinesis. On the one hand, phragmoplast microtubules, deliver vesicles and cell wall components to the division plane (Samuels et al., 1995). On the other hand, membrane proteins in the cell plate or cell plate assembly matrix appear to anchor microtubule plus ends (Austin et al., 2005). The diversity of microtubule-related and membrane-related mutants enables us to precisely dissect the processes underlying cytokinesis in plants.

Mutant	Wild-type gene encodes	Function during cytokinesis	Reference
clasp-1	Microtubule-associated protein (CLIP-associated protein)	determination of the division plane	(Ambrose et al., 2007)
mor-1-1	Microtubule-associated protein (Microtubule organizing 1)		(Kawamura et al., 2006)
trs120-4	subunit of TRAPPII (tethering complex)	execution of cytokinesis	(Thellmann et al., 2010)
club-2/trs130-2			(Jaber et al., 2010)
keu^{T282} ***(keule)***	Sec1/Munc18 (SM) protein		(Assaad et al., 2001)
keu^{mm125} ***(keule)***			
hik^{G235} **(*hinkel*)**	Kinesin		(Strompen et al., 2002)
ple-2 ***(pleiade)***	Microtubule associated protein 65 (bundles microtubules)		(M.-T. Hauser unpublished; Steiner et al., 2016)
ple-3 ***(pleiade)***			
ple-4 ***(pleiade)***			(Müller et al., 2004)
mas-5 ***(massue)***	GSL8 (putative callose synthase)	cell plate insertion	(Thiele et al., 2009)
exo84b-2 ***(exocyst)***	Subunit of exocyst (tethering complex)	cell plate maturation	(Fendrych et al., 2010; Rybak et al., 2014)

Table 1. Mutants analysed in this thesis. For more information about the mutants and additional *exocyst* mutant lines, used in the thesis, see the supplemental information of the publications.

1.2. Microtubule arrays required for cytokinesis

Microtubules, first described as such in 1963 (Ledbetter and Porter, 1963), consist of non-covalently bound α- and β-tubulin heterodimers. The interaction between both tubulin subunits is GTP-dependent and generates protofilaments. At least 13 protofilaments form a structure called "microtubule". Microtubules are required for a large variety of processes including cell division, organelle positioning or the maintenance of cell shape (Kollman et al., 2011). Six different α-tubulin genes and at least nine β-tubulin genes exist in *Arabidopsis thaliana* (Kopczak et al., 1992; Snustad et al., 1992).

Contrary to animals and fungi, plants lack central microtubule organising centres such as centrosomes. Instead, microtubule organising centres are rather pleiotropic in plants and multiple nucleation sites have been described. In addition to the nuclear envelope, the cell cortex also shows nucleation activity at sites with and without pre-existing microtubules (Stoppin et al., 1994; Shaw et al., 2003; Bruaene et al., 2004). The new microtubules tend to nucleate at an angle of 40° to the pre-existing ones (Murata et al., 2005). Other studies point to the existence of undefined nucleation sites at the spindle poles (Chan et al., 2003). The main protein of microtubule nucleation, γ-tubulin, is conserved over kingdoms and occurs as two isoforms in *Arabidopsis thaliana* (Pastuglia et al., 2006). It is part of the γ-tubulin ring complex (Murata et al., 2007).

The dynamic interplay between polymerisation (assembly), depolymerisation (catastrophe) and variable nucleation enables microtubules to respond rapidly to a variety of intrinsic and extrinsic cues. Microtubule-associated proteins (MAPs) play a significant role in this rapid adaptation (Kollman et al., 2011). Some of the MAPs stabilise and promote polymerisation of microtubules, others destabilise or sever microtubules. In addition, some MAPs help to form bundles via microtubule crosslinking, while others move material or organelles along these microtubule bundles (Lodish et al., 2000). Altogether, this leads to timely and spatially well-organised microtubule arrays during cell division and other intra- and extra- cellular events (Figure 2). With all the degrees of freedom the microtubule arrays have at the minus end, it will be interesting to see whether there are mechanisms at the plus end that give the microtubule arrays structure and stability.

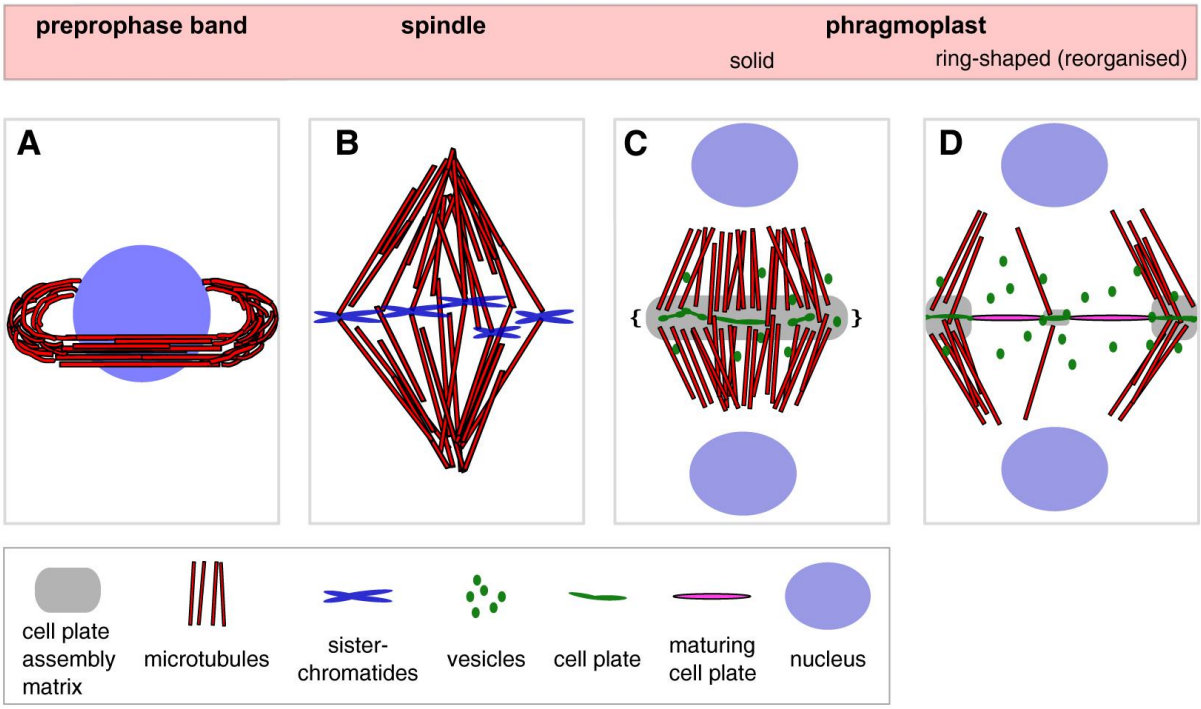

Figure 2. Microtubule arrays in plants.
(A) The preprophase band delineates the future division site.
(B) The metaphase spindle separates the sister-chromatids.
(C) In telophase, a barrel-like phragmoplast, consisting of two opposing sets of microtubules is formed between two daughter nuclei. The opposing sets of microtubules are separated by the so called midzone (brackets).
(D) The phragmoplast expands centrifugally, leading the cell plate towards the cortical division site, where it gets attached to the lateral wall.

1.2.1. Preprophase band

The basic geometry of a cell intrinsically gives some cues as to the position of the division plane. For instance, the division occurs perpendicular to the long axis of the cell (Hofmeister, 1863). A microtubule array, the preprophase band, marks the future division plane in a more precise manner (Figure 2A; Pickett-Heaps and Northcote, 1966).

Selective depolymerisation and remodelling of cortical interphase microtubules gives rise to the preprophase microtubule array (Dhonukshe and Gadella, 2003; Vos et al., 2004). *De novo* microtubule nucleation might also add to the formation of the microtubule array, as components of the γ-tubulin ring complex localise to the preprophase band (Janski et al., 2012). Cortical actin filaments constrict the preprophase band to an area called the cortical division zone (Liu et al., 2011b). The constricted zone is actin-depleted and persists throughout mitosis and cytokinesis (Hoshino et al., 2003; Panteris, 2008). The constricting actin filaments, also known as microfilament twin peaks, are thought to guide the phragmoplast and cell plate towards the cortical division site (CDS) (Figure 3; Sano et al., 2005; Panteris, 2008). The cortical division site is the confined cortical division zone, where

the cell plate gets inserted into the lateral wall (Lipka et al., 2015). Although the disassembly of the preprophase band takes place well ahead of nuclear breakdown, the orientation of the cell plate can be predicted by its position (McMichael and Bednarek, 2013). Some proteins remain at the cortical division site after the disassembly of the preprophase band and highlight this site throughout mitosis and cytokinesis (Müller et al., 2006; Walker et al., 2007; Xu et al., 2008).

1.2.2. Phragmoplast

The phragmoplast is the cytokinetic microtubule array in higher plants, in contrast to the phycoplast of algae (Figure 2C, D; Pickett-Heaps, 1974). Evolutionary, the phragmoplast first appeared in plant-related green algae such as *Coleochaete* and *Chara*. Contrary to the phycoplast, the phragmoplast is not arranged parallel, but perpendicular to the division plane (Ledbetter and Porter, 1963; Graham et al., 2000). Similarly, the actin microfilaments, the other cytoskeletal component of the phragmoplast, organise themselves perpendicular to the division plane (Zhang et al., 1993).

After completing anaphase, phragmoplast microtubules emerge from polymers of the former mitotic spindle (Figure 1A, Figure 2B; Staehelin and Hepler, 1996). Consistently, introduction of fluorescently labelled brain tubulin shows structural continuity of microtubule arrays throughout cytokinesis in stamen hair cells of *Tradescantia virginiana* (Zhang et al., 1990). A bipolar array of two opposite sets of microtubules is assembled at the division site. As cytokinesis proceeds, microtubules are added to the array at the plus end, in proximity of the division zone, and shortened at the minus end, near the chromosomes. This process is also known as treadmilling. A barrel-like structure is generated with a midzone between the two opposing sets of microtubules (Figure 2C). Subsequently, the phragmoplast microtubules relocalise from the middle to the periphery and encircle the expanding cell plate (Figure 2D; Lee and Liu, 2013). This is realised via microtubule depolymerisation at the centre of the phragmoplast and assembly at its leading edge (Liu et al., 2011a). After insertion of the cell plate in the lateral wall, phragmoplast microtubules get depolymerised.

Although plants lack centrosomes and display dynamic microtubule plus ends and minus ends (Shaw et al., 2003), they are able to establish higher-order microtubule arrays such as the phragmoplast (Figure 2). So far, the establishment and maintenance of the phragmoplast is not fully understood. Localisation patterns of microtubule plus end and minus end proteins and fluorescence motility experiments point to a model that exceeds simple treadmilling from the minus end (nuclei) to the plus end (midzone; Figure 2C) (Van Damme et al., 2004; Zeng

et al., 2009; Smertenko et al., 2011). Consistently, the turnover rate of microtubules is very high during this phase (Hush et al., 1994). Another open question is the possible interdigitation of opposite microtubules in the phragmoplast midzone. On the one hand, no overlap of anti-parallel microtubules was observed for the majority of microtubules in cryofixed/freeze substituted somatic *Arabidopsis thaliana* cells. This led to speculation as to the existence of a mechanism that stabilises microtubule plus ends inside the cell plate assembly matrix (Austin et al., 2005). On the other hand, interdigitation was observed in endosperm cells and also in a subset of microtubules in cryofixed/freeze substituted somatic cells (Hepler and Jackson, 1968; Ho et al., 2011). It will be interesting to see whether the organisation of the phragmoplast microtubules at the plus end is determined not only by microtubule-related proteins but also by membrane-related proteins.

A microtubule-related protein family, known to be localised to the phragmoplast, might be responsible for the correct reorganisation of the phragmoplast. The microtubule-associated protein 65 (MAP65) family consists of nine members in *Arabidopsis thaliana* (Hussey et al., 2002), and is known to form homodimers to promote anti-parallel microtubule bundling *in vitro*. This binding is achieved by the conserved C-terminal part of the proteins (Smertenko et al., 2004; Gaillard et al., 2008). AtMAP65-1, AtMAP65-2 and PLEIADE/AtMAP65-3 are involved in the correct execution of cytokinesis. All three proteins localise to the phragmoplast and display cytokinesis-specific phenotypes as single or double mutants (Sasabe et al., 2011a). *pleiade,* however, exhibits the most pronounced cytokinesis-related defects of the protein family and, in addition, an abnormally wide midzone (Table 1; Figure 2C; Müller et al., 2004; Caillaud et al., 2008).

1.3. Membrane compartments required for cytokinesis

Besides microtubules, two membrane compartments are crucial for plant cytokinesis. The first compartment, the trans-Golgi network/early endosome (TGN/EE) (Figure 3), contributes material to the division plane. In addition to newly synthesised proteins, polysaccharides such as xyloglucans or arabinogalactans are transported in TGN/EE-derived vesicles (Seguí-Simarro et al., 2004; McMichael and Bednarek, 2013). The arriving vesicles form a membranous network, which develops into a cell plate, the second essential membrane compartment (Figure 3). Several membrane fusions and the alteration of the protein and polysaccharide composition let the cell plate mature into a cross wall. Callose is a juvenile trait of the cell plate compared to the parental cell wall. After cell plate maturation, callose, which is synthesised at the cell plate, is removed and cellulose becomes the predominant

luminal component of the nascent cross wall. Finally, the two daughter cells are divided via a new cross wall, flanked by a plasma membrane on either side (Samuels et al., 1995).

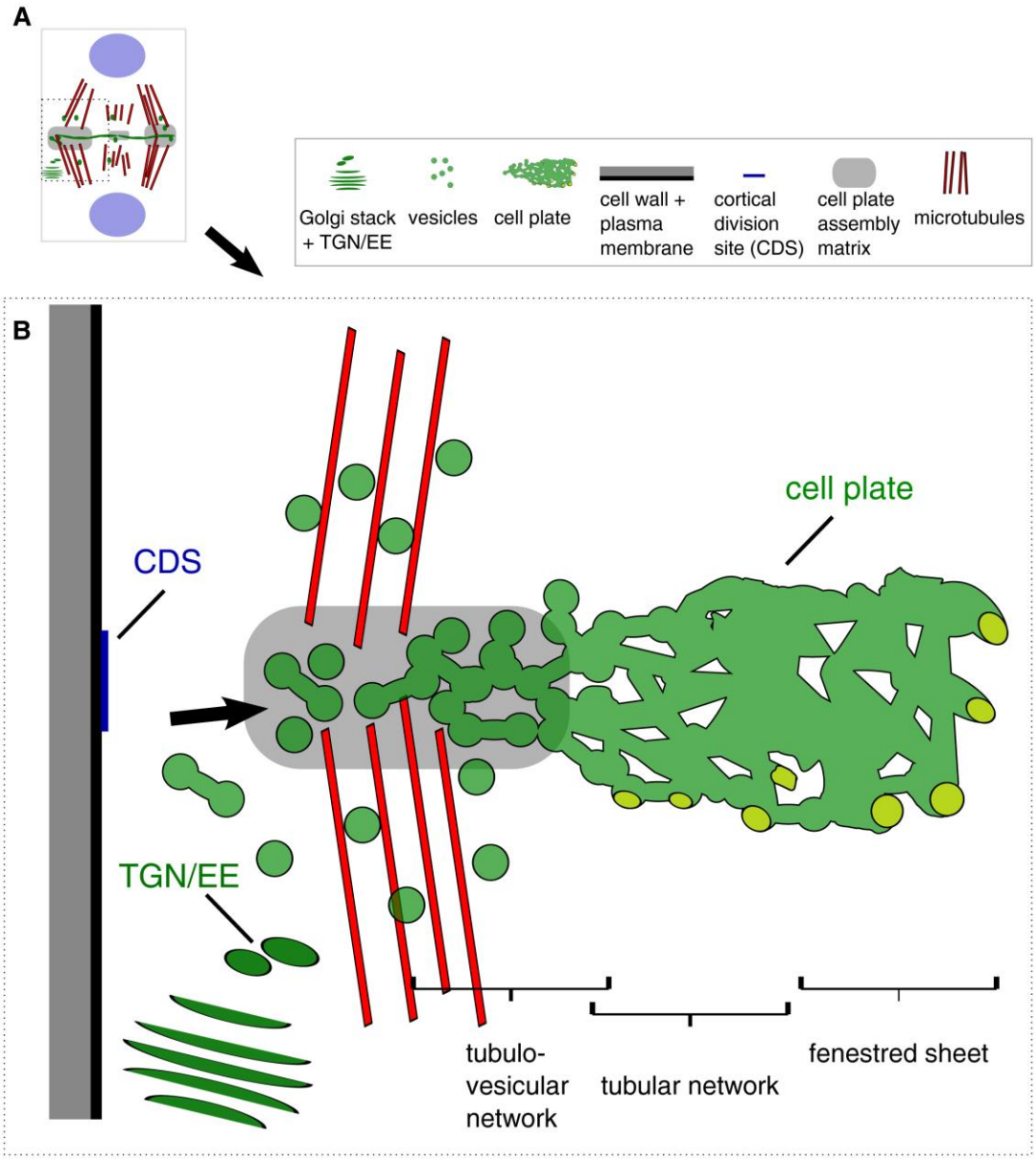

Figure 3. Membrane dynamics during cell plate development.
(A) Somatic cell during cell plate expansion.
(B) TGN/EE and Golgi-derived vesicles are delivered along phragmoplast microtubules (red) to the division plane. Right after arrival at the division plane, membrane fusion generates dumbbell-shaped cell plate initials (arrow). A tubulovesicular network arises by subsequent rounds of fusion in the cell plate assembly matrix. The tubulovesicular network is successively transformed into a tubular network and a planar fenestrated sheet. The cell plate centrifugally expands towards the cortical division site (CDS). The CDS marks the site of cell plate insertion into the lateral cell wall. Adapted from Jürgens (2005).

1.3.1. The trans-Golgi network/ early endosome (TGN/EE)

The TGN/EE was initially perceived as part of the Golgi stack adjacent to the *trans*-Golgi cisterna within the Golgi matrix (L A Staehelin and Moore, 1995). It was later proposed that the TGN/EE is structurally divided in early and late sub-compartments (Staehelin and Kang, 2008). Consistently, super-resolution confocal microscopy has identified two types of TGN/EEs: the Golgi-associated TGN/EE and the Golgi-released independent TGN/EE (Uemura et al., 2014). Additionally, it has been observed that clusters of vesicles leave the TGN/EE and traffic together towards the plasma membrane or cell plate (Toyooka et al., 2009). It is now generally accepted that the TGN/EE is a highly diverse and plastic compartment.

The main function of the TGN/EE is to deliver proteins from the Golgi apparatus to the plasma membrane, lysosomes, vacuoles and extracellular space (Griffiths and Simons, 1986). However, the TGN/EE is also involved in retrograde transport from the plasma membrane. A marker for the recycling endosome (Geldner et al., 2003) also co-aggregates with TGN/EE markers in Brefeldin A (BFA)-compartments (Dettmer et al., 2006; Lam et al., 2007; Chow et al., 2008). It is not clear whether the recycling endosome is connected with the TGN/EE, a matured form of the TGN/EE, or a discrete compartment (Viotti et al., 2010). Consistent with its central function in trafficking, TGN/EE-specific proteins also play a critical role in plant-pathogen resistance (Uemura et al., 2012a) and salt tolerance (Kim and Bassham, 2011; Uemura et al., 2012b). Taken together, the TGN/EE is a transfer site for information from the plasma membrane and the secretory pathway (Dettmer et al., 2006; Uemura and Nakano, 2013; Viotti et al., 2010). The TGN/EE acts as the main hub in the cell and distributes vesicles, proteins and polysaccharides to their destined organelles. During cytokinesis, the TGN/EE delivers vesicles and material for the cell plate to the division plane (Chow et al., 2008).

1.3.2. The Cell Plate

Bisecting two newly divided plant cells requires the formation of a new cross wall. This process starts after the separation of the chromosomes at late anaphase. Golgi and TGN/EEs form the so-called ‘Golgi-belt’ around the determined division plane (Figure 1A; Nebenführ et al., 2000). From there a cloud of TGN/EE-derived vesicles accumulates at the equatorial plane and instantly initiate fusion. The first round of membrane fusion leads to hourglass-like intermediates, which get turned into a dumbbell-shaped vesicle-tubule-vesicle structures (Figure 3; arrow). Dynamin-related proteins are involved in forming this structures (Otegui et

al., 2001; McMichael and Bednarek, 2013). Hundreds of simultaneous executed fusion events give rise to a continuous, interwoven tubulovesicular network (Figure 3). The fusion events take place in a ribosome excluding network, known as the cell plate assembly matrix. This matrix contains a high density of clathrin-coated vesicles and microtubule plus ends of the phragmoplast. Upon phragmoplast replacement to the leading edge, the cell plate turns into a smooth tubular network (Figure 3) and expands centrifugally. During this phase the two nuclei already start to reform. In the next step, the membranous, interwoven mesh develops to a fenestrated sheet (Figure 3) whilst connecting with the parental plasma membrane. Membrane fusions take place at several sites at the same time (Samuels et al., 1995; Seguí-Simarro et al., 2004). Once this connection is established, the cell plate starts to flatten (Gunning, 1982) and finally gets attached to the lateral cell wall (Schopfer and Hepler, 1991). Although cell plate formation follows this specific sequence of events, these fusion events are not timely separated and may occur at different places at the same time as the cell plate expands centrifugally (Figure 3; Samuels et al., 1995).

1.4. Membrane trafficking machinery

Inter- and intra-compartmental trafficking of proteins is mediated by vesicles. Vesicles bud from one compartment and get delivered along microtubules to their destined compartment. During cytokinesis and other cellular processes a lot of vesicle fusion occurs at the same time. To prevent incorrect fusion, different proteins localised on the vesicles and in their periphery are involved in specific vesicle fusion. Tethering factors are responsible for the first contact between vesicles, prior to the fusion event (Cao et al., 1998). Monomeric GTPases are important regulators of membrane tethering in the secretory and endocytic pathways. Guanine nucleotide Exchange Factor (GEFs) mediate the switch from an inactive GDP-bound state to an active GTP-bound state (Pan and Wessling-Resnick, 1998). RabAs are the largest group of GTPases in plant trafficking (Vernoud et al., 2003). SNAP (soluble N-ethylmaleimide-sensitive factor attachment protein) receptor (SNARE) proteins are required for the actual fusion of the membranes (Weber et al., 1998). Sec1/Munc18 (SM) proteins interact with SNARE proteins to realise the membrane fusion. All these proteins together are required for correct homo- and heterotypic membrane fusion (Figure 4).

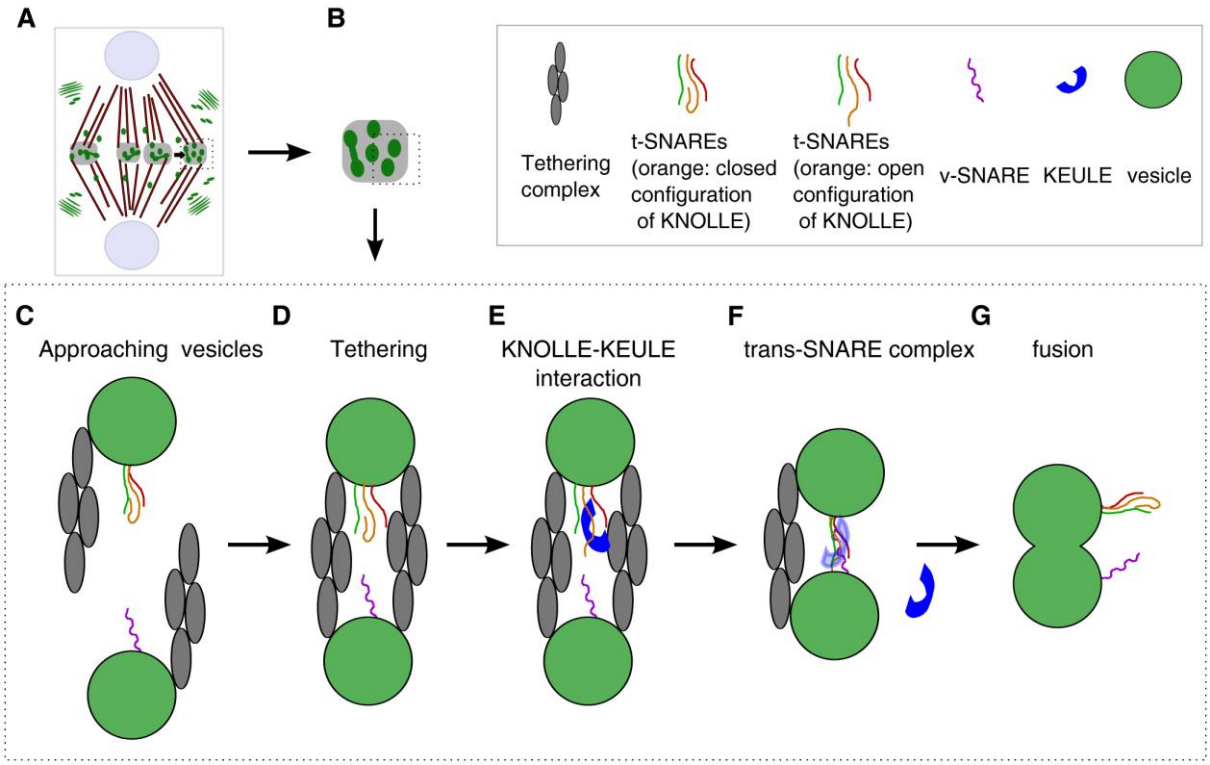

Figure 4. Schematic of the main components during vesicle tethering and fusion.
(A) Cell plate initiation stage of a somatic cell.
(B) Close-up of the cell plate assembly matrix, within which vesicle fusion takes place **(C-G).**
(C) Two approaching vesicles, each with a multisubunit tethering complex (grey ovals) and SNARE proteins.
(D) Multisubunit tethering complexes mediate the first contact between the vesicles.
(E) The SM protein KEULE (blue) binds to the open configuration of the syntaxin KNOLLE (orange).
(F) A trans-SNARE complex is established between the v-SNARE (purple) and the t-SNAREs (red, light green, orange). Whether KEULE remains bound (transparent blue) or gets released after the trans-SNARE complex formation (blue) remains unclear.
(G) This interaction brings the two vesicles to a close proximity and enables fusion. To simplify the illustration, components of just one trans-SNARE complex are depicted and the GTPases, NSFs and SNAPs were omitted. Modified from (Park et al., 2012).

1.4.1. Tethering factors during cytokinesis

The first specific physical contact between the trafficking vesicle and its target membrane is described as tethering (Figure 4D; Cao et al., 1998). This tethering process is regulated by two kinds of molecules, coiled-coil proteins and multisubunit complexes (Sztul and Lupashin, 2006). Several tethering factors are specifically required for vesicle fusion at different steps throughout the secretory pathway.

The multisubunit complexes can be attributed to particular inter- or intra- organellar transport. The specificity and trafficking properties of the tethering complexes were mainly investigated in yeast (or human cells for EARP). Retrograde and anterograde transport between the endoplasmic reticulum (ER) and the Golgi apparatus and intra Golgi transport is realised by the Dependence on Sly1 (Dsl1), the Conserved Oligomeric Golgi (COG) and the Transport

Protein Particle I (TRAPP I) tethering complexes (Reilly et al., 2001; Sacher et al., 2001; Suvorova et al., 2002; Zolov and Lupashin, 2005). Vesicle fusion at the trans-Golgi face, endosomes and vacuoles is mediated by the Golgi-Associated Retrograde Protein (GARP), the Endosome-Associated Recycling Protein (EARP), the endosomal Class C core Vacuole/Endosome Tethering (CORVET) and the Homotypic fusion and Protein Sorting (HOPS) tethering complexes (Conibear and Stevens, 2000; Wurmser et al., 2000; Schindler et al., 2015).

Two further multisubunit tethering complexes, the TRAPP II and exocyst, mediate late Golgi transport and exocytosis, respectively (TerBush et al., 1996; Sacher et al., 1998, 2001).

In addition to the six TRAPP I subunits, the TRAPP II complex consists of three further subunits, TRS120, TRS130 and TRS65 (Table 2; Sacher et al., 2001; Yu and Liang, 2012). All of the subunits except for TRS65 are conserved in plants (Thellmann et al., 2010). In yeast and mammals, the TRAPPII complex serves as a Rab GEF for monomeric GTPases that are homologs of the plant RabA family (Jones et al., 2000; Morozova et al., 2006). Recent studies in yeast strengthen these findings that TRAPPII shows Rab GEF activity predominantly for homologs of the plant RabA family; however, some studies in yeast and mammals show contradictory results (reviewed by Kim et al., 2016). So far in plants, colocalisation of TRAPPII subunits with members of the RabA family has been reported but no Rab GEF activity has been documented (Qi et al., 2011; Qi and Zheng, 2011). RabA family members are involved in vesicle transport from the TGN/EE to the plasma membrane and are required for cell plate development (Chow et al., 2008; Feraru et al., 2012; Preuss et al., 2004; Davis et al., 2015). This suggests a possible regulatory function of TRAPPII during plant cytokinesis, as the RabA GTPases are the key regulators of vesicle fusion during cytokinesis (Chow et al., 2008).

Subunit (yeast)	TRAPP complex	Required for tethering in following compartments (yeast)	Subunit group/comments
Bet3	I, II and III	ER-to-Golgi	Core subunit; (Sacher et al., 2001)
Bet5	I, II and III		
Trs23	I, II and III		
Trs31	I, II and III		
Trs20	I, II and III		Adaptor; (Sacher et al., 2001)
Trs33	I, II and III		TRAPPI-associated; (Sacher et al., 2001)
Tca17	II*	post Golgi; TGN/EE	Adaptor; paralog of Trs20; (Montpetit and Conibear, 2009)
Trs65	II		Not conserved in plants; (Liang et al., 2007)
Trs120	II		TRAPPII-specific; (Sacher et al., 2001)
Trs130	II		
Trs85	III	Autophagosome	TRAPPIII-specific; (Sacher et al., 2008)

Table 2. TRAPP tethering complexes. Orthologs in plants exist for all subunits, but the functions of TRAPP I and TRAPP III in plants are so far unknown. TRAPP II functions in plants also in post-Golgi trafficking.*Tca17 is a sub-stoichiometric component of the TRAPPII tethering complex (Rybak et al., 2014; Kim et al., 2016).

The exocyst complex in mammals and yeast consists of eight subunits that are encoded as single or multiple isoforms in the *Arabidopsis thaliana* genome (Table 3; Guo et al., 1999; Matern et al., 2001; Synek et al., 2006). In mammals and yeast, the exocyst is required for polarised secretion. For instance, the exocyst complex localises to the tip of the growing neurite in neuronal cells (Hazuka et al., 1999). In budding yeast the exocyst complex is present at the tip/neck and in dividing fission yeast at the cleavage furrow (TerBush and Novick, 1995; Fielding et al., 2005). In addition, the exocyst complex was shown to interact with a Rab GTPase (Novick and Guo, 2002). This hints to a role during cytokinesis, as cell division can be seen as a special form of polarised secretion.

Both the TRAPPII and the exocyst tethering complexes are in some way involved in cytokinesis (Fendrych et al., 2010; Jaber et al., 2010; Thellmann et al., 2010), but neither their exact localisation nor their exact function during cytokinesis had so far been described.

Subunit (yeast)	Isoforms in *Arabidopsis thaliana*	Required for tethering in following compartments	Reference
Sec3	2	plasma membrane (exocytosis)	(Elias et al., 2003)
Sec5	2		
Sec6	1		
Sec8	1		
Sec10	1		
Sec15	2		
Exo70	22		(Synek et al., 2006)
Exo84	3		(Elias et al., 2003)

Table 3. Exocyst tethering complex. Multiple isoforms exist for almost all exocyst subunits in plants (Synek et al., 2006).

1.4.2. SNARE and SM proteins required for cytokinesis

The transport of newly synthesised proteins through the secretory pathway occurs via vesicles (Palade, 1975). Vesicles bud off the donor membrane and fuse with the acceptor membrane of the following organelle. After tethering the vesicle to the acceptor membrane, the fusion is mediated by SNARE proteins (Chen and Scheller, 2001).

SNAP receptor proteins (SNARE) are receptors for N-ethylmaleimide sensitive factors (NSF) and soluble NSF attachment proteins (SNAP) (Söllner et al., 1993). These receptors can be roughly divided into two groups, the v-SNAREs and the t-SNAREs (Figure 4), indicating their localisation at the vesicle or target membrane respectively. Fusion occurs when the right (R-type) v-SNARE interacts with the right (Qa-, Qb-, Qc-type) t-SNAREs. This interaction is highly specific and enables multiple targeted fusions of different vesicles at the same time (McNew et al., 2000). Upon arrival of the vesicle at the target membrane, a trans-SNARE-complex consisting of four α-helices is created (Figure 4F). Consequently, the trans-SNARE complex brings the membranes in close proximity to each other so that fusion can occur (Figure 4G; Weber et al., 1998). Sec1/Munc18 (SM) proteins are positive or negative regulators of SNARE interaction (Burgoyne and Morgan, 2007; Südhof and Rothman, 2009). Different SM families have distinct binding mechanisms. Most of them bind to the closed conformation of syntaxins (SNARE proteins), dependent or independent of their SNARE motifs. Other SM proteins bind to the open conformation (Dulubova et al., 2003; Park et al.,

2012). SNARE proteins get recycled back into their non-binding configuration in the presence of NSF and SNAP proteins.

In plants, the cytokinesis-specific syntaxin KNOLLE/AtSYP111 (Lauber et al., 1997) gets delivered to the cell plate via the Golgi and TGN/EE (Chow et al., 2008). At the cell plate, KNOLLE forms a trans-SNARE-complex with AtSNAP33 (Heese et al., 2001) and the v-SNAREs, AtVAMP721 and AtVAMP722 (Zhang et al., 2011). The SM protein KEULE/AtSEC11 (Waizenegger et al., 2000; Assaad et al., 2001) stabilises the open form of KNOLLE and favours the formation of the trans-SNARE complex (Figure 4E; Park et al., 2012). This interaction suggests that KEULE's predominant role is the regulation of KNOLLE during cytokinesis. However, trafficking studies with BFA and involvement of KEULE, but not KNOLLE, in tip growth, indicates additional roles of KEULE (Assaad et al., 2001; Reichardt et al., 2007; Park et al., 2012).

1.5. Cell cycle regulation of phragmoplast microtubule dynamics

The core cell cycle genes are conserved over a broad range of species (Vandepoele et al., 2002). Key regulators of the cell cycle such as cyclins and cyclin-dependent kinases (CDKs) are amongst these genes. However, plants differ in some aspects of the cell cycle regulation compared to animals. Plants have additional CDKs, such as CDKBs, but lack other proteins such as polo-like kinases that are required for the cell cycle regulation in animals (Sasabe and Machida, 2012).

Cell cycle progression through the M-phase of plants involves three important transitions. First, entry into mitosis, the G2/M transition, which is controlled by CDKA, CDKBs and cyclin B (Figure 5A; Gutierrez, 2009; Tank and Thaker, 2011; Scofield et al., 2014). Second, the metaphase to anaphase transition that is controlled via specific cyclin degradation. The anaphase promoting complex marks cyclins as targets for degradation in the proteasome. This is also true for other kingdoms (Figure 5B; Weingartner et al., 2004; Heyman and Veylder, 2012). Third, during cytokinesis the lateral phragmoplast expansion is controlled by a mitogen-activated protein (MAP) kinase cascade that is regulated in a cell cycle-dependent manner (Figure 5C; Sasabe et al., 2011b).

Dephosphorylation of the kinesin 7 member HINKEL/AtNACK1 activates the MAP kinase cascade that is conserved in tobacco and *Arabidopsis thaliana*. While entering telophase, the phragmoplast microtubules debundle towards the centre and get translocated to the leading edge of the cell plate. Phosphorylation of PLEIADE/AtMAP65-3 and other members of the

microtubule-associated protein 65 (MAP65) family by this mitogen-activated protein (MAP) kinase cascade causes the debundling of microtubules at the centre of the phragmoplast (Takahashi et al., 2004; Sasabe et al., 2011a).

Microtubules are known to be important for cell cycle progression. For example, as targets of the described MAP kinase cascade or as part of a control mechanism, called the spindle assembly checkpoint (SAC) (Musacchio, 2015). On the other hand, not much is known about the contributions of the membranes in the progression through the cell cycle.

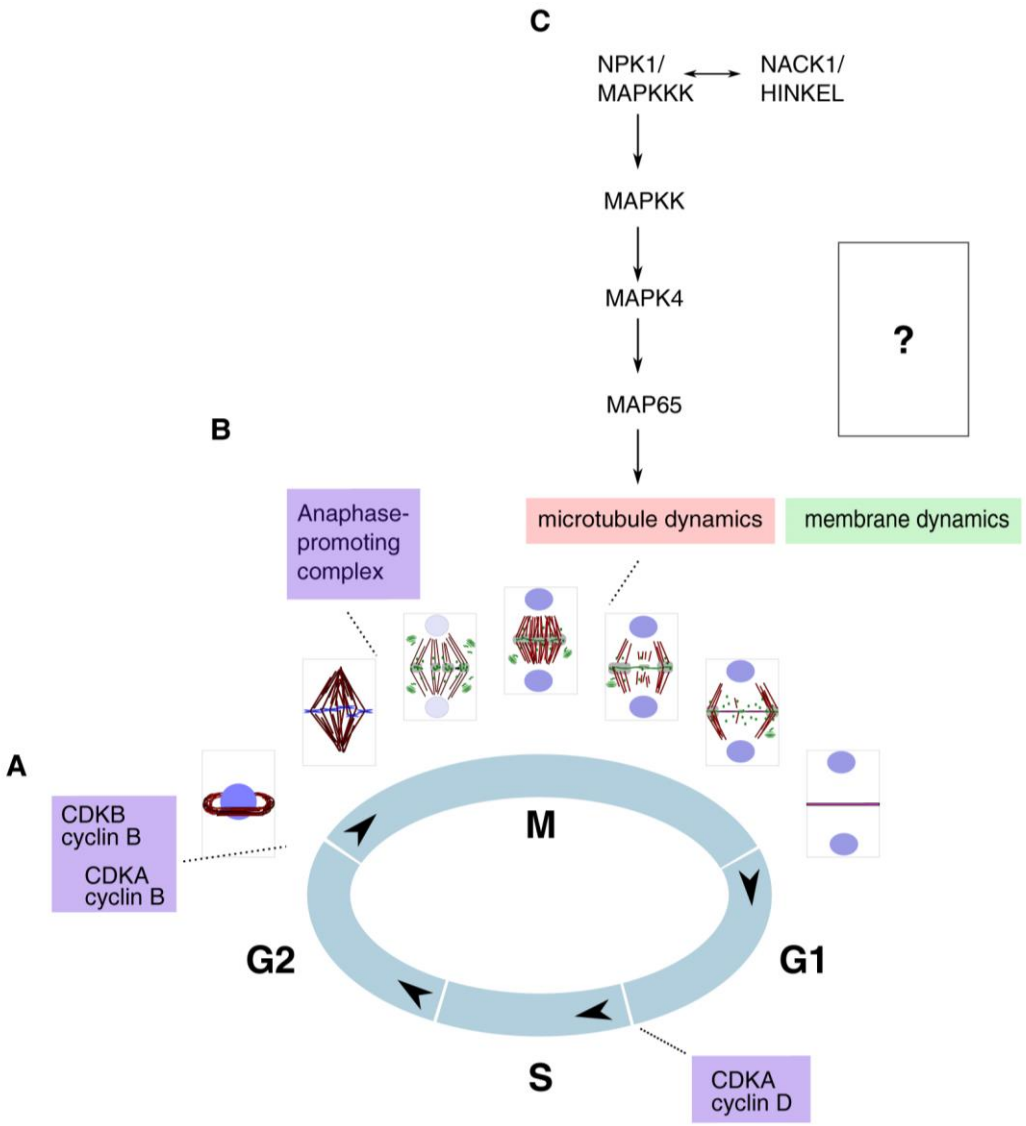

Figure 5. Progression through the M-phase (mitosis/cytokinesis) of the cell cycle.
(A) Entry into the M-phase is coordinated via the interaction of B-type cyclins with CDKA and plant-specific CDKBs. Additionally, CDKA also regulates the G1/S transition with D-type cyclins.
(B) The anaphase-promoting complex marks cyclins for degradation in the proteasome.
(C) During cytokinesis, a plant-specific mitogen-activated protein (MAP) kinase cascade regulates the reorganisation of the phragmoplast microtubules. The role of the cell plate in progression through the cell cycle is still unknown (question mark).

1.6. Objectives

Open questions in plant cytokinesis

Although the principles of plant cytokinesis are known, there are still many open questions. The formation of the cell plate requires a large amount of vesicles being delivered to the division plane. Whether the cell plate arises solely from TGN/EE-derived vesicles or additionally also from endocytic vesicles remains elusive. The cell plate is a transient compartment that emerges during cytokinesis. It is not clear so far, whether the cell plate is just a sink for plasma membrane proteins and cell wall polysaccharides during cytokinesis or a compartment distinct from the mature cell wall. Furthermore, the interplay between membranes and microtubules is crucial for a correct cell plate formation. A great number of membrane-related and microtubule-related proteins required for cytokinesis are known (Table 1). However, the molecular link between membranes and microtubules during cytokinesis is still missing. In addition, the molecular functions of some of the proteins involved in cytokinesis (Table 1-3) are so far not entirely understood. Although most of the cell cycle machinery is conserved across kingdoms, not much is known about the transmission of cell cycle cues to the membranes during plant cytokinesis. The open questions were split into three chapters, to thoroughly address each topic.

Identity of the cell plate; role of the tethering complexes; sorting behaviour

The first chapter focused on the identity of the cell plate, the role of the two tethering complexes, TRAPPII and exocyst, and the sorting behaviour of proteins and polysaccharides at the cell plate. Two hypotheses as to the identity of the cell plate were tested. The first hypothesis assumes the cell plate to be at the same time a TGN/EE and a plasma membrane compartment. The second considers the identity of the cell plate to be sequential throughout cytokinesis, first a TGN/EE then a plasma membrane compartment. Except for the involvement in cytokinesis, not much is known about the localisation pattern or function of the TRAPPII and exocyst tethering complexes during cytokinesis. Therefore, localisation studies, interaction studies and mutant analyses were conducted. The hypothesis that the cell plate acts as a sink for plasma membrane proteins was tested with localisation studies of plasma membrane proteins and polysaccharides in mutant backgrounds of the two tethering complexes.

Membrane and microtubules; additional role of KEULE

The second chapter of this thesis focused on the dynamics of membrane- and microtubule-related proteins and their interdependence during cytokinesis. To this effect, the localization dynamics of microtubule and membrane markers were monitored throughout cytokinesis. In addition, the effect of microtubule-related mutants on cell plate formation and, conversely, the effect of a membrane-related mutant on phragmoplast reorganisation was tested. The sorting behaviour at the cell plate was monitored. The syntaxin KNOLLE and the SM protein KEULE play a crucial role during vesicle fusion in plant cytokinesis. Some aspects of the interaction between KEULE and KNOLLE were still unclear. Besides the re-evaluation of the interaction, the sorting of both proteins was compared throughout cytokinesis.

Interaction between membranes and microtubules; cell cycle cues

In the third chapter of the thesis the main goal was to find a possible anchor mechanism for microtubule plus ends at the cell plate or in the cell plate assembly matrix. To this end, an interaction study with membrane-related proteins was conducted. Possible microtubule-related hits were evaluated and further analysed.

2. Embedded Publications

2.1. Publication 1: Plant cytokinesis is orchestrated by the sequential action of the TRAPPII and exocyst tethering complexes (Appendices 1-2)

Summary of publication 1

The first publication of this thesis, *plant cytokinesis is orchestrated by the sequential action of the TRAPPII and exocyst tethering complexes*, was published in *Developmental Cell* in June 2014.

Creating a new wall between two recently divided plant cells is a complex process that requires the biogenesis of a new compartment, the cell plate. The physical properties of the cell plate and cross wall differ. The cell plate changes from being fluid and deformable to being flat and rigid after insertion into the lateral wall in *Tradescantia* stamen hair cells (Mineyuki and Gunning, 1990). Cell plates also change their growth kinetics from slow and undirected to fast and directed upon contact with the lateral walls in *Arabidopsis* shoot cells (Cutler and Ehrhardt, 2002). Moreover, the composition of polysaccharides are quite different in the cell plate compared to the cross wall (Moore and Staehelin, 1988; Samuels et al., 1995; Seguí-Simarro et al., 2004). Although these physical and kinetic alterations in structure and composition are identified, little is known about the coordination and regulation of the transition from a juvenile cell plate to a mature cross wall.

The major thrust of this publication was to test two hypotheses as to the identity of the cell plate. The first hypothesis postulates that the cell plate has a mosaic identity, simultaneously consisting of TGN-derived and plasma membrane compartments, and the second that it has a sequential identity as it progresses from biogenesis to insertion and maturation. Analysing two tethering complexes throughout cytokinesis provided evidence in favour for the sequential identity hypothesis. The exocyst tethering complex has been shown to be involved in cytokinesis and polarised exocytosis (He and Guo, 2009; Fendrych et al., 2010). Similarly, the two plant specific subunits of the TRAPPII tethering complex, AtTRS120 and CLUB/AtTRS130, have been shown to be required for plant cytokinesis (Jaber et al., 2010; Thellmann et al., 2010; Qi et al., 2011).

In localisation studies, TRS120-GFP could be seen at the cell plate at the initiation phase of cytokinesis and it persisted at the cell plate until its insertion into the lateral cell wall (App. 1 Figure 1). EXO84b-GFP, a subunit of exocyst implicated in cytokinesis (Fendrych et al.,

2010; Heider and Munson, 2012) also localised to the cell plate at the onset of cytokinesis. Thereafter, EXO84b-GFP was diffuse, with a cloud-like appearance around the cell plate. Towards the end of cytokinesis EXO84b-GFP appeared at the cell plate and the fluorescence increased until it peaked at the new cross wall (App. 1 Figure 1). For both tethering complexes, all the subunits of the same complex we tested shared the same localisation pattern throughout cytokinesis (App. 1 Figure 2; App. 2 Figure S1). Colocalisation with the microtubule marker mCherry-TUA5 showed that TRS120-GFP and EXO84b-GFP appeared at the phragmoplast assembly stage. TRS120-GFP fluorescence persisted along the entire cell plate during the solid phragmoplast stage, while EXO84b-GFP fluorescence was diffuse around the plate during this stage. At the ring-shaped phragmoplast stage, TRS120-GFP localised to the leading edges with the microtubules and then gradually got weaker and disappeared. EXO84b-GFP, on the other hand, started to relocalise to the cell plate at the ring-shaped phragmoplast stage and became stronger and reached its peak fluorescence at the newly formed cross wall after the microtubules had already depolymerised (App. 1 Figure 2; App. 2 Figure S2). Colocalisation of both tethering complexes together confirmed these findings and showed overlap at the onset of cytokinesis and at the moment of cell plate insertion into the lateral walls (App. 1 Figure 3; App. 2 Figure S3). This indicates a sequential activity of both tethering factors during cytokinesis.

The localisation at the onset of cytokinesis might point to a function for both during cell plate biogenesis. However, and contrary to *TRAPPII* mutants, *exocyst* mutants had no visible cell plate biogenesis defect. No cell wall stubs or incomplete cross walls were found in *exo84b-2* via confocal microscopy (App. 1 Figure 3). Even electron microscopy failed to reveal small gaps or cross wall breaks in the *exo84b-2* mutant. *trs120-4* mutants, on the other hand, exhibited a range of cross wall defects, including stubs, incomplete cross walls, and “beads on a string-like” structures (App. 1 Figure 4; App. 2 Figure S4). Towards the end of cytokinesis, *exocyst* mutants varied in their behaviour compared to the wild type. For instance, the cytokinesis-specific syntaxin KNOLLE appeared already at the early ring-shaped phragmoplast stage as a punctate stain around the cell plate in *exo84b-2*, compared to the late ring-shaped phragmoplast stage in the wild type. Additionally, the polysaccharide composition of the cell plate and cross wall differed in the *exo84b-2* mutant in contrast to the wild type (App. 1 Figure 3, 5). In conclusion, the TRAPPII but not the exocyst complex is required for the biogenesis of the cell plate. The exocyst complex rather appears to be involved in cell plate maturation.

Another issue we addressed was whether active sorting of proteins and polysaccharides contributes to the identity of the cell plate. The analysis of cell wall polysaccharides via immunostaining showed that in *club/trs130-2* as well as in *exo84b-2,* the deposition of methyl-esterified pectins and AGP glycans at the cell plate, cross wall and lateral walls was altered compared to the wild type. In line with this, it is interesting to see that just *club/trs130-2* influenced the sorting behaviour of EXO84b-GFP, while the localisation of the TRAPPII complex was unaffected in *exo84b-2* mutants. EXO84b-GFP exhibited neither the cloud-like appearance during cell plate formation and expansion nor the characteristic peak fluorescence during cell plate initiation and nascent cross wall. The signal intensity of EXO84b-GFP was rather uniform at the cell plate and cross walls. Four other plasma membrane proteins showed similar results: they labelled the cell plate, cross walls and lateral walls differentially in the wild type but uniformly in *club/trs130-2* root tip cells (App. 1 Figure 5; App. 2 Figure S3, S5). We conclude that the TRAPPII complex is required for the correct sorting of proteins at the cell plate.

We next assessed the physical interaction between both tethering complexes. Mass spectrometry of purified proteins from anti-GFP pull downs of CLUB-GFP and TRS120-GFP identified multiple hits of the exocyst complex, including at least one isoform of each subunit (Table 3). This interaction was confirmed by co-immunoprecipitation of three exocyst subunits in CLUB-GFP and TRS120-GFP pull-downs via western blot and antibodies against the three subunits. Additionally, TRS120 was found in a yeast two-hybrid screen with EXO70H7 as a bait (App. 1 Figure 6; App. 2 Figure S6, S7). These results support a physical interaction between both tethering complexes.

Further analysis of the proteomic data revealed that TRAPPII subunits clustered on scatter plots at higher signal intensities than exocyst subunits. Likewise, the phenotypes of both complexes are quite different. *TRAPPII* mutants display classical cytokinesis defects such as bloated cells and incomplete walls. By contrast, the phenotype of *exo84b-2* was reminiscent of those of cell wall-related mutants, with radial swelling and cell wall breaks in vacuolated cells. In addition, both complexes did not colocalise in non-dividing cells (App. 1 Figure 6). This points to a transient interaction of both complexes and strengthened the model of a sequential function of the two complexes during cytokinesis.

In summary, the TRAPPII tethering complex and the exocyst tethering complex exhibit a transient physical interaction. We postulate that both complexes sequentially coordinate the development of the cell plate. The TRAPPII complex is required for the biogenesis of and

proper sorting at the cell plate. Thereafter, the exocyst complex is responsible for cell plate maturation. This sequential order of the two tethering complexes may enable the correct and timely delivery of the right proteins and polysaccharides to or at the cell plate or cross wall (App. 1 Figure 7).

Contributions to Publication 1

I performed a great deal of microscopy work for this study, including confocal laser scanning microscopy, environmental scanning electron microscopy and transmission electron microscopy. I taught myself the Imaris software (Bitplane) and prepared the 3D reconstructions of Focused Ion Beam/Scanning Electron Microscope micrographs. After image acquisition, I carried out quantitative analyses including, heat maps, line graphs and the measurement of the mitotic index. For the final manuscript I prepared the major complement of the figures and movies, critically appraised the manuscript and gave input for the writing.

2.2. Publication 2: The Membrane-Associated Sec1/Munc18 KEULE is Required for Phragmoplast Microtubule Reorganisation During Cytokinesis in *Arabidopsis* (Appendices 3-4)

Summary of Publication 2

The second article summarised in this thesis, *The Membrane-Associated Sec1/Munc18 KEULE is Required for Phragmoplast Microtubule Reorganization During Cytokinesis in Arabidopsis*, was published in *Molecular Plant* in April 2016.

Phragmoplast microtubules are postulated to transport vesicles to the division site to deliver the membrane and cargo required for cell plate biogenesis and expansion (Seguí-Simarro et al., 2004). When proteins required for microtubule nucleation are knocked out or down, the cells exhibit not only abnormal phragmoplasts but also cell plate defects (Pastuglia et al., 2006; Zeng et al., 2009). In *Physcomitrella*, downregulation of three microtubule-associated protein 65 (MAP65) genes additionally affect cell plate organisation (Kosetsu et al., 2013). Conversely, little is known about the effect of membrane proteins on the organisation of microtubule arrays during cytokinesis. SM proteins positively or negatively control the trans-SNARE complex formation during membrane fusion. The plant SM protein KEULE interacts with the plant-specific syntaxin KNOLLE. However, experiments with the membrane-trafficking blocking drug, Brefeldin A, and the root hair defect of *keule* mutants, but not *knolle* mutants, indicates additional roles of KEULE (Assaad et al., 2001; Reichardt et al., 2007).

To identify the dynamics and role of proteins involved in cellular processes such as phragmoplast reorganisation, it is important to work with functional, native protein fusions. To this end, we constructed and characterised a functional P_{KEU}::KEULE-GFP gene fusion (App. 4 Figure S1). KEULE-GFP was localised in the cytosol in non-dividing cells and to the cell plate in dividing cells throughout cytokinesis. At the end of cytokinesis, it aggregated at the edges of the cell plate, similar to what was shown in (Wu et al., 2013) with P_{35S}::KEULE-GFP in tobacco BY-2 suspension cells. Unlike other membrane proteins, KEULE-GFP does not seem to be trafficked through the TGN towards the plane of cell division. It did not colocalise with the TGN markers VHAa1-mRFP and SYP61-CFP (App. 3 Figure 1; App. 4 Figure S1; Dettmer et al., 2006; Drakakaki et al., 2012). This points to a TGN-independent recruitment of KEULE-GFP to the cell plate.

Immobilised KNOLLE bound native KEULE extracted from non-dividing *Arabidopsis* tissues better than from dividing tissues (App. 3 Figure 1). This indicates regulation of the KEULE-KNOLLE interaction does not just dependent on the pure presence of KNOLLE during mitosis/cytokinesis. Consistently, the movement and sorting behaviour of KNOLLE-YFP and KEULE-GFP at the cell plate differs. KNOLLE-YFP (Völker et al., 2001) and its close homologue SYP121-GFP (Collins et al., 2003) do not localise predominantly to the leading edges at the end of telophase like KEULE-GFP, but their localisation at the cell plate is rather uniform throughout cytokinesis. These proteins also vary in their removal from the cell plate. Whereas KNOLLE gets delivered to the vacuole, SYP121 and KEULE follow a different path (App. 3 Figure 2). Furthermore, the delivery of KEULE but not KNOLLE to the cell plate was perturbed in a TRAPPII mutant, *trs120-4*. Interestingly, an *exocyst* mutant *exo84b-2* had no influence on the recruitment of KEULE to the cell plate. Consistently, KEULE colocalised with P_{UBQ}::TRS120-mCherry, a TRAPPII subunit, but not with SEC6-mRFP, an exocyst subunit, throughout cytokinesis (App. 3 Figure 3). This indicates that the TRAPPII tethering complex is required for correct sorting of KEULE at the cell plate. The sorting behaviour of KEULE to, at and from the cell plate differs compared to the cytokinesis-specific syntaxin KNOLLE.

To test whether microtubules drive membrane dynamics at the cell plate or vice versa, the ability to reorganise to the leading edge of the cell plate was analysed with representative markers. In agreement with the broadly accepted view, the relocalisation of the microtubule marker GFP-PLEIADE to the leading edges at the transition from the solid to the ring-shaped phragmoplast stage occurred faster than that of the membrane markers KEULE-GFP and TRS120-GFP. Even though microtubule translocation precedes membrane displacement at the cell plate, the transport of KEULE-GFP to the plate and the distribution during cytokinesis over the plate was not altered in *hik*^{G235} and *ple-4* mutants (Table 1), which have been shown to affect phragmoplast array organisation (App. 3 Figure 4; App. 4 Figure S2). Microtubule reorganisation precedes membrane translocation at the cell plate. Microtubule-related proteins do not change the localisation patterns of KEULE.

Thorough analysis of both microtubule-related mutants, *hik*^{G235} and *ple*-4, revealed defects in phragmoplast reorganisation from the solid to the ring-shaped stage in telophase cells. Cell plate formation was normal in both mutants (App. 3 Figure 5). In addition, we monitored phragmoplast array organisation and cell plate formation in two further microtubule-related mutants, *clasp1-1* and *mor1-1* (temperature-sensitive) (Table 1). *clasp1-1* did not show any

defect in phragmoplast reorganisation or in cell plate formation. By contrast, *mor1-1* exhibited partially reorganised phragmoplasts in 36.2% telophase cells. Of the four microtubule-related mutants we analysed, *mor1-1* mutants were the most severely affected in cell plate formation (App. 3 Table 1; App. 4 Figure S3). Surprisingly, the membrane-related *keule* mutants, which had strong cell plate defects, as confirmed by focused ion beam/scanning electron micrographs (FIB/SEM) analysis, had a severe defect in reorganising phragmoplast microtubules in telophase cells: 86% of *keule* phragmoplasts were still solid in telophase cells (App. 3 Figure 6; App. 4 Figure S4). This defect seems to be independent of cell plate formation. Cell plates, monitored with anti-KNOLLE, were fully assembled in 78% of cases in *keule* mutants (App. 3 Table 1; Figure 6). Cell plate formation was most impaired in *mor1-1* mutants and *keule* displayed the most severe impairment in phragmoplast reorganisation.

In conclusion, KEULE-GFP appears in the cytosol during interphase and localises to the cell plate during cytokinesis. The behaviour of membrane proteins, including KEULE, is differential at the cell plate. KEULE-GFP seems not to be recruited to the cell plate via the TGN, but rather from the cytosol. The recruitment of KEULE-GFP to the cell plate appears to be controlled by the TRAPPII but not the exocyst tethering complex. A comparison of cytokinesis-defective mutants revealed that, among microtubule-related mutants, cell plate assembly was most disturbed in *mor1-1* mutants. Among all mutants tested, phragmoplast reorganisation was most severely impaired in *keule* mutants. In addition to its well documented role in membrane fusion (Waizenegger et al., 2000; Park et al., 2012), KEULE appears to play an important role in the reorganisation of the phragmoplast microtubule array.

Contributions to Publication 2

In this publication Farhah Assaad and I designed the experiments. All of the live imaging with the confocal laser scanning microscopy, with the exception of Figure 3A and Figure S2 (A-D), were performed by myself. The imaging of the fixed samples and the resulting numbers for the table was the cumulative effort of myself and former students in the laboratory of Farhah Assaad. I performed environmental scanning electron microscopy with the help of Eva Facher. The KEULE-GFP construct was carried out by Lin Müller; I carried out the complementation assay and the localisation analysis of KEULE-GFP in wild-type and mutant backgrounds. The 3D reconstructions of Focused Ion Beam/Scanning Electron Microscope micrographs were carried out by myself. Farhah Assaad and I did the data analysis. I prepared the figures and movies, critically appraised the manuscript and gave input for the writing.

2.3. Publication 3: Cell-cycle regulated PLEIADE/AtMAP65-3 links membrane and microtubule dynamics during plant cytokinesis (Appendices 5-6)

Summary of Publication 3

The third manuscript described in this thesis, *cell-cycle regulated PLEIADE/AtMAP65-3 links membrane and microtubule dynamics during plant cytokinesis*, was accepted by *The Plant Journal* in June 2016.

It is known that a large quantity of stable microtubule plus ends terminate in the cell plate assembly matrix. Around 30% of these stable plus ends are in the vicinity of the cell plate, at a fixed distance of ~ 30 nm (Austin et al., 2005). This is within the range of less than 50 nm where microtubule plus ends have been shown to be captured from the plasma membrane (Small and Kaverina, 2003). These findings point to an anchoring mechanism for microtubules at the cell plate, but the actual link between this membrane compartment and the cytoskeleton is still missing.

Immunoprecipitation experiments with mass spectrometry readout were conducted with membrane proteins as baits to discover possible links between membranes and microtubules at the division plane. The resulting dataset was mined for microtubule-associated proteins. We used three membrane proteins as baits, KEULE and the two plant-specific TRAPPII subunits; these were selected on the basis that their localization dynamics closely followed phragmoplast microtubule translocation throughout cytokinesis. Various KEULE fusions did not yield any significant microtubule-related result in dividing or non-dividing tissue. However, several tubulin isoforms and some plus end microtubule tracking proteins co-purified with the two TRAPPII subunits (App. 5 Table I; App. 6 Table S2). In addition the microtubule-associated protein 65 (MAP65) family, which plays an important role in bundling microtubules during cytokinesis *in vitro* (Gaillard et al., 2008; Smertenko et al., 2004), was also identified in the screen. AtMAP65-1 was significantly enriched in the immunoprecipitations of both TRAPPII subunits TRS120-GFP and CLUB-GFP. Additionally, it had a significant enrichment over the control and the co-expression coefficients were positively correlated to the TRAPPII subunits (App. 5 Table I; App. 6 Figure S1; Table S2). For subsequent experiments we focused on the MAP65 family.

AtMAP65-1, AtMAP65-2 and PLEIADE/AtMAP65-3 are known to act redundantly during cytokinesis (Sasabe et al., 2011a). To confirm the mass spectrometry result, we conducted binary interaction assays (yeast two-hybrid and bimolecular fluorescence complementation).

In our hands, full-length CLUB/AtTRS130 and AtTRS120 were poorly expressed in yeast, so truncations for each specific TRAPPII subunit were constructed. These truncations were generated after a phylogenetic analysis. A yeast two-hybrid assay revealed the interaction between PLEIADE/AtMAP65-3 and the plant specific fragment C3 of CLUB/AtTRS130, but not the other two fragments C1 and C2. Bimolecular fluorescence complementation assays corroborated binary interaction between the C3 CLUB truncation and the full length TRS120 with AtMAP65-1 and PLEIADE/AtMAP65-3. Interestingly, this interaction was localised to structures that resembled cortical microtubules, while the interaction of AtTRS120 with CLUB/AtTRS130 was localised to the cytosol and plasma membrane (App. 5 Figure 1). Binary interactions confirm the connection between TRAPPII and MAP65 family.

For a genetic interaction we focused on PLEIADE/AtMAP65-3 of the MAP65 family because its phenotype resembled most the one of other cytokinesis-specific mutants such as *keule* and *TRAPPII* (Smertenko et al., 2004). A hypomorphic, viable *ple-2* allele was crossed with a null seedling-lethal allele of AtTRS120. Analysis of *ple-2 trs120-4* double mutants showed a synergistic enhancement of the percentage of cells with incomplete cross walls in hypocotyl cells as compared to *trs120-4* and *ple-2* single mutants (App. 5 Figure 2). Furthermore, TRS120-mCherry co-localised with GFP-PLEIADE throughout cytokinesis, with both constructs reorganising towards the leading edges of the cell plate (App. 5 Figure 3; App. 6 Figure S2). p*le-2 trs120-4* double mutants show a synergistic genetic interaction and fluorescently tagged proteins of PLEIADE/ATMAP65-3 and AtTRS120 colocalise throughout cytokinesis.

Mutation at the *TRAPPII* locus had no influence on the delivery or localisation of PLEIADE/AtMAP65-3 to or at the cell plate. Conversely, mutation at the *PLEIADE/AtMAP65-3* locus also did not markedly perturb the appearance of TRAPPII at the cell plate: TRS120-GFP resided on the cell plate and relocalised to its leading edges correctly in *ple-4* mutants. The more diffuse appearance of the cell plate localisation in *ple-4* mutants could also be seen with the FM4-64 stain and is presumably due to the larger midzone characteristic of *pleiade* mutants (App. 5 Figure 4). TRAPPII does not act as a direct anchor for PLEIADE/AtMAP65-3 at the cell plate and PLEIADE/AtMAP65-3 is not required for the recruitment of TRAPPII to the cell plate.

Since TRAPPII and PLEIADE/AtMAP65-3 had no influence on each other's localisation pattern during cytokinesis, we focused more thoroughly on the genetic interaction. p*le-2 trs120-4* double mutants showed interesting accumulations of four or more nuclei in the

absence of even rudimentary cell walls. A twenty-fold enhancement of four or more nuclei in one cell was seen in *the* double mutants compared to *ple-2* single mutants. In *trs120-4* mutants at least rudimentary cross walls were always found. This result points to the uncoupling of the nuclear cycle and cytokinesis in the double mutants. The absence of even vestigial cell walls in focused ion beam/scanning electron micrographs of *ple-4* single mutants reinforced this result of an uncoupling of the nuclear cycle and cytokinesis (App. 5 Figure 5).

We tested our hypothesis that the role of this interaction is to transmit cell cycle cues to the cell plate membranes. We expected additional phenotypes of the *TRAPPII* mutants, similar to those of *NtMAP65* mutants in tobacco that are insensitive to cell cycle cues. The non-phosphorylatable *NtMAP65* mutants are not able to correctly reorganise the phragmoplast microtubules (Sasabe et al., 2006). Interestingly, the *TRAPPII* mutants have similar problems to correctly reorganise the phragmoplast microtubules from the solid to the ring-shaped phragmoplast stage (App. 6 Figure S3). The phenotype of *TRAPPII* mutants resembles the phenotype of non-phosphorylatable *NtMAP65-1* mutants.

In conclusion, several lines of evidence point to an interaction between the TRAPPII tethering complex and members of the MAP65 family. This interaction has no influence on either the anchoring of PLEIADE/AtMAP65-3 at the cell plate or on the delivery of AtTRS120 to the cell plate. We propose that this interaction might integrate membrane dynamics with microtubule dynamics and cell cycle cues.

Contributions to Publication 3

With the help of Farhah Assaad I designing the experiments for this work. For the binary interaction assays I prepared the constructs and Heather E. McFarlane (Bimolecular fluorescence complementation) and Melina Altmann (Yeast Two-Hybrid) performed the experiments. For the mass spectrometry screen, I did the biochemical work (Co-Immunoprecipitation, Western Blot) with the KEULE protein, which in the end did not show significant results. The screen was continued with the TRAPPII pull downs (performed by Katarzyna Rybak). I obtained the double mutants and analysed them with the help of Farhah Assaad and Eva Facher. The confocal laser scanning microscopy of live and fixed samples except Figure 1C was performed by me as well as the 3D reconstructions of FIB/SEM micrographs. For this publication I performed the majority of the data analysis, prepared the figures and movies and assisted in writing the manuscript.

3. Discussion

3.1. Role of TRAPPII and exocyst tethering complexes during cytokinesis

Sequential origin of the cell plate

Taken together, our data supports a sequential model for the origin of the cell plate. The two tethering complexes TRAPPII and exocyst are assigned to tether vesicles at the TGN/EE (TRAPPII) or at the plasma membrane (exocyst). Therefore, the localisation and function of both complexes during cytokinesis gives a good prediction of the cell plate identity for each developmental stage. There are four stages of cell plate development during plant cytokinesis: initiation, biogenesis, expansion and maturation (Figure 6). Our findings pertaining to the two tethering complexes indicate that the cell plate is mainly a TGN/EE compartment, with some exceptions towards the end of cytokinesis. The sole localisation of the exocyst complex at the initiation step is no definite evidence for an additional plasma membrane identity of the cell plate at the onset of cytokinesis. The change between the tethering complexes might be the reason for the alteration in polysaccharide composition, because the complexes tether vesicles with different cargo derived from different origins. Further evidence that the cell plate arises from Golgi-derived vesicles, is the positive cell plate staining throughout cytokinesis of JIM7, a methyl-esterified pectin. Methyl-esterified pectins are synthesised in the Golgi and thereafter deposited in a highly esterified form in the cell wall (Clausen et al., 2003).

Contrary to our findings, Dhonukshe et al. (2006) reported that endocytosis significantly contributes to cell plate formation. This would suggest that the cell plate is rather a plasma membrane than a TGN/EE compartment. However, some endocytosis experiments in Dhonukshe et al. (2006) are based on the amphiphilic dye FM4-64. The dye is often used for endocytic experiments, but the results have to be analysed with caution. FM4-64 does not exclusively stain endocytic vesicles and compartments but also, after 15 min, already Golgi stacks and other compartments (Bolte et al., 2004). Consistently, FM4-64 was shown to label TGN/EE-assigned compartments before it labels PVC-assigned compartments in *Arabidopsis* roots (Chow et al., 2008). The difference between the positive cell plate staining of JIM7 by our group compared to the negative cell plate staining by Dhonukshe et al. (2006) could be due to the different plant systems they were obtained. Our group used *Arabidopsis* root tips in contrast to tobacco BY-2 suspension cells used by Dhonukshe et al. (2006). Additionally, Dhonukshe et al. (2006) showed colocalisation of GNOM, an Arf-GEF of the recycling endosome and some pre-vacuolar compartment (PVC) markers such as Rab-F2 with

KNOLLE at the cell plate. It is not clear what kind of tissue was used for these experiments. I guess that the GNOM immunostaining experiments were conducted in fixed *Arabidopsis* root cells and the experiments with the PVC markers maybe in tobacco BY-2 cells. However, live imaging by Chow et al. (2008) with the same markers and additional PVC markers such as GFP-BP80 could not verify these observations in *Arabidopsis* root cells. Immunostaining can be a powerful tool in cell biology, however, it is prone to produce artefacts without the right controls and the sufficient number of biological replicates. Furthermore, additional studies concur with our results that the secretory pathway is the predominant source of vesicles for cell plate formation. For instance, the inhibition of TGN/EE trafficking via concanamycin A treatment leads to cytokinesis defects while sole impairment of endocytosis with wortmanin shows no cell plate formation defect (Reichardt et al., 2007).

Towards the end of cytokinesis the cell plate matures into a cross wall and starts to exhibit a plasma membrane identity. We show that a cell wall AGP glycan marker (Moller et al., 2008) labels cell plates after insertion into the lateral wall. Consistently, mutants of a multivesicular body-localised ESCRT-I sorting complex subunit show cytokinesis defects (Spitzer et al., 2006). Otegui et al. (2001) states that approximately 70% of the cell plate is removed during maturation. This recycling process from the cell plate is most likely executed by the ESCRT machinery (Van Damme et al., 2008). The involvement in the recycling of juvenile traits from the cell plate could explain the cytokinesis-related phenotype of ESCRT I. Additionally, during cell plate maturation pectins and xyloglucans from the parental cell wall and proteins derived from the plasma membrane occur at the maturing cell plate (Baluska et al., 2005; Van Damme et al., 2011). Furthermore, after cell-plate insertion, KNOLLE localization at the cell plate depends on correct sterol-dependent endocytosis (Boutté et al., 2010).

Tethering factors contribute to the specificity of vesicle trafficking.

Specificity in vesicle trafficking is determined at numerous steps: budding of the donor membrane, transport, contact and fusion with the target membrane. Various distinct coat proteins and Arf GTPases form transport vesicles at the donor membrane (Schekman and Orci, 1996; Vernoud et al., 2003). Vesicle transport is mediated via microtubule-associated proteins (MAPs) such as motor proteins (Jürgens, 2005). At the target membrane, tethering factors promote the first specific contact. In our case, the TRAPPII specifically tethers TGN-vesicles and the exocyst plasma membrane vesicles. Actual fusion of the membranes is accomplished by SNARE proteins and assisted by SM-proteins. The large number of SNARE proteins, with compartment-specific localisation, points to an important role of SNARE

proteins in determining the specificity at the target membrane (Lipka et al., 2007). Several lines of evidence, however, suggest that SNARE proteins do not suffice to ensure the specificity. For example, during periods of polarised growth in yeast, plasma membrane SNAREs, Sso1p and Sso2p, fuse vesicles to specific parts of the membrane, even though the SNAREs are distributed over the entire plasma membrane (Brennwald et al., 1994). Similarly, the cytokinesis-specific t-SNARE KNOLLE is localised over the entire cell plate, while the TRAPPII tethering complex relocalises to the growing part of the cell plate. Although localisation does not provide definite evidence for the function of a protein, it still gives a hint as to where the protein or complex is required. Additionally, SNAREs form random complexes *in vitro* (Yang et al., 1999). This indicates that additional mechanisms such as tethering are crucial for the specificity of vesicle trafficking.

The TRAPPII and exocyst are required at different stages of cell plate development (Figure 6)
The physical contact between both tethering complexes and the observation that TRAPPII sorts the exocyst suggests that there might be some form of coordination between the two complexes. In addition, the sequential localisation of the two complexes during cytokinesis and the different mutant phenotypes led us to propose a "relay race" model (Figure 6). Both complexes act at different stages during cytokinesis and coordinate transitions via a transient interaction. According to their localisation pattern, both complexes may be required for the regulation of cell plate initiation (Figure 6A). Subsequently, the TRAPPII complex gives the cell plate a juvenile TGN identity and drives the biogenesis and expansion of the cell plate (Figure 6B-C). The maturation from a TGN/EE to a plasma membrane compartment is promoted by the exocyst complex. The cell plate loses its juvenile traits, including the removal of KNOLLE at the late ring-shaped phragmoplast stage (arrowhead) (Figure 6 D).

During the phragmoplast assembly stage, all exocyst subunits showed a bright signal at the cell plate (Figure 6A). This made us speculate about a role of exocyst during initiation of cytokinesis. In favour of a role during initiation, electron tomographs showed vesicles being tethered in the very beginning of cytokinesis by exocyst resembling tethering molecules. (Seguí-Simarro et al., 2004). However, these structures could also be different tethering complexes or proteins. To verify these structures as exocyst positive complexes, immunostaining with nanogold-antibodies against exocyst epitopes would, for instance, be required. Mutant analysis of *exo70a1* also suggest a possible involvement of exocyst during initiation of cytokinesis. Aberrant, donut-shaped FM4-64 positive structures were identified in early stages of cytokinesis, but normal cell plates were found during later stages (Fendrych et

al., 2010). The aberrant, donut-shaped structures might be vesicles or FM4-64 stained compartments around the division plane and not yet cell plate initials. From my personal experience, I know it is hard to find cells that are going to divide in mutants. Without the appropriate cell plate marker, such as KNOLLE, and sufficient optical resolution it is hard to distinguish cell plate initials from other vesicles or compartments around the division plane. Additionally, the timing is very important when you want to catch the exact same moment of cell plate initiation in wild type and mutant cells. Without a marker such as tubulin, it is difficult to pinpoint the start of the cell plate formation. A combination of a FM4-64 stain with a KNOLLE fusion protein as a cell plate marker and a tubulin fusion protein should clarify, if the donut-shaped FM4-64 structures are cell plate initials. A correct initiation of cytokinesis has to be coordinated with the cell cycle machinery. In *Saccharomyces cerevisiae*, cell-cycle-dependent phosphorylation of EXO84 inhibits the assembly of the exocyst complex and thus may coordinate the cell cycle and the initiation of cytokinesis (Luo et al., 2013). Our results suggest that in plants the TRAPPII tethering complex is involved in the coordination of cell cycle cues with cytokinesis. Whether or not the exocyst tethering complex is also required in this context in plants remains to be determined.

Confocal and electron microscopy analyses verified the importance of the TRAPPII complex in cell plate biogenesis. Patchy or incomplete cell plates and cross walls were identified in meristematic root cells of TRAPPII mutants in *Arabidopsis thaliana*. Contrary to the cell plate localisation of the methyl-esterified pectin JIM7, in the wild type, no signal was detectable in *club-2/trs130-2* mutants. TRAPPII additionally localised to the rapid expanding parts of the cell plate. The TRAPPII signal first accumulates at the centre of the division plane, where the first membrane fusions take place. Subsequently, TRAPPII relocalises to the actively growing leading edges of the cell plate.

In addition to the possible involvement of the exocyst complex during cell plate initiation at the onset of cytokinesis, more solid evidence points to involvement of the exocyst in the maturation of the cell plate. The exocyst complex localises to the insertion sites and to already expanded parts of the cell plate. Additionally, KNOLLE gets prematurely removed from telophase plates in *exo84b-2* mutants compared to FM4-64 and TRS120-GFP, which behaved normally. The removal of KNOLLE can be seen as one of the first steps of maturation from a cell plate to a cross wall. Another line of evidence is the altered relative content of some polysaccharides, namely methyl-esterified pectins and AGP glycans, in the cell plates, cross walls and lateral walls in *exo84b-2* mutants.

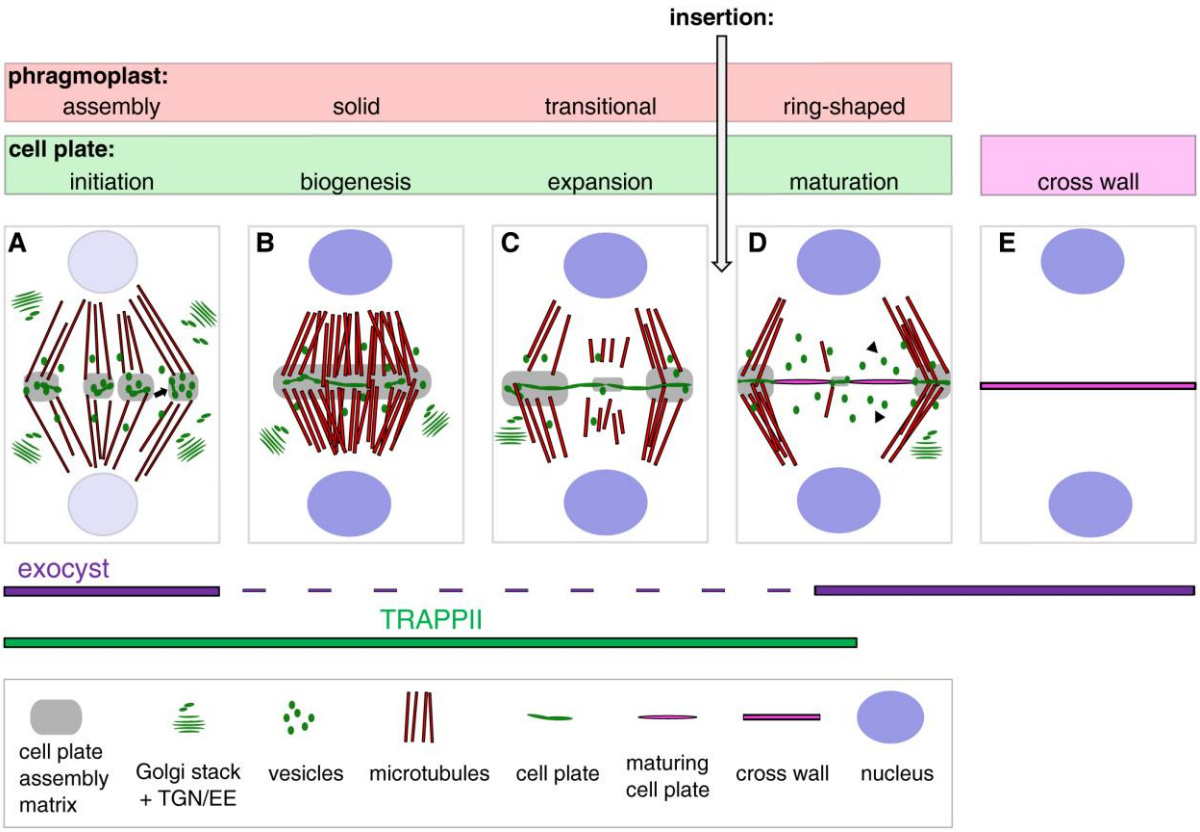

Figure 6 "Relay Race" model for the sequential but overlapping action of the TRAPPII and exocyst. Four stages of cytokinesis (A-D).
(A) Two opposite sets of phragmoplast microtubules arise from former spindle microtubules. A 'Golgi-belt', consisting of the Golgi apparatus and trans-Golgi network/early endosomes (TGN/EE) surrounds the division plane. Right after arrival, vesicles fuse to dumbbell-shaped cell plate initials (arrow).
(B) The microtubules arrange into a barrel-like structure at the solid phragmoplast stage and further fusion initiates cell plate biogenesis within a cell plate assembly matrix.
(C) The cell plate expands centrifugally towards the lateral cell walls. The phragmoplast microtubules reorganise into a ring-shaped pattern surrounding the expanding cell plate.
(D) Cell plate maturation occurs upon insertion into the parental cell walls. The cell plate loses its juvenile traits, including the removal of KNOLLE (arrowheads).
(E) The mature cell plate, namely the cross wall, divides the cell into two daughter cells, flanked on either side by plasma membranes.
In our "relay race" model, we assume that both tethering complexes, TRAPPII (green bar) and exocyst (purple bar), are required for the initiation of cytokinesis. Thereafter, cell plate biogenesis and expansion are driven by the TRAPPII complex, while the exocyst seems to be required towards the end of cytokinesis for the maturation of the cell plate. Adapted from (Seguí-Simarro et al., 2004) with permission from the American Society of Plant Biologists).

Relevance of the sequential function of tethering factors in other kingdoms

Although plant cytokinesis differs from cytokinesis in animals and fungi, we postulate that the TRAPPII and exocyst tethering complexes sequentially coordinate cytokinesis in other kingdoms. In *Drosophila*, for example, the two complexes are also required sequentially during cytokinesis. Cleavage furrow ingression is disturbed in a TRS120 ortholog, the *bru*

mutant (Robinett et al., 2009). Towards the end of cytokinesis, the exocyst is required for secretory vesicle-mediated abscission at the midbody (Gromley et al., 2005; Neto et al., 2013). Additionally, mutant analysis showed that exocyst is involved in cell separation during the final steps of cytokinesis rather than processes during early stages of cytokinesis in fission yeast (Wang et al., 2002). The exocyst traffics enzymes to the medial region, which digest the primary septum after the cell wall is completed and the cell membranes have closed (Martín-Cuadrado et al., 2005). A recent study in fission yeast showed that the TRAPPII complex tethers secretory vesicles at the cleavage furrow and the exocyst vesicles at the rim of the division plane. In the same study, both complexes also show overlapping localisation during ring maturation; however, the localisation of both complexes seems to be independent of each other (Wang et al., 2016). Based on localisation studies and mutant analysis, Wang et al. (2016) rule out physical interaction between both complexes in fission yeast. However, the interaction between both complexes might also be transient, similar to the mechanism in plants. Further interaction assays have to be conducted to verify or rule out the interaction between both complexes in fission yeast.

Taken all together, the cell plate is a distinct compartment that arises mainly from TGN/EE-derived vesicles and matures into a cross wall, flanked by plasma membranes on each side. The tethering complexes contribute to the specificity of vesicle trafficking throughout cytokinesis. Furthermore, the transitions through the different stages of cell plate development are coordinated by the sequential yet overlapping work of two tethering complexes. This sequential coordination seems not just to be true for plant cytokinesis, but also quite likely for cytokinesis in other kingdoms.

3.2. The TRAPPII tethering complex is required for sorting at the cell plate

Sorting at the cell plate

Proteins are sorted actively to, at and from the cell plate. In addition to its role during cell plate biogenesis, the TRAPPII complex is required for this differential sorting. Active sorting stands in contrast with the assumption that the cell plate acts as a sink for plasma membrane proteins. Müller et al. (2003) and Reichardt et al. (2007, 2011) documented that newly synthesised plasma membrane syntaxins, SYP121, SYP112 and SYP132, under the control of the cytokinesis-specific KNOLLE promoter, are directed to the cell plate. This favours the assumption that trafficking via the TGN/EE may be by default, polarised toward the division plane rather than the plasma membrane during cytokinesis (Touihri et al., 2011). However,

our analysis of the dynamics of several plasma membrane proteins and polysaccharides in *TRAPPII* mutants compared to the wild type contradicts this assumption of the cell plate as a sink. Plasma membrane proteins and polysaccharides are differentially localised to the cell plate, cross wall, plasma membrane or mature cell wall in the wild type. In *TRAPPII* mutants, the ability to differentially sort proteins appears to be lost. The plasma membrane proteins localise to the cell plate and other compartments with equal intensity in *club-2/trs130-2* mutants. For this analysis, cell plates were selected, which were normally assembled, so that mislocalisation due to cell plate defects could be excluded. Other cytokinesis-defective mutants did not show a comparable sorting problem. One explanation could be that proteins have to pass through the TGN/EE to reach the plasma membrane. If this passage is blocked, proteins simply accumulate in endomembrane compartments in the *TRAPPII* mutants. Consistently, Golgi transport to the cell wall has been shown to be impaired in TRAPPII mutants (Qi et al., 2011). However, proteins could still be transported to the plasma membrane via unconventional protein secretion. Proteins transported to the plasma membrane via unconventional secretion either lack a signal peptide or bypass the Golgi apparatus, despite their signal peptide. Unconventional protein secretion occurs mainly but not exclusively upon pathogen attack or under stress conditions (Ding et al., 2014). Even though we cannot exclude the explanation that most proteins have to pass through the TGN/EE, this cannot explain the highly differential sorting we observe. The specific appearance of the exocyst subunits as clouds around the cell plate, which is disrupted in *club-2/trs130* mutants, indicates a more direct influence of the TRAPPII complex on protein sorting. The cell plate appears as a transient compartment with a distinct identity to the nascent cross wall or mature plasma membrane.

Sorting of KEULE at the cell plate

The TRAPPII complex rather than the exocyst complex seems to be required for the sorting of the SM protein KEULE at the cell plate. Localisation at the cell plate of KEULE is perturbed in *trs120-4* mutants, but not in *exo84b-2* mutants. However, a possible regulation of KEULE through the exocyst cannot be totally excluded. Sec6, a subunit of exocyst, was shown to interact with KEULE (Wu et al., 2013). With respect to the cytokinesis-related defects of *exo84b-2* rather than the gametophytic lethal phenotype of *sec6* (Fendrych et al., 2010; Wu et al., 2013), our mutant analysis was carried out with *exo84b-2*. The *exo84b-2* single mutants show a strong seedling lethal phenotype, but rather weak cellular cytokinesis-specific defects. We detected no cell wall stubs or bloated cells in *Arabidopsis* root tips in

exo84b-2 single mutants. Additionally, just 2% of the leave cells of *exo84b-2* single mutants analysed by Fendrych et al. (2010) exhibited cell wall stubs. Maybe the *exo84b-2* single mutant is not enough to see an effect on the sorting behaviour. In light of the multiple paralogs of exocyst subunits in *Arabidopsis thaliana* (Table 3), a double or triple mutant analysis or experiments with mutants of other subunits of the exocyst complex might be required. Alternatively, both complexes could work again sequentially in sorting KEULE. The TRAPPII complex could solely be required for sorting at the cell plate. The transport of KEULE to the cell plate could be TRAPPII-independent, as KEULE does not localise to TGN/EE compartments. TRAPPII, on the other hand, mainly tethers TGN/EE vesicles. In addition, KEULE and TRAPPII predominantly colocalise on the cell plate throughout cytokinesis. The exocyst could be required for the recruitment of KEULE to the plasma membrane. Both the exocyst and KEULE are needed for polarised secretion in tip growth (Assaad et al., 2001; Hála et al., 2008).

Similarities of TRAPPII with other proteins required for sorting

TRAPPII and ECHIDNA, a protein required for sorting at the TGN/EE (Gendre et al., 2011), show similar sorting properties. The *Arabidopsis* ECHIDNA is thought to be involved in formation of secretory vesicles at the TGN/EE and secretion of polysaccharides and newly synthesised proteins to the plasma membrane (Boutté et al., 2013; McFarlane et al., 2013). ECHIDNA, like TRAPPII, differentially sorts proteins. ECHIDNA, for example, is required for trafficking of the auxin influx carrier AUX1, but not the auxin efflux carrier PIN3 (Boutté et al., 2013; McFarlane et al., 2013). Similarly, TRAPPII influences the localisation of AUX1 and PIN2, but not PIN1, in root tips (Qi and Zheng, 2011; Qi et al., 2011).

In conclusion, the cell plate is not a sink for plasma membrane proteins during cytokinesis, but rather a distinct compartment where active sorting occurs. The TRAPPII complex is required for differential sorting at the cell plate.

3.3. Re-evaluating the interaction between KEULE and KNOLLE

The interaction between the SM protein KEULE and the cytokinesis-specific syntaxin KNOLLE is crucial for vesicle fusion during cytokinesis. Aside from stabilizing the open form of KNOLLE (Park et al., 2012), it seems that KEULE might have some additional functions during cytokinesis and other cellular processes. This is reflected by the differential appearance and dynamics of KNOLLE and KEULE during cytokinesis. For example, KNOLLE appears in a punctate manner at the onset of cytokinesis, resembling the signal of

TGN/EE compartments (Chow et al., 2008). In contrast, KEULE expressed from its endogenous promoter is localised to the cytosol and does not colocalise with two TGN/EE markers. Our data are consistent with the observation that another TGN marker and P_{KNOLLE}::KEULE-HA do not colocalise (Park et al., 2012). Our observation concerning KEULE's cytosolic localisation differs from the exclusive cell plate localisation described by Wu et al. (2013), and from the punctate appearance described by Park et al. (2012). However, both laboratories did not use endogenously expressed KEULE, but fusion proteins expressed under the control of either the 35S promoter (Wu et al., 2013) or the KNOLLE promoter (Park et al., 2012). This could be the reason for the different localisation patterns. Furthermore, KEULE and KNOLLE differ in their response to BFA treatment. At the end of cytokinesis, KNOLLE accumulates in BFA compartments, while KEULE is insensitive to this traffic inhibiting drug (Reichardt et al., 2007; Park et al., 2012). Another difference between both proteins is the dependence of KEULE on TRAPPII for trafficking at the cell plate. KNOLLE seems to be TRAPPII-independent. Furthermore, the localisation dynamics at the cell plate differs between both proteins. Whereas KNOLLE is distributed evenly over the expanding cell plate, KEULE largely relocalises to the leading edges. Additionally, towards the end of cytokinesis KNOLLE is delivered to vacuoles and degraded (Reichardt et al., 2011), while KEULE seems to be degraded in a different way. In contrast to KNOLLE, KEULE appears also to be involved in other cellular processes, such as polarised secretion during tip growth. *keule* mutants show a defective root growth phenotype (Assaad et al., 2001; Söllner et al., 2002). Consistent with the fact that SNAREs can randomly bind other SNAREs *in vitro* (Yang et al., 1999), the SM protein KEULE is also able to bind other t-SNAREs such as the plasma membrane t-SNARE SYP121 (Karnik et al., 2015).

Taken together, KEULE seems to be involved in cellular processes other than facilitating the formation of a trans-SNARE complex by binding the cytokinesis-specific syntaxin KNOLLE.

3.4. Phenotypic analysis of cytokinesis-defective mutants

Cell plate formation and phragmoplast reorganisation in microtubule-related mutants

Cytokinesis-defective mutants are in general characterised by cell wall stubs, multinucleate cells, bloated cells and seedling lethality. The severe impairment in their morphogenesis and their pleiotropic phenotypes makes it difficult to assign a primary defect to a specific mutant. Our comparative and quantitative analysis concentrated on the formation of the cell plate and the organisation of the phragmoplast. Of four microtubule-related mutants, *hinkel*, *pleiade*,

clasp-1 and *mor1-1* (Table 1), *mor1-1* showed the greatest impairment in cell plate formation and phragmoplast organisation. Cell plate defects in *mor1-1* mutants have already been reported (Whittington et al., 2001; Eleftheriou et al., 2005; Kawamura et al., 2006), but no quantitative analysis and comparison to other microtubule-related mutants had been conducted. Interestingly, *clasp-1,* which is also impaired in preprophase band organisation (Ambrose et al., 2007), did not show comparable cell plate formation or orientation defects as *mor1-1*. The involvement of *hinkel* and *pleiade* in phragmoplast organisation and the similar canonical phenotype to the membrane-related *keule* led us to speculate that *hinkel* and *pleiade* might have a more pronounced cell plate defect. However, both did not show any defect in cell plate formation. Similar effects of microtubule-related mutants on cell plate formation have been reported for knock-outs or knock-downs of proteins involved in microtubule nucleation (Pastuglia et al., 2006; Zeng et al., 2009). Downregulation of three MAP65 genes also affected cell plate organisation in the moss *Physcomitrella* (Kosetsu et al., 2013). The redundancy of the MAP65 family at the cell plate in *Arabidopsis thaliana* (Sasabe et al., 2011a) could be a reason why single mutant analysis of *ple-4* (PLEIADE/AtMAP65-3) did not show a similar cell plate defect in our study.

Phragmoplast reorganisation from the solid to the ring-shaped phragmoplast stage (Figure 2C-D) was impaired in all microtubule-related mutants, except for *clasp-1*. *mor1-1* showed again more severe defects than the other mutants, although it was the only mutant used in this study that was not a null mutant and that did not show seedling-lethality. The temperature-sensitive allele *mor1-1* reveals a defect after two days at the restrictive temperature. We additionally used histological sections of embryos of some seedling lethal mutants, to obtain comparable amounts of cell divisions as in *mor1-1*. However, all experiments suggest that *mor1-1* is the most impaired of the microtubule–related mutants in cell plate formation and phragmoplast reorganisation.

Membrane-related keule mediates phragmoplast microtubule reorganisation

The membrane-related mutant *keule* was even more impaired in reorganising the phragmoplast microtubules than *mor1-1*. Some studies already pointed to additional microtubule defects in cells treated with membrane-related drugs (Samuels and Staehelin, 1996; Yasuhara and Shibaoka, 2000). The defect of *keule* mutants to reorganise the phragmoplast suggests a regulatory mechanism of the membranes on phragmoplast microtubules during cytokinesis. The cell plate assembly matrix has been postulated to act as a possible anchor for microtubule plus ends. A physical link between the cell plate and the

phragmoplast has been assumed, after fully intact phragmoplasts (cell plate with the two opposing sets of microtubules) have been isolated from synchronised, dividing BY-2 cells. Phragmoplasts can only resist these mechanical forces used to isolate them if they are connected to some sort of cell plate-associated structures (Kakimoto and Shibaoka, 1992; Seguí-Simarro et al., 2004). As an interactor of membrane proteins such as KNOLLE and SEC6, KEULE might act as the link between the membranes and the microtubules of the phragmoplast. However, our proteomic data contradicts this assumption. Neither MAPs nor tubulins have been identified as positive hits in KEULE immunoprecipitation experiments with mass spectrometry readout. How KEULE regulates phragmoplast reorganisation remains elusive and further research has to be conducted on this topic. One possible means of regulation could be via an interaction with the TRAPP II tethering complex, as KEULE was a reproducible hit in the CLUB-GFP immunoprecipitation.

In Conclusion, microtubules and membranes are highly coordinated throughout cytokinesis. Some microtubule-related proteins have an effect on cell plate assembly and vice versa membrane-related proteins such as KEULE seem to be required for phragmoplast reorganisation in a yet unknown fashion.

3.5. Interaction between microtubules and membranes

Microtubule addition at the phragmoplast exceeds simple treadmilling

The treadmilling model, where tubulin dimers are added at the dynamic plus end and depolymerised at the minus end, is challenged by findings of localisation patterns of plus end or minus end proteins. The plus-end tracking protein EB1 (Van Damme et al., 2004; Chan et al., 2005) and components of the γ-tubulin ring complex (Liu et al., 1994; Dryková et al., 2003; Kumagai et al., 2003; Zeng et al., 2009) are localised throughout the phragmoplast, not just at their specific ends. Furthermore, fluorescence recovery after photobleaching experiments in tobacco BY-2 cells and *in silico* point to a more complex process in phragmoplast nucleation and maintenance than simple treadmilling from one end to the other (Smertenko et al., 2011). These findings suggest a model whereby microtubules do not have a specific nucleation site but get nucleated along pre-existing microtubules, at the surface of the forming nuclei and by free γ-tubulin ring complexes. The polarity is determined at the onset of phragmoplast assembly and the newly made microtubules adopt the polarity of the pre-existing microtubules and thus maintain the asymmetry of the array (Smertenko et al., 2011).

Interdigitation of phragmoplast microtubules

In *Haemanthus katherinae* endosperm cells it was shown that the phragmoplast consists of two anti-parallel, polar sets of microtubules overlapping in the midzone (Hepler and Jackson, 1968; Euteneuer and McIntosh, 1980). A similar interdigitation was observed in chemically fixed caulonemal cells of the moss *Physcomitrella patens* (Hiwatashi et al., 2008) and in a subset of microtubules of cryofixed/freeze substituted cells of *Arabidopsis thaliana* (Ho et al., 2011). The microtubule-associated protein, PLEIADE/AtMAP65-3, is able to cross-link anti-parallel microtubules *in vitro* with its distinct C-terminal microtubule binding site (Ho et al., 2011, 2012). In addition, it is localised in a narrow fashion to the phragmoplast midzone (Müller et al., 2004; Van Damme et al., 2004). This suggests that PLEIADE/AtMAP65-3 is required for crosslinking anti-parallel microtubules at the phragmoplast midzone. However, no overlap of anti-parallel microtubules was seen for the majority of the microtubules in cryofixed/freeze substituted somatic *Arabidopsis thaliana* cells. This was strengthened by the numerous occurrence of microtubules ending in this zone (Samuels et al., 1995; Otegui and Staehelin, 2000). The organisation of the phragmoplast microtubules might function in the same fashion as the organisation of the spindle microtubules. Some spindle microtubules are attached to the kinetochore of the chromatids, while others are crosslinked via motor proteins or MAPs with opposite spindle microtubules. This ensures that the opposite spindle halves stay attached, while the chromatids are separated (Bannigan et al., 2008; Zhang and Dawe, 2011). The kinetochore could also be part of a stabilising mechanism for the spindle, as centrosomes are missing in plants (Bannigan et al., 2008). Similarly, different types of phragmoplast microtubules could organise the transitions during cytokinesis. Some microtubules might bundle with anti-parallel microtubules of the opposite phragmoplast half. PLEIADE/AtMAP65-3 could be responsible for crosslinking anti-parallel microtubules at the midzone while other microtubules deliver material and vesicles to the division plane. This could explain the interdigitation of some, but not all, microtubules at the phragmoplast midzone.

TRAPPII and MAP65 family interaction

Microtubule plus ends have been shown to be captured at a distance of less than 50 nm from the plasma membrane (Small and Kaverina, 2003). In the cell plate assembly matrix, non-overlapping microtubule plus ends terminate approximately 30 nm from the cell plate (Austin et al., 2005). This suggests a mechanism in the cell plate or cell plate assembly matrix that links the phragmoplast microtubules to the cell plate membranes. KEULE seems to be

required in another way for phragmoplast reorganisation than as a physical link between microtubules and membranes. However, the interaction between the tethering complex TRAPPII and the microtubule-associated protein 65 (MAP65) family seems more likely to be the missing link between membranes and microtubules. The microtubule-associated protein, PLEIADE/AtMAP65-3, seems to be required for crosslinking anti-parallel microtubules at the phragmoplast midzone. Additionally, PLEIADE/AtMAP65-3 may also be needed for stabilising the phragmoplast and organising the transitions between the microtubule arrays. The transition between the arrays has to be coordinated with the cell plate. The TRAPPII tethering complex is required for biogenesis of the cell plate and sorting at the cell plate. Furthermore, TRAPPII relocalises to the expanding part of the cell in the same manner as phragmoplast microtubules. Multisubunit tethering complexes, such as TRAPPII, are able to tether vesicles in a range of 30 nm (Chia and Gleeson, 2014). This distance would be enough to interact with microtubules or MAPs in the cell plate assembly matrix. Co-immunoprecipitation, binary interaction assays, synergistic genetic interaction, co-expression and colocalisation indicate a strong interaction between TRAPPII and the MAP65 family. However, localisation studies did not reveal TRAPPII as an anchor for PLEIADE/AtMAP65-3 at the cell plate. Conversely, PLEIADE/AtMAP65-3 is also not required for the recruiting of TRAPPII to the cell plate. It seems that the interaction between TRAPPII and PLEIADE/AtMAP65-3 has a different purpose than to mediate the localisation of either protein or complex.

3.6. Cell cycle-dependent regulation of microtubule array transitions

The twenty-fold enhancement of clumped nuclei in p*le-2 trs120-4* double mutants compared to *ple-2* single mutants prompted us to look for a connection to the cell-cycle.

Already during preprophase, microtubule-related proteins are regulated via cell cycle-specific kinases. In late prophase, cyclin-dependent kinase A (CDKA) is activated by cyclin B and thereafter localises to and promotes disassembly of the preprophase band (Figure 7A; Imajuku et al., 2001; Weingartner et al., 2001). Phosphorylation of microtubule-associated proteins (MAPs) by the CDKA kinase may have an inhibitory effect on their functions at the preprophase band. Also, preprophase band-associated motor proteins seem to be negatively cell cycle-dependent regulated through CDKA phosphorylation (Imajuku et al., 2001; Vanstraelen et al., 2006; Malcos and Cyr, 2011).

The spindle assembly checkpoint (SAC) assures that all chromosomes are correctly oriented and attached to the spindle microtubules before the cell advances from metaphase to

anaphase. The localisation of PLEIADE/AtMAP65-3 at the anaphase spindle, the coregulated expression with spindle-assembly checkpoint genes (Menges et al., 2005) and the recent report of an interaction of PLEIADE/AtMAP65-3 with SAC proteins in *Arabidopsis thaliana* (Figure 7B; Paganelli et al., 2015), indicates the involvement of PLEIADE/AtMAP65-3 with the spindle-assembly checkpoint complex.

The mitogen-activated protein (MAP) kinase cascade is regulated in a cell cycle-dependent manner and, in turn, targets MAP65 proteins during phragmoplast reorganisation (Figure 7C; Sasabe et al., 2006, 2011a, 2011b; Kosetsu et al., 2013). The interaction of the plant-specific moiety of CLUB/AtTRS130 with PLEIADE/AtMAP65-3 highlights the unique features of plant cytokinesis. This includes the phragmoplast microtubule array and its plant-specific cell cycle regulation by the MAP kinase cascade.

TRAPPII is required for biogenesis of the cell plate throughout cytokinesis (Figure 6), which delineates an effective margin for cell cycle regulation. The involvement of PLEIADE/AtMAP65-3 with the SAC checkpoint complex indicates that besides the transmission of cell cycle progression cues, PLEIADE/AtMAP65-3 might also transmit chromosome attachment cues to spindle microtubules. The TRAPPII-MAP65 interaction could enable the coordination of these cues with membrane dynamics during cytokinesis. Our findings provide a conceptual framework for the integration of cell cycle cues with microtubule and membrane dynamics during cytokinesis. So far, not much is known about cell cycle checkpoints after the SAC (Musacchio, 2015). The TRAPPII-MAP65 interaction could be a safeguard mechanism that coordinates the cell cycle progression with the completion of cell plate formation during cytokinesis.

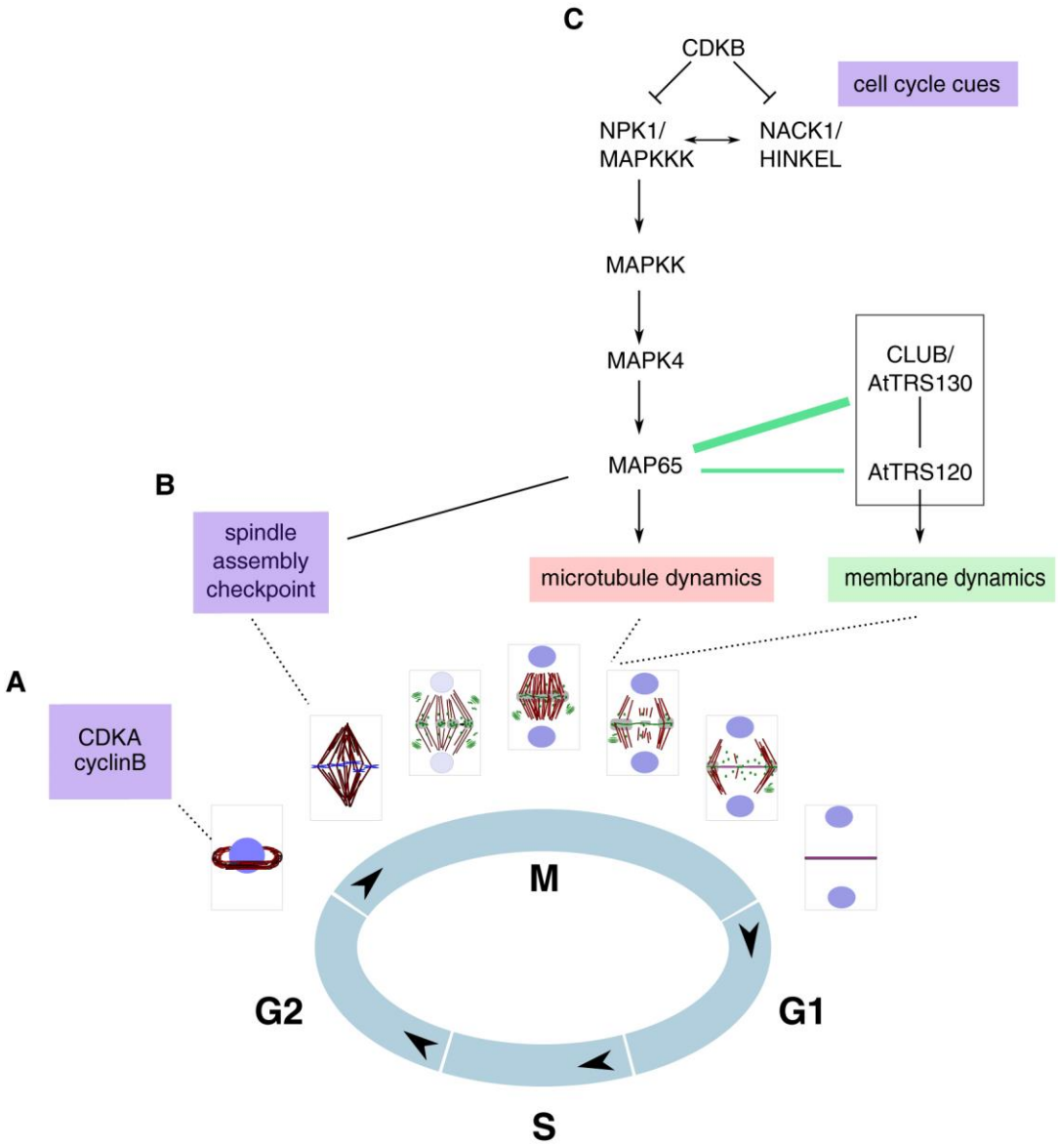

Figure 7. Cell cycle regulation and checkpoints during M-phase (mitosis/cytokinesis).
(A) The preprophase band and microtubule-associated proteins (MAPs) at the preprophase band get regulated via CDKA and cyclin B.
(B) The spindle assembly checkpoint (SAC) controls the transition from metaphase to anaphase. The correct orientation and attachment of the chromatids to the microtubules is checked via the SAC. PLEIADE/AtMAP65-3 interacts with SAC proteins.
(C) The MAP kinase cascade is regulated via CDKs and may be a possible link between the progression of cytokinesis and the cell cycle. The TRAPPII-MAP65 interaction might be a safeguard mechanism that coordinates cell cycle cues with microtubule and membrane dynamics during cytokinesis.

4. Concluding remarks and perspectives

In summary, this thesis helps to further understand the processes underlying plant cytokinesis. The cell plate is a distinct compartment and not simply a sink for plasma membrane proteins or cell wall polysaccharides during cytokinesis. Proteins and polysaccharides are actively sorted to, at and from the cell plate. This active sorting at the cell plate is most likely mediated by the TRAPPII tethering complex. Cell plate development can be broken down into for stages: initiation, biogenesis, expansion and maturation (Figure 6). The TRAPPII and the exocyst tethering complexes sequentially mediate the transitions between these stages. The TRAPPII complex gives the cell plate a TGN/EE identity and drives cell plate formation throughout cytokinesis. The maturation of the juvenile cell plate to a mature cross wall is mainly mediated by the exocyst complex.

Plant cytokinesis is distinct from cytokinesis in other kingdoms. There are many things unique in plant cytokinesis such as the phragmoplast, CDKB or the regulation of the phragmoplast via a MAP kinase cascade. Despite these differences, the sequential coordinated work of the two tethering complexes during cytokinesis seem universally conserved (Neto et al., 2013; Wang et al., 2016). It will be interesting to see, whether this sequential and coordinated action of two distinct complexes can also be applied to other processes in plants or other kingdoms. So far, sequential action is known for complexes that share core subunits but differ in a few subunits. For example, the ubiquitination of cyclin E depends on the sequential function of SCF complexes containing one variable subunit in mammals (van Drogen et al., 2006).

The cell plate and the phragmoplast strongly depend on each other throughout cytokinesis. However, the mechanism that anchors the phragmoplast microtubules to the cell plate membranes is still missing. The SM-protein KEULE seems to be required for phragmoplast reorganisation, in addition to its role in facilitating the formation of a trans-SNARE complex by binding the cytokinesis-specific syntaxin KNOLLE. How exactly KEULE is involved in the reorganisation of phragmoplast microtubules remains elusive. The TRAPPII-MAP65 interaction does also not anchor microtubules at the cell plate. Maybe other proteins such as motor proteins are the missing link. Motor proteins could connect the cell plate to phragmoplast microtubules in a similar manner as they connect other organelles to microtubules (Knoblach and Rachubinski, 2015). Many plus end directed kinesins are known to be required for maintaining the structure, the reorganisation and stability of the phragmoplast (Lee and Liu, 2000; Strompen et al., 2002; Tanaka et al., 2004).

The TRAPPII-MAP65 interaction appears to be required for the transmission of cell cycle cues to the cell plate. This might comprise a safeguard mechanism that coordinates the completion of cytokinesis with the cell cycle progression. Further molecular experiments have to be carried out to fully understand this interaction and its meaning in plant cytokinesis. It will be interesting to see whether TRAPPII is also a direct substrate of the MAP kinase cascade (Figure 7C). This would strengthen the hypothesis that this interaction comprises a safeguard mechanism for cytokinesis. TRAPPII and MAP65-3 would be directly regulated by the kinase cascade and coordinate the information via their interaction with each other.

5. References

Ambrose, J.C., Shoji, T., Kotzer, A.M., Pighin, J.A., and Wasteneys, G.O. (2007). The Arabidopsis CLASP gene encodes a microtubule-associated protein involved in cell expansion and division. Plant Cell *19*, 2763–2775.

Assaad, F.F., Huet, Y., Mayer, U., and Jürgens, G. (2001). The cytokinesis gene KEULE encodes a Sec1 protein that binds the syntaxin KNOLLE. J. Cell Biol. *152*, 531–543.

Austin, J.R., Seguí-Simarro, J.M., and Staehelin, L.A. (2005). Quantitative analysis of changes in spatial distribution and plus-end geometry of microtubules involved in plant-cell cytokinesis. J. Cell Sci. *118*, 3895–3903.

Baluska, F., Liners, F., Hlavacka, A., Schlicht, M., Van Cutsem, P., McCurdy, D.W., and Menzel, D. (2005). Cell wall pectins and xyloglucans are internalized into dividing root cells and accumulate within cell plates during cytokinesis. Protoplasma *225*, 141–155.

Bannigan, A., Lizotte-Waniewski, M., Riley, M., and Baskin, T.I. (2008). Emerging molecular mechanisms that power and regulate the anastral mitotic spindle of flowering plants. Cell Motil. Cytoskeleton *65*, 1–11.

Bolte, S., Talbot, C., Boutte, Y., Catrice, O., Read, N.D., and Satiat-Jeunemaitre, B. (2004). FM-dyes as experimental probes for dissecting vesicle trafficking in living plant cells. J. Microsc. *214*, 159–173.

Boutté, Y., Frescatada-Rosa, M., Men, S., Chow, C.-M., Ebine, K., Gustavsson, A., Johansson, L., Ueda, T., Moore, I., Jürgens, G., et al. (2010). Endocytosis restricts Arabidopsis KNOLLE syntaxin to the cell division plane during late cytokinesis. EMBO J. *29*, 546–558.

Boutté, Y., Jonsson, K., McFarlane, H.E., Johnson, E., Gendre, D., Swarup, R., Friml, J., Samuels, L., Robert, S., and Bhalerao, R.P. (2013). ECHIDNA-mediated post-Golgi trafficking of auxin carriers for differential cell elongation. Proc. Natl. Acad. Sci. U. S. A. *110*, 16259–16264.

Brennwald, P., Kearns, B., Champion, K., Keränen, S., Bankaitis, V., and Novick, P. (1994). Sec9 is a SNAP-25-like component of a yeast SNARE complex that may be the effector of Sec4 function in exocytosis. Cell *79*, 245–258.

Bruaene, N.V., Joss, G., and Oostveldt, P.V. (2004). Reorganization and in Vivo Dynamics of Microtubules during Arabidopsis Root Hair Development. Plant Physiol. *136*, 3905–3919.

Burgoyne, R.D., and Morgan, A. (2007). Membrane Trafficking: Three Steps to Fusion. Curr. Biol. *17*, R255–R258.

Caillaud, M.-C., Lecomte, P., Jammes, F., Quentin, M., Pagnotta, S., Andrio, E., de Almeida Engler, J., Marfaing, N., Gounon, P., Abad, P., et al. (2008). MAP65-3 microtubule-associated protein is essential for nematode-induced giant cell ontogenesis in Arabidopsis. Plant Cell *20*, 423–437.

Cao, X., Ballew, N., and Barlowe, C. (1998). Initial docking of ER-derived vesicles requires Uso1p and Ypt1p but is independent of SNARE proteins. EMBO J. *17*, 2156–2165.

Chan, J., Calder, G.M., Doonan, J.H., and Lloyd, C.W. (2003). EB1 reveals mobile microtubule nucleation sites in Arabidopsis. Nat. Cell Biol. *5*, 967–971.

Chan, J., Calder, G., Fox, S., and Lloyd, C. (2005). Localization of the microtubule end binding protein EB1 reveals alternative pathways of spindle development in Arabidopsis suspension cells. Plant Cell *17*, 1737–1748.

Chen, Y.A., and Scheller, R.H. (2001). SNARE-mediated membrane fusion. Nat. Rev. Mol. Cell Biol. *2*, 98–106.

Chia, P.Z.C., and Gleeson, P.A. (2014). Membrane tethering. F1000Prime Rep. *6*.

Chow, C.-M., Neto, H., Foucart, C., and Moore, I. (2008). Rab-A2 and Rab-A3 GTPases define a trans-golgi endosomal membrane domain in Arabidopsis that contributes substantially to the cell plate. Plant Cell *20*, 101–123.

Clausen, M.H., Willats, W.G.T., and Knox, J.P. (2003). Synthetic methyl hexagalacturonate hapten inhibitors of anti-homogalacturonan monoclonal antibodies LM7, JIM5 and JIM7. Carbohydr. Res. *338*, 1797–1800.

Collins, N.C., Thordal-Christensen, H., Lipka, V., Bau, S., Kombrink, E., Qiu, J.-L., Hückelhoven, R., Stein, M., Freialdenhoven, A., Somerville, S.C., et al. (2003). SNARE-protein-mediated disease resistance at the plant cell wall. Nature *425*, 973–977.

Conibear, E., and Stevens, T.H. (2000). Vps52p, Vps53p, and Vps54p Form a Novel Multisubunit Complex Required for Protein Sorting at the Yeast Late Golgi. Mol. Biol. Cell *11*, 305–323.

Cutler, S.R., and Ehrhardt, D.W. (2002). Polarized cytokinesis in vacuolate cells of Arabidopsis. Proc. Natl. Acad. Sci. U. S. A. *99*, 2812–2817.

Davis, D.J., McDowell, S.C., Park, E., Hicks, G., Wilkop, T.E., and Drakakaki, G. (2015). The RAB GTPase RABA1e localizes to the cell plate and shows distinct subcellular behavior from RABA2a under Endosidin 7 treatment. Plant Signal. Behav. *10*, e984520.

De Storme, N., and Geelen, D. (2013). Cytokinesis in plant male meiosis. Plant Signal. Behav. *8*.

Dettmer, J., Hong-Hermesdorf, A., Stierhof, Y.-D., and Schumacher, K. (2006). Vacuolar H+-ATPase activity is required for endocytic and secretory trafficking in Arabidopsis. Plant Cell *18*, 715–730.

Dhonukshe, P., and Gadella, T.W.J. (2003). Alteration of microtubule dynamic instability during preprophase band formation revealed by yellow fluorescent protein-CLIP170 microtubule plus-end labeling. Plant Cell *15*, 597–611.

Dhonukshe, P., Baluska, F., Schlicht, M., Hlavacka, A., Samaj, J., Friml, J., and Gadella, T.W.J. (2006). Endocytosis of cell surface material mediates cell plate formation during plant cytokinesis. Dev. Cell *10*, 137–150.

Ding, Y., Robinson, D.G., and Jiang, L. (2014). Unconventional protein secretion (UPS) pathways in plants. Curr. Opin. Cell Biol. *29*, 107–115.

Drakakaki, G., van de Ven, W., Pan, S., Miao, Y., Wang, J., Keinath, N.F., Weatherly, B., Jiang, L., Schumacher, K., Hicks, G., et al. (2012). Isolation and proteomic analysis of the SYP61 compartment reveal its role in exocytic trafficking in Arabidopsis. Cell Res. *22*, 413–424.

van Drogen, F., Sangfelt, O., Malyukova, A., Matskova, L., Yeh, E., Means, A.R., and Reed, S.I. (2006). Ubiquitylation of cyclin E requires the sequential function of SCF complexes containing distinct hCdc4 isoforms. Mol. Cell *23*, 37–48.

Dryková, D., Cenklová, V., Sulimenko, V., Volc, J., Dráber, P., and Binarová, P. (2003). Plant gamma-tubulin interacts with alphabeta-tubulin dimers and forms membrane-associated complexes. Plant Cell *15*, 465–480.

Dulubova, I., Yamaguchi, T., Arac, D., Li, H., Huryeva, I., Min, S.-W., Rizo, J., and Sudhof, T.C. (2003). Convergence and divergence in the mechanism of SNARE binding by Sec1/Munc18-like proteins. Proc. Natl. Acad. Sci. U. S. A. *100*, 32–37.

Eleftheriou, E.P., Baskin, T.I., and Hepler, P.K. (2005). Aberrant cell plate formation in the Arabidopsis thaliana microtubule organization 1 mutant. Plant Cell Physiol. *46*, 671–675.

Elias, M., Drdova, E., Ziak, D., Bavlnka, B., Hala, M., Cvrckova, F., Soukupova, H., and Zarsky, V. (2003). The exocyst complex in plants. Cell Biol. Int. *27*, 199–201.

Euteneuer, U., and McIntosh, J.R. (1980). Polarity of midbody and phragmoplast microtubules. J. Cell Biol. *87*, 509–515.

Fendrych, M., Synek, L., Pečenková, T., Toupalová, H., Cole, R., Drdová, E., Nebesářová, J., Šedinová, M., Hála, M., Fowler, J.E., et al. (2010). The Arabidopsis Exocyst Complex Is Involved in Cytokinesis and Cell Plate Maturation. Plant Cell *22*, 3053–3065.

Feraru, E., Feraru, M.I., Asaoka, R., Paciorek, T., De Rycke, R., Tanaka, H., Nakano, A., and Friml, J. (2012). BEX5/RabA1b regulates trans-Golgi network-to-plasma membrane protein trafficking in Arabidopsis. Plant Cell *24*, 3074–3086.

Fielding, A.B., Schonteich, E., Matheson, J., Wilson, G., Yu, X., Hickson, G.R.X., Srivastava, S., Baldwin, S.A., Prekeris, R., and Gould, G.W. (2005). Rab11-FIP3 and FIP4 interact with Arf6 and the exocyst to control membrane traffic in cytokinesis. EMBO J. *24*, 3389–3399.

Gaillard, J., Neumann, E., Van Damme, D., Stoppin-Mellet, V., Ebel, C., Barbier, E., Geelen, D., and Vantard, M. (2008). Two Microtubule-associated Proteins of Arabidopsis MAP65s Promote Antiparallel Microtubule Bundling. Mol. Biol. Cell *19*, 4534–4544.

Geldner, N., Anders, N., Wolters, H., Keicher, J., Kornberger, W., Muller, P., Delbarre, A., Ueda, T., Nakano, A., and Jürgens, G. (2003). The Arabidopsis GNOM ARF-GEF mediates endosomal recycling, auxin transport, and auxin-dependent plant growth. Cell *112*, 219–230.

Gendre, D., Oh, J., Boutté, Y., Best, J.G., Samuels, L., Nilsson, R., Uemura, T., Marchant, A., Bennett, M.J., Grebe, M., et al. (2011). Conserved Arabidopsis ECHIDNA protein mediates trans-Golgi-network trafficking and cell elongation. Proc. Natl. Acad. Sci. U. S. A. *108*, 8048–8053.

Gillmor, C.S., Roeder, A.H.K., Sieber, P., Somerville, C., and Lukowitz, W. (2016). A Genetic Screen for Mutations Affecting Cell Division in the Arabidopsis thaliana Embryo Identifies Seven Loci Required for Cytokinesis. PLOS ONE *11*, e0146492.

Graham, L.E., Cook, M.E., and Busse, J.S. (2000). The origin of plants: body plan changes contributing to a major evolutionary radiation. Proc. Natl. Acad. Sci. U. S. A. *97*, 4535–4540.

Griffiths, G., and Simons, K. (1986). The trans Golgi network: sorting at the exit site of the Golgi complex. Science *234*, 438–443.

Gromley, A., Yeaman, C., Rosa, J., Redick, S., Chen, C.-T., Mirabelle, S., Guha, M., Sillibourne, J., and Doxsey, S.J. (2005). Centriolin Anchoring of Exocyst and SNARE Complexes at the Midbody Is Required for Secretory-Vesicle-Mediated Abscission. Cell *123*, 75–87.

Gunning, B.E.S. (1982) The cytokinetic apparatus: its development and spatial regulation. In The Cytoskeleton in Plant Growth and Development. Edited by Lloyd, C.W. pp. 229-292. Academic Press, London.

Guo, W., Grant, A., and Novick, P. (1999). Exo84p is an exocyst protein essential for secretion. J. Biol. Chem. *274*, 23558–23564.

Gutierrez, C. (2009). The Arabidopsis Cell Division Cycle. Arab. Book e0120.

Hála, M., Cole, R., Synek, L., Drdová, E., Pečenková, T., Nordheim, A., Lamkemeyer, T., Madlung, J., Hochholdinger, F., Fowler, J.E., et al. (2008). An Exocyst Complex Functions in Plant Cell Growth in Arabidopsis and Tobacco. Plant Cell *20*, 1330–1345.

Hazuka, C.D., Foletti, D.L., Hsu, S.C., Kee, Y., Hopf, F.W., and Scheller, R.H. (1999). The sec6/8 complex is located at neurite outgrowth and axonal synapse-assembly domains. J. Neurosci. Off. J. Soc. Neurosci. *19*, 1324–1334.

He, B., and Guo, W. (2009). The Exocyst Complex in Polarized Exocytosis. Curr. Opin. Cell Biol. *21*, 537–542.

Heese, M., Gansel, X., Sticher, L., Wick, P., Grebe, M., Granier, F., and Jurgens, G. (2001). Functional characterization of the KNOLLE-interacting t-SNARE AtSNAP33 and its role in plant cytokinesis. J. Cell Biol. *155*, 239–249.

Heider, M.R., and Munson, M. (2012). Exorcising the exocyst complex. Traffic Cph. Den. *13*, 898–907.

Hepler, P.K., and Jackson, W.T. (1968). Microtubules and early stages of cell-plate formation in the endosperm of Haemanthus katherinae Baker. J. Cell Biol. *38*, 437–446.

Heyman, J., and Veylder, L.D. (2012). The Anaphase-Promoting Complex/Cyclosome in Control of Plant Development. Mol. Plant *5*, 1182–1194.

Hiwatashi, Y., Obara, M., Sato, Y., Fujita, T., Murata, T., and Hasebe, M. (2008). Kinesins Are Indispensable for Interdigitation of Phragmoplast Microtubules in the Moss Physcomitrella patens. Plant Cell *20*, 3094–3106.

Ho, C.-M.K., Hotta, T., Guo, F., Roberson, R.W., Lee, Y.-R.J., and Liu, B. (2011). Interaction of Antiparallel Microtubules in the Phragmoplast Is Mediated by the Microtubule-Associated Protein MAP65-3 in Arabidopsis. Plant Cell *23*, 2909–2923.

Ho, C.-M.K., Lee, Y.-R.J., Kiyama, L.D., Dinesh-Kumar, S.P., and Liu, B. (2012). Arabidopsis Microtubule-Associated Protein MAP65-3 Cross-Links Antiparallel Microtubules toward Their Plus Ends in the Phragmoplast via Its Distinct C-Terminal Microtubule Binding Domain[W]. Plant Cell *24*, 2071–2085.

Hofmeister W. (1863). Zusätze und Berichtigungen zu den 1851 veröffentlichten Untersuchungen der Entwicklung höherer Krytogamen. Jahrb. Wiss. Bot. 3, 259–293

Hoshino, H., Yoneda, A., Kumagai, F., and Hasezawa, S. (2003). Roles of actin-depleted zone and preprophase band in determining the division site of higher-plant cells, a tobacco BY-2 cell line expressing GFP-tubulin. Protoplasma *222*, 157–165.

Hush, J.M., Wadsworth, P., Callaham, D.A., and Hepler, P.K. (1994). Quantification of microtubule dynamics in living plant cells using fluorescence redistribution after photobleaching. J. Cell Sci. *107 (Pt 4)*, 775–784.

Hussey, P.J., Hawkins, T.J., Igarashi, H., Kaloriti, D., and Smertenko, A. (2002). The plant cytoskeleton: recent advances in the study of the plant microtubule-associated proteins MAP-65, MAP-190 and the Xenopus MAP215-like protein, MOR1. Plant Mol. Biol. *50*, 915–924.

Imajuku, Y., Ohashi, Y., Aoyama, T., Goto, K., and Oka, A. (2001). An upstream region of the Arabidopsis thaliana CDKA;1 (CDC2aAt) gene directs transcription during trichome development. Plant Mol. Biol. *46*, 205–213.

Jaber, E., Thiele, K., Kindzierski, V., Loderer, C., Rybak, K., Jürgens, G., Mayer, U., Söllner, R., Wanner, G., and Assaad, F.F. (2010). A putative TRAPPII tethering factor is required for cell plate assembly during cytokinesis in Arabidopsis. New Phytol. *187*, 751–763.

Janski, N., Masoud, K., Batzenschlager, M., Herzog, E., Evrard, J.-L., Houlné, G., Bourge, M., Chabouté, M.-E., and Schmit, A.-C. (2012). The GCP3-Interacting Proteins GIP1 and GIP2 Are Required for γ-Tubulin Complex Protein Localization, Spindle Integrity, and Chromosomal Stability. Plant Cell *24*, 1171–1187.

Jones, S., Newman, C., Liu, F., and Segev, N. (2000). The TRAPP complex is a nucleotide exchanger for Ypt1 and Ypt31/32. Mol. Biol. Cell *11*, 4403–4411.

Jürgens, G. (2005). Cytokinesis in higher plants. Annu. Rev. Plant Biol. *56*, 281–299.

Kakimoto, T., and Shibaoka, H. (1992). Synthesis of Polysaccharides in Phragmoplasts Isolated from Tobacco BY-2 Cells. Plant Cell Physiol. *33*, 353–361.

Karnik, R., Zhang, B., Waghmare, S., Aderhold, C., Grefen, C., and Blatt, M.R. (2015). Binding of SEC11 indicates its role in SNARE recycling after vesicle fusion and identifies two pathways for vesicular traffic to the plasma membrane. Plant Cell *27*, 675–694.

Kawamura, E., Himmelspach, R., Rashbrooke, M.C., Whittington, A.T., Gale, K.R., Collings, D.A., and Wasteneys, G.O. (2006). MICROTUBULE ORGANIZATION 1 Regulates Structure and Function of Microtubule Arrays during Mitosis and Cytokinesis in the Arabidopsis Root. Plant Physiol. *140*, 102–114.

Kim, S.-J., and Bassham, D.C. (2011). TNO1 Is Involved in Salt Tolerance and Vacuolar Trafficking in Arabidopsis. Plant Physiol. *156*, 514–526.

Kim, J.J., Lipatova, Z., and Segev, N. (2016). TRAPP Complexes in Secretion and Autophagy. Front. Cell Dev. Biol. *4*.

Knoblach, B., and Rachubinski, R.A. (2015). Motors, Anchors, and Connectors: Orchestrators of Organelle Inheritance. Annu. Rev. Cell Dev. Biol. *31*, 55–81.

Kollman, J.M., Merdes, A., Mourey, L., and Agard, D.A. (2011). Microtubule nucleation by γ-tubulin complexes. Nat. Rev. Mol. Cell Biol. *12*, 709–721.

Kopczak, S.D., Haas, N.A., Hussey, P.J., Silflow, C.D., and Snustad, D.P. (1992). The small genome of Arabidopsis contains at least six expressed alpha-tubulin genes. Plant Cell *4*, 539–547.

Kosetsu, K., Keijzer, J. de, Janson, M.E., and Goshima, G. (2013). MICROTUBULE-ASSOCIATED PROTEIN65 Is Essential for Maintenance of Phragmoplast Bipolarity and Formation of the Cell Plate in Physcomitrella patens. Plant Cell *25*, 4479–4492.

Kumagai, F., Nagata, T., Yahara, N., Moriyama, Y., Horio, T., Naoi, K., Hashimoto, T., Murata, T., and Hasezawa, S. (2003). Gamma-tubulin distribution during cortical microtubule reorganization at the M/G1 interface in tobacco BY-2 cells. Eur. J. Cell Biol. *82*, 43–51.

L A Staehelin, and Moore, and I. (1995). The Plant Golgi Apparatus: Structure, Functional Organization and Trafficking Mechanisms. Annu. Rev. Plant Physiol. Plant Mol. Biol. *46*, 261–288.

Lam, S.K., Siu, C.L., Hillmer, S., Jang, S., An, G., Robinson, D.G., and Jiang, L. (2007). Rice SCAMP1 defines clathrin-coated, trans-golgi-located tubular-vesicular structures as an early endosome in tobacco BY-2 cells. Plant Cell *19*, 296–319.

Lauber, M.H., Waizenegger, I., Steinmann, T., Schwarz, H., Mayer, U., Hwang, I., Lukowitz, W., and Jürgens, G. (1997). The Arabidopsis KNOLLE protein is a cytokinesis-specific syntaxin. J. Cell Biol. *139*, 1485–1493.

Ledbetter, M.C., and Porter, K.R. (1963). A “Microtubule” in Plant Cell Fine Structure. J. Cell Biol. *19*, 239–250.

Lee, Y.R., and Liu, B. (2000). Identification of a phragmoplast-associated kinesin-related protein in higher plants. Curr. Biol. CB *10*, 797–800.

Lee, Y.-R.J., and Liu, B. (2013). The rise and fall of the phragmoplast microtubule array. Curr. Opin. Plant Biol. *16*, 757–763.

Liang, Y., Morozova, N., Tokarev, A.A., Mulholland, J.W., and Segev, N. (2007). The role of Trs65 in the Ypt/Rab guanine nucleotide exchange factor function of the TRAPP II complex. Mol. Biol. Cell *18*, 2533–2541.

Lipka, E., Herrmann, A., and Mueller, S. (2015). Mechanisms of plant cell division. Wiley Interdiscip. Rev. Dev. Biol. *4*, 391–405.

Lipka, V., Kwon, C., and Panstruga, R. (2007). SNARE-ware: the role of SNARE-domain proteins in plant biology. Annu. Rev. Cell Dev. Biol. *23*, 147–174.

Liu, B., Joshi, H.C., Wilson, T.J., Silflow, C.D., Palevitz, B.A., and Snustad, D.P. (1994). gamma-Tubulin in Arabidopsis: gene sequence, immunoblot, and immunofluorescence studies. Plant Cell *6*, 303–314.

Liu, B., Hotta, T., Ho, C.-M.K., and Lee, Y.-R.J. (2011a). Microtubule Organization in the Phragmoplast. In The Plant Cytoskeleton, B. Liu, ed. (Springer New York), pp. 207–225.

Liu, P., Qi, M., Xue, X., and Ren, H. (2011b). Dynamics and functions of the actin cytoskeleton during the plant cell cycle. Chin. Sci. Bull. *56*, 3504–3510.

Lodish, H., Berk, A., Zipursky, S.L., Matsudaira, P., Baltimore, D., and Darnell, J. (2000). Microtubule Dynamics and Associated Proteins.

Lukowitz, W., Mayer, U., and Jürgens, G. (1996). Cytokinesis in the Arabidopsis embryo involves the syntaxin-related KNOLLE gene product. Cell *84*, 61–71.

Luo, G., Zhang, J., Luca, F.C., and Guo, W. (2013). Mitotic phosphorylation of Exo84 disrupts exocyst assembly and arrests cell growth. J. Cell Biol. *202*, 97–111.

Malcos, J.L., and Cyr, R.J. (2011). An ungrouped plant kinesin accumulates at the preprophase band in a cell cycle-dependent manner. Cytoskelet. Hoboken NJ *68*, 247–258.

Martín-Cuadrado, A.B., Morrell, J.L., Konomi, M., An, H., Petit, C., Osumi, M., Balasubramanian, M., Gould, K.L., del Rey, F., and de Aldana, C.R.V. (2005). Role of Septins and the Exocyst Complex in the Function of Hydrolytic Enzymes Responsible for Fission Yeast Cell Separation. Mol. Biol. Cell *16*, 4867–4881.

Matern, H.T., Yeaman, C., Nelson, W.J., and Scheller, R.H. (2001). The Sec6/8 complex in mammalian cells: characterization of mammalian Sec3, subunit interactions, and expression of subunits in polarized cells. Proc. Natl. Acad. Sci. U. S. A. *98*, 9648–9653.

McFarlane, H.E., Watanabe, Y., Gendre, D., Carruthers, K., Levesque-Tremblay, G., Haughn, G.W., Bhalerao, R.P., and Samuels, L. (2013). Cell wall polysaccharides are mislocalized to the Vacuole in echidna mutants. Plant Cell Physiol. *54*, 1867–1880.

McMichael, C.M., and Bednarek, S.Y. (2013). Cytoskeletal and membrane dynamics during higher plant cytokinesis. New Phytol. *197*, 1039–1057.

McNew, J.A., Parlati, F., Fukuda, R., Johnston, R.J., Paz, K., Paumet, F., Söllner, T.H., and Rothman, J.E. (2000). Compartmental specificity of cellular membrane fusion encoded in SNARE proteins. Nature *407*, 153–159.

Menges, M., de Jager, S.M., Gruissem, W., and Murray, J.A.H. (2005). Global analysis of the core cell cycle regulators of Arabidopsis identifies novel genes, reveals multiple and highly specific profiles of expression and provides a coherent model for plant cell cycle control. Plant J. Cell Mol. Biol. *41*, 546–566.

Mineyuki, Y. (1999). The Preprophase Band of Microtubules: Its Function as a Cytokinetic Apparatus in Higher Plants. In International Review of Cytology, K.W. Jeon, ed. (Academic Press), pp. 1–49.

Mineyuki, Y., and Gunning, B.E.S. (1990). A role for preprophase bands of microtubules in maturation of new cell walls, and a general proposal on the function of preprophase band sites in cell division in higher plants. J. Cell Sci. *97*, 527–537.

Moller, I., Marcus, S.E., Haeger, A., Verhertbruggen, Y., Verhoef, R., Schols, H., Ulvskov, P., Mikkelsen, J.D., Knox, J.P., and Willats, W. (2008). High-throughput screening of monoclonal antibodies against plant cell wall glycans by hierarchical clustering of their carbohydrate microarray binding profiles. Glycoconj. J. *25*, 37–48.

Montpetit, B., and Conibear, E. (2009). Identification of the novel TRAPP associated protein Tca17. Traffic Cph. Den. *10*, 713–723.

Moore, P.J., and Staehelin, L.A. (1988). Immunogold localization of the cell-wall-matrix polysaccharides rhamnogalacturonan I and xyloglucan during cell expansion and cytokinesis inTrifolium pratense L.; implication for secretory pathways. Planta *174*, 433–445.

Morozova, N., Liang, Y., Tokarev, A.A., Chen, S.H., Cox, R., Andrejic, J., Lipatova, Z., Sciorra, V.A., Emr, S.D., and Segev, N. (2006). TRAPPII subunits are required for the specificity switch of a Ypt-Rab GEF. Nat. Cell Biol. *8*, 1263–1269.

Müller, I., Wagner, W., Völker, A., Schellmann, S., Nacry, P., Küttner, F., Schwarz-Sommer, Z., Mayer, U., and Jürgens, G. (2003). Syntaxin specificity of cytokinesis in Arabidopsis. Nat. Cell Biol. *5*, 531–534.

Müller, S., Smertenko, A., Wagner, V., Heinrich, M., Hussey, P.J., and Hauser, M.-T. (2004). The plant microtubule-associated protein AtMAP65-3/PLE is essential for cytokinetic phragmoplast function. Curr. Biol. CB *14*, 412–417.

Müller, S., Han, S., and Smith, L.G. (2006). Two kinesins are involved in the spatial control of cytokinesis in Arabidopsis thaliana. Curr. Biol. CB *16*, 888–894.

Murata, T., Sonobe, S., Baskin, T.I., Hyodo, S., Hasezawa, S., Nagata, T., Horio, T., and Hasebe, M. (2005). Microtubule-dependent microtubule nucleation based on recruitment of γ-tubulin in higher plants. Nat. Cell Biol. *7*, 961–968.

Murata, T., Tanahashi, T., Nishiyama, T., Yamaguchi, K., and Hasebe, M. (2007). How do Plants Organize Microtubules Without a Centrosome? J. Integr. Plant Biol. *49*, 1154–1163.

Musacchio, A. (2015). The Molecular Biology of Spindle Assembly Checkpoint Signaling Dynamics. Curr. Biol. *25*, 3017.

Nebenführ, A., Frohlick, J.A., and Staehelin, L.A. (2000). Redistribution of Golgi stacks and other organelles during mitosis and cytokinesis in plant cells. Plant Physiol. *124*, 135–151.

Neto, H., and Gould, G.W. (2011). The regulation of abscission by multi-protein complexes. J. Cell Sci. *124*, 3199–3207.

Neto, H., Kaupisch, A., Collins, L.L., and Gould, G.W. (2013). Syntaxin 16 is a master recruitment factor for cytokinesis. Mol. Biol. Cell *24*, 3663–3674.

Novick, P., and Guo, W. (2002). Ras family therapy: Rab, Rho and Ral talk to the exocyst. Trends Cell Biol. *12*, 247–249.

Olsen, O.-A. (2007). Endosperm: Developmental and Molecular Biology (Springer Science & Business Media).

Otegui, M., and Staehelin, L.A. (2000). Syncytial-type cell plates: a novel kind of cell plate involved in endosperm cellularization of Arabidopsis. Plant Cell *12*, 933–947.

Otegui, M.S., Mastronarde, D.N., Kang, B.H., Bednarek, S.Y., and Staehelin, L.A. (2001). Three-dimensional analysis of syncytial-type cell plates during endosperm cellularization visualized by high resolution electron tomography. Plant Cell *13*, 2033–2051.

Paganelli, L., Caillaud, M.-C., Quentin, M., Damiani, I., Govetto, B., Lecomte, P., Karpov, P.A., Abad, P., Chabouté, M.-E., and Favery, B. (2015). Three BUB1 and BUBR1/MAD3-related spindle assembly checkpoint proteins are required for accurate mitosis in Arabidopsis. New Phytol. *205*, 202–215.

Palade, G. (1975). Intracellular aspects of the process of protein synthesis. Science *189*, 347–358.

Pan, J.Y., and Wessling-Resnick, M. (1998). GEF-mediated GDP/GTP exchange by monomeric GTPases: A regulatory role for Mg2+? BioEssays *20*, 516–521.

Panteris, E. (2008). Cortical actin filaments at the division site of mitotic plant cells: a reconsideration of the “actin-depleted zone.” New Phytol. *179*, 334–341.

Park, M., Touihri, S., Müller, I., Mayer, U., and Jürgens, G. (2012). Sec1/Munc18 protein stabilizes fusion-competent syntaxin for membrane fusion in Arabidopsis cytokinesis. Dev. Cell *22*, 989–1000.

Pastuglia, M., Azimzadeh, J., Goussot, M., Camilleri, C., Belcram, K., Evrard, J.-L., Schmit, A.-C., Guerche, P., and Bouchez, D. (2006). γ-Tubulin Is Essential for Microtubule Organization and Development in Arabidopsis. Plant Cell *18*, 1412–1425.

Peirson, B.N., Bowling, S.E., and Makaroff, C.A. (1997). A defect in synapsis causes male sterility in a T-DNA-tagged Arabidopsis thaliana mutant. Plant J. Cell Mol. Biol. *11*, 659–669.

Pickett-Heaps, J. (1974). The evolution of mitosis and the eukaryotic condition. Biosystems *6*, 37–48.

Pickett-Heaps, J.D., and Northcote, D.H. (1966). Organization of microtubules and endoplasmic reticulum during mitosis and cytokinesis in wheat meristems. J. Cell Sci. *1*, 109–120.

Preuss, M.L., Serna, J., Falbel, T.G., Bednarek, S.Y., and Nielsen, E. (2004). The Arabidopsis Rab GTPase RabA4b Localizes to the Tips of Growing Root Hair Cells. Plant Cell *16*, 1589–1603.

Qi, X., and Zheng, H. (2011). Arabidopsis TRAPPII is functionally linked to Rab-A, but not Rab-D in polar protein trafficking in trans-Golgi network. Plant Signal. Behav. *6*, 1679–1683.

Qi, X., Kaneda, M., Chen, J., Geitmann, A., and Zheng, H. (2011). A specific role for Arabidopsis TRAPPII in post-Golgi trafficking that is crucial for cytokinesis and cell polarity. Plant J. Cell Mol. Biol. *68*, 234–248.

Reichardt, I., Stierhof, Y.-D., Mayer, U., Richter, S., Schwarz, H., Schumacher, K., and Jürgens, G. (2007). Plant cytokinesis requires de novo secretory trafficking but not endocytosis. Curr. Biol. CB *17*, 2047–2053.

Reichardt, I., Slane, D., El Kasmi, F., Knöll, C., Fuchs, R., Mayer, U., Lipka, V., and Jürgens, G. (2011). Mechanisms of functional specificity among plasma-membrane syntaxins in Arabidopsis. Traffic Cph. Den. *12*, 1269–1280.

Reilly, B.A., Kraynack, B.A., VanRheenen, S.M., and Waters, M.G. (2001). Golgi-to-endoplasmic reticulum (ER) retrograde traffic in yeast requires Dsl1p, a component of the ER target site that interacts with a COPI coat subunit. Mol. Biol. Cell *12*, 3783–3796.

Robinett, C.C., Giansanti, M.G., Gatti, M., and Fuller, M.T. (2009). TRAPPII is required for cleavage furrow ingression and localization of Rab11 in dividing male meiotic cells of Drosophila. J. Cell Sci. *122*, 4526–4534.

Rybak, K., Steiner, A., Synek, L., Klaeger, S., Kulich, I., Facher, E., Wanner, G., Kuster, B., Zarsky, V., Persson, S., et al. (2014). Plant cytokinesis is orchestrated by the sequential action of the TRAPPII and exocyst tethering complexes. Dev. Cell *29*, 607–620.

Sacher, M., Jiang, Y., Barrowman, J., Scarpa, A., Burston, J., Zhang, L., Schieltz, D., Yates, J.R., Abeliovich, H., and Ferro-Novick, S. (1998). TRAPP, a highly conserved novel complex on the cis-Golgi that mediates vesicle docking and fusion. EMBO J. *17*, 2494–2503.

Sacher, M., Barrowman, J., Wang, W., Horecka, J., Zhang, Y., Pypaert, M., and Ferro-Novick, S. (2001). TRAPP I implicated in the specificity of tethering in ER-to-Golgi transport. Mol. Cell *7*, 433–442.

Sacher, M., Kim, Y.-G., Lavie, A., Oh, B.-H., and Segev, N. (2008). The TRAPP complex: insights into its architecture and function. Traffic Cph. Den. *9*, 2032–2042.

Samuels, A.L., and Staehelin, L.A. (1996). Caffeine inhibits cell plate formation by disrupting membrane reorganization just after the vesicle fusion step. Protoplasma *195*, 144–155.

Samuels, A.L., Giddings, T.H., and Staehelin, L.A. (1995). Cytokinesis in tobacco BY-2 and root tip cells: a new model of cell plate formation in higher plants. J. Cell Biol. *130*, 1345–1357.

Sano, T., Higaki, T., Oda, Y., Hayashi, T., and Hasezawa, S. (2005). Appearance of actin microfilament "twin peaks" in mitosis and their function in cell plate formation, as visualized in tobacco BY-2 cells expressing GFP-fimbrin. Plant J. Cell Mol. Biol. *44*, 595–605.

Sasabe, M., and Machida, Y. (2012). Regulation of organization and function of microtubules by the mitogen-activated protein kinase cascade during plant cytokinesis. Cytoskelet. Hoboken NJ *69*, 913–918.

Sasabe, M., Soyano, T., Takahashi, Y., Sonobe, S., Igarashi, H., Itoh, T.J., Hidaka, M., and Machida, Y. (2006). Phosphorylation of NtMAP65-1 by a MAP kinase down-regulates its activity of microtubule bundling and stimulates progression of cytokinesis of tobacco cells. Genes Dev. *20*, 1004–1014.

Sasabe, M., Kosetsu, K., Hidaka, M., Murase, A., and Machida, Y. (2011a). Arabidopsis thaliana MAP65-1 and MAP65-2 function redundantly with MAP65-3/PLEIADE in cytokinesis downstream of MPK4. Plant Signal. Behav. *6*, 743–747.

Sasabe, M., Boudolf, V., Veylder, L.D., Inzé, D., Genschik, P., and Machida, Y. (2011b). Phosphorylation of a mitotic kinesin-like protein and a MAPKKK by cyclin-dependent kinases (CDKs) is involved in the transition to cytokinesis in plants. Proc. Natl. Acad. Sci. *108*, 17844–17849.

Schekman, R., and Orci, L. (1996). Coat Proteins and Vesicle Budding. Science *271*, 1526–1533.

Schindler, C., Chen, Y., Pu, J., Guo, X., and Bonifacino, J.S. (2015). EARP is a multisubunit tethering complex involved in endocytic recycling. Nat. Cell Biol. *17*, 639–650.

Schopfer, C.R., and Hepler, P.K. (1991). Distribution of Membranes and the Cytoskeleton During Cell Plate Formation in Pollen Mother Cells of Tradescantia. J. Cell Sci. *100*, 717–728.

Scofield, S., Jones, A., and Murray, J.A.H. (2014). The plant cell cycle in context. J. Exp. Bot. *65*, 2557–2562.

Seguí-Simarro, J.M., Austin, J.R., White, E.A., and Staehelin, L.A. (2004). Electron tomographic analysis of somatic cell plate formation in meristematic cells of Arabidopsis preserved by high-pressure freezing. Plant Cell *16*, 836–856.

Shaw, S.L., Kamyar, R., and Ehrhardt, D.W. (2003). Sustained Microtubule Treadmilling in Arabidopsis Cortical Arrays. Science *300*, 1715–1718.

Small, J.V., and Kaverina, I. (2003). Microtubules meet substrate adhesions to arrange cell polarity. Curr. Opin. Cell Biol. *15*, 40–47.

Smertenko, A.P., Chang, H.-Y., Wagner, V., Kaloriti, D., Fenyk, S., Sonobe, S., Lloyd, C., Hauser, M.-T., and Hussey, P.J. (2004). The Arabidopsis microtubule-associated protein AtMAP65-1: molecular analysis of its microtubule bundling activity. Plant Cell *16*, 2035–2047.

Smertenko, A.P., Piette, B., and Hussey, P.J. (2011). The Origin of Phragmoplast Asymmetry. Curr. Biol. *21*, 1924–1930.

Snustad, D.P., Haas, N.A., Kopczak, S.D., and Silflow, C.D. (1992). The small genome of Arabidopsis contains at least nine expressed beta-tubulin genes. Plant Cell *4*, 549–556.

Söllner, R., Glässer, G., Wanner, G., Somerville, C.R., Jürgens, G., and Assaad, F.F. (2002). Cytokinesis-defective mutants of Arabidopsis. Plant Physiol. *129*, 678–690.

Söllner, T., Whiteheart, S.W., Brunner, M., Erdjument-Bromage, H., Geromanos, S., Tempst, P., and Rothman, J.E. (1993). SNAP receptors implicated in vesicle targeting and fusion. Nature *362*, 318–324.

Spitzer, C., Schellmann, S., Sabovljevic, A., Shahriari, M., Keshavaiah, C., Bechtold, N., Herzog, M., Müller, S., Hanisch, F.-G., and Hülskamp, M. (2006). The Arabidopsis elch mutant reveals functions of an ESCRT component in cytokinesis. Dev. Camb. Engl. *133*, 4679–4689.

Staehelin, L.A., and Hepler, P.K. (1996). Cytokinesis in Higher Plants. Cell *84*, 821–824.

Staehelin, L.A., and Kang, B.-H. (2008). Nanoscale architecture of endoplasmic reticulum export sites and of Golgi membranes as determined by electron tomography. Plant Physiol. *147*, 1454–1468.

Steiner, A., Müller, L., Rybak, K., Vodermaier, V., Facher, E., Thellmann, M., Ravikumar, R., Wanner, G., Hauser, M.-T., and Assaad, F.F. (2016). The Membrane-Associated Sec1/Munc18 KEULE is Required for Phragmoplast Microtubule Reorganization During Cytokinesis in Arabidopsis. Mol. Plant *9*, 528–540.

Stoppin, V., Vantard, M., Schmit, A.C., and Lambert, A.M. (1994). Isolated Plant Nuclei Nucleate Microtubule Assembly: The Nuclear Surface in Higher Plants Has Centrosome-like Activity. Plant Cell *6*, 1099–1106.

Strompen, G., El Kasmi, F., Richter, S., Lukowitz, W., Assaad, F.F., Jürgens, G., and Mayer, U. (2002). The Arabidopsis HINKEL gene encodes a kinesin-related protein involved in cytokinesis and is expressed in a cell cycle-dependent manner. Curr. Biol. CB *12*, 153–158.

Südhof, T.C., and Rothman, J.E. (2009). Membrane fusion: grappling with SNARE and SM proteins. Science *323*, 474–477.

Suvorova, E.S., Duden, R., and Lupashin, V.V. (2002). The Sec34/Sec35p complex, a Ypt1p effector required for retrograde intra-Golgi trafficking, interacts with Golgi SNAREs and COPI vesicle coat proteins. J. Cell Biol. *157*, 631–643.

Synek, L., Schlager, N., Eliás, M., Quentin, M., Hauser, M.-T., and Zárský, V. (2006). AtEXO70A1, a member of a family of putative exocyst subunits specifically expanded in land plants, is important for polar growth and plant development. Plant J. Cell Mol. Biol. *48*, 54–72.

Sztul, E., and Lupashin, V. (2006). Role of tethering factors in secretory membrane traffic. Am. J. Physiol. Cell Physiol. *290*, C11-26.

Takahashi, Y., Soyano, T., Sasabe, M., and Machida, Y. (2004). A MAP kinase cascade that controls plant cytokinesis. J. Biochem. (Tokyo) *136*, 127–132.

Tanaka, H., Ishikawa, M., Kitamura, S., Takahashi, Y., Soyano, T., Machida, C., and Machida, Y. (2004). The AtNACK1/HINKEL and STUD/TETRASPORE/AtNACK2 genes, which encode functionally redundant kinesins, are essential for cytokinesis in Arabidopsis. Genes Cells Devoted Mol. Cell. Mech. *9*, 1199–1211.

Tank, J.G., and Thaker, V.S. (2011). Cyclin dependent kinases and their role in regulation of plant cell cycle. Biol. Plant. *55*, 201–212.

TerBush, D.R., and Novick, P. (1995). Sec6, Sec8, and Sec15 are components of a multisubunit complex which localizes to small bud tips in Saccharomyces cerevisiae. J. Cell Biol. *130*, 299–312.

TerBush, D.R., Maurice, T., Roth, D., and Novick, P. (1996). The Exocyst is a multiprotein complex required for exocytosis in Saccharomyces cerevisiae. EMBO J. *15*, 6483–6494.

Thellmann, M., Rybak, K., Thiele, K., Wanner, G., and Assaad, F.F. (2010). Tethering Factors Required for Cytokinesis in Arabidopsis. Plant Physiol. *154*, 720–732.

Thiele, K., Wanner, G., Kindzierski, V., Jürgens, G., Mayer, U., Pachl, F., and Assaad, F.F. (2009). The timely deposition of callose is essential for cytokinesis in Arabidopsis. Plant J. Cell Mol. Biol. *58*, 13–26.

Touihri, S., Knöll, C., Stierhof, Y.-D., Müller, I., Mayer, U., and Jürgens, G. (2011). Functional anatomy of the Arabidopsis cytokinesis-specific syntaxin KNOLLE. Plant J. *68*, 755–764.

Toyooka, K., Goto, Y., Asatsuma, S., Koizumi, M., Mitsui, T., and Matsuoka, K. (2009). A mobile secretory vesicle cluster involved in mass transport from the Golgi to the plant cell exterior. Plant Cell *21*, 1212–1229.

Uemura, T., and Nakano, A. (2013). Plant TGNs: dynamics and physiological functions. Histochem. Cell Biol. *140*, 341–345.

Uemura, T., Kim, H., Saito, C., Ebine, K., Ueda, T., Schulze-Lefert, P., and Nakano, A. (2012a). Qa-SNAREs localized to the trans-Golgi network regulate multiple transport pathways and extracellular disease resistance in plants. Proc. Natl. Acad. Sci. *109*, 1784–1789.

Uemura, T., Ueda, T., and Nakano, A. (2012b). The physiological role of SYP4 in the salinity and osmotic stress tolerances. Plant Signal. Behav. *7*, 1118–1120.

Uemura, T., Suda, Y., Ueda, T., and Nakano, A. (2014). Dynamic behavior of the trans-golgi network in root tissues of Arabidopsis revealed by super-resolution live imaging. Plant Cell Physiol. *55*, 694–703.

Van Damme, D., Bouget, F.-Y., Van Poucke, K., Inzé, D., and Geelen, D. (2004). Molecular dissection of plant cytokinesis and phragmoplast structure: a survey of GFP-tagged proteins. Plant J. Cell Mol. Biol. *40*, 386–398.

Van Damme, D., Inzé, D., and Russinova, E. (2008). Vesicle Trafficking during Somatic Cytokinesis. Plant Physiol. *147*, 1544–1552.

Van Damme, D., Gadeyne, A., Vanstraelen, M., Inzé, D., Van Montagu, M.C.E., De Jaeger, G., Russinova, E., and Geelen, D. (2011). Adaptin-like protein TPLATE and clathrin recruitment during plant somatic cytokinesis occurs via two distinct pathways. Proc. Natl. Acad. Sci. U. S. A. *108*, 615–620.

Vandepoele, K., Raes, J., De Veylder, L., Rouzé, P., Rombauts, S., and Inzé, D. (2002). Genome-Wide Analysis of Core Cell Cycle Genes in Arabidopsis. Plant Cell *14*, 903–916.

Vanstraelen, M., Van Damme, D., De Rycke, R., Mylle, E., Inzé, D., and Geelen, D. (2006). Cell cycle-dependent targeting of a kinesin at the plasma membrane demarcates the division site in plant cells. Curr. Biol. CB *16*, 308–314.

Vernoud, V., Horton, A.C., Yang, Z., and Nielsen, E. (2003). Analysis of the Small GTPase Gene Superfamily of Arabidopsis. Plant Physiol. *131*, 1191–1208.

Viotti, C., Bubeck, J., Stierhof, Y.-D., Krebs, M., Langhans, M., van den Berg, W., van Dongen, W., Richter, S., Geldner, N., Takano, J., et al. (2010). Endocytic and secretory traffic in Arabidopsis merge in the trans-Golgi network/early endosome, an independent and highly dynamic organelle. Plant Cell *22*, 1344–1357.

Völker, A., Stierhof, Y.D., and Jürgens, G. (2001). Cell cycle-independent expression of the Arabidopsis cytokinesis-specific syntaxin KNOLLE results in mistargeting to the plasma membrane and is not sufficient for cytokinesis. J. Cell Sci. *114*, 3001–3012.

Vos, J.W., Dogterom, M., and Emons, A.M.C. (2004). Microtubules become more dynamic but not shorter during preprophase band formation: A possible "search-and-capture" mechanism for microtubule translocation. Cell Motil. Cytoskeleton *57*, 246–258.

Waizenegger, I., Lukowitz, W., Assaad, F., Schwarz, H., Jürgens, G., and Mayer, U. (2000). The Arabidopsis KNOLLE and KEULE genes interact to promote vesicle fusion during cytokinesis. Curr. Biol. *10*, 1371–1374.

Walker, K.L., Müller, S., Moss, D., Ehrhardt, D.W., and Smith, L.G. (2007). Arabidopsis TANGLED identifies the division plane throughout mitosis and cytokinesis. Curr. Biol. CB *17*, 1827–1836.

Wang, H., Tang, X., Liu, J., Trautmann, S., Balasundaram, D., McCollum, D., and Balasubramanian, M.K. (2002). The multiprotein exocyst complex is essential for cell separation in Schizosaccharomyces pombe. Mol. Biol. Cell *13*, 515–529.

Wang, N., Lee, I.-J., Rask, G., and Wu, J.-Q. (2016). Roles of the TRAPP-II Complex and the Exocyst in Membrane Deposition during Fission Yeast Cytokinesis. PLOS Biol *14*, e1002437.

Weber, T., Zemelman, B.V., McNew, J.A., Westermann, B., Gmachl, M., Parlati, F., Söllner, T.H., and Rothman, J.E. (1998). SNAREpins: minimal machinery for membrane fusion. Cell *92*, 759–772.

Weingartner, M., Binarova, P., Drykova, D., Schweighofer, A., David, J.P., Heberle-Bors, E., Doonan, J., and Bögre, L. (2001). Dynamic recruitment of Cdc2 to specific microtubule structures during mitosis. Plant Cell *13*, 1929–1943.

Weingartner, M., Criqui, M.-C., Mészáros, T., Binarova, P., Schmit, A.-C., Helfer, A., Derevier, A., Erhardt, M., Bögre, L., and Genschik, P. (2004). Expression of a Nondegradable Cyclin B1 Affects Plant Development and Leads to Endomitosis by Inhibiting the Formation of a Phragmoplast. Plant Cell *16*, 643–657.

Whittington, A.T., Vugrek, O., Wei, K.J., Hasenbein, N.G., Sugimoto, K., Rashbrooke, M.C., and Wasteneys, G.O. (2001). MOR1 is essential for organizing cortical microtubules in plants. Nature *411*, 610–613.

Wu, J., Tan, X., Wu, C., Cao, K., Li, Y., and Bao, Y. (2013). Regulation of cytokinesis by exocyst subunit SEC6 and KEULE in Arabidopsis thaliana. Mol. Plant.

Wurmser, A.E., Sato, T.K., and Emr, S.D. (2000). New Component of the Vacuolar Class C-Vps Complex Couples Nucleotide Exchange on the Ypt7 Gtpase to Snare-Dependent Docking and Fusion. J. Cell Biol. *151*, 551–562.

Xu, X.M., Zhao, Q., Rodrigo-Peiris, T., Brkljacic, J., He, C.S., Müller, S., and Meier, I. (2008). RanGAP1 is a continuous marker of the Arabidopsis cell division plane. Proc. Natl. Acad. Sci. U. S. A. *105*, 18637–18642.

Yang, B., Gonzalez, L., Prekeris, R., Steegmaier, M., Advani, R.J., and Scheller, R.H. (1999). SNARE interactions are not selective. Implications for membrane fusion specificity. J. Biol. Chem. *274*, 5649–5653.

Yasuhara, H., and Shibaoka, H. (2000). Inhibition of Cell-Plate Formation by Brefeldin A Inhibited the Depolymerization of Microtubules in the Central Region of the Phragmoplast. Plant Cell Physiol. *41*, 300–310.

Yu, S., and Liang, Y. (2012). A trapper keeper for TRAPP, its structures and functions. Cell. Mol. Life Sci. CMLS *69*, 3933–3944.

Zeng, C.J.T., Lee, Y.-R.J., and Liu, B. (2009). The WD40 Repeat Protein NEDD1 Functions in Microtubule Organization during Cell Division in Arabidopsis thaliana. Plant Cell *21*, 1129–1140.

Zhang, H., and Dawe, R.K. (2011). Mechanisms of plant spindle formation. Chromosome Res. Int. J. Mol. Supramol. Evol. Asp. Chromosome Biol. *19*, 335–344.

Zhang, D., Wadsworth, P., and Hepler, P.K. (1990). Microtubule dynamics in living dividing plant cells: confocal imaging of microinjected fluorescent brain tubulin. Proc. Natl. Acad. Sci. U. S. A. *87*, 8820–8824.

Zhang, D., Wadsworth, P., and Hepler, P.K. (1993). Dynamics of microfilaments are similar, but distinct from microtubules during cytokinesis in living, dividing plant cells. Cell Motil. Cytoskeleton *24*, 151–155.

Zhang, L., Zhang, H., Liu, P., Hao, H., Jin, J.B., and Lin, J. (2011). Arabidopsis R-SNARE proteins VAMP721 and VAMP722 are required for cell plate formation. PloS One *6*, e26129.

Zolov, S.N., and Lupashin, V.V. (2005). Cog3p depletion blocks vesicle-mediated Golgi retrograde trafficking in HeLa cells. J. Cell Biol. *168*, 747–759.

Acknowledgments

First of all I want to thank Farhah for the perfect supervision over the last five years. Farhah was always a demanding, but fair supervisor. I am really glad that I chose to work in her group for my doctoral thesis. Also many thanks for the advice and help throughout the writing process of the thesis.

I also thank the members of my examining committee: Prof. Dr. Ralph Hückelhoven, Prof. Dr. Jörg Durner and Prof. Dr. Ramon Torrez-Ruiz for the time they invest to evaluate my thesis.

I am also grateful for Kasia that she patiently introduced me into the daily routine of the lab work and for her helping hand when needed. Furthermore, I want to thank all the current and former members of our group (Nils, Raksha, Felix etc.) for their help, the discussions and the fun during the last years.

I am really glad and thankful that our group was part of the botany department: Beate always helped me with the paper work, the gardeners took care of my plants, Sepp took care of everything else and the technical assistants helped me with media, protocols and orders. I really enjoyed the great atmosphere and discussions at work, but also the fun times outside of work with all the members of the botany department, especially Michl, Timo, Steffi, Christian and Chrisi. Many thanks also to Inês of the chair of Plant Systems Biology for the help with my thesis.

I want to thank Gerhard Wanner and all the members of the Ultrastructural Research group of the LMU Munich for the fruitful cooperation over the past years. I always enjoyed to deliver or pick up samples. Many thanks also to Eva Facher from the Biology Department I of the LMU Munich for the help with the Environmental Electron microscope.

I am thankful for the effective cooperation with Prof. Dr. Bernhardt Küster and Susan Kläger of the Proteomics and Bioanalytics chair of the TUM Munich.

Many thanks to Prof. Staffan Persson and Heather McFarlane from the University of Melbourne for the successful cooperation and the opportunity to use the spinning disc confocal microscope of your group.

Last but not least I am very grateful for the help and support of my friends and family throughout the ups and downs of the thesis. Especially Andi for last minute corrections of my thesis. Special thanks and “bisous” to Margaux, for your help, support and encouragement throughout the whole time and especially towards the end. I am really lucky to have you by my side.

Appendix

Developmental Cell
Article

Plant Cytokinesis Is Orchestrated by the Sequential Action of the TRAPPII and Exocyst Tethering Complexes

Katarzyna Rybak,[1] Alexander Steiner,[1] Lukas Synek,[2] Susan Klaeger,[3] Ivan Kulich,[4] Eva Facher,[5,6] Gerhard Wanner,[6] Bernhard Kuster,[3] Viktor Zarsky,[2,4] Staffan Persson,[7,8] and Farhah F. Assaad[1,*]
[1]Botany, Technische Universität München, 85354 Freising, Germany
[2]Institute of Experimental Botany, Academy of Sciences of the Czech Republic, 165 02 Prague 6, Czech Republic
[3]Chair for Proteomics and Bioanalytics, Technische Universität München, 85354 Freising, Germany
[4]Department of Experimental Plant Biology, Faculty of Science, Charles University, 128 44 Prague 2, Czech Republic
[5]Department Biologie I, Ludwig-Maximillians Universität, Systematische Botanik und Mykologie, 80638 Munich, Germany
[6]Department Biologie I, Ludwig-Maximillians Universität, 82152 Planegg-Martinsried, Germany
[7]Max-Planck-Institut für Molekulare Pflanzenphysiologie, 14476 Potsdam, Germany
[8]ARC Centre of Excellence in Plant Cell Walls, School of Botany, University of Melbourne, Parkville, VIC 3010, Australia
*Correspondence: farhah@wzw.tum.de
http://dx.doi.org/10.1016/j.devcel.2014.04.029

SUMMARY

Plant cytokinesis is initiated in a transient membrane compartment, the cell plate, and completed by a process of maturation during which the cell plate becomes a cross wall. How the transition from juvenile to adult stages occurs is poorly understood. In this study, we monitor the *Arabidopsis* transport protein particle II (TRAPPII) and exocyst tethering complexes throughout cytokinesis. We show that their appearance is predominantly sequential, with brief overlap at the onset and end of cytokinesis. The TRAPPII complex is required for cell plate biogenesis, and the exocyst is required for cell plate maturation. The TRAPPII complex sorts plasma membrane proteins, including exocyst subunits, at the cell plate throughout cytokinesis. We show that the two tethering complexes physically interact and propose that their coordinated action may orchestrate not only plant but also animal cytokinesis.

INTRODUCTION

Cytokinesis is the partitioning of the cytoplasm following nuclear division. In plants, this occurs in a transient membrane compartment called the cell plate. Following its biogenesis and expansion, the cell plate is inserted into the lateral walls of the parent cell. A number of changes in the properties and composition of the plate occur thereafter, and insertion thus appears to trigger the maturation of the cell plate into a cross wall. Live imaging of asymmetric cytokinetic events has documented a dramatic change in the growth dynamics of nascent cell plates upon anchoring to one side of the cell: whereas cell plate movements prior to insertion could best be described as tentative, cell plate growth becomes rapid and highly directional upon connecting with a lateral wall (Cutler and Ehrhardt, 2002). Similarly, time-lapse images of *Tradescantia* stamen hair cells show fluid and wrinkled cell plates becoming stiff and flat after insertion into the parent cell walls (Mineyuki and Gunning, 1990). This difference in appearance requires cellulose synthesis (Mineyuki and Gunning, 1990), and immunohistochemistry has in fact shown that cellulose is a major component of mature cross walls (Samuels et al., 1995). This is in contrast to cell plates, in which the principle luminal polysaccharide is callose (Samuels et al., 1995; Seguí-Simarro et al., 2004). The abundance of other cell wall polysaccharides, including pectins and xyloglucans, also differs between cell plates and cross walls (Moore and Staehelin, 1988). Although it is apparent that the composition of cell plate membranes and polysaccharides changes as this juvenile compartment matures into a cross wall, the mechanisms that coordinate these transitions remain unclear.

In contrast to plants, cytokinesis in animal cells occurs by means of a ring of actin and myosin that contracts to pinch a cell in two (Neto and Gould, 2011). This process requires extensive cell-surface expansion, which is achieved by the delivery of membranes from the recycling endosome to the cleavage furrow (Robinett et al., 2009). The completion of animal cytokinesis, via a process referred to as abscission, requires the delivery of secretory vesicles to a scaffold assembled at the midbody (Gromley et al., 2005). The regulation of the transition between furrow ingression and abscission is poorly understood. Thus, in both plant and animal cells, cytokinesis requires the regulation in time and space of a series of successive steps, and in neither kingdom have the underlying mechanisms been elucidated.

Although plants and animals adopt different strategies for cytokinesis, a number of conserved molecular components are shared. These include Rab GTPases and other factors that are required for vesicle tethering. Tethering refers to the initial contact between donor and recipient membranes and represents a highly selective trafficking step that precedes and facilitates vesicle docking and fusion (see Thellmann et al., 2010, and references therein). The *Arabidopsis* Rab-A subfamily of small GTPases is the only one that labels the cell plate throughout cytokinesis (Chow et al., 2008). Similarly, the orthologous Rab11 class is the only one that has been shown to be required for and present throughout animal cytokinesis (Yu et al., 2007).

CellPress

Developmental Cell
TRAPPII and Exocyst Function in Plant Cytokinesis

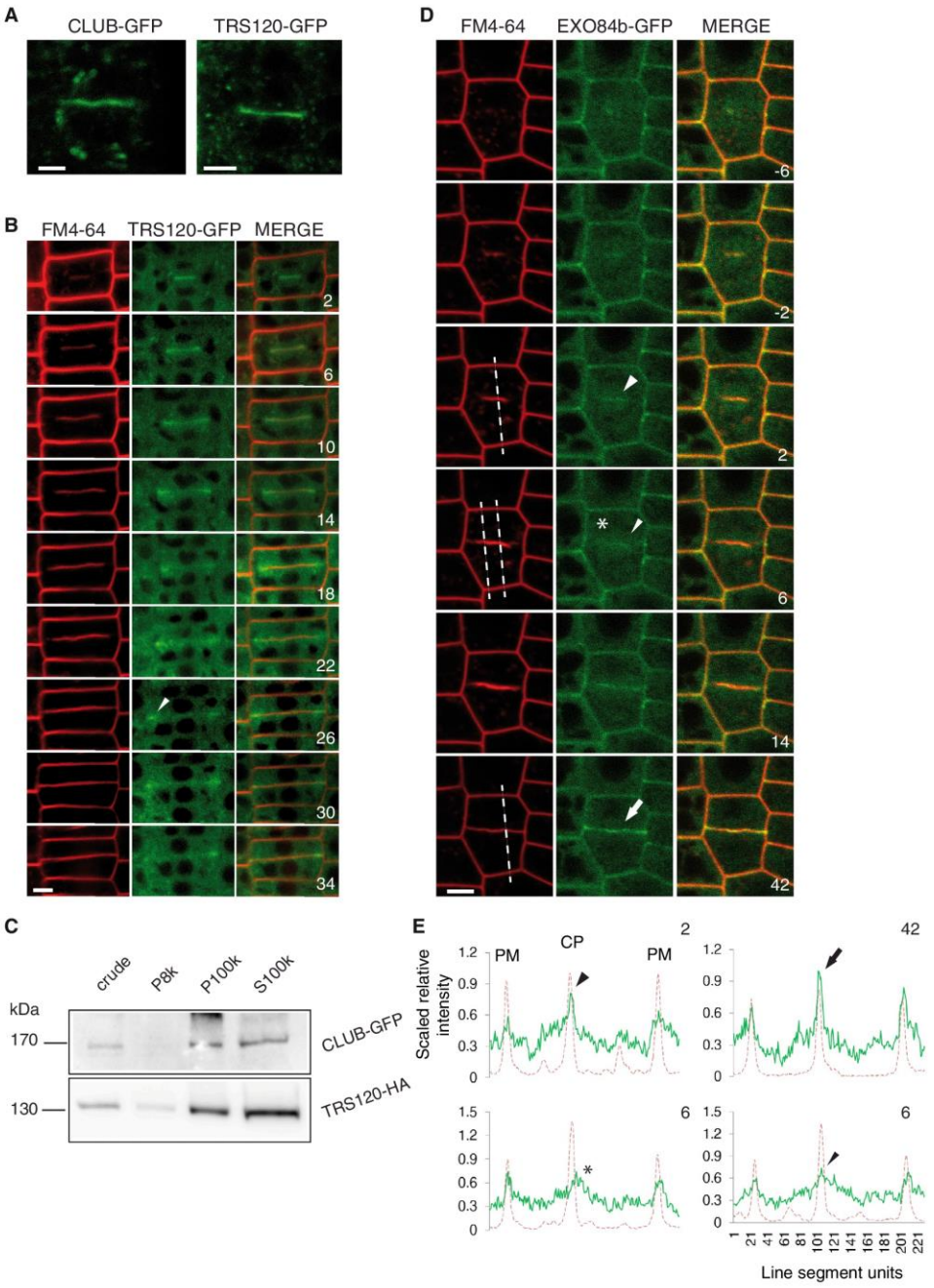

Figure 1. Localization Dynamics of TRAPPII and Exocyst Gene Fusions

(A) Cell plate localization of P_{UBQ}::CLUB-GFP (left) and P_{TRS120}::TRS120-GFP (right).

(B and D) Time lapses of P_{TRS120}::TRS120-GFP (B) and P_{EXO84b}::EXO84b-GFP (D) with FM4-64 are shown, with minutes indicated in the right panel. The 0 min time point corresponds to cell plate initiation. Arrowhead in (B) points to leading edge of cell plate.

(C) Cell fractionation showing that CLUB-GFP and TRS120-HA can be detected in both the membrane (P100k) and soluble (S100k) fractions.

(legend continued on next page)

Developmental Cell
TRAPPII and Exocyst Function in Plant Cytokinesis

Two distinct tethering complexes, the transport protein particle II (TRAPPII) and exocyst, have been implicated in cytokinesis in both the plant and animal kingdoms (McMichael and Bednarek, 2013; Neto and Gould, 2011). The yeast TRAPPII complex acts as a guanine nucleotide exchange factor for Rab GTPases and is required for intra- and post-Golgi traffic; it consists of the hexameric TRAPPI complex and of three additional subunits (Trs65, Trs120, and Trs130; Yu and Liang, 2012). All subunits but one (Trs65) are conserved in plants (Thellmann et al., 2010). The exocyst is a conserved octameric complex required for polarized secretion (reviewed in Heider and Munson, 2012). The *Arabidopsis* genome encodes single or multiple isoforms of all exocyst subunits (Sec3, Sec5, Sec6, Sec8, Sec10, Sec15, Exo70, and Exo84; Cvrckova et al., 2001; Synek et al., 2006).

The *Arabidopsis* TRAPPII complex was first identified in a screen for cytokinesis-defective mutants (Jaber et al., 2010); mutation at the *CLUB* locus gave rise to seedlings with multinucleate cells, cell wall stubs as well as an amorphous, club-shaped overall appearance, hence the name (Söllner et al., 2002). Positional cloning identified *CLUB* as a homolog of the yeast Trs130 TRAPPII-specific subunit (Jaber et al., 2010). The two conserved *Arabidopsis* TRAPPII subunits, CLUB/AtTRS130 and AtTRS120, have been shown to be required for cell plate formation (Jaber et al., 2010; Thellmann et al., 2010; Qi et al., 2011), but their localization dynamics during cytokinesis has not been determined to date. A number of studies have addressed the role of the exocyst in plant cytokinesis. The EXO70A1 and EXO84b exocyst subunits localize to nascent cell plates and postcytokinetic cross walls and were found to be involved in cytokinesis (Fendrych et al., 2010). The SEC6 exocyst subunit interacts with the Sec1/Munc18 protein KEULE, and pollen-rescued *sec6* mutant embryos have been reported to have a canonical *keule*-like phenotype, with multinucleate cells and cell wall stubs (Wu et al., 2013). However, such cytokinesis defects were not observed in embryo lethal *sec3a* exocyst mutants of *Arabidopsis* (Zhang et al., 2013). In brief, the literature on the role of the exocyst in cell plate formation is internally inconsistent, and there is no clear consensus as regards the cell plate localization of the exocyst throughout cytokinesis.

The finding that both the TRAPPII and exocyst tethering complexes are required for plant cytokinesis is intriguing. The TRAPPII complex is functionally related to Rab-A but not Rab-D family members in *Arabidopsis* and colocalizes with Rab-A1c (Qi et al., 2011; Qi and Zheng, 2011). It is thereby thought to label *trans*-Golgi network (TGN) compartments. By contrast, the exocyst partitions between the cytoplasm and the plasma membrane, where it forms distinct, transient foci (Fendrych et al., 2013; Zhang et al., 2013). This raises the question as to whether the cell plate may have a mosaic identity, consisting simultaneously of both TGN and plasma membrane components. An alternative hypothesis would postulate a sequential identity for the cell plate as it undergoes initiation, biogenesis, expansion, and maturation. In this study, we simultaneously monitor the TRAPPII and exocyst complexes throughout cytokinesis. Our data support a sequential identity for the cell plate. In addition, we show that the TRAPPII complex regulates the localization of the exocyst at the cell plate and that the two complexes physically interact. We present a model for the sequential yet overlapping, coordinated action of the TRAPPII and exocyst complexes in cytokinesis.

RESULTS

The Appearance of the TRAPPII and Exocyst Complexes at the Cell Plate Is Predominantly Sequential, with a Brief Overlap at the Onset and End of Cytokinesis

We first set out to elucidate the localization dynamics of TRAPPII and exocyst subunits throughout cytokinesis. CLUB/AtTRS130 and AtTRS120 GFP fusions, expressed under the control of ubiquitin and/or native promoters, were shown to be functional (Figures S1A–S1C available online) and found to reside on the cell plate (Figures 1A and 1B). As CLUB/AtTRS130 and AtTRS120 show very similar localization dynamics at the cell plate (Figure S2), we continued predominantly with TRS120 gene fusions, which yielded a brighter signal. TRS120-GFP appeared at the cell equator at the onset of cytokinesis and labeled the cell plate throughout cytokinesis, disappearing after cell plate insertion into the lateral cell walls (Figure 1B; Movie S1). TRAPPII gene fusions appeared to localize in the cytoplasm as well as on membrane structures (Figure 1B; Figure S2); upon cell fractionation, CLUB-GFP and TRS120-hemagglutinin (HA) gene fusions were found in both the soluble and membrane fractions (Figure 1C). It thus appears that these subunits shuttle between the cytosol and endomembrane compartments. In contrast to the TRAPPII subunits, EXO84b-GFP appeared at the cell equator at the onset and at the end of cytokinesis and labeled membranes associated with newly deposited cross walls after cytokinesis (Figure 1D; Movie S2; Fendrych et al., 2010). In expanding cell plates, peak EXO84b-GFP fluorescence was typically not at the cell plate, but rather present as a diffuse cloud around the plate; this was often observed in discontinuous patches of the cell plate (Figures 1D and 1E, 6 min time point; Figure S5D; Movie S2) and could be seen throughout the biogenesis and expansion phases of cytokinesis (Figure S1I). The localization dynamics of different TRAPPII and exocyst subunits did not appear to be due to overexpression of the fusion proteins and was robust over a considerable range of protein expression levels (Figures S1D–S1K; Movies S1, S2, and S3). Furthermore, different subunits of each complex behaved similarly (Figures 2A and 2B).

To better monitor the different stages of cytokinesis, we used a microtubule marker, mCherry-TUA5 (Gutierrez et al., 2009). The onset of cytokinesis is characterized by the assembly of the phragmoplast, which is a transient array of polar microtubules nucleated from spindle microtubules. A solid phragmoplast subsequently arises from lateral expansion of phragmoplast initials. As cells enter telophase, microtubules are translocated

(E) Line graphs, corresponding to panels shown in (D), depict scaled relative fluorescence intensity, with FM4-64 used to position the plasma membranes (PM) and cell plate (CP). The arrowhead at 2 min points to an initial signal at the cell plate, the arrow at 42 min points to peak signal at the cross wall. At 6 min the signal is more diffuse, with a cloud-like appearance on the left (asterisk) and weak signal at the cell plate on the right (arrowhead). Scale bars, 5 μm.
See also Figures S1 and S2 and Movies S1 and S2.

Developmental Cell
TRAPPII and Exocyst Function in Plant Cytokinesis

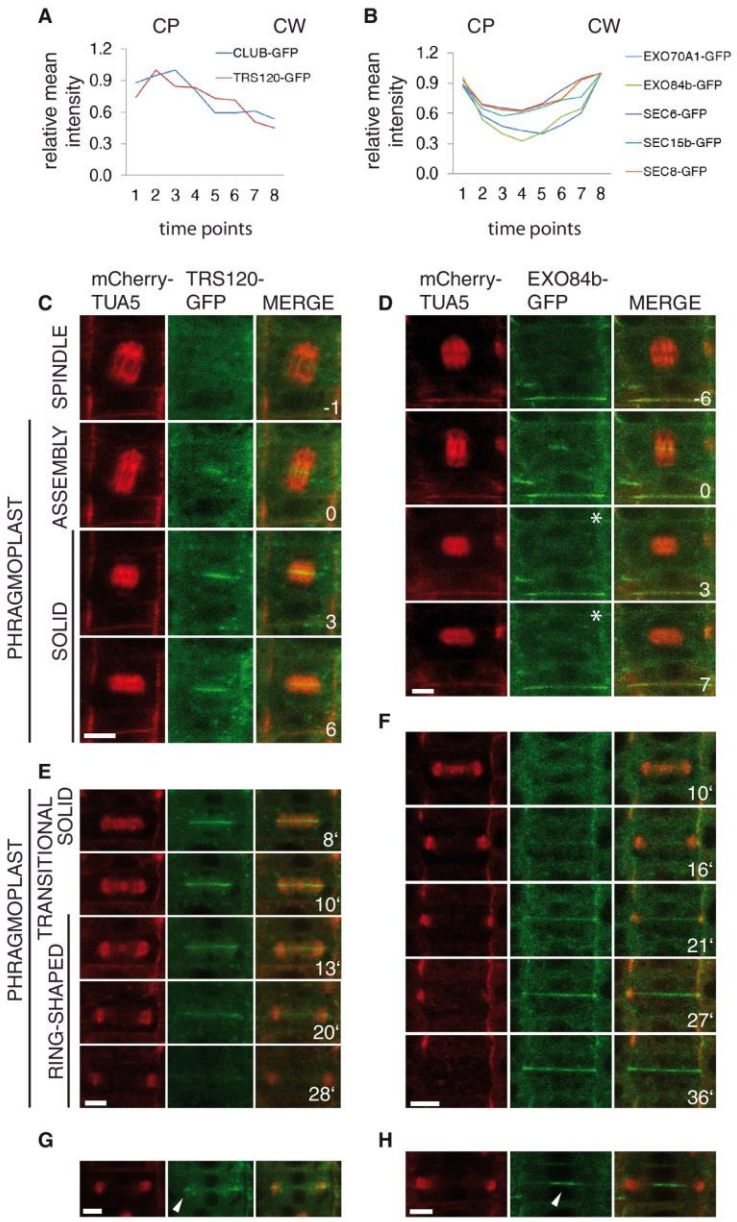

Figure 2. Localization of TRAPPII and Exocyst Gene Fusions and Phragmoplast Microtubule Dynamics

(A and B) Mean signal intensity at the CP or cross walls (CW). The value 1.0 is set at maximal CP signal in (A) and maximal CW signal in (B). (A) TRAPPII subunits show peak fluorescence at the cell plate and are absent at the cross wall. (B) All exocyst subunits monitored (SEC6, SEC8, SEC15b, EXO70A1, and EXO84b; Fendrych et al., 2010) follow a localization dynamics we refer to as "strong-weak/diffuse-strong."

(C–H) Time lapses of P_{TRS120}::TRS120-GFP (C and E) and P_{EXO84b}::EXO84b-GFP (D and F) with mCherry-TUA5 are shown, with minutes indicated in the right panel.

(C and D) Anaphase-telophase transition. The 0 min time point corresponds to cell plate initiation. Star in (D) at 3 and 7 designates barely detectable, diffuse EXO84b-GFP cytosolic signal.

(E and F) Telophase. The time-lapse segments start at the solid phragmoplast stage, which occurs on average 8 min after cell plate initiation, hence the labeling 8′, etc.

(G and H) Ring-shaped phragmoplast stage. Arrowhead in (G) points to leading edge of cell plate. Arrowhead in (H) points to first appearance of the exocyst subunit. The brief window in time shown in (G) and (H) was missed in the time lapses shown in (E) and (F). This is because the fluorescence was low and photobleaching extensive, such that time lapses were carried out with 4 min intervals. Scale bars, 5 μm.

See also Figure S2 and Movies S1, S2, and S3.

to the leading edges of the phragmoplast, giving rise to a ring-shaped phragmoplast (McMichael and Bednarek, 2013). TRS120-GFP and EXO84b-GFP first appeared at the cell equator at the phragmoplast assembly stage (Figures 2C and 2D; Figure S2). At the solid phragmoplast stage, however, TRS120-GFP fluorescence at the cell plate reached a peak (Figure 2C; Figure S2B), whereas the EXO84b-GFP signal became weak and diffuse (Figure 2D; Figure S2C). At the ring-shaped phragmoplast, TRS120-GFP relocated to the leading edges of the cell plate (Figure 2G; Figure S2B) and then gradually disappeared (Figure 2E; Figure S2B). The EXO84b-GFP fluorescence remained weak and diffuse until this time point (Figures 2F and 2H). Thereafter, the EXO84b-GFP signal gradually increased (Figure 2F; Figure S2C; Fendrych et al., 2010) to reach peak fluorescence throughout the cross wall as the phragmoplast disappeared (Figure 2F; Figure S2C).

An analysis of colocalization was undertaken with TRS120 and three exocyst subunits (SEC6, EXO70A1, and EXO84b) with different combinations of mCherry or monomeric red fluorescent protein (mRFP) and GFP tags. All three combinations yielded the same results (Figure 3A; Figure S3; data not shown). Whereas peak fluorescence of TRS120 was seen during cell plate formation, peak fluorescence of the exocyst subunit was associated with cross walls, where TRS120 was absent (Figures 3A and 3B). A brief overlap between the two tethering complexes could be seen not only at the onset of cytokinesis (Figure 3A, 0 min) but also as of a time point at which the TRS120 signal began to decrease at the cell plate and increase

DEVCEL 2970

Developmental Cell
TRAPPII and Exocyst Function in Plant Cytokinesis

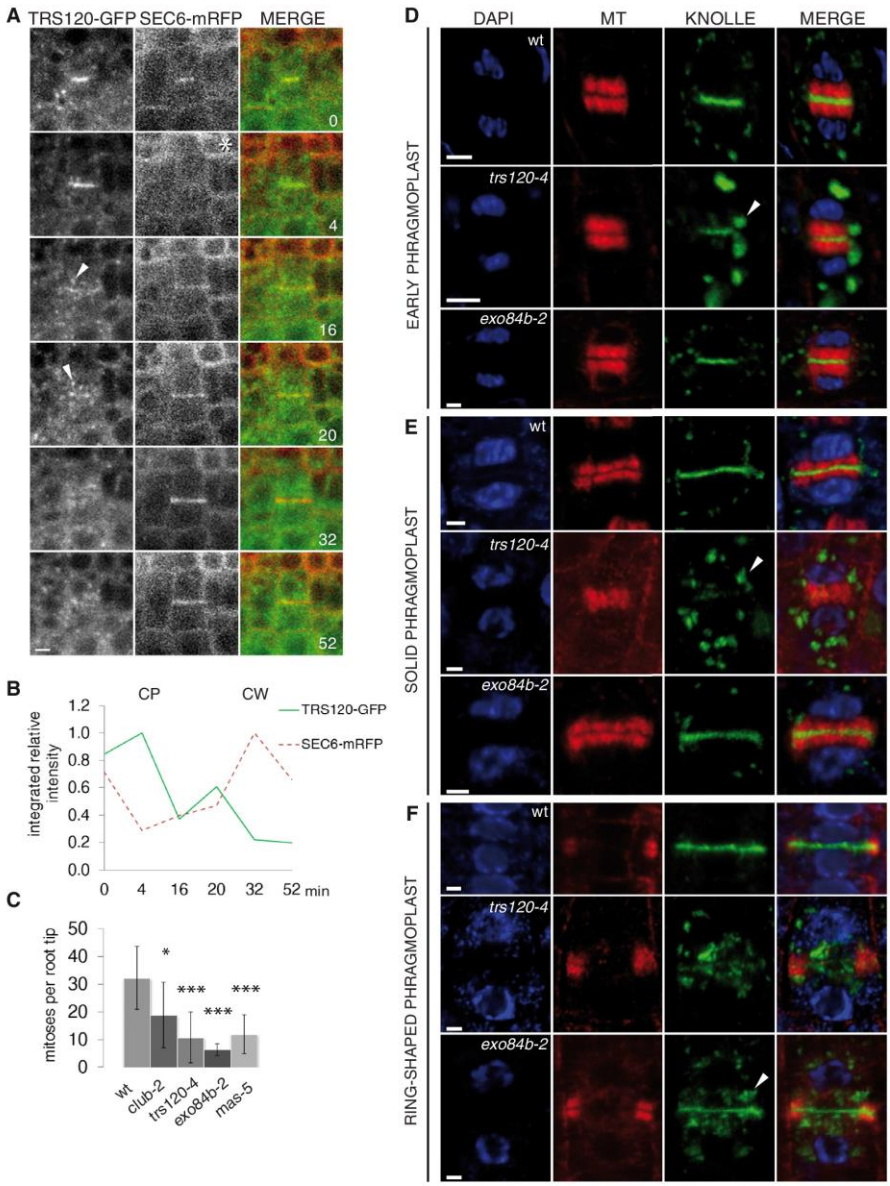

Figure 3. Colocalization of TRAPPII and Exocyst Subunits as well as Cell Plate Biogenesis and Maturation in Wild-Type and Mutant Backgrounds

(A and B) Time lapse of P_{UBQ}::TRS120-mCherry and P_{35S}::SEC6-mRFP, with minutes indicated in the right panel. (A) z stack projections generated with a spinning disk confocal microscope. Star at 4 min designates barely detectable, diffuse SEC6-mRFP cytosolic signal. Arrowheads at 16 and 20 min point to TRS120 recycling from the cell plate. Scale bar, 5 μm. Line graph (B) shows integrated signal intensity per unit area at the cell plate or cross wall, with peak signals set at 1.0.

(C) Mitotic index (mean ± SD) of wild-type (WT) and mutant root tips. All mutants show a significantly lower mitotic index than the wild-type ($n > 15$, $^{*}p \leq 0.01$ and $^{***}p \leq 0.0001$; Student's t test).

(D–F) Antibody stains of root tips: DAPI/nucleus (blue), microtubules (MT, red), KNOLLE protein (green), and merge. The cell-cycle stage is indicated on the left and the genotype in the first column. Arrowheads point to large KNOLLE-positive compartments surrounding thin or absent cell plates in *trs120-4* (D–F) and surrounding telophase plates in *exo84b-2* (F). See text for a detailed description. Scale bars, 2 μm.

See also Figure S3.

in intracellular compartments (Figure 3A, 16 min). Our analysis of SEC6 is discrepant with the findings of Wu et al. (2013), who describe a similar SEC6-GFP fusion as labeling cell plate membranes throughout cytokinesis, and of reorganizing to the leading edges at the end of cytokinesis. This discrepancy might be attributed to the fact that Wu et al. (2013) used tobacco BY2 protoplasts for localization. The consensus (based on this study, Fendrych et al., 2010, and Zhang et al., 2013) in meristematic cells of root tips and embryos is that the exocyst signal is weak during the solid phragmoplast stages.

Taken together, our data show that the appearance of the TRAPPII and exocyst complexes was predominantly sequential. The overlap between the complexes occurred at two key transitions: during the phragmoplast assembly stage at the onset of cytokinesis, and at the late ring-shaped phragmoplast stage, which is concomitant with cell plate insertion into the lateral walls at the end of cytokinesis.

The TRAPPII Complex Is Required for Cell Plate Biogenesis, and the Exocyst Is Required for Cell Plate Maturation

We next compared cell plate formation and maturation in TRAPPII and exocyst mutants. TRAPPII mutants of *Arabidopsis* are seedling lethal, whereas exocyst mutants range from gametophytic lethality to viability (see Supplemental Experimental Procedures), depending presumably on the degree of redundancy between paralogs. To compare TRAPPII and exocyst mutant phenotypes of similar strength, we screened 54 insertion lines in exocyst subunits for strong cytokinesis defects (see Supplemental Experimental Procedures). The screen identified one exocyst mutant, *exo84b-2*, with a seedling lethal phenotype of roughly equal strength as TRAPPII mutants in terms of growth and meristem dysfunction, and we therefore focused on it in this study. Wild-type and mutant root tips were stained with DAPI to determine nuclear stages and labeled with α-microtubule and α-KNOLLE antibodies to visualize phragmoplast microtubules and cell plate membranes, respectively (Figures 3C–3F). The stains revealed that the mitotic index of *exo84b-2* root meristems (Figure 3C) was significantly lower than that of TRAPPII mutants ($p = 0.004$ for an average of *club-2* and *trs120-4*) and of other canonical cytokinesis-defective mutants such as *massue* (Thiele et al., 2009; $p = 0.002$ for *mas-5*), which made it difficult to obtain a large number of cytokinetic cells. Throughout the early-to-late solid phragmoplast stages, *trs120-4*, but not *exo84b-2*, mutants showed a defect in cell plate biogenesis (Figures 3D and 3E). Indeed, 84% of *trs120* and *club* cell plates were absent, patchy, thin, or incomplete ($n = 183$), whereas 92% of *exo84b-2* ($n = 48$) and 84% of wild-type ($n = 115$) cell plates appeared complete at this stage. Although *exo84b-2* mutants did not exhibit anomalies at the beginning of cytokinesis, they differed from the wild-type at the end of cytokinesis. In the wild-type, KNOLLE is actively removed from the cell plate as of the late ring-shaped phragmoplast stage, once the plate has fully expanded to reach the lateral walls. In *exo84b-2* mutants, KNOLLE prematurely appeared as a punctate stain at the cell plate, already at early ring-shaped phragmoplast stages (Figure 3F, arrowhead). This was also observed in *trs120-4* mutants, but, in this case, the solid and ring-shaped phragmoplast stages did not considerably differ (compare Figure 3E with Figure 3F).

As cell plate formation was not impaired in *exo84b-2*, possible explanations for the premature removal of KNOLLE include impaired stability or maturation of the cell plate. We reasoned that impaired cell plate stability would result in incomplete cross walls and cell wall stubs. FM4-64 stains, however, failed to detect such defects in *exo84b-2* root meristems, even though stubs have been observed in leaf cells in this mutant, as have guard cells with incomplete ventral walls (Fendrych et al., 2010). As confocal microscopy cannot resolve small cell wall gaps, we applied focused ion beam/scanning electron microscopy (FIB/SEM), which allows for 3D reconstructions of high-resolution images of entire cells (Figure 4). FIB/SEM tomographic data sets failed to reveal reproducible cell wall defects in *exo84b-2* (Figure 4B; $n > 200$ cells), but detected frequent (33%, $n = 33$ cells) stubs and incomplete walls in *trs120-4* mutants (Figure 4C; Figure S4). Transmission electron microscopy (TEM) also failed to reveal reproducible cross wall defects in *exo84b-2* root tips (Figure 4E), but cross walls in *trs120-4* root tips occasionally resembled beads on a string (Figure 4F). In summary, antibody stains, FIB/SEM, and TEM revealed cell plate biogenesis defects in TRAPPII, but not in *exo84b-2*, mutants.

To assess cell plate and cross wall maturation in *exo84b-2*, we carried out a survey with 13 different antibodies against cell wall polysaccharides, including callose, cellulose, xyloglucans, pectins, and α1-acid glycoprotein (AGP) glycans (see Supplemental Experimental Procedures). We focused on methyl-esterified pectins (JIM7 antibody, Clausen et al., 2003), as this labeled the cell plate throughout cytokinesis (Figure 5A, wild-type, left panels), and on AGP glycans (LM14 antibody, Moller et al., 2008) as a good marker for nascent cross walls and mature cell walls. In *club-2* mutants there was almost no JIM7 signal at the cell plate (Figure 5A, middle panels). In *exo84b-2*, cell plate labeling was variable and was often ectopically detected on lateral walls and cross walls (Figure 5A, right panels; Figure 5B), which were rarely detected in the wild-type (Figure 5A, left panels; Figure 5B). In contrast to JIM7, which labeled the cell plate throughout cytokinesis, LM14 was predominantly seen on lateral walls and labeled cell plates only after insertion (as inferred from late ring-shaped phragmoplast microtubules having reached the outer edges of the cell) into the lateral walls in the wild-type (Figure 5C, left panels). In *club-2*, cell walls were often weakly labeled, and LM14-positive compartments were ectopically seen in the cytosol (Figure 5C, middle panels). In *exo84b-2*, the wall stains were somewhat punctate; telophase plates were often labeled to a greater extent than the wild-type, with little signal on lateral walls (Figure 5C, right panels). We conclude that the relative content of methyl-esterified pectins and AGP glycans was altered in the cell plates, cross walls, and lateral walls of both TRAPPII and exocyst mutants.

The TRAPPII Complex Is Required for Protein Sorting at the Cell Plate

We next asked whether the TRAPPII complex is required for the targeting of the exocyst to the cell plate or plasma membrane, and whether, conversely, the exocyst regulates TRAPPII localization. TRS120-GFP targeting to expanding cell plates did not

Developmental Cell
TRAPPII and Exocyst Function in Plant Cytokinesis

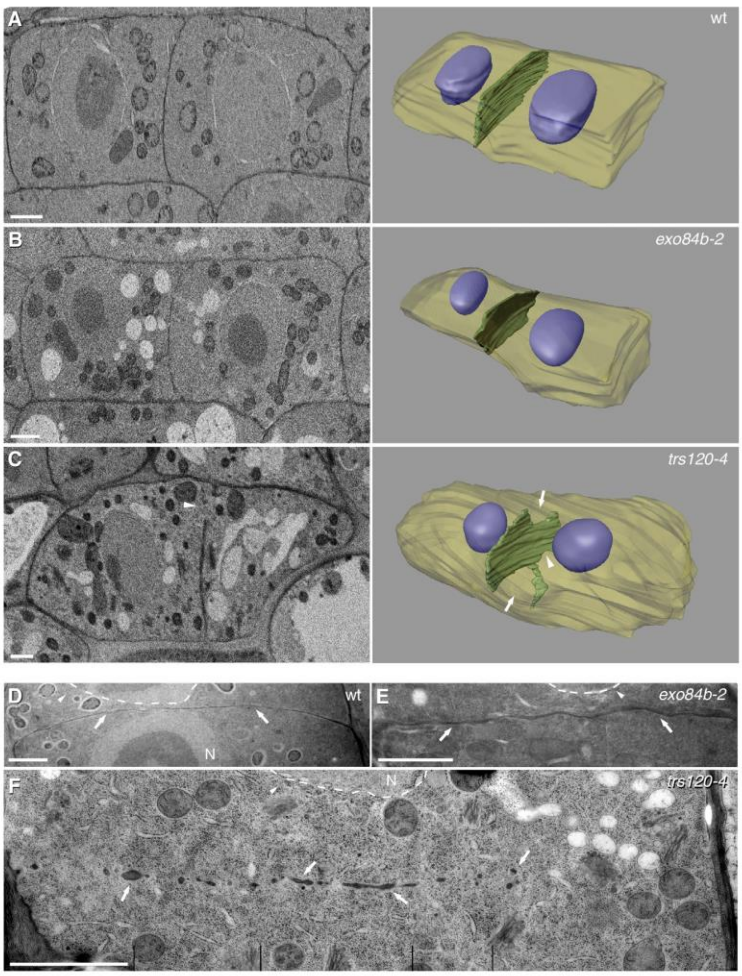

Figure 4. Electron Micrographs of High-Pressure Frozen, Freeze-Substituted 5-Day-Old Root Tips

Wild-type (A and D), *exo84b-2* (B and E), and *trs120-4* (C and F).

(A–C) Single slices of FIB/SEMs are shown on the left and 3D reconstructions of entire stacks on the right.

(B) Note the regular shape of the cell and the complete cross wall, as in the wild-type.

(C) Arrowhead points to the same cell wall gap in the micrograph (left) and 3D reconstruction (right). Arrows point to other gaps in the same cross wall. See Figure S4 for selected micrographs from the same series showing 3D reconstruction.

(D–F) TEMs. Arrowheads point to interphase nuclei, as evidenced by decondensed DNA (N) and a fully formed nuclear envelope (surrounded by a dotted white line). Note the complete cross walls in (D) and (E) and contrast this to the incomplete cross wall in (F; arrows), which has the appearance of beads on a string. Scale bars, 2 μm.

appear to be perturbed in the *exo84b-2* mutant background (Figure S3D). By contrast, EXO84b-GFP had a dramatically altered, punctate appearance in the *club/trs130-2* mutant background (Figure 5D; Figure S5D). The features we invariably detected in the wild-type, namely, a clear membrane signal during cell plate initiation and cross wall maturation versus a diffuse cloud during cell plate expansion, were never seen in *club-2* mutants (n = 100 wild-type and n = 130 *club-2* seedlings). Enrichment factors at expanding cell plates (signal intensity at the cell plate compared to the signal at the plasma membrane and as normalized against FM4-64 values; see Experimental Procedures) were significantly different between the wild-type and *club-2* ($p = 0.004$; Figures 5F and 5G; Figure S5D). This suggests that the TRAPPII complex may, directly or indirectly, be required to target the exocyst to cell plate initials and to maturing cell plates at the onset and end of cytokinesis. It is tempting to speculate that it might also be required to sort the exocyst away from expanding cell plates during the juvenile phase of cytokinesis.

We compared the exocyst subunits with four other plasma membrane proteins: SYP121 and SYP122, and the auxin efflux carriers PIN1 and PIN2 (Collins et al., 2003; Assaad et al., 2004; Benková et al., 2003; Abas et al., 2006). In the wild-type, plasma membrane markers and polysaccharide stains labeled the cell plate, lateral walls, and cross wall compartments differentially (Figures 5A–5F; Figures S5D and S5E). In *club-2* mutants, by contrast, cell plates were labeled with equal relative intensity as the surrounding plasma membrane (Figures 5A–5E and 5G; Figures S5D and S5E). In other words, enrichment factors at the cell plate ranged from 9.5 to 0.3 in the wild-type, but oscillated around 1.0 in *club-2* (compare Figure 5F with Figure 5G). The two markers most enriched at the cell plate in the wild-type, namely, JIM7 and SYP121-GFP, were almost completely absent at both the cell plate and plasma membrane or cell wall in *club-2* mutants (Figures 5A and 5E; Figure S5D). Taken together, the data show that *club/trs130* mutants appeared to have lost the ability to differentially exclude or target membrane proteins from or to the cell plate during different stages of cytokinesis.

The TRAPPII and Exocyst Complexes Physically Interact

The colocalization of the TRAPPII and exocyst complexes at key transitions at the beginning and end of cytokinesis as well as the dependence of exocyst localization on TRAPPII function prompted us to ask whether the two tethering complexes physically interact. The TRAPPII complex consists of nine conserved subunits encoded by ten genes, and the exocyst complex of eight subunits encoded by 36 genes in *Arabidopsis*. To gauge which subunits might interact, we carried out anti-GFP pull-downs of CLUB-GFP and TRS120-GFP fusions in planta and identified

CellPress

Developmental Cell
TRAPPII and Exocyst Function in Plant Cytokinesis

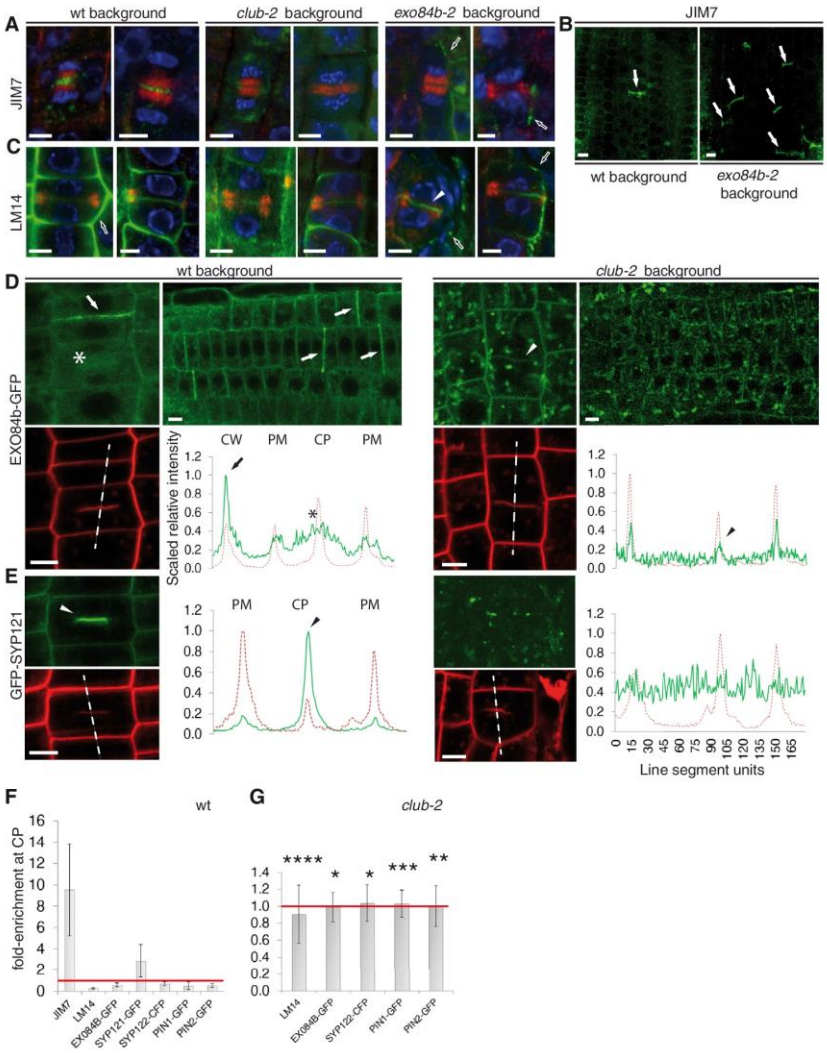

Figure 5. Cell Wall Polysaccharides and Protein Sorting at the Cell Plate

(A–C) Cell wall polysaccharide stains in root tips: DAPI/nucleus (blue), microtubules (red), and JIM7 or LM14 (green).

(A) JIM7 antibody stain. In the wild-type (two left panels), JIM7-positive staining was detected on 97% of cell plates (n = 127). In *club-2* (middle panels), JIM7 staining was absent in 94% of cell plates (n = 68), and in *exo84b-2* (right panels) it was absent from 79% of cell plates (n = 33), but was often detected on lateral walls (white-rimmed black arrow).

(B) Overviews of root tips showing ectopic cross wall stain (arrows) in *exo84b-2* mutants. These were more than 10-fold more frequent in the mutant than in the wild-type, in which a rare event is shown.

(C) LM14 antibody stain. In the wild-type (two left panels), LM14-positive staining was weak or absent in 83% of expanding cell plates (n = 88). In *club-2* (middle panels), LM14 staining was present as of the ring-shaped phragmoplast in 67% of cell plates (n = 12); the stain was often punctate at the cell wall, and cell plates were labeled with the same intensity as lateral and cross walls. In *exo84b-2* (right panels) the stain was often punctate on lateral walls (white-rimmed black arrows; n = 7) and could be seen on nascent cross walls (arrow; n = 6).

(D and E) Protein sorting at the cell plate. Left panels represent the wild-type and right panels *club-2* mutant backgrounds. The line graphs depict scaled relative fluorescence intensity, with FM4-64 (red) used to position the PM, CP, and the CW (arrow). (D) P_{EXO84b}::EXO84b-GFP. Asterisk indicates a cloud in the wild-type (left) and the arrowhead a small peak *club-2* (right); earlier time points show the same localization pattern. (E) P_{SYP121}::GFP-SYP121. Scale bars, 5 μm.

(F and G) Fold-enrichment at the cell plate (compared to PM or CW) in the wild-type (F) and *club-2* (G). Mean ± SD and n ≥ 10 cells, with the following exceptions in (G): n = 5 for EXO84b, n = 5 for SYP122, and n = 8 for PIN1; see Supplemental Experimental Procedures. *p < 0.005, **p < 0.001, ***p < 0.0001, and ****p < 0.00001 (Student's t test).

See also Figures S3 and S5.

the purified proteins by mass spectrometry. This approach yielded ten hits including at least one isoform of each exocyst subunit (Figures 6A and 6B; Figure S6; Table S1). Western blots of the CLUB-GFP and AtTRS120-GFP pull-downs with antibodies against the exocyst subunits EXO84b, EXO70A1, and SEC6 confirmed an interaction between the TRAPPII and exocyst complexes (Figure S7A). In an independent approach, a yeast two-hybrid screen with EXO70H7 as a bait identified AtTRS120, which documents a direct physical interaction between these subunits of the two tethering complexes (Figure S7B). We conclude that the TRAPPII and exocyst complexes physically interact.

An analysis of the proteomics data suggests that only a small pool of the TRAPPII bait interacts with exocyst components. This can be seen by the clustering of the two complexes in scatter plots, with the TRAPPII components consistently having a higher intensity than the exocyst components (Figure 6A; Figure S6A). This could simply be due to a looser association between the two complexes than within a single complex, which would differentially affect the disruption of protein complexes during sample preparation. If the TRAPPII and exocyst were to form a stoichiometric complex in plant cells, however, one might predict that TRAPPII and exocyst mutants would have similar phenotypes, which is not the case. Rather, we observed salient differences between TRAPPII and exocyst mutants: TRAPPII mutants had canonical cytokinesis defects, including bloated cells and incomplete walls (Figures 6D and 6E), whereas *exo84b-2* had a cell wall-related defect, namely, broken walls in vacuolate cells (Fendrych et al., 2010), radial swelling, and isodiametric in lieu of elongated cells, for example in the hypocotyl (Figures 6D and 6G). These features are characteristic of cell wall mutants such as *procuste* and *rsw1* (Fagard et al., 2000; Peng et al., 2000). As the TRAPPII and exocyst subunits do not colocalize in nondividing cells (other than the cytosolic pools; Figure S3C) and only transiently colocalize in dividing cells, the data are consistent with a model whereby the two complexes would transiently interact during key transitions at the onset and end of cytokinesis.

DISCUSSION

Our data support a model for the sequential, yet overlapping, coordinated action of the TRAPPII and exocyst complexes in the regulation of plant cytokinesis (Figure 7). Plant cytokinesis can be broken down into four stages: initiation, biogenesis, expansion, and maturation (Figure 7). At the end of cytokinesis, the cell plate has matured into a cross wall flanked on either side by plasma membranes. Based on their localization patterns, we speculate that the TRAPPII and exocyst complexes coordinate the spatiotemporal regulation of cell plate initiation. Thereafter, the TRAPPII complex gives the juvenile compartment a TGN identity and drives its rapid growth, whereas the exocyst mediates the maturation process that enables the transition from TGN to plasma membrane identity (Figure 7). We propose that this switch in membrane identity drives the observed changes in polysaccharide composition, because the tethering complexes would tether different vesicle populations carrying different cargo to the cell plate or cross wall. Coordination between the complexes is implicated by the observation that the TRAPPII complex sorts the exocyst complex at the cell plate, and by the physical interaction between the complexes. We refer to this model as a "relay race" model, in which two protein complexes act as players in a relay race, each having a different role (as in being responsible for a different lap), and interacting transiently to coordinate transitions (as in passing the buck to each other between laps).

The strong initial signal at the cell plate seen with all exocyst subunits during the phragmoplast assembly stage raises the question as to the role of the exocyst in the initiation of cytokinesis. Electron tomographs of this stage document vesicles tethered by Y-shaped complexes that strongly resemble the exocyst as well as dumbbell-shaped cell plate precursors arising from initial fusion events (Seguí-Simarro et al., 2004; Figure 7). Interestingly, Fendrych et al. (2010) detected aberrant, donut-shaped FM4-64-positive membranes at the equator of root tips cells of *exo70a1* mutants at the onset of cytokinesis, but normal cell plates at later stages. A recent study in budding yeast has shown that the assembly of the exocyst is inhibited during mitosis by the cell-cycle-dependent phosphorylation of Exo84p (Luo et al., 2013). This provides a very interesting link between cell-cycle progression and membrane traffic during mitosis. To avoid bisecting the nucleus, this level of coordination is also required for the initiation of plant cytokinesis, and it will be interesting to see whether this is mediated by the exocyst.

A role for the TRAPPII complex in cell plate biogenesis is substantiated by patchy or incomplete plates and cross walls we detected with TEM, SEM, and confocal microscopy. Consistently, the TRAPPII complex was invariably associated with rapidly expanding regions, initially at the center and at later stages of the cell cycle at the leading edges of the cell plate. Although EXO84b does not appear to be required for cell plate formation, three lines of evidence suggest that it may play a role in cell plate maturation. First, the exocyst localized to the insertion site (Fendrych et al., 2010) and to areas of the cell plate that had already expanded. Second, we observed premature removal of KNOLLE from telophase plates in *exo84b-2*. This phenotype cannot readily be attributed to a general membrane recycling defect, as FM4-64 and TRS120 dynamics in the *exo84b-2* did not differ from that of the wild-type. The loss of KNOLLE as a juvenile trait can be considered as a first important step in the maturation of the cell plate into a cross wall, and its removal is an active process that is likely to require the action of the ESCRT complex (Spitzer et al., 2009). A third line of evidence was the altered relative content of methyl-esterified pectins and of AGP glycans in the cell plates, cross walls, and lateral walls of *exo84b-2* mutant root tips. Pectins are synthesized in the Golgi and deposited in the cell wall in a highly esterified form; in the cell wall, they undergo demethylesterification via a set of enzymes referred to as pectin methylesterases (PMEs) (Clausen et al., 2003). Our observation of JIM7-positive staining at the cell plate throughout cytokinesis supports the view that the cell plate is derived from Golgi/TGN- rather than endocytotic vesicles. This is discrepant with reports from Dhonukshe et al. (2006), but consistent with the observations of Chow et al. (2008). The absence of JIM7-positive staining in *club/trs130* mutant cell plates is yet another line of evidence for a role of the TRAPPII complex in cell plate biogenesis. The ectopic JIM7 staining seen in lateral and cross walls in

Developmental Cell
TRAPPII and Exocyst Function in Plant Cytokinesis

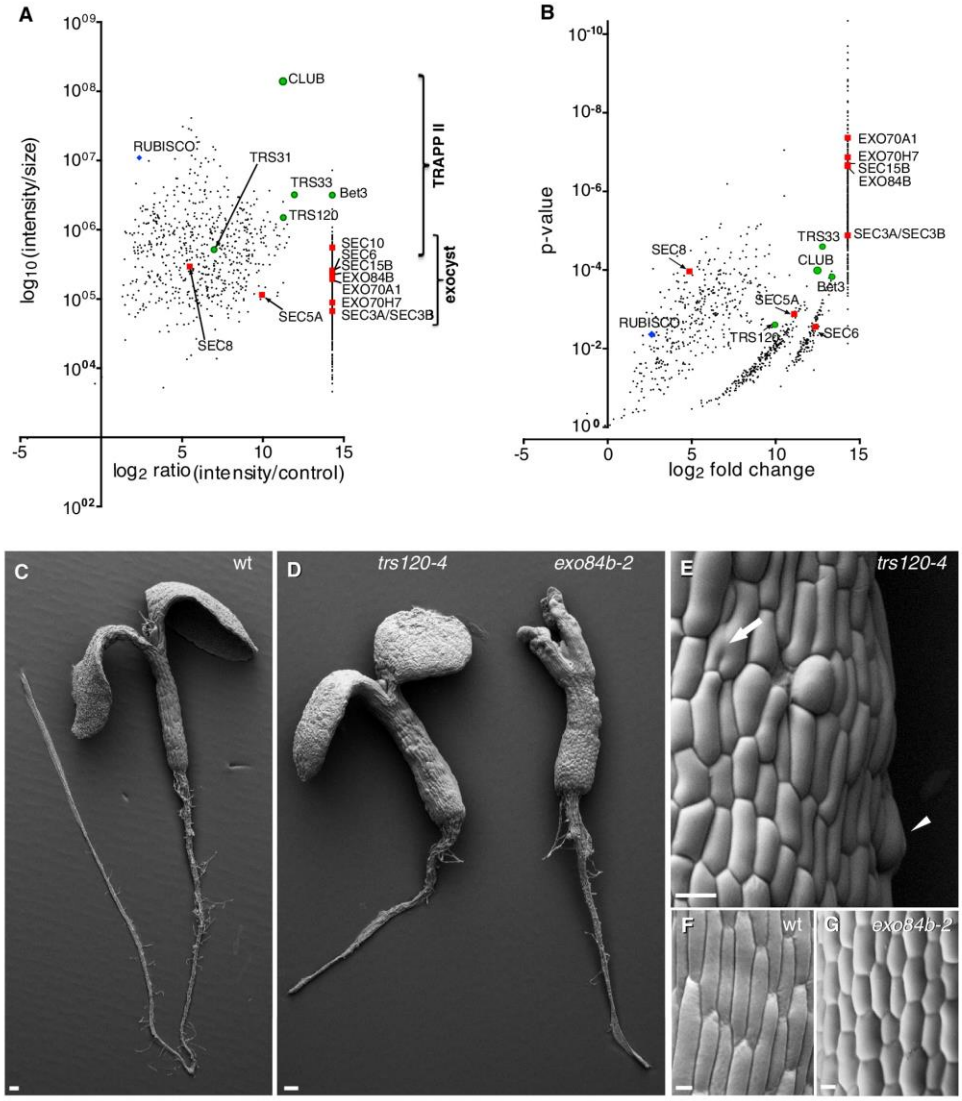

Figure 6. Physical Interaction between the TRAPPII and Exocyst Complexes and Mutant Phenotypes

(A and B) Scatter plots showing all the copurified proteins in a CLUB-GFP immunoprecipitate. Each protein is represented by at least five unique peptides and was present in all three biological replicates. The ratio was calculated for each protein as the intensity of the signal in the experiment divided by its intensity in the soluble GFP empty vector control. Green circles, TRAPPII subunits; red squares, exocyst subunits; blue diamond, rubisco.

(A) Signal intensity (normalized against protein size, $\log_{10}$ scale) against the signal ratio ($\log_2$ scale). The CLUB-GFP bait has the highest intensity, as expected. An artificial line is formed to the right for proteins that had no signal in the control; these were attributed a random value so as not to appear at infinity on the plot. Rubisco is the most abundant protein in plant tissues and was found in the experiment and control at relatively comparable intensities (low $\log_2$ ratio). Note that TRAPPII subunits have a higher average signal intensity than exocyst subunits.

(B) The p value (Student's t test; depicted along a negative $\log_{10}$ scale, but labeled with actual values) is plotted against the signal ratio. Note that a large number of exocyst components have lower p values than the actual bait, due to the fact that they had no signal in the empty vector control. Shown are hits with $p < 0.02$.

(C–G) SEMs of seedlings. (C and D) Overviews. (E–G) Close-ups. (C and F) Wild-type. (D, left; and E) *trs120-4*. In (E) the arrow points to a cell wall stub and the arrowhead to a bloated cell. (D, right; and G) *exo84b-2*. Scale bars, 100 μm (C and D); 20 μm (E–G).

See also Figures S6 and S7.

Developmental Cell
TRAPPII and Exocyst Function in Plant Cytokinesis

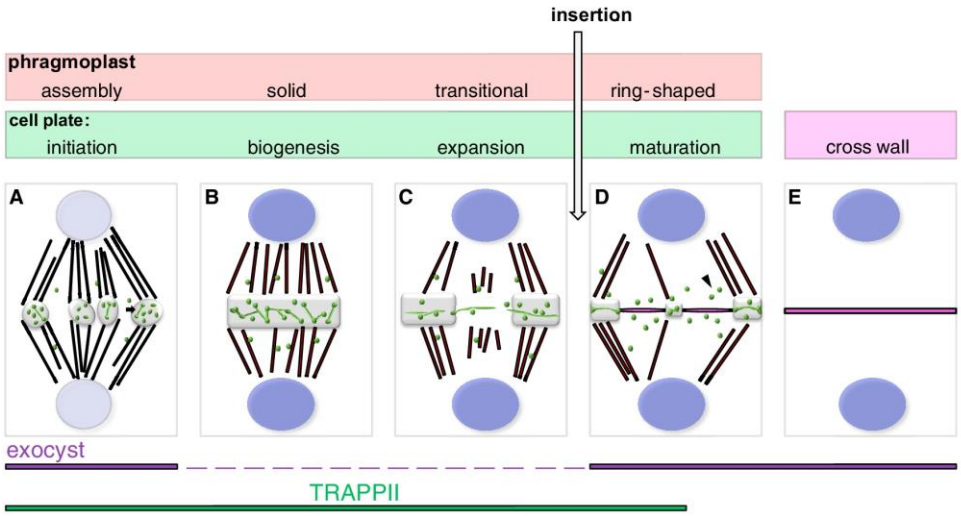

Figure 7. "Relay Race" Model for the Sequential but Overlapping and Coordinated Action of the TRAPPII and Exocyst Complexes
Cytokinesis is broken down into four stages (top, A–D; adapted from Seguí-Simarro et al., 2004 with permission from the American Society of Plant Biologists).
(A) The phragmoplast is assembled from opposite sets of polar spindle microtubules (red rod-like structures). A first round of vesicle fusion gives rise to dumbbell-shaped cell plate initials (arrow).
(B) At the solid phragmoplast stage, cell plate biogenesis occurs within a cell plate assembly matrix (CPAM; gray) via further rounds of membrane fusion.
(C) Cell plate expansion is driven by the reorganization of phragmoplast microtubules and membrane addition at the leading edges of the cell plate.
(D) Insertion occurs once the expanding cell plate has reached the parental walls. This event triggers maturation, which is accompanied by the loss of juvenile traits, including the removal of KNOLLE from cell plate membranes (arrowheads).
(E) At the end of cytokinesis, the cell plate has matured into a cross wall (fuchsia) flanked on either side by plasma membranes (black contour lines).
Bottom: We postulate that the TRAPPII (dark green bar) and exocyst (purple bars) complexes are both required for the initiation of cytokinesis. Thereafter, the TRAPPII complex drives cell plate biogenesis and expansion, and the exocyst complex appears to be required for cell plate maturation (see text for details).
Red, phragmoplast microtubules; green, cell plate membranes; pink, mature cell plates and cross wall; blue, nuclei (light blue, dividing nuclei); gray, CPAM.

exo84b-2 could reflect a deficiency in cell wall PMEs, or a general defect in pectin recycling from mother cell walls.

In addition to a role in cell plate biogenesis, we show in this study that the TRAPPII complex is required for protein sorting at the cell plate. We monitored the localization dynamics of five plasma membrane proteins as well as the presence of a variety of cell wall polysaccharides in the cell plates of wild-type versus *club/trs130* root tips. Contrary to the view that the cell plate acts as a sink for plasma membrane proteins expressed during cytokinesis (Müller et al., 2003), we found that the dozen markers we monitored were differentially localized to the cell plate, plasma membrane, newly formed cross walls, or mature cell walls in the wild-type. By contrast, *club/trs130* mutants appeared to have lost the ability to distinguish between these compartments: the default localization pattern for the membrane or polysaccharide markers we imaged was that they accumulated in intracellular compartments and that they labeled the cell plate with roughly equal relative intensity as the plasma membrane or cross/lateral walls. Mislocalization cannot readily be attributed to cell plate aberrations in *club/trs130* mutants, seeing as we chose among mutant plates ones that had a fairly normal appearance on the basis of FM4-64 staining. Furthermore, sorting did not appear to be affected in other cytokinesis-defective mutants of similar overall appearance (K.R. and F.F.A., unpublished data). A trivial explanation would be that trafficking to the plasma membrane requires prior passage through the TGN, which is a TRAPPII compartment, and that plasma membrane proteins merely accumulate in an endomembrane compartment in TRAPPII mutants; TRAPPII mutants of *Arabidopsis* have in fact been shown to be impaired in Golgi transport to the cell wall (Qi et al., 2011). Although we cannot formally exclude this explanation, we do not feel that it accounts for the highly differential sorting we observed at the cell plate. Of nine plasma membrane markers, for example, the five exocyst subunits were the only ones to be present as a diffuse cloud around the cell plate during the anaphase-telophase transition, yet enriched at cross wall membranes during telophase (see also Fendrych et al., 2010; Zhang et al., 2013). This specific pattern was disrupted in *club/trs130* mutants, as were all other differential localization patterns. Taken together, our data suggest that the TRAPPII complex is required not only for the biogenesis of the cell plate but also for its identity as a transient compartment distinct from newly formed cross walls and mature parental walls.

The *Arabidopsis* ECHIDNA protein is also involved in protein sorting at the cell plate (Gendre et al., 2011). ECHIDNA is thought to be required for the genesis of secretory vesicles at the TGN, and, accordingly, for the secretion of cell wall polysaccharides and for the deposition of de novo-synthesized membrane proteins such as the auxin influx carrier AUX1 at the plasma

CellPress

Developmental Cell
TRAPPII and Exocyst Function in Plant Cytokinesis

membrane (Boutté et al., 2013; Gendre et al., 2013; McFarlane et al., 2013). The trafficking of the auxin efflux carrier PIN3 to the plasma membrane, however, does not require ECHIDNA function (Boutté et al., 2013). Similarly, the TRAPPII complex is required for the polar localization of AUX1 and PIN2, but not PIN1, in root tips (Qi et al., 2011; Qi and Zheng, 2011). These observations highlight the differential regulation of trafficking to the plasma membrane as well as the highly sophisticated nature of post-Golgi trafficking in plants. It will be interesting to see whether ECHIDNA and the TRAPPII complex act in concert and/or in parallel to regulate the diverse functions of the plant TGN.

We postulate that the sequential, coordinated action of the TRAPPII and exocyst complexes may also be required for the spatiotemporal regulation of cytokinesis in fungi and in animals. Mutations in the *bru* gene of *Drosophila*, a TRAPPII-specific Trs120 ortholog, specifically cause failure of cleavage furrow ingression (Robinett et al., 2009). Rab11 localization to the cleavage furrow depends on *bru*, and *bru* and Rab11 interact genetically (Robinett et al., 2009). Although the TRAPPII complex may be required for cleavage furrow ingression, the exocyst appears to be required at the terminal phase of cytokinesis, namely, at the midbody for secretory vesicle-mediated abscission (Gromley et al., 2005; Neto et al., 2013; reviewed by Neto and Gould, 2011). Similarly, in fission yeast exocyst mutants are not defective at early stages of cytokinesis, which include actomyosin ring and division septum assembly, but are specifically impaired in cell separation at the end of cytokinesis (Wang et al., 2002). The exocyst targets hydrolytic enzymes to the septum that in turn digest the primary septum and surrounding wall and thereby enable cell separation (Martín-Cuadrado et al., 2005).

Although cell plate assembly and maturation in plants versus contractile ring and midbody assembly and function in animals comprise very different strategies for cytokinesis, there are some interesting common ancestral components. In the primitive red alga *Cyanidium caldarium* RK-1, for example, cytokinesis occurs by means of a contractile ring (Suzuki et al., 1995). Also, in the alga *Spirogyra* cytokinesis is initiated by a cleavage furrow and completed via a cell plate (McIntosh et al., 1995). Conversely, somatic cytokinesis in higher plants can be considered to be initiated by a cell plate and completed by a centripetal (from the outside in, like the furrow) process (Van Damme et al., 2011). Indeed, cell plate anchoring and insertion into the lateral walls occur via a TGN-independent centripetal recruitment pathway (Van Damme et al., 2011). Regardless of evolutionary considerations, however, we suggest that, across kingdoms, the TRAPPII complex is required to mediate membrane addition during an initial growth phase of cytokinesis, and the exocyst later during cytokinesis for cell separation.

We have suggested a model whereby key transitions in membrane identity and function are mediated by the sequential yet overlapping and coordinated action of two tethering complexes. The cell plate is a transient compartment that, once cytokinesis is completed, matures into a cross wall, flanked on either side by plasma membranes. While the predominant role of the cell plate is growth, the cell wall lends the plant cell positional information, support, and tensile strength, and the plasma membrane represents a highly regulated interface between the inner and outer surfaces of plant cells. Thus, the cell plate is an interesting example of a membrane compartment whose composition and function change as it undergoes biogenesis, expansion, and maturation. There are many other examples for which this is the case. Upon fungal infection, for example, a feeding structure called the haustorium is formed. The haustorium is surrounded by an extrahaustorial membrane, which is contiguous with but distinct from the host plasma membrane (Koh et al., 2005). It will be interesting to see whether the model of sequential coordinated action by two different tethering complexes can be applied to situations other than cytokinesis in which membrane identity and function are sequentially regulated in time and space.

EXPERIMENTAL PROCEDURES

Lines and Growth Conditions

Due to their seedling lethality, mutant lines were propagated as hetero- or hemi-zygotes. Insertion lines were selected via the TAIR and NASC websites (Swarbreck et al., 2008). Plants were grown in the greenhouse throughout the year, under controlled temperature conditions and with supplemental light, or under controlled growth chamber conditions (16/8 hr photoperiod at 250 μmol $m^{-2}s^{-1}$). Seedlings were surface sterilized, stratified at 4°C for 2 days, and plated on Murashige and Skoog medium supplemented with 1% sucrose and B5 vitamins (Sigma). The root tips of 5-day-old plate-grown seedlings were used for light, confocal, and electron microscopies.

Antibody Stains and Confocal Microscopy

Antibody stains were carried out as described by Völker et al. (2001), with anti-KNOLLE (rabbit, 1:2,000; Lauber et al., 1997), anti-tubulin (mouse, 1:2,500; Sigma), JIM7 (rat monoclonal, 1:10; Carbosource), and LM14 (rat monoclonal, 1:10; PlantProbes). Secondary antibodies are described in the Supplemental Experimental Procedures. Nuclei were stained with 1 mg/ml DAPI (Sigma). A FluoView 1000 confocal laser scanning microscope (Olympus) was used as well as a CSU-X1 Yokogawa spinning disk head fitted to a Nikon Ti-E inverted microscope.

Electron Microscopy

For SEM of fresh material, samples were placed onto stubs and examined immediately in low vacuum with a Zeiss (LEO) VP 438 scanning electron microscope operated at 15 kV. Electron micrographs were digitally recorded from the backscattered electron-signal. For electron microscopy, root tips were placed in aluminum platelets, infiltrated with BSA, and fixed by high-pressure freezing (Leica Microsystems HPM100 system). Freeze substitution was performed in acetone with 2% osmium tetroxide and 0.2% uranyl acetate, including 5% water. The FIB serial sectioning was performed using a Zeiss-Auriga workstation. FIB/SEM tomographic data sets were obtained via the "slice and view" technique using a Zeiss Auriga 60 dual-beam instrument. A Zeiss EM912 Omega transmission electron microscope was used for TEM.

Coimmunoprecipitation

Coimmunoprecipitation experiments were carried out on 3 g of inflorescences using GFP-trap beads (Chromotek), as described by Park et al. (2012), with the following modifications: we supplemented both the lysis and washing buffers with a protease inhibitor cocktail for plants (Sigma-Aldrich P9599) and added 1 mM phenylmethanesulfonylfluoride every 45 min. An inhibitor of proteasome activity (Sigma-Aldrich C2211) was also added to the lysis buffer. The washing buffer (50 mM Tris [pH 7.5] and 0.2% [v/v] Triton X-100) was supplemented with 200 mM NaCl. Cell fractionation, mass spectrometry, peptide and protein identification, data analysis, and western blot procedures are described in the Supplemental Experimental Procedures.

Statistics and Image Analysis

The p values were determined with the Student's two-tailed t test and set at a cutoff of 2%. Images were processed with Adobe Photoshop and assembled with Adobe Illustrator. 3D reconstructions were carried out with Imaris software (Bitplane). Images were analyzed with ImageJ (NIH). Line graphs of

Developmental Cell
TRAPPII and Exocyst Function in Plant Cytokinesis

mean signal intensities (Figure 2) were corrected for photobleaching during the course of a time lapse. Enrichment factors (Figure 5) were computed as mean signal intensity at the cell plate divided by the mean signal intensity at the plasma membrane or cell wall. For the plasma membrane markers, these values were normalized against FM4-64 cell plate/plasma membrane intensities. The entire cell plate and surrounding plasma membrane or cell wall were traced, where these were clearly delineated; these criteria excluded JIM7 and SYP121 in *club-2* mutants as these had a punctate appearance and failed to label either the cell plate or the cell wall/plasma membrane compartments. We used at least ten cells per measurement in the wild-type, but in *club-2* mutants the sample size was lower in three cases (see figure legend). This is due to the difficulty of detecting cell plates in a mutant with a low mitotic index that is impaired in cell plate biogenesis and FM4-64 uptake. Thus, in the case of EXO84b-GFP, we were only able to detect five cell plates in 130 mutant seedlings.

SUPPLEMENTAL INFORMATION

Supplementary Information includes Supplemental Experimental Procedures, seven figures, one table, and three movies and can be found with this article online at http://dx.doi.org/10.1016/j.devcel.2014.04.029.

ACKNOWLEDGMENTS

We thank Prof. Grill and members of the Botany Department for support. Silvia Dobler helped with sample preparation. Matyas Fendrych prepared the EXO84b antibody. Alex Ivakov helped with spinning disk confocal microscopy. Ngoc Nguyen provided technical assistance. We thank TAIR and NASC for insertion lines. Thanks to Heather McFarlane for useful suggestions and a critical evaluation of the manuscript. We are grateful to Eva Benkova and Christian Luschnig for sharing published resources. Distribution of the JIM7 antibody was supported in part by NSF grant DBI-0421683 and RCN 009281. K.R. and A.S. were supported by DFG grants AS110/4-6 and AS110/5-1; L.S. and V.Z. by Czech Science Foundation grants GPP501/11/P853 and GACR P305/11/1629, respectively; and I.K. by a Charles University grant (Prague project 658112). S.P. was funded by the Max Planck Gesellschaft. This research was funded by DFG grants to F.F.A. and G.W.

Received: August 2, 2013
Revised: February 13, 2014
Accepted: April 25, 2014
Published: May 29, 2014

REFERENCES

Abas, L., Benjamins, R., Malenica, N., Paciorek, T., Wiśniewska, J., Moulinier-Anzola, J.C., Sieberer, T., Friml, J., and Luschnig, C. (2006). Intracellular trafficking and proteolysis of the Arabidopsis auxin-efflux facilitator PIN2 are involved in root gravitropism. Nat. Cell Biol. *8*, 249–256.

Assaad, F.F., Qiu, J.L., Youngs, H., Ehrhardt, D., Zimmerli, L., Kalde, M., Wanner, G., Peck, S.C., Edwards, H., Ramonell, K., et al. (2004). The PEN1 syntaxin defines a novel cellular compartment upon fungal attack and is required for the timely assembly of papillae. Mol. Biol. Cell *15*, 5118–5129.

Benková, E., Michniewicz, M., Sauer, M., Teichmann, T., Seifertová, D., Jürgens, G., and Friml, J. (2003). Local, efflux-dependent auxin gradients as a common module for plant organ formation. Cell *115*, 591–602.

Boutté, Y., Jonsson, K., McFarlane, H.E., Johnson, E., Gendre, D., Swarup, R., Friml, J., Samuels, L., Robert, S., and Bhalerao, R.P. (2013). ECHIDNA-mediated post-Golgi trafficking of auxin carriers for differential cell elongation. Proc. Natl. Acad. Sci. USA *110*, 16259–16264.

Chow, C.-M., Neto, H., Foucart, C., and Moore, I. (2008). Rab-A2 and Rab-A3 GTPases define a trans-golgi endosomal membrane domain in Arabidopsis that contributes substantially to the cell plate. Plant Cell *20*, 101–123.

Clausen, M.H., Willats, W.G., and Knox, J.P. (2003). Synthetic methyl hexagalacturonate hapten inhibitors of anti-homogalacturonan monoclonal antibodies LM7, JIM5 and JIM7. Carbohydr. Res. *338*, 1797–1800.

Collins, N.C., Thordal-Christensen, H., Lipka, V., Bau, S., Kombrink, E., Qiu, J.L., Hückelhoven, R., Stein, M., Freialdenhoven, A., Somerville, S.C., and Schulze-Lefert, P. (2003). SNARE-protein-mediated disease resistance at the plant cell wall. Nature *425*, 973–977.

Cutler, S.R., and Ehrhardt, D.W. (2002). Polarized cytokinesis in vacuolate cells of Arabidopsis. Proc. Natl. Acad. Sci. USA *99*, 2812–2817.

Cvrckova, F., Elias, M., Hala, M., Obermeyer, G., and Zarsky, V. (2001). Small GTPases and conserved signalling pathways in plant cell morpho-genesis: from exocytosis to the exocyst. In Cell Biology of Plant and Fungal Tip Growth, A. Geitmann, M. Cresti, and I.B. Heath, eds. (Amsterdam: IOS Press), pp. 105–122.

Dhonukshe, P., Baluska, F., Schlicht, M., Hlavacka, A., Samaj, J., Friml, J., and Gadella, T.W., Jr. (2006). Endocytosis of cell surface material mediates cell plate formation during plant cytokinesis. Dev. Cell *10*, 137–150.

Fagard, M., Desnos, T., Desprez, T., Goubet, F., Refregier, G., Mouille, G., McCann, M., Rayon, C., Vernhettes, S., and Höfte, H. (2000). PROCUSTE1 encodes a cellulose synthase required for normal cell elongation specifically in roots and dark-grown hypocotyls of Arabidopsis. Plant Cell *12*, 2409–2424.

Fendrych, M., Synek, L., Pecenková, T., Toupalová, H., Cole, R., Drdová, E., Nebesárová, J., Sedinová, M., Hála, M., Fowler, J.E., and Zársky, V. (2010). The Arabidopsis exocyst complex is involved in cytokinesis and cell plate maturation. Plant Cell *22*, 3053–3065.

Fendrych, M., Synek, L., Pecenková, T., Drdová, E.J., Sekeres, J., de Rycke, R., Nowack, M.K., and Zársky, V. (2013). Visualization of the exocyst complex dynamics at the plasma membrane of Arabidopsis thaliana. Mol. Biol. Cell *24*, 510–520.

Gendre, D., Oh, J., Boutté, Y., Best, J.G., Samuels, L., Nilsson, R., Uemura, T., Marchant, A., Bennett, M.J., Grebe, M., and Bhalerao, R.P. (2011). Conserved Arabidopsis ECHIDNA protein mediates trans-Golgi-network trafficking and cell elongation. Proc. Natl. Acad. Sci. USA *108*, 8048–8053.

Gendre, D., McFarlane, H.E., Johnson, E., Mouille, G., Sjödin, A., Oh, J., Levesque-Tremblay, G., Watanabe, Y., Samuels, L., and Bhalerao, R.P. (2013). Trans-Golgi network localized ECHIDNA/Ypt interacting protein complex is required for the secretion of cell wall polysaccharides in Arabidopsis. Plant Cell *25*, 2633–2646.

Gromley, A., Yeaman, C., Rosa, J., Redick, S., Chen, C.-T., Mirabelle, S., Guha, M., Sillibourne, J., and Doxsey, S.J. (2005). Centriolin anchoring of exocyst and SNARE complexes at the midbody is required for secretory-vesicle-mediated abscission. Cell *123*, 75–87.

Gutierrez, R., Lindeboom, J.J., Paredez, A.R., Emons, A.M.C., and Ehrhardt, D.W. (2009). Arabidopsis cortical microtubules position cellulose synthase delivery to the plasma membrane and interact with cellulose synthase trafficking compartments. Nat. Cell Biol. *11*, 797–806.

Heider, M.R., and Munson, M. (2012). Exorcising the exocyst complex. Traffic *13*, 898–907.

Jaber, E., Thiele, K., Kindzierski, V., Loderer, C., Rybak, K., Jürgens, G., Mayer, U., Söllner, R., Wanner, G., and Assaad, F.F. (2010). A putative TRAPPII tethering factor is required for cell plate assembly during cytokinesis in Arabidopsis. New Phytol. *187*, 751–763.

Koh, S., André, A., Edwards, H., Ehrhardt, D., and Somerville, S. (2005). Arabidopsis thaliana subcellular responses to compatible Erysiphe cichoracearum infections. Plant J. *44*, 516–529.

Lauber, M.H., Waizenegger, I., Steinmann, T., Schwarz, H., Mayer, U., Hwang, I., Lukowitz, W., and Jürgens, G. (1997). The Arabidopsis KNOLLE protein is a cytokinesis-specific syntaxin. J. Cell Biol. *139*, 1485–1493.

Luo, G., Zhang, J., Luca, F.C., and Guo, W. (2013). Mitotic phosphorylation of Exo84 disrupts exocyst assembly and arrests cell growth. J. Cell Biol. *202*, 97–111.

Martín-Cuadrado, A.B., Morrell, J.L., Konomi, M., An, H., Petit, C., Osumi, M., Balasubramanian, M., Gould, K.L., Del Rey, F., and de Aldana, C.R. (2005). Role of septins and the exocyst complex in the function of hydrolytic enzymes responsible for fission yeast cell separation. Mol. Biol. Cell *16*, 4867–4881.

McFarlane, H.E., Watanabe, Y., Gendre, D., Carruthers, K., Levesque-Tremblay, G., Haughn, G.W., Bhalerao, R.P., and Samuels, L. (2013). Cell

wall polysaccharides are mislocalized to the Vacuole in *echidna* mutants. Plant Cell Physiol. *54*, 1867–1880.

McIntosh, K., Pickett-Heaps, J.D., and Gunning, B.E.S. (1995). Cytokinesis in Spirogyra: Integration of Cleavage and Cell-Plate Formation. Int. J. Plant Sci. *156*, 1–8.

McMichael, C.M., and Bednarek, S.Y. (2013). Cytoskeletal and membrane dynamics during higher plant cytokinesis. New Phytol. *197*, 1039–1057.

Mineyuki, Y., and Gunning, B.E.S. (1990). A role for preprophase bands of microtubules in maturation of new cell walls, and a general proposal on the function of the preprophase band sites in cell division in higher plants. J. Cell Sci. *97*, 527–537.

Moller, I., Marcus, S.E., Haeger, A., Verhertbruggen, Y., Verhoef, R., Schols, H., Ulvskov, P., Mikkelsen, J.D., Knox, J.P., and Willats, W. (2008). High-throughput screening of monoclonal antibodies against plant cell wall glycans by hierarchical clustering of their carbohydrate microarray binding profiles. Glycoconj. J. *25*, 37–48.

Moore, P.J., and Staehelin, L.A. (1988). Immunogold localization of the cell-wall-matrix polysaccharides rhamnogalacturonan I and xyloglucan during cell expansion and cytokinesis inTrifolium pratense L.; implication for secretory pathways. Planta *174*, 433–445.

Müller, I., Wagner, W., Völker, A., Schellmann, S., Nacry, P., Küttner, F., Schwarz-Sommer, Z., Mayer, U., and Jürgens, G. (2003). Syntaxin specificity of cytokinesis in Arabidopsis. Nat. Cell Biol. *5*, 531–534.

Neto, H., and Gould, G.W. (2011). The regulation of abscission by multi-protein complexes. J. Cell Sci. *124*, 3199–3207.

Neto, H., Kaupisch, A., Collins, L.L., and Gould, G.W. (2013). Syntaxin 16 is a master recruitment factor for cytokinesis. Mol. Biol. Cell *24*, 3663–3674.

Park, M., Touihri, S., Müller, I., Mayer, U., and Jürgens, G. (2012). Sec1/Munc18 protein stabilizes fusion-competent syntaxin for membrane fusion in Arabidopsis cytokinesis. Dev. Cell *22*, 989–1000.

Peng, L., Hocart, C.H., Redmond, J.W., and Williamson, R.E. (2000). Fractionation of carbohydrates in Arabidopsis root cell walls shows that three radial swelling loci are specifically involved in cellulose production. Planta *211*, 406–414.

Qi, X., and Zheng, H. (2011). Arabidopsis TRAPPII is functionally linked to Rab-A, but not Rab-D in polar protein trafficking in trans-Golgi network. Plant Signal. Behav. *6*, 1679–1683.

Qi, X., Kaneda, M., Chen, J., Geitmann, A., and Zheng, H. (2011). A specific role for Arabidopsis TRAPPII in post-Golgi trafficking that is crucial for cytokinesis and cell polarity. Plant J. *68*, 234–248.

Robinett, C.C., Giansanti, M.G., Gatti, M., and Fuller, M.T. (2009). TRAPPII is required for cleavage furrow ingression and localization of Rab11 in dividing male meiotic cells of Drosophila. J. Cell Sci. *122*, 4526–4534.

Samuels, A.L., Giddings, T.H., Jr., and Staehelin, L.A. (1995). Cytokinesis in tobacco BY-2 and root tip cells: a new model of cell plate formation in higher plants. J. Cell Biol. *130*, 1345–1357.

Seguí-Simarro, J.M., Austin, J.R., 2nd, White, E.A., and Staehelin, L.A. (2004). Electron tomographic analysis of somatic cell plate formation in meristematic cells of Arabidopsis preserved by high-pressure freezing. Plant Cell *16*, 836–856.

Söllner, R., Glässer, G., Wanner, G., Somerville, C.R., Jürgens, G., and Assaad, F.F. (2002). Cytokinesis-defective mutants of Arabidopsis. Plant Physiol. *129*, 678–690.

Spitzer, C., Reyes, F.C., Buono, R., Sliwinski, M.K., Haas, T.J., and Otegui, M.S. (2009). The ESCRT-related CHMP1A and B proteins mediate multivesicular body sorting of auxin carriers in Arabidopsis and are required for plant development. Plant Cell *21*, 749–766.

Suzuki, K., Kawazu, T., Mita, T., Takahashi, H., Itoh, R., Toda, K., and Kuroiwa, T. (1995). Cytokinesis by a contractile ring in the primitive red alga Cyanidium caldarium RK-1. Eur. J. Cell Biol. *67*, 170–178.

Swarbreck, D., Wilks, C., Lamesch, P., Berardini, T.Z., Garcia-Hernandez, M., Foerster, H., Li, D., Meyer, T., Muller, R., Ploetz, L., et al. (2008). The Arabidopsis Information Resource (TAIR): gene structure and function annotation. Nucleic Acids Res. *36* (Database issue), D1009–D1014.

Synek, L., Schlager, N., Eliás, M., Quentin, M., Hauser, M.-T., and Zárský, V. (2006). AtEXO70A1, a member of a family of putative exocyst subunits specifically expanded in land plants, is important for polar growth and plant development. Plant J. *48*, 54–72.

Thellmann, M., Rybak, K., Thiele, K., Wanner, G., and Assaad, F.F. (2010). Tethering factors required for cytokinesis in Arabidopsis. Plant Physiol. *154*, 720–732.

Thiele, K., Wanner, G., Kindzierski, V., Jürgens, G., Mayer, U., Pachl, F., and Assaad, F.F. (2009). The timely deposition of callose is essential for cytokinesis in Arabidopsis. Plant J. *58*, 13–26.

Van Damme, D., Gadeyne, A., Vanstraelen, M., Inzé, D., Van Montagu, M.C., De Jaeger, G., Russinova, E., and Geelen, D. (2011). Adaptin-like protein TPLATE and clathrin recruitment during plant somatic cytokinesis occurs via two distinct pathways. Proc. Natl. Acad. Sci. USA *108*, 615–620.

Völker, A., Stierhof, Y.D., and Jürgens, G. (2001). Cell cycle-independent expression of the Arabidopsis cytokinesis-specific syntaxin KNOLLE results in mistargeting to the plasma membrane and is not sufficient for cytokinesis. J. Cell Sci. *114*, 3001–3012.

Wang, H., Tang, X., Liu, J., Trautmann, S., Balasundaram, D., McCollum, D., and Balasubramanian, M.K. (2002). The multiprotein exocyst complex is essential for cell separation in Schizosaccharomyces pombe. Mol. Biol. Cell *13*, 515–529.

Wu, J., Tan, X., Wu, C., Cao, K., Li, Y., and Bao, Y. (2013). Regulation of cytokinesis by exocyst subunit SEC6 and KEULE in Arabidopsis thaliana. Mol. Plant *6*, 1863–1876.

Yu, S., and Liang, Y. (2012). A trapper keeper for TRAPP, its structures and functions. Cell. Mol. Life Sci. *69*, 3933–3944.

Yu, X., Prekeris, R., and Gould, G.W. (2007). Role of endosomal Rab GTPases in cytokinesis. Eur. J. Cell Biol. *86*, 25–35.

Zhang, Y., Immink, R., Liu, C.-M., Emons, A.M., and Ketelaar, T. (2013). The Arabidopsis exocyst subunit SEC3A is essential for embryo development and accumulates in transient puncta at the plasma membrane. New Phytol. *199*, 74–88.

Supplemental Information

Supplemental Data

Supplemental Experimental Procedures

Supplemental References

Supplemental Data

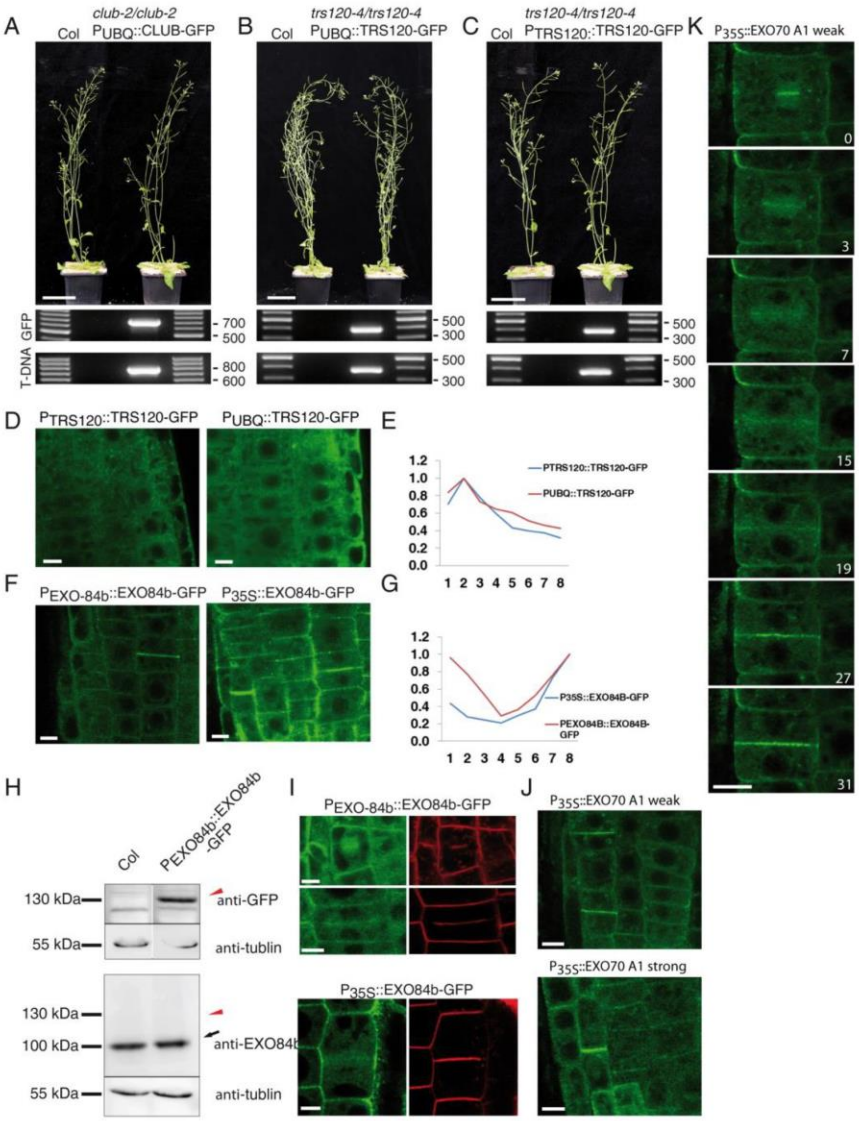

Figure S1. Fusion protein functionality, expression levels and localization dynamics (related to Figures 1 and 2).

(A-C) Complementation analysis. In each panel, the rescued mutant (right) did not differ from the wild type Columbia control (left). PCR analysis (see Supplemental Experimental Procedures) was used to detect the presence of the GFP fusions and to assess the genotype of the plants (presence or absence of T-DNA insertion).
(A) *club-2/club-2* hemizygous for P_{UBQ}::CLUB-GFP
(B) *trs120-4/trs120-4* hemizygous for P_{UBQ}::TRS120-GFP
(C) *trs120-4/trs120-4* hemizygous for P_{TRS120}::TRS120-GFP

(D-K) The effect of fusion protein expression levels on localization dynamics. Confocal settings and image processing were the same for D, F and J, such that the fluorescence intensity can be compared between the lines. See Movies S1-S3 for localization dynamics.
(D, E) TRS120-GFP fusions (see Movie S1). (D) P_{TRS120}::TRS120-GFP (left) and P_{UBQ}::TRS120-GFP (right). (E) The circa three-fold difference in TRS120-GFP fusion protein expression levels had no reproducible effect on localization dynamics throughout cytokinesis. Blue: Endogenous promoter. Red: Ubiquitin promoter.
(F, G) EXO84b-GFP fusions (see Movie S2). (F) P_{EXO84b}::EXO84b-GFP (left) and P_{35S}:: EXO84b -GFP (Fendrych et al., 2010; right). (G) The circa two-fold difference in EXO84b-GFP fusion protein expression levels had no reproducible effect on localization dynamics throughout cytokinesis. Blue: Endogenous promoter. Red: P35S promoter.
(H) Western blots with antibodies against GFP, EXO84B and alpha tubulin as a loading control. The P_{EXO84b}::EXO84b-GFP fusion protein (red arrowhead) is clearly visible with the GFP antibody but not detected with the anti-EXO84b antibody at exposure levels that readily detect the endogenous protein (black arrow) in the same sample. Thus, the GFP fusion protein expression levels were considerably weaker than the endogenous protein, which is consistent with its low fluorescence intensity.
(I) A diffuse cloud is seen throughout the cell plate biogenesis (top panel) and expansion stages (middle and lower panels), and with both promoters. P_{EXO84b}::EXO84b-GFP (top and middle) and P_{35S}::EXO84b-GFP (bottom). The plates shown in the middle and bottom panels are almost fully expanded, just prior to insertion.
(J, K) P_{35S}::EXO70A1-GFP fusions (see Movie S3). (J) Weakly expressing line (top); strongly expressing line (bottom). (K) Time lapse of weakly expressing line shown in (J).

Bars = 5 cm in (A-C) and 5 µm in (D-K).

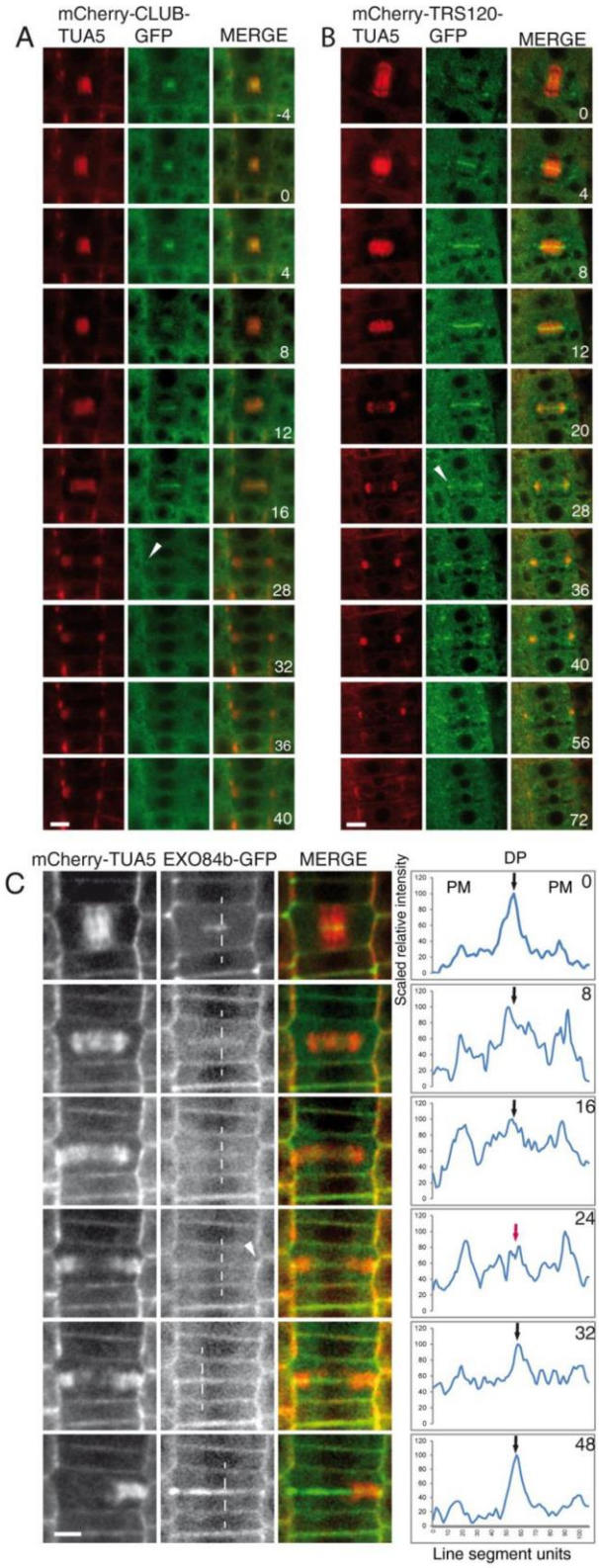
A
mCherry-CLUB-TUA5
GFP
MERGE
-4
0
4
8
12
16
28
32
36
40
B
mCherry-TRS120-TUA5
GFP
MERGE
0
4
8
12
20
28
36
40
56
72
C
mCherry-TUA5
EXO84b-GFP
MERGE
DP
PM
PM
0
8
16
24
32
48
Scaled relative intensity
Line segment units

Figure S2. CLUB-GFP, TRS120-GFP and EXO84b-GFP and phragmoplast microtubule localization dynamics throughout cytokinesis (related to Figures 1 and 2).

Time lapses of GFP fusions with mCherry-TUA5 are shown, with minutes indicated in the rightmost panel.

(A,B) TRAPPII gene fusions imaged with a CSLM. Arrowheads point to the leading edge of the cell plate, where P_{UBQ}::CLUB-GFP (A) and P_{UBQ}::TRS120-GFP (B) have relocated at the ring-shaped phragmoplast stage. Note that the TRS120-GFP signal is sharper and brighter than that of CLUB-GFP. The 0 min time point corresponds to cell plate initiation.

(C) P_{EXO84b}::EXO84b-GFP imaged with a spinning disk confocal microscope. Z stack projections are shown. Arrowhead in the second panel (at 24 min) points to the insertion site in the lateral walls. The line graphs represent the relative signal intensity. The arrow points to the division plane (DP). PM: plasma membrane. Note the dip at the division plane at 24 minutes, suggesting that EXO84b-GFP is sorted away from the cell plate at this time point (red arrow). Clear peaks at the division plane can be seen at the onset of cytokinesis (0 min) and at the cross wall at the end of cytokinesis (48 min).

Bars = 5 µm.

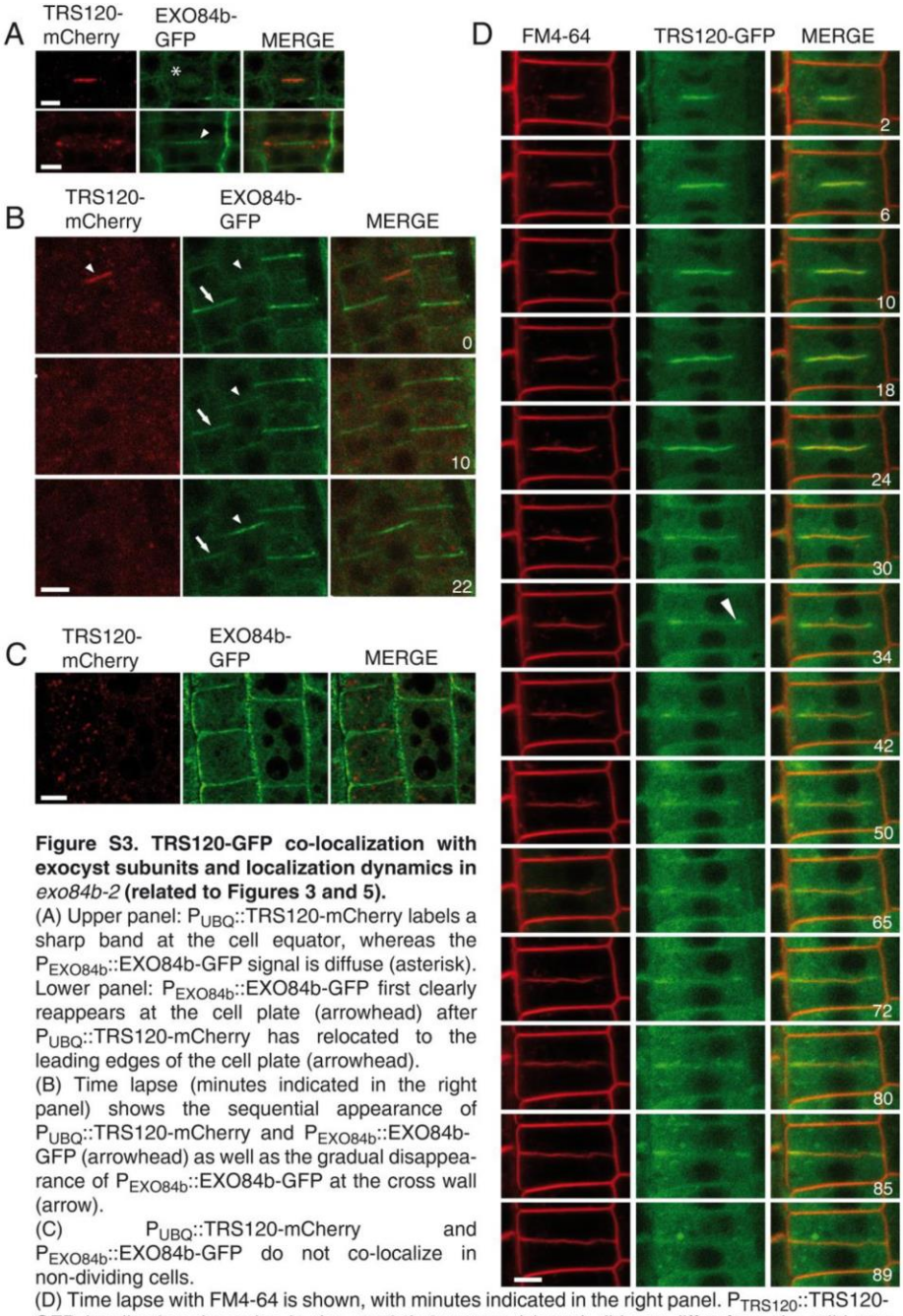

Figure S3. TRS120-GFP co-localization with exocyst subunits and localization dynamics in *exo84b-2* (related to Figures 3 and 5).
(A) Upper panel: P_{UBQ}::TRS120-mCherry labels a sharp band at the cell equator, whereas the P_{EXO84b}::EXO84b-GFP signal is diffuse (asterisk). Lower panel: P_{EXO84b}::EXO84b-GFP first clearly reappears at the cell plate (arrowhead) after P_{UBQ}::TRS120-mCherry has relocated to the leading edges of the cell plate (arrowhead).
(B) Time lapse (minutes indicated in the right panel) shows the sequential appearance of P_{UBQ}::TRS120-mCherry and P_{EXO84b}::EXO84b-GFP (arrowhead) as well as the gradual disappearance of P_{EXO84b}::EXO84b-GFP at the cross wall (arrow).
(C) P_{UBQ}::TRS120-mCherry and P_{EXO84b}::EXO84b-GFP do not co-localize in non-dividing cells.
(D) Time lapse with FM4-64 is shown, with minutes indicated in the right panel. P_{TRS120}::TRS120-GFP localization dynamics in the *exo84b-2* mutant (shown) did not differ from the wild type (compare to Figure 2B). Note relocalization of the signal to the leading edges of the cell plate (arrowhead at 34 min), as in the wild type (Figure 2B).
Bars = 5 µm.

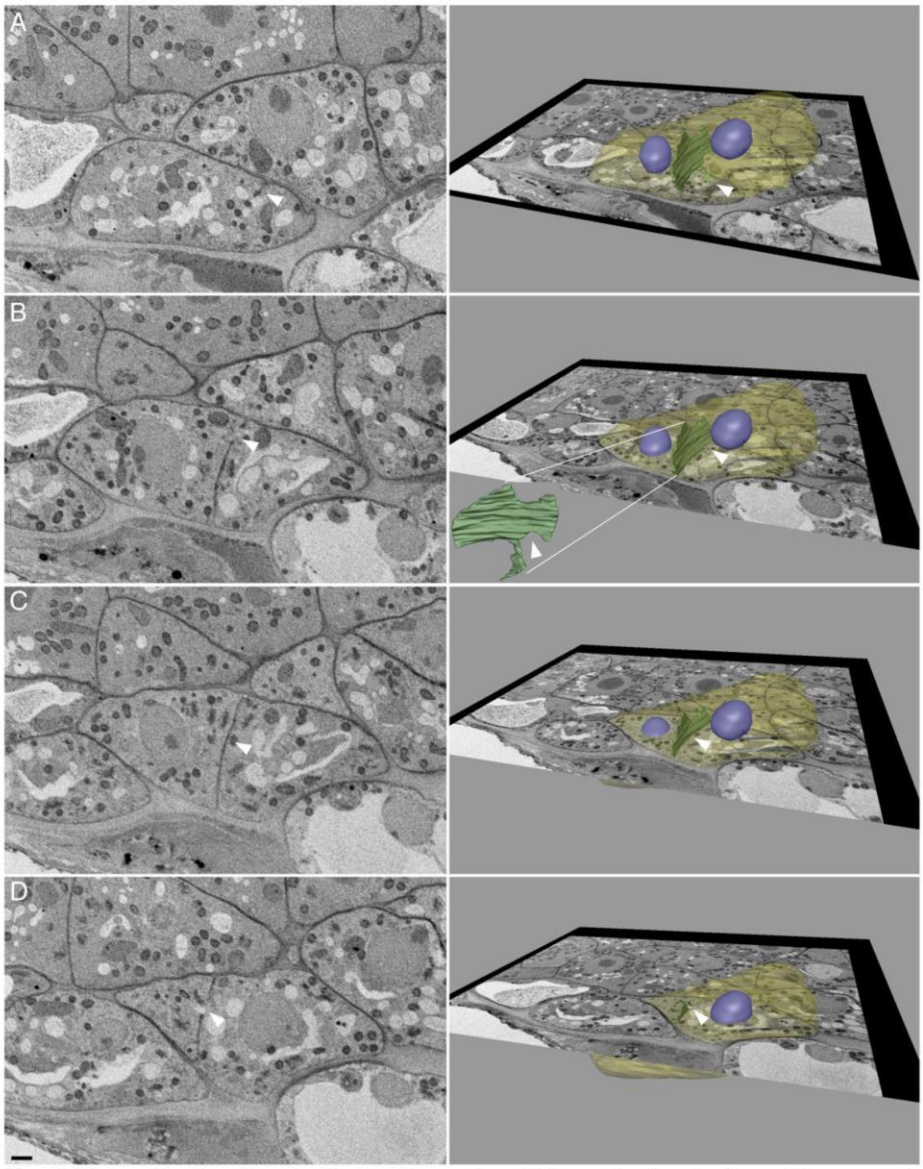

Figure S4. Focused Ion Beam/Scanning Electron Micrographs and 3D reconstruction of an incomplete cross wall in *trs120-4* (related to Figure 4).
(A-D) Selected slices of a single stack. Electron micrographs are shown on the left and 3D reconstructions on the right. Arrowheads point to different features of the same cross wall.
(A) Cell wall stub.
(B) Cell wall gap.
(C) Complete cross wall.
(D) Cell wall gap (distinct from B).
Bar = 2 µm

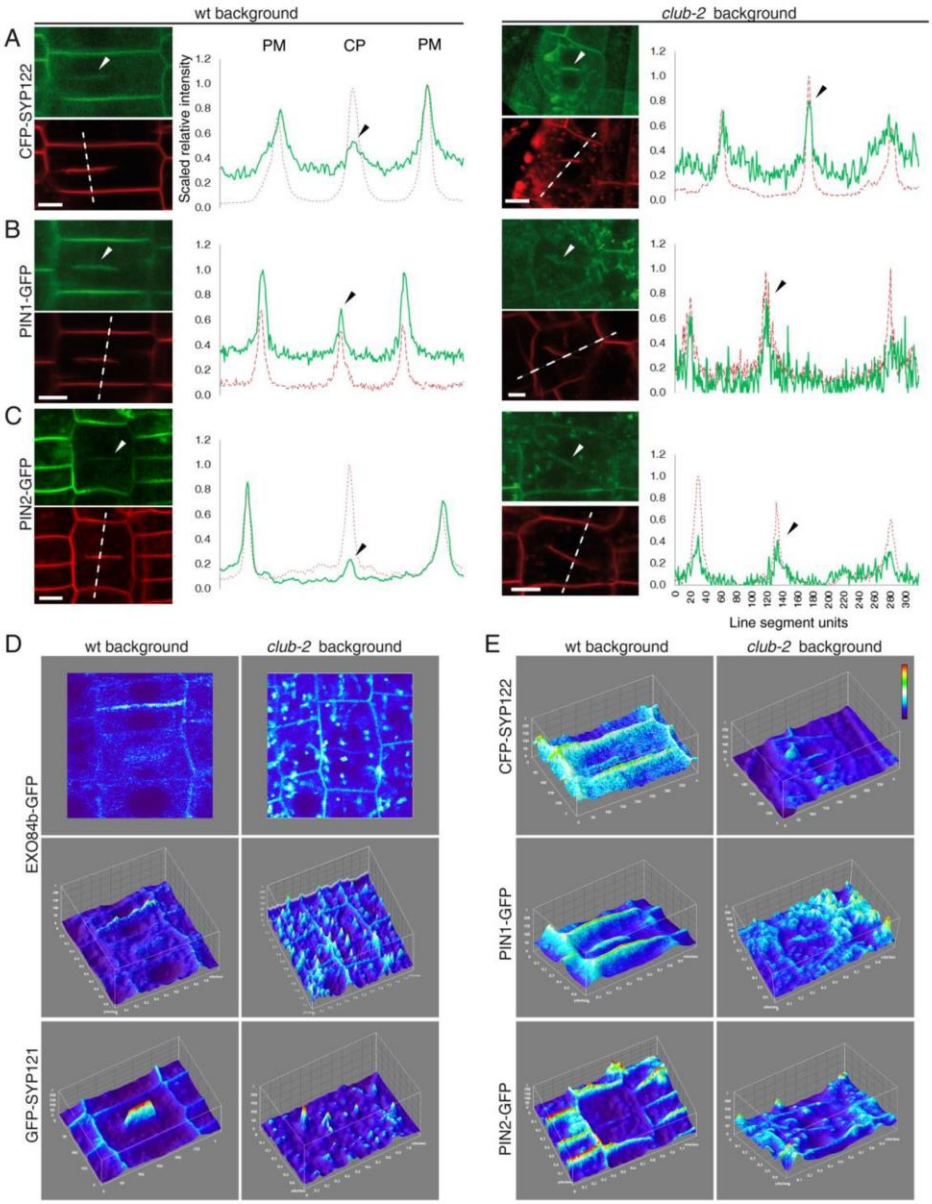

Figure S5. Protein sorting at the cell plate (related to Figure 5).
(A-E) Left panels represent the wild type and right panels *club-2* mutant backgrounds. The line graphs depict scaled relative fluorescence intensity, with FM4-64 (red) used to position the plasma membranes (PM) and cell plate (CP).
(A) P_{35S}::CFP-SYP122.
(B) P_{PIN1}::PIN1-GFP.
(C) P_{PIN2}::PIN2-GFP.
Arrowheads point to signal at the cell plate. Note the punctate appearance of all plasma membrane markers in *club-2*. Bars = 5 µm.
(D, E). Heatmaps of panels in Figure 5D and 5E (D) and S5A-S5C (E). Only the green (GFP or CFP) channels are shown. These 2D or 3D graphical representations show that the signal intensity is fairly uniform along entire cell plates. Bar in panel E (upper right) depicts signal intensity, with red for maximum and blue for minimum levels.

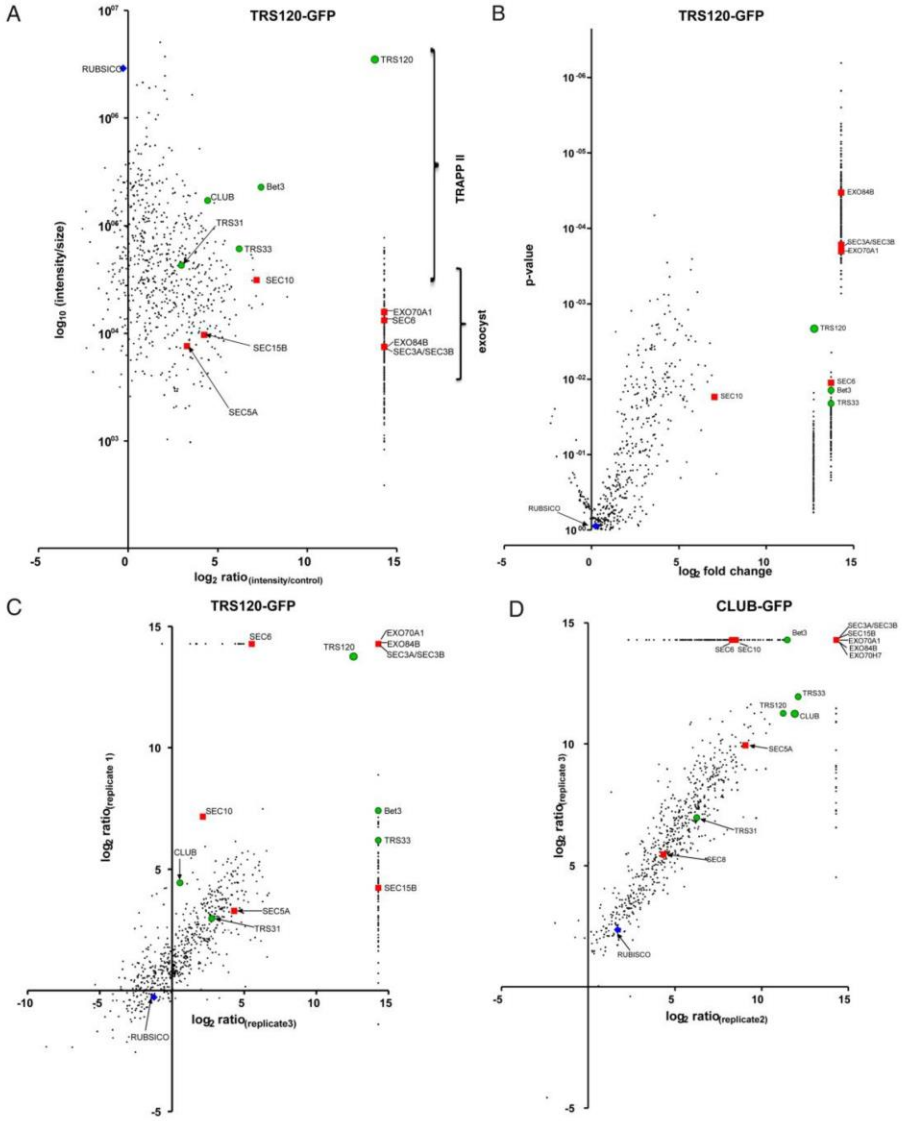

Figure S6. Proteomic analysis of CLUB-GFP and TRS120-GFP immunoprecipitates (IPs, related to Figure 6).
(A-D). Scatter plots showing all the hits in a pull down experiment with TRS120-GFP (A-C) or CLUB-GFP (D) as a bait. Each protein is represented by at least five unique peptides and was present in all three biological replicates. The ratio was calculated for each protein as the intensity of the signal in the experiment divided by its intensity in the soluble GFP empty vector control. Green circles: TRAPPII subunits; red squares: exocyst subunits; blue diamond: rubisco.
(A) Signal intensity (normalized against protein size, log10 scale) against the signal ratio (log2 scale). The TRS120-GFP bait has the highest intensity, as expected. An artificial line is formed to the right for proteins that had no signal in the control – these were attributed a random value so as not to appear at infinity on the plot. Rubisco is the most abundant protein in plant tissues and was found in the experiment and control at relatively comparable intensities (low log2 ratio). Note that TRAPPII subunits have a higher average signal intensity than exocyst subunits.
(B) The p value (Student's test; depicted along a negative log10 scale but labeled with actual values) is plotted against the signal ratio. Note that a large number of exocyst components have lower p values than the actual bait, due to the fact that they had no signal in the empty vector control. Shown are hits with $p < 0.02$.
(C, D) Reproducibility for TRS120-GFP (C) and CLUB-GFP (D) IPs can be seen as a straight line seen when two replicates are plotted against each other. The horizontal and vertical lines and their intersection represent proteins that had no signal in the control in either replicate or in both.

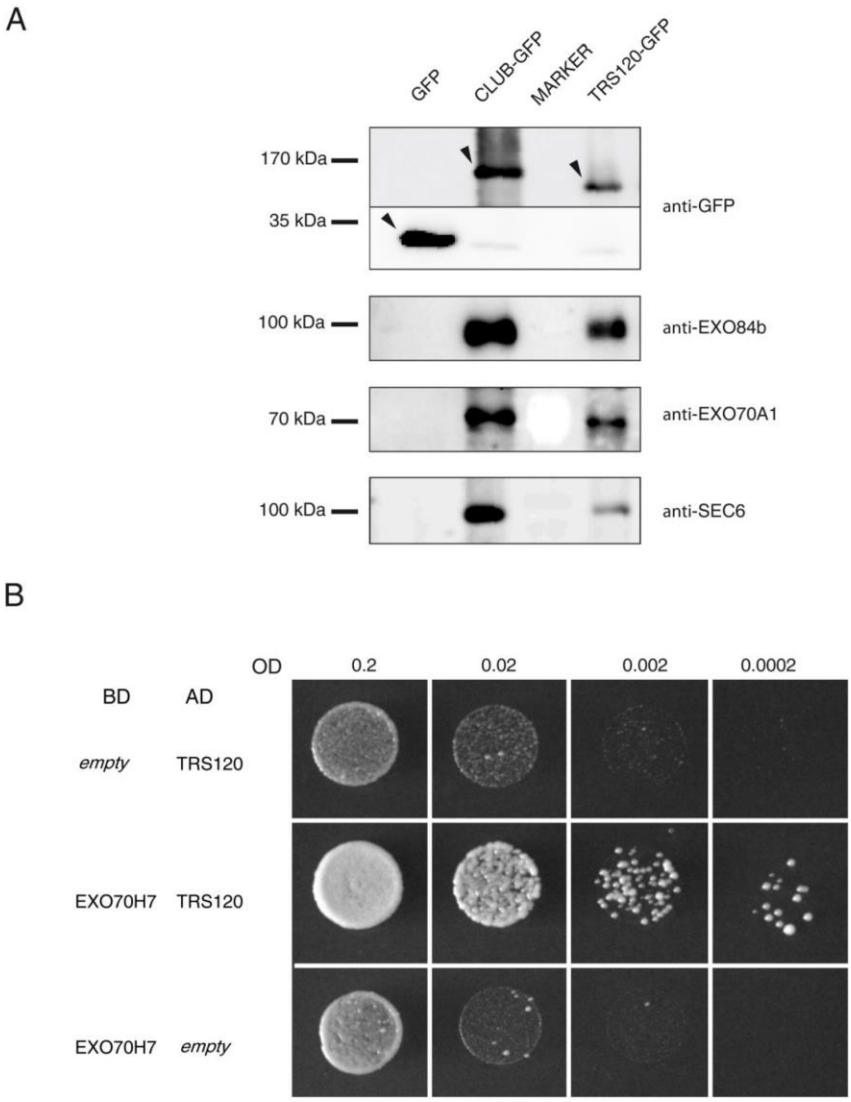

Figure S7. Physical interaction between TRAPPII and exocyst (related to Figure 6).
(A) Western blots of anti-GFP imunoprecipitates. Antibodies used to probe the blots are described at the right of the panels. An anti-GFP antibody detects GFP, CLUB-GFP or TRS120-GFP (arrowheads). Specific bands are seen in the CLUB-GFP and TRS120-GFP IPs but not in the GFP empty cassette control for antibodies against exocyst subunits EXO84b, EXO70A1 and SEC6. Three biological replicates were performed for each transgenic line.
(B) A yeast two-hybrid screen with EXO70H7 (fused to GAL4 BD) interacts with a c-terminal fragment of AtTRS120 (fused to GAL4 AD). Serial dilutions are shown with OD 0.2, 0.02, 0.002 and 0.0002. The empty vector controls (top and lower panels) only grew at the high concentrations (OD 0.2).

AGI number	Gene descrip-tion	CLUB-GFP IP				TRS120-GFP IP			
		average number of unique peptides	Average Log2 (ratio)	standard deviation	p-Value	average number of unique peptides	Average Log2 (ratio)	standard deviation	p-Value
TRAPPII components									
AT5G54440	CLUB/ AtTRS130	121	12	1,6	0,0001				
AT5G11040	TRS120	40	10	2,3	0,0025	72	12	2,4	0,002
AT3G05000	TRS33	9	13	1,3	2,54E-05	5	12	4,7	0,02
AT5G54750	Bet3	10	13	1,6	1,50E-04	9	12	4,0	0,014
AT5G58030	TRS31	6	9	4,4	0,012				
exocyst components									
AT5G59730	EXO70H7	7	14/0	0,0	1,35E-07				
AT5G49830	EXO84B	10	14/0	0,0	2,28E-07	9	14.29/0	0,0	3,36E-05
AT3G10380	SEC8	23	5	0,6	1,08E-04				
AT1G47550, AT1G47560	SEC3A, SEC3B	10	14/0	0,0	1,33E-05	7	14.29/0	0,0	1,65E-04
AT5G03540	EXO70A1	11	14/0	0,0	4,34E-08	6	14.29/0	0,0	0,0002
AT4G02350	SEC15B	14	14/0	0,0	2,15E-07				
AT1G71820	SEC6	11	12	3,3	2,80E-04	8	11	5,1	0,011
AT5G12370	SEC10	21	10	3,7	0,0078	19	6	3,2	0,017
AT1G76850	SEC5A	9	11	2,8	0,0013				

Table S1. Analysis of CLUB-GFP and TRS120-GFP immunoprecipitates via mass spectrometry (Related to Figure 6).
Shown proteins correspond to subunits of the TRAPPII and exocyst complexes. The data are based on three biological replicates. AGI: Arabidopsis genome initiative accessions (www.arabidopsis.org). a: The log2 intensity ratio for each protein was calculated from its signal intensity in the experiment divided by its intensity in the control. Note that the log2 ratios for the exocyst subunits are comparable to those of the TRAPPII subunits, supporting their identification as a complex. b: P values (< 0.02) were calculated using the t-test (two-sided). This table lists only TRAPPII and exocyst components detected in the IPs. For a graphical representation of all the co-purified proteins, see Figures 6 and S6.

Movie legends

Movie S1. P_{TRS120}::TRS120-GFP and P_{UBQ}::TRS120-GFP localization dynamics throughout cytokinesis (related to Figures 1, 2, 3, S1 and S2).

Movie S2. P_{EXO84b}::EXO84b-GFP and P_{35S}::EXO84b-GFP localization dynamics throughout cytokinesis (related to Figures 1, 2, 5 and S1).

Movie S3. P_{35S}::EXO70A1-GFP weakly and strongly expressing lines: localization dynamics throughout cytokinesis (related to Figures 2 and S1).

Supplemental Experimental Procedures

Lines used in this study

Insertion lines were selected via the TAIR and NASC web sites (Swarbreck *et al.*, 2008).

Allele	AGI gene identification	Polymorphism	Intron/exon	Accession number	Reference
club-2	At5g54440	SALK_039353	Intron	N539353	Jaber et al., 2010
trs120-4	At5g11040	SAIL_1285_D07	Intron	N879232	Thelmann et al., 2010
exo84b-2	At5g49830	SAIL_736_A04	Intron	N832876	Fendrych et al., 2010
mas-5	At2g36850	SALK_015454	Intron	N515454	Thiele et al., 2009

Mutant lines used in this study. All lines are seedling lethal; note that the *tsr120-4* allele we used (Thellmann et al., 2010) is distinct from the hypomorphic allele later named tsr120-4 by Qi et al., 2011.

Exocyst insertion lines surveyed for this study						
Allele	AGI gene identification	Polymorphism	Intron/exon	Accession number	Comment	Reference
sec3a	At1g47550	SALK_145185	Intron	N645185	embryo lethal	Zhang et al., 2013
sec5a-1	At1g76850	SALK_010127.56	Intron	N510127	viable	Hala et al., 2008
sec5a-2		GABI_731C01	Exon	N329010		
sec5b-1	At1g21170	SALK_001525	Intron	N501525	viable	Hala et al., 2008
sec6-1	At1g71820	SALK_078235.54	Intron	N578235	male gametophytic lethal	Hala et al., 2008; Wu et al., 2013
sec6-2		SALK_072337	Exon	N572337		
sec8-1	At3g10380	SALK_057409.49	Intron	N557409	male gametophytic lethal	Cole et al., 2005
sec8-3		SALK_026204	Intron	N526204		
sec8-4		SALK_118129	Intron	N618129	viable	
sec8-6		SALK_091118	Exon	N591118	viable	
sec8		SAIL_553_A07	Exon	N823395		
		SALK_027307.36	Exon	N527307		
		SALK_039659.53	Exon	N539659		
sec10	At5g12370	SALK_101637.54	Exon	N601637		
		SALK_146417.17	Intron	N646417		
		SALK_120710.53	Exon	N620710		
		SALK_146418.55	Exon	N646418		
sec15a-1	At3g56640	SALK_006302.46	Exon	N506302	male gametophytic lethal	Hala et al., 2008
sec15a-2		SALK_067498	Exon	N567498		
sec15b	At4g02350	SALK_042723.35	Exon	N542723		
exo70A1-1	At5g03540	SALK_014826	Intron	N514826	sterile dwarf[a]	Synek et al, 2006; Hala et al., 2008
exo70A1-2		SALK_135462.38	Exon	N635462		
exo70A1-3		SALK_026036.52	Intron	N526036		
		SALK_026036C	Intron	N665607*		
exo70A2	At5g52340	GABI_824D06	Exon	N329594		
exo70A3	At5g52350	SAIL_860_A02	Exon	N838557		
		SALK_046855.44	Intron	N546855		
		SALK_046855C	Intron	N668196		
		SALK_046993.44	Intron	N546993		
exo70B1	At5g58430	GABI_114C03	Exon	N328817		
		GABI_156G02	Exon	N414954		
exo70B2	At1g07000	SAIL_621_F02	Exon	N859934		
exo70B2-2		SAIL_339_D07	Exon	N873298	viable	Pečenková et al., 2011
exo70C1	At5g13150	GABI_100A02	Exon	N328778		
exo70D1	At1g72470	SALK_067007.28	Exon	N567007		
exo70D2	At1g54090	SALK_003651.25	Exon	N503651		

Allele	AGI gene identification	Polymorphism	Intron/exon	Accession number	Comment	Reference
exo70D3	At3g14090	SAIL_175_D08	Exon	N871831		
		GABI_747E03	Exon	N329494		
exo70E1	At3g29400	GABI_576F04	Exon	N304920		
		SALK_084145.48	Exon	N584145		
exo70F1	At5g50380	SALK_068101.40	Exon	N568101		
		SALK_109094.18	Exon	N609094		
exo70G1	At4g31540	SALK_074915.54	Exon	N574915		
		SALK_074915C	Exon	N672731		
		SALK_124115.54	Exon	N624115		
exo70G2	At1g51640	SALK_097393.49	Exon	N859942		
		SALK_066920.27	Exon	N566920		
exo70H1	At3g55150	SALK_042456.34	Exon	N542456	viable	Pečenková et al., 2011
		SAIL_189_D12	Exon	N808914		
exo70H3	At3g09530	GABI_651C10	Exon	N328929		
exo70H4	At3g09520	SALK_023593.51	Exon	N523593		
		SALK_080458.46	Exon	N580458		
exo70H5	At2g28640	SALK_132040.26	Exon	N859587		
exo70H6	At1g07725	GABI_768C01	Exon	N329559		
		SAIL_673_A11	Exon	N829423		
exo70H7	At5g59730	GABI_058G08	Exon	N328529		
		SALK_072673.42	Exon	N860008		
exo70H8	At2g28650	SALK_014867.55	Exon	N514867		
		SALK_106117.30	Exon	N606117		
		SALK_125606.35	Exon	N860026		
***exo84b*-1**	At5g49830	GABI_459C01	Intron	N443993	seedling lethal	Fendrych et al., 2010
exo84b-2		SAIL_736_A04	Intron	N832876	seedling lethal	

Insertion lines in exocyst mutants surveyed for seedling lethal cytokinesis-defective phenotypes. We indicate the overall segregation or phenotype for published lines only. For unpublished lines, our survey focused only on the identification of canonical cytokinesis defective phenotypes and segregation analysis was preliminary. a: exo70A1 mutants are very stunted in their growth and produce seeds only very rarely. b: SALK_026036C in EXO70A1 segregated the desired phenotype but was discarded because its phenotype, stronger than that of null alleles, appeared to be synthetically enhanced by a background mutation.

Molecular techniques

Standard molecular techniques were used for subcloning (Sambrook at al., 1989). DNA was isolated from rosette leaves or influorescences of soil-grown plants. CTAB minipreps were prepared as described by Assaad et al. (2001). PCR analysis was carried out with GoTaq (Promega) for standard purposes or with high fidelity PfuUltra II fusion HS DNA polymerase for gene fusions (Agilent Technology inc., Santa Clara, USA). Restriction enzymes were from Promega, NEB or Fermentas. All constructs were introduced into *Agrobacterium tumefaciens* strain GV3101 (Koncz and Shell, 1986) and plants were transformed using the simplified floral-dip method as described in Clough and Bent (1998). T1 plants were selected for transformants on Murashige and Skoog (MS) medium containing 50 µg/ml kanamycin. TRAPPII fusion constructs are described in the table below; Exocyst GFP fusions have been described elsewhere (Fendrych et al., 2010)

Construct	*Arabidopsis thaliana* line	Vector	Template	Primers sequence	
P_{UBQ}:CLUB-GFP	Columbia	pCambia2300-GFP AscI/AatII	F24B18	Forward	5'-ATAGGCGCGCCATGGCGA ACTACT-3'
				Reverse	5'-TATGACGTCCTTGACAGGTAAGCAGT-3'
P_{UBQ}::TRS120-GFP	*trs120-4*/+	pCAMBIA2300-GFP AscI/AatII	pBeloBAC11	Forward	5'-ATAGGCGCGCCATGGAACCTGTCG-3'*
				Reverse	5'-TATGACGTCCAGTGCACCTCCAGCTA-3'
P_{TRS120}::TRS120-GFP	*trs120-4*/+	P_{UBQ}::TRS120-GFP KpnI/AscI	pBeloBAC11	Forward	5'-ATAGGTACCTAGAGAGCCCATGCAATA AAGGAG-3'
				Reverse	5'-TATGGCGCGCCGGCGAGATCAGAGAA GGA-3'
P_{UBQ}::TRS120-mCherry	Columbia, P_{UBQ}::GFP-EXO70A1 (Fendrych et al., 2010)	P_{UBQ}::TRS120-GFP AatII/XbaI	mCherry-mini-SOG C1 (Shu et al., 2011)	Forward	5'-ATATCTAGACTCCGGATTACTTGTACAG CTCGTCCATGCCGCCGGTGGAGTGGCGG CCC-3'
				Reverse	5'-ATAGACGTCGCTGCTGCCGCTGCCGCT GCGGCAGCGGCCATGGTGAGCAAGGGC G AGGAG-3'
P_{TRS120}:TRS120-HA	*trs120-3*/+	pEarleyGate301	F24B18	Forward	5'-GGGGACAAGTTTGTACAAAAAAGCAG G CTCCAGACTTGACAGTAACAATAGGCA -3'
				Reverse	5'-GGGGACCACTTTGTACAAGAAAGCTG GGTCCTTGACAGGTAAGCAGTAGGAAGA A-3'

P_{UBQ}::TRS120-GFP and P_{UBQ}::TRS130/CLUB-GFP gene fusions were constructed by inserting the TRS120 and TRS130/CLUB genomic sequences in the modified binary vector pCAMBIA2300-GFP. P_{TRS120}::TRS120-GFP was constructed by replacing the UBQ promoter in P_{UBQ}::TRS120-GFP with 1kb of endogenous genomic DNA upstream of the AtTRS120 coding sequence. P_{UBQ}::TRS120-mCherry was constructed by replacing GFP with mCherry in P_{UBQ}::TRS120-GFP. P_{TRS120}::TRS120-HA was constructed via the Gateway system (Invitrogen) in the pEarleyGate 301 vector (ABRC). * In the forward primer for P_{UBQ}::TRS120-GFP, GAC was replaced by GTC to optimize restriction enzyme sites for subcloning.

Yeast two hybrid analysis

Yeast two-hybrid analysis was performed as described (Hála et al.2010). The Matchmaker GAL4 Two-Hybrid System 3 (Clontech) was used according to the manufacturer's instructions. EXO70H7 coding sequences were cloned into pGADT7 and pGBKT7 using genomic DNA as a template, as this is a single exon gene. A 2037 base pair C-terminal fragment of AtTRS120 (bp 1524-3561) was identified as a positive hit in the yeast two hybrid screen.

	Yeast strain				
P_{ADH1}::GAL4BD: EXO70H7	AH109	pGBKT7, EcoRI/XhoI	Arabidopsis genomic DNA	Forward	5'-ACCGAATTCATGGGGAAGCATTTATTCCGATC-3'
				Reverse	5'-CACCTCGAGCTCATTCAATGACTACTACGTCC-3'
P_{ADH1}::GAL4AD: TRS120	AH109	pACT2	Cell suspension cDNA library (Bhalerao et al. 1999)		

Genotyping and complementation analysis

All mutant lines were seedling lethal and therefore generated as hemizygotes. Genotyping was carried out with the primers described in the table below. Surface sterilization and growth media were as described by Assaad et al. (1996). For complementation analysis, hemizygous lines were transformed. Because the gene fusions carried full-length genomic sequences, the transgenic lines were selfed over three generations. Mutants rescued by the gene fusion construct segregated roughly 50% cytokinesis-defective mutant seedlings and 100% of their progeny carried both the T-DNA insertion and the gene fusion construct.

Genotype	Primer sequence		LB primer	Tm [°C]
genotype (T-DNA insertion)				
club-2	Forward	5'-CTCGTCCAAGGAGCGGCAAG-3'	LBa1	59,5
	Reverse	5'-GGCACGAACAGGGACCCAAA-3'*		
trs120-4	Forward	5'-TGATTGAGCATGGTTTTCTGGAG-3'	LB3	58,9
	Reverse	5'-TGTCCACTTGGGAGGAATGG-3'*		
exo84b-2	Forward	5'-TGTAGATGTGCTGGTAAGAGC-3'	LB3	57,9
	Reverse	5'-TGGTTCACGTAGTGGGCCATCG-3'*		
GFP fusion			Reverse primer	
CLUB	Forward	5'-GATGAGGTGTTATATGAAGTCA-3'	GFP[a]	58,8
TRS120	Forward	5'-GCGTAGGCTGGGACGTG-3'		

*The primers markeded by an asterisks were used together with the T-DNA left border LB primer to amplify the DNA insertion and flanking genomic sequences, as described at http://signal.salk.edu. Annealing times were 30 sec for all primer pairs. T-DNA primers were: LBa1: TGGTTCACGTAGTGGGCCATCG; Lb3: TAGCATCTGAATTTCATAACCAATCTCGATACAC and a: GFP-reverse primer: 5'-GGCATGGCGGACTTGAAGA-3'.

Confocal microscopy and image analysis

Spinning disk confocal micrscopy was carried out according to Sampathkumar et al., 2011; briefly, roots were imaged on a confocal microscope equipped with a CSU-X1 Yokogawa spinning disc head fitted to a Nikon Ti-E inverted microscope, a CFI APO TIRF 100x N.A. 1.49 oil immersion objective, an evolve charge-coupled device camera (Photometrics Technology), and a 1.2x lens between the spinning disc and camera. For CSLM, images were acquired with the Fluoview 1000 acquisition software (Olympus). Due to weak fluorescence and extensive photobleaching of the samples, time lapses were taken at four minute intervals. For the time lapse movies, however, we used an Olympus Fluorview 1000 equipped with a high sensitivity

detector unit with two gallium arsenide phosphide photomultipliers. This enabled us to carry out extended time lapses at one minute intervals.

Antibody stains

Root tips were fixed in paraformaldehyde, permeablized and stained according to Völker et al., 2001. For a survey of cell wall polysaccharides in wild-type and mutant root tips, and in addition to JIM7 and LM14, the following antibodies were used: CCRC-M1, CCRC-M2 and CCRC-M7 (mouse, Carbo Source, 1:10, Puhlmann et al., 1994); CCRC-M38 (mouse, 1:10, Carbo Source , Pattathil et al., 2010); JIM5 (rat, 1:10, Knox et al., 1990); LM5 (rat, 1:10, Plant Probes , Jones et al., 1997); LM6 (rat, 1:10, Plant Probes, Willats et al., 1998); LM15 (rat, 1:10, Plant Probes, Marcus et al., 2008); LM25 (rat, 1:5, Plant Probes, Pedersen et al., 2012) and CBM3a (1:100, Plant Probes, Blake at al., 2006). For tubulin we also used anti-tubulin (sheep, 1:200, Cytoskeleton). Secondary antibodies were Cy3-conjugated anti-mouse (goat, 1:400; Jackson ImmunoResearch); Alexa Fluor® 488-conjugated anti-rat (goat, 1:100; Molecular Probes) and Alexa Fluor® 488-conjugated anti-rabbit (goat, 1:600; Molecular Probes); anti-HIS (mouse, 1:100, Sigma H-1029) and anti-sheep Alexa Fluor 488 (donkey, 1:100, Jackson ImmunoResearch).

Cell fractionation

The cell fractionation protocol was according to Isono and Schwechheimer (2010). Briefly, 1 g of frozen in liquid nitrogen plant tissue was homogenized (1 min, 1600U/min) on an ice-filled cooling jacket in 6 ml of ice-cold protein extraction buffer (50 mM Tris-HCl pH 7.5, 100mM NaCl, 10% glycerol (w/v) supplemented with 1x protease inhibitor cocktail (S8830, Sigma Aldrich), MG132 (C2211, Sigma Aldrich) and 1mM PMSF. Samples were allowed to cool for 30 s on ice between homogenization cycles (Isono and Schwechheimer, 2010). The crude lysate was centrifuged at 8000 x g, 4˚C for 15 minutes to obtain cell associated membrane fraction (P8K). The supernatant (S8K) was subsequently spinned down at 100 000 x g 4˚C for 1 hour to obtain P100K containing membrane fraction and S100K containing soluble proteins.

Western Blot Analysis

Standard Western blot analysis was performed according to Sambrook at al. (1989). 8 % SDS-PAGE gels were blotted onto PVDF Immobilon-P membranes (Millipore). Polyclonal mouse anti-EXO84b was raised against the full length protein, and polyclonal rabbit anti-EXO70A1 was raised against C-terminal 250 amino acids (Appronex, Czech Republic). Primary antibodies were used at the following concentrations: polyclonal anti-GFP, 1:2000 (A11122, Invitrogen); polyclonal mouse anti-SEC6, 1:1000 (Hala et al., 2008); polyclonal rabbit anti-EXO70 A1, 1:4000 and polyclonal mouse anti-EXO84b, 1:2000. As secondary antibodies, we used either anti-rabbit or anti-mouse Horseradish peroxidase–conjugated antibodies (Pierce, Thermo Scientific) or anti-HA-Peroxidase (3F10), 1:1000 (Roche) together with the SuperSignal West FemtoMaxiumum Sensitivity Substrate (Pierce, Thermo Scientific).

Electron Microscopy

Following high-pressure freezing and freeze substitution, infiltration was carried out as described by Assaad et al., 1996. Infiltrated samples were embedded in Spurr,

and ultrathin sections were cut with a diamond knife and mounted onto collodion coated copper grids. The sections were post- stained with aqueous lead citrate (100 mM, pH 13.0). The FIB serial sectioning was performed by a Zeiss-Auriga workstation. The resin block was trimmed with a pyramitome (LKB) with glass knives so that vertical faces allowed lateral milling of the cells by the FIB. Tomographic datasets were obtained using the ‘‘slice and view’’ technique using a Zeiss Auriga 60 dual beam instrument (Carl Zeiss Microscopy, Oberkochen, Germany). For slicing with the focused ion beam, the conditions were as follows: 2 nA milling current of the Ga-emitter; with each step 30 to 60 nm of the Epon was removed with the FIB. SEM images were recorded with an aperture of 60 µm in the high current mode at 1.5 kV of the in-lens EsB detector with the EsB grid set to 1,350 - 1,400 V. Line averaging 4 was performed. The pixel size was 30 x 30 nm. The pixel dimensions of a recorded image were 2,048 x 1,536 pixel. The time to acquire one frame was 90 s. The slice and view process was repeated 130 to 1350 times to obtain the datasets. The contrast of the images was inversed, so that they appeared like a conventional bright field TEM image.

LC-MS/MS analysis

The rationale for the proteomics approach is described by Cox and Mann (2008). NanoflowLc-MS/MS was performed by coupling an EksigentnanoLC-Ultra 1D+ (Eksigent, Dublin, CA) to a Velos-LTQ-Orbitrap (Thermo Scientific, Bremen, Germany). Peptides were first delivered to a trap column (100 µm inner diameter (i.d.) x 2 cm, packed with 5 µm C18 resin, Reprosil PUR AQ, Dr. Maisch, Ammerbuch, Germany) at a flow rate of 5 µl/min in 100% solvent A (0.1% FA in HPLC grade water). After 10 min of loading and washing, peptides were transferred to an analytical column (75 µm i.d. x 40 cm C18 column Reprosil GOLD, 3 µm, Dr. Maisch, Ammerbuch, Germany) and separated using a 210 min gradient from 4% to 32% solvent B (0.1% FA in acetonitrile) at 300 nL/min flowrate. Data acquisition occurred in data dependent mode, automatically switching between MS and MS^2. Full scan MS spectra were acquired in the Orbitrap at 30,000 resolution. Tandem mass spectra were generated for up to 10 peptide precursors by using higher energy collisional dissociation (HCD) and analyzed in the Orbitrap.

Peptide and Protein Identification/ Data analysis

Raw MS files were loaded into the MaxQuant software (version 1.3.0.3) and searched against an Arabidopsis thaliana RefSeq database (003702_RefSeq.fasta) using carbamidomethyl cysteine as fixed modification, oxidation of Methionin and acetylation of protein N-terminus as variable modifications. Trypsin was specified as proteolytic enzyme and up to 2 missed cleavages were allowed. Mass tolerance of precursor ion was set to 6 ppm and for fragment ions to 20 ppm. Protein identifications were filtered to 0.01% peptide and false discovery rates. Label free quantification and match between runs was enabled, using a retention time window of 2 min. For data evaluation, Max Quant data were loaded into Perseus Software (1.4.0.11) and filtered for reverse identifications (false positives) and contaminants. Intensity values were used to calculate protein ratios between sample and control experiment. Proteins that were included in the final data set were present in all three biological replicates and satisfied the stringent criteria of being represented by a

minimum of five unique peptides. P-values (cutoff at < 0.02) were calculated for all proteins over three biological replicates using a two-tailed Student's t-test.

Supplemental References

Assaad, F.F., Mayer, U., Wanner, G., and Jürgens, G. (1996). The KEULE gene is involved in cytokinesis in Arabidopsis. Mol. Gen. Genet. *253*, 267-277.

Assaad, H., Huet, Y., Mayer, M. and Jürgens, G. (2001). The Cytokinesis Gene KEULE Encodes a Sec1 Protein That Binds the Syntaxin KNOLLE. J. Cell Biol. *152*, 531-543.

Bhalerao, R.P., Salchert, K., Bakó, L., Okrész, L., Szabados, L., Muranaka, T., Machida, Y., Schell, J., and Koncz, C. (1999). Regulatory interaction of PRL1 WD protein with Arabidopsis SNF1-like protein kinases. Proc. Natl. Acad. Sci. USA. *96*, 5322-5327.

Blake, A.W., McCartney, L., Flint, J.E., Bolam, D.N., Boraston, A.B., Gilbert, H.J., and Knox, J.P.(2006). Understanding the biological rationale for the diversity of cellulose-directed carbohydrate-binding modules in prokaryotic enzymes. J. Biol. Chem. *281*, 29321-29329.

Clough, S.J., and Bent, A.F. (1998). Floral dip: a simplified method for Agrobacterium-mediated transformation of Arabidopsis thaliana. Plant J. *16*, 735-743.

Cole, R.A., Synek, L., Zarsky, V., and Fowler, J.E. (2005). SEC8, a Subunit of the Putative Arabidopsis Exocyst Complex, Facilitates Pollen Germination and Competitive Pollen Tube Growth. Plant Physiol. *138*, 2005-2018.

Cox, J., and Mann, M. (2008). MaxQuant enables high peptide identification rates, individualized p.p.b.-range mass accuracies and proteome-wide protein quantification. Nat Biotechnol. *26*, 1367-1372.

Hala, M., Cole, R., Synek, L., Drdova, E., Pecenkova, T., Nordheim, A., Lamkemeyer, T., Madlung, J., Hochholdinger, F., Fowler, J.E., et al. (2008). An exocyst complex functions in plant cell growth in Arabidopsis and tobacco. Plant Cell *20*, 1330-1345.

Isono, E., and Schwechheimer, R. (2010). Co-immunoprecipitation and protein blots. Methods Mol. Biol. *655*, 377-387.

Jones L., Seymour G.B., and Knox, J.P. (1997). Localization of pectic galactan in tomato cell walls using a monoclonal antibody specific to (1[->]4)-[beta]-D-galactan. Plant Physiol. *113*, 1405–1412.

Knox, J.P. , Linstead, P.J., King, J., Cooper C., and Roberts, K. (1990). Pectin esterification is spatially regulated both within cell walls and between developing tissues of root apices. Planta *181*, 512-521.

Koncz, C., and Schell, J. (1986). The promoter of TL-DNA gene 5 controls the tissue-specific expression of chimaeric genes carried by a novel type of Agrobacterium binary vector. Mol. Gen. Genet. *204*, 383-396.

Marcus, S.E., Verhertbruggen, Y., Hervé, C., Ordaz-Ortiz, J.J., Farkas, V., Pedersen, H.L., Willats, W.G., and Knox, J.P. (2008). Pectic homogalacturonan masks abundant sets of xyloglucan epitopes in plant cell walls. BMC Plant Biol. *8*, 60.

Pattathil, S., Avci, U., Baldwin, D., Swennes, A.G., McGill, J.A., Popper, Z., Bootten, T., Albert, A., Davis, R.H., Chennareddy, C., Dong et al. (2010). A Comprehensive Toolkit of Plant Cell Wall Glycan-Directed Monoclonal Antibodies. Plant Physiol. *153*, 514-525.

Pecenková, T., Hála, M., Kulich, I., Kocourková, D., Drdová, E., Fendrych, M., Toupalová, H., and Zársky, V. (2011). The role for the exocyst complex subunits Exo70B2 and Exo70H1 in the plant-pathogen interaction. J. Exp. Bot. 62, 2107-16.

Pedersen, H.L., Fangel, J.U., McCleary, B., Ruzanski, C., Rydahl, M.G., Ralet, M.C., Farkas, V., von Schantz, L., Marcus, S.E., Andersen, M.C. et al. (2012). Versatile high resolution oligosaccharide microarrays for plant glycobiology and cell wall research. J. Biol. Chem. *47*, 39429-39438.

Puhlmann, J., Bucheli, E. , Swain, M. J., Dunning, N., Albersheim, P., Darvill, A. G., and Hahn M. G. (1994). Generation of monoclonal antibodies against plant cell wall polysaccharides. I. Characterization of a monoclonal antibody to a terminal alpha-(1,2)-linked fucosyl-containing epitope. Plant Physiol. *104*, 699-710.

Sambrook, J., Fritsch, E.F., and Maniatis, T. (1989). Molecular cloning: A laboratory Manual. II edn. (New York: Cold Spring Harbourn Laboratory Press).

Sampathkumar, A., Lindeboom, J.J., Debolt, S., Gutierrez, R., Ehrhardt, D.W., Ketelaar, T., and Persson, S. (2011). Live cell imaging reveals structural associations between the actinand microtubule cytoskeleton in Arabidopsis. Plant Cell *23*, 2302-2313.

Shu, X., Lev-Ram, V., Deerinck, T.J., Qi, Y., Ramko, E.B., Davidson, M.W., Jin, Y., Ellisman, M.H., Tsien, R.Y., and McIntosh, J.R. (2011). A Genetically Encoded Tag for Correlated Light and Electron Microscopy of Intact Cells, Tissues, and Organisms.PLoSBiol9, e1001041.

Willats, W.G., Marcus, S.E., and Knox, J.P. (1998). Generation of monoclonal antibody specific to (1-->5)-alpha-L-arabinan. Carbohydr. Res. *308*, 149-152.

Please cite this article in press as: Steiner et al., The Membrane-Associated Sec1/Munc18 KEULE is Required for Phragmoplast Microtubule Reorganization During Cytokinesis in *Arabidopsis*, Molecular Plant (2016), http://dx.doi.org/10.1016/j.molp.2015.12.005

Molecular Plant
Research Article

CellPress
PARTNER JOURNAL

The Membrane-Associated Sec1/Munc18 KEULE is Required for Phragmoplast Microtubule Reorganization During Cytokinesis in *Arabidopsis*

Alexander Steiner[1], Lin Müller[1], Katarzyna Rybak[1], Vera Vodermaier[3], Eva Facher[2], Martha Thellmann[1], Raksha Ravikumar[1], Gerhard Wanner[2], Marie-Theres Hauser[3] and Farhah F. Assaad[1,*]

[1]Botany Department, School of Life Sciences, Technische Universität München, Emil-Ramann-Street 4, 85354 Freising, Germany

[2]Department Biologie I, Ludwig-Maximillians Universität, 82152 Planegg-Martinsried, Germany

[3]Department of Applied Genetics and Cell Biology, University of Natural Resources and Life Sciences, 1190 Vienna, Austria

***Correspondence: Farhah F. Assaad (farhah@wzw.tum.de)**

http://dx.doi.org/10.1016/j.molp.2015.12.005

ABSTRACT

Cytokinesis, the partitioning of the cytoplasm following nuclear division, requires extensive coordination between membrane trafficking and cytoskeletal dynamics. In plants, the onset of cytokinesis is characterized by the assembly of a bipolar microtubule array, the phragmoplast, and of a transient membrane compartment, the cell plate. Little is known about the coordination between membrane deposition at the cell plate and the dynamics of phragmoplast microtubules. In this study, we monitor the localization dynamics of microtubule and membrane markers throughout cytokinesis. Our spatiotemporal resolution is consistent with the general view that microtubule dynamics drive membrane movements. Nonetheless, we provide evidence for active sorting at the cell plate and show that this is, at least in part, mediated by the TRAPPII tethering complex. We also characterize phragmoplast microtubule organization and cell plate formation in a suite of cytokinesis-defective mutants. Of four mutant lines with defects in phragmoplast microtubule organization, only *mor1* microtubule-associated mutants exhibited aberrant cell plates. Conversely, the mutants with the strongest impairment in phragmoplast microtubule reorganization are *keule* alleles, which have a primary defect in membrane fusion. Our findings identify the SEC1/Munc18 protein KEULE as a central regulatory node in the coordination of membrane and microtubule dynamics during plant cytokinesis.

Key words: cytokinesis, cell plate, phragmoplast microtubule, KEULE, KNOLLE, PLEIADE/MAP65-3

Steiner A., Müller L., Rybak K., Vodermaier V., Facher E., Thellmann M., Ravikumar R., Wanner G., Hauser M.-T., and Assaad F.F. (2016). The Membrane-Associated Sec1/Munc18 KEULE is Required for Phragmoplast Microtubule Reorganization During Cytokinesis in *Arabidopsis*. Mol. Plant. ■■, 1–13.

INTRODUCTION

Microtubules are polar filamentous structures, with minus ends that are associated with microtubule organizing centers (MTOCs) and plus ends that are free to explore the cytosol. Several features of plant microtubule dynamics are unique. First, plant MTOCs are pleiotropic rather than central. Second, whereas in animal cells the minus end is stable and the plus end dynamic, in plants both the plus and minus ends are dynamic (Shaw, 2013). Combined, this removes the majority of the constraints associated with central MTOCs such as centrioles in animal cells. Yet this enhanced degree of freedom does not appear to compromise microtubule organization in plants, as demonstrated by the presence of higher-order plant microtubule arrays. Plant microtubule dynamics have been extensively documented in cortical arrays (Ehrhardt, 2008). Ordered cortical array patterns are not correlated with the patterns of microtubule nucleation sites. This is because microtubule bundles are not anchored and because they are nucleated at dispersed sites along pre-existing microtubules at the cell cortex (Murata et al., 2005). After nucleation, the majority of the microtubules are released from their nucleation sites (Shaw et al., 2003; Shaw, 2013). Significantly, polymerization-biased instability at the plus end and slow depolymerization at the minus end lead to hybrid

Published by the Molecular Plant Shanghai Editorial Office in association with Cell Press, an imprint of Elsevier Inc., on behalf of CSPB and IPPE, SIBS, CAS.

Please cite this article in press as: Steiner et al., The Membrane-Associated Sec1/Munc18 KEULE is Required for Phragmoplast Microtubule Reorganization During Cytokinesis in *Arabidopsis*, Molecular Plant (2016), http://dx.doi.org/10.1016/j.molp.2015.12.005

treadmilling. This is much more frequent in plant cells than in animal cells and results in a sustained migration of microtubules along the cell cortex, leading to polymer interactions, reorientation, and bundling (Shaw et al., 2003). Because plant microtubule minus ends can be nucleated at different places and at different times, and because they are not stable, plus end capture mechanisms and membrane anchors may play a particularly important role in the stability of higher-order microtubule arrays in plants. However, little is known about the role of membranes in organizing microtubules.

Plant cytokinesis is an excellent system for elucidating the mechanisms underlying the spatiotemporal coordination between membrane and cytoskeletal dynamics. The formation of a nascent cross wall is initiated during late anaphase within a transient membrane compartment referred to as the cell plate. The onset of cytokinesis is characterized by the assembly of the phragmoplast, which is an array of polar microtubules and actin microfilaments. Phragmoplast microtubules, which nucleate from spindle microtubules, are initially organized in a solid antiparallel array, with their plus ends facing the emerging cell plate. As cells enter telophase, microtubules are translocated to the leading edges of the cell plate, giving rise to a ring-shaped phragmoplast (McMichael and Bednarek, 2013). Thus, three consecutive higher-order arrays characterize mitosis and cytokinesis in plants: the spindle, the solid phragmoplast, and the ring-shaped phragmoplast. Recent studies have addressed the transition from the solid to the ring-shaped phragmoplast (Murata et al., 2013; for review, see Lee and Liu, 2013). The centrifugal expansion that underlies this transition is a result of continuous microtubule assembly at the periphery of the phragmoplast concomitant with the disassembly of microtubules at the center of the phragmoplast (Smertenko et al., 2011). Phragmoplast microtubules are postulated to guide the transport of vesicles to the division site to deliver the membrane and cargo required for cell plate biogenesis and expansion (Samuels et al., 1995; Seguí-Simarro et al., 2004; Chow et al., 2008). However, membrane deposition at the cell plate and phragmoplast microtubule dynamics have not been thoroughly been teased apart to date.

The coordination of microtubule and membrane dynamics during cytokinesis in plant somatic cells has been addressed with genetic or pharmacological analyses and electron tomography. A number of studies have shown that disrupting phragmoplast microtubule components affects cell plate formation and/or expansion. First, the downregulation or knockout of augmin, γ-tubulin, or γ-TuRC MT-nucleating components gives rise to aberrant phragmoplasts and cell plate defects (Binarová et al., 2006; Pastuglia et al., 2006; Zeng et al., 2009; Nakamura et al., 2010; Ho et al., 2011; Hotta et al., 2012). Second, the simultaneous downregulation of three MAP65 genes gives rise to a delay in cell plate expansion in *Physcomitrella* (Kosetsu et al., 2013). Third, kinesin mutants in several double-mutant combinations, or the kinesin-interacting TIO kinase, exhibit cell plate formation or expansion defects (Oh et al., 2005, 2008; Vanstraelen et al., 2006; Lee et al., 2007). Conversely, only a few studies have addressed the role of cell plate membranes on phragmoplast microtubule arrays. First, a quantitative analysis of microtubule plus end geometry via electron tomography has suggested that microtubule plus ends may be

Coordination of Membrane and Microtubule Dynamics

stabilized by as yet unknown components of the cell plate assembly matrix and that a possible microtubule-cell plate association appears to be temporarily disrupted as the phragmoplast transitions from the solid to the ring-shaped stage (Austin et al., 2005). Second, disrupting membrane dynamics with brefeldin-A (BFA) or caffeine inhibits microtubule depolymerization and blocks expansion of the phragmoplast microtubule array (Yasuhara et al., 1995; Yasuhara and Shibaoka, 2000). Although caffeine has been shown to disrupt membrane reorganization during the early stages of cell plate biogenesis (Samuels and Staehelin, 1996), the primary target of this drug remains to be unequivocally determined. What role, if any, cell plate membranes or trafficking components may play in organizing phragmoplast microtubules and in regulating their dynamics remains unclear.

Trafficking components known to play a pivotal role during plant cytokinesis include the syntaxin KNOLLE (SYP111) and the Sec1/Munc18 protein KEULE (SEC11; Lukowitz et al., 1996; Assaad et al., 1996, 2001; Boruc and Van Damme, 2015). KNOLLE appears in trans-Golgi network (TGN)-associated compartments during late prophase, labels the cell plate throughout cytokinesis, and is targeted to the vacuole for degradation at the end of cytokinesis (Lauber et al., 1997; Reichardt et al., 2007, 2011; Chow et al., 2008). KEULE has been shown to bind to and stabilize the open form of KNOLLE, enabling it to form the trans-SNARE complexes that are required for membrane fusion (Park et al., 2012). A constitutively open form of KNOLLE has been reported to suppress the *keule* null mutant phenotype (Park et al., 2012). Based on this observation, it has been proposed that KEULE's sole role is to regulate KNOLLE. From a phylogenetic perspective, this model appears surprising. Indeed, the *Arabidopsis* genome encodes a total of six Sec1/Munc18 genes, of which three are in the KEULE family, and 24 SNAREs, of which nine are in the KNOLLE family; this would lead to the assumption that KEULE might regulate t-SNARES other than KNOLLE (Sanderfoot et al., 2000). Consistently, *keule* mutants have a more pleiotropic phenotype than *knolle* mutants, as seen, for instance, in their root hair phenotype (Assaad et al., 2001). KEULE/SEC11 has in fact been shown to bind the plasma membrane t-SNARE SYP121, a member of the KNOLLE family that is implicated in secretory traffic (Karnik et al., 2015). KEULE and KNOLLE also differ with respect to their trafficking routes, with KNOLLE accumulating in BFA compartments and being delivered to the cell plate via the TGN, and KEULE, in contrast, being BFA insensitive (Reichardt et al., 2007, 2011; Park et al., 2012).

Although KEULE and KNOLLE physically interact at the cell plate, mutant analysis shows that they are delivered to the cell plate independently of each other. It is not clear how KEULE is recruited to the division plane during cytokinesis. A default model would postulate that delivery routes are simply dictated by the orientation and arrangement of phragmoplast microtubules in higher-order solid or ring-shaped arrays. Alternatively, and in light of the physical interaction between KEULE and the exocyst (Wu et al., 2013), it is possible that the exocyst recruits KEULE to the cell plate. The exocyst is a tethering complex that has been shown to play a role in plant cytokinesis, in concert with the TRAPPII tethering complex (Fendrych et al., 2010; Wu et al., 2013; Rybak et al., 2014).

Please cite this article in press as: Steiner et al., The Membrane-Associated Sec1/Munc18 KEULE is Required for Phragmoplast Microtubule Reorganization During Cytokinesis in *Arabidopsis*, Molecular Plant (2016), http://dx.doi.org/10.1016/j.molp.2015.12.005

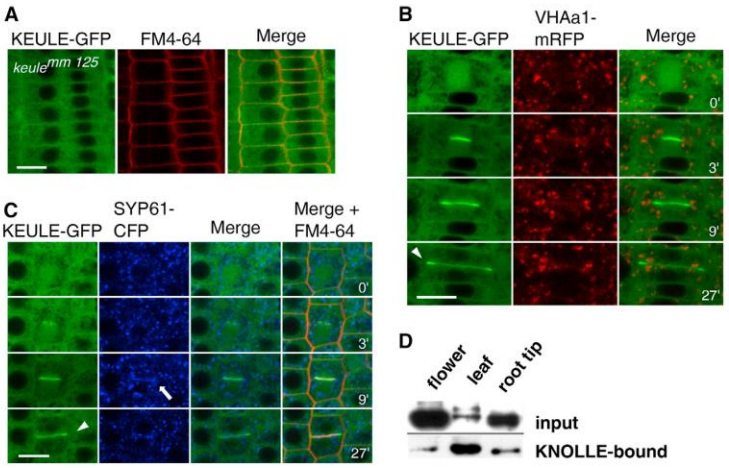

Figure 1. Characterization of KEULE-GFP.
(A) P_{KEU}::KEULE-GFP with FM4-64 in non-dividing cells. Homozygous *keule*^{mm125} mutant rescued by the construct. Note cytosolic localization pattern.
(B and C) Time lapses are shown, with minutes indicated in the right panel. Arrowheads point to the leading edges of the cell plate (CP). **(B)** P_{KEU}::KEULE-GFP with P_{VHAa1}::VHAa1-mRFP. **(C)** P_{KEU}::KEULE-GFP with P_{SYP61}::SYP61-CFP and FM4-64. Arrow points to the CP.
(D) T7-KNOLLE *in vitro* pull-down with protein extracts from different tissues. Western blot probed with anti-KEULE peptide antibody (Assaad et al., 2001). Note that, although more KEULE is present in flowers and root tips than in leaves, more KEULE protein is bound to the KNOLLE affinity column in leaf extracts.
Bars represent 10 μm. See Supplemental Figure 1 for the functionality of the P_{KEU}::KEULE-GFP gene fusion.

In this study, we exploited a new functional KEULE-GFP fusion together with known membrane trafficking markers to characterize the emergence and dynamics of the cell plate from mitosis to cytokinesis. To study the dynamics of phragmoplast microtubule arrays, we used a new functional phragmoplast-specific GFP-PLEIADE/AtMAP65-3 fusion, as well as an alpha-tubulin marker. We find that KEULE differs from KNOLLE in many respects, notably in its localization dynamics and sorting. We show that the TRAPPII tethering complex but not the exocyst EXO84b component is required for sorting KEULE at the cell plate. Using KEULE-GFP to probe membrane dynamics throughout cytokinesis, we find that membrane movements lag behind phragmoplast microtubule dynamics. We further monitored phragmoplast microtubule array organization and cell plate formation in a collection of cytokinesis-defective mutants. While most microtubule organization mutants did not exhibit a strong cell plate phenotype, *keule* mutants, with a primary defect in membrane traffic, were more severely impaired in phragmoplast microtubule reorganization than microtubule-related mutants. Our findings suggest KEULE as a central regulator in the coordination of membrane and microtubule dynamics during cytokinesis.

RESULTS

KEULE-GFP Is Cytosolic during Interphase and Associates with the Cell Plate throughout Cytokinesis

KEULE has been shown to be associated with the cell plate in tobacco BY2 cells (Wu et al., 2013) and in embryos or root tips (Park et al., 2012), but a detailed spatiotemporal localization dynamics of a functional fusion throughout cytokinesis is lacking. We have previously documented that NH_2- and COOH-terminal GFP fusions of the KEULE full-length coding sequence under the transcriptional control of the 35S promoter fail to rescue *keule* mutants (Assaad et al., 2001). For a functional fusion, we therefore used genomic sequences spanning the native promoter, 5′UTR and first eight exons. The ensuing COOH-terminal GFP fusion rescued the *keule* mutant phenotype (Supplemental Figure 1; Supplemental Experimental Procedures). KEULE-GFP had a cytosolic appearance in interphase cells (Figure 1A) but was cell plate-associated throughout cytokinesis, accumulating at the periphery of the expanding cell plate (as has been shown by Wu et al., 2013; Figure 1B and 1C; Supplemental Figure 1). This localization pattern differs from the punctate appearance in anti-HA antibody stains of an HA-tagged KEULE fusion, expressed from the KNOLLE promoter (Park et al., 2012), and of the exclusively cell plate-positive appearance of a GFP-KEULE fusion, expressed from the constitutive 35S promoter (Wu et al., 2013). It also differs from the punctate localization patterns of KNOLLE and RabA2/A3, which have been shown to label the cell plate throughout cytokinesis (Lauber et al., 1997; Chow et al., 2008). As the cell plate is considered to be a TGN-derived compartment, we compared KEULE localization dynamics with that of two TGN markers, VHAa1-mRFP and SYP61-CFP (Dettmer et al., 2006; Drakakaki et al., 2012; Kim and Brandizzi, 2014). KEULE differed from both TGN markers, both in the extent of its cell plate association and in the observation that it did not have a punctate appearance (Figure 1B and 1C). Park et al. (2012) similarly report that KEULE does not co-localize with the TGN marker ARF1. In conclusion, KEULE-GFP is a functional fusion that behaves as a cytosolic or cell plate-associated marker, and not as a TGN marker.

The KEULE-KNOLLE Interaction Is Increased in Non-dividing Leaf Cells

KEULE is only peripherally associated with membranes (Assaad et al., 2001) and its cell plate association is likely due to a direct physical interaction with the cytokinesis-specific syntaxin KNOLLE, expressed exclusively during mitosis (Lauber et al., 1997; Assaad et al., 2001; Park et al., 2012). We re-evaluated KEULE's ability to bind KNOLLE *in vitro*. To this end, we ran pull-down assays in which bacterially expressed T7-epitope tagged KNOLLE was immobilized on immune-affinity columns and incubated with plant extracts. Native KEULE extracted from *Arabidopsis* dividing tissues such as influorescences and root tips did not bind T7-KNOLLE as efficiently as KEULE extracted from non-dividing tissues such as leaves (Figure 1D). Our findings could explain why only little binding was seen *in vivo*

Please cite this article in press as: Steiner et al., The Membrane-Associated Sec1/Munc18 KEULE is Required for Phragmoplast Microtubule Reorganization During Cytokinesis in *Arabidopsis*, Molecular Plant (2016), http://dx.doi.org/10.1016/j.molp.2015.12.005

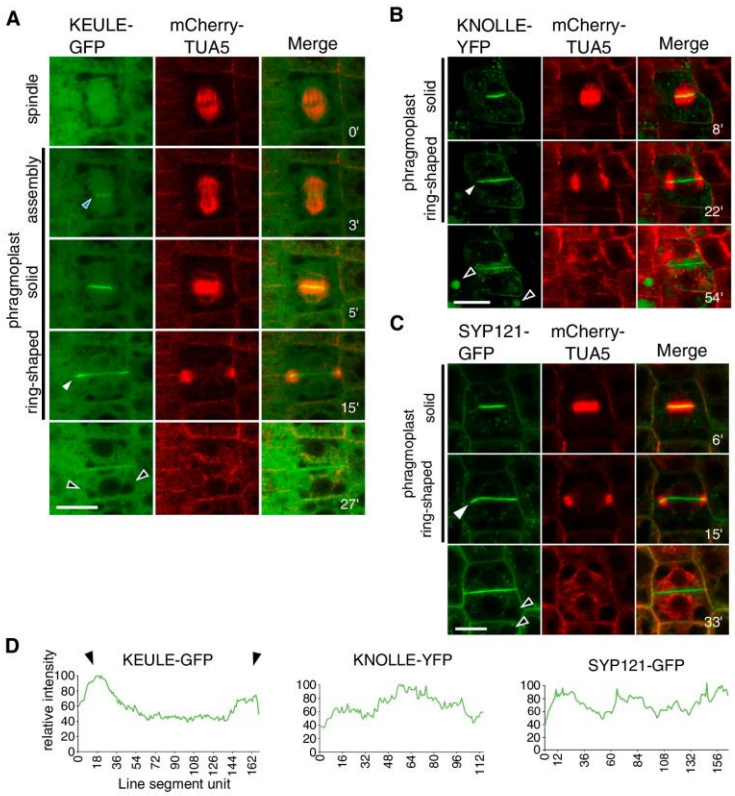

Figure 2. Localization Dynamics of Membrane and Microtubule Markers During Cytokinesis.

(A–C) Time lapses are shown, with minutes indicated in the right panel. Microtubule array stages are indicated on the left. Arrowheads point to the leading edges of the cell plate. Bars represent 10 μm. **(A)** P_{KEU}::KEULE-GFP with mCherry-TUA5. The signal accumulates at the cell equator as of the phragmoplast assembly stage (white-rimmed blue arrowhead). **(B)** P_{KN}::KNOLLE-YFP with mCherry-TUA5. **(C)** P_{SYP121}::SYP121-GFP with mCherry-TUA5. White-rimmed black arrowheads point to vacuoles. Note signal in vacuoles in **(B)** and the absence of a vacuolar signal in **(A)** and **(C)**.

(D) Line graphs of the cell plate at the ring-shaped phragmoplast stage from P_{KEU}::KEULE-GFP, P_{KN}::KNOLLE-YFP, P_{SYP121}::SYP121-GFP depicting fluorescence intensity along the Y axis. Note that, in contrast to P_{KEU}::KEULE-GFP, neither KNOLLE nor SYP121 reorganize to the periphery of the CP at the ring-shaped phragmoplast stage.

between KEULE and KNOLLE isolated from influorescences or seedings (Park et al., 2012) and suggest that the KEULE-KNOLLE interaction is not simply dictated by the presence of KNOLLE during mitosis/cytokinesis but also subject to additional layers of regulation.

KEULE-GFP and KNOLLE-YFP Localization Dynamics Differ

We next set out to monitor the localization dynamics of membrane markers during cytokinesis. To better monitor cell-cycle stages, microtubules were labeled with mCherry-TUA5 (Gutierrez et al., 2009). KEULE-GFP first appeared at the cell equator during the phragmoplast assembly stage; it subsequently labeled the entire cell plate during the solid phragmoplast stage and accumulated at the leading edges of the cell plate at the ring-shaped phragmoplast stage (Figure 2A). The behavior of KNOLLE/SYP111 and of its close homolog SYP121 during the transition from the solid to the ring-shaped phragmoplast has not been quantified to date. We found that KNOLLE-YFP (Völker et al., 2001) did not label the periphery of the cell plate as clearly as KEULE-GFP (Figure 2B and 2D). SYP121-GFP (Collins et al., 2003) also failed to accumulate at the leading edges of the cell plate at the ring-shaped phragmoplast stage (Figure 2C and 2D). Contrary to KNOLLE-YFP, KEULE-GFP was never seen in the vacuole, regardless of the cell-cycle stage (compare Figure 2A versus 2B; Reichardt et al., 2011). This shows that membrane movements are highly differentiated and sorted at the cell plate.

The TRAPPII Complex Is Required for KEULE Localization

The observation that active sorting appears to take place led to the hypothesis that tethering factors might regulate KEULE and/or KNOLLE localization dynamics. Two tethering complexes have been shown to be required for cytokinesis: the TRAPPII complex and the exocyst (Fendrych et al., 2010; Jaber et al., 2010; Rybak et al., 2014). A direct physical interaction between KEULE and the exocyst SEC6 subunit has, in fact, been documented (Wu et al., 2013). To test whether the exocyst recruits KEULE to the cell plate, we monitored KEULE-GFP localization dynamics in an exocyst mutant background. As *sec6* mutants are gametophytic lethal (Wu et al., 2013), we chose the seedling-lethal *exo84b-2* mutant, which exhibits cytokinesis-related phenotypes (Fendrych et al., 2010; Rybak et al., 2014). KEULE-GFP dynamics, however, were unperturbed in this mutant background (Figure 3A). In contrast, the KEULE-GFP signal was reduced and punctate in appearance in a TRAPPII mutant, *trs120-4*, as opposed to being cytosolic or cell plate-localized as in the wild-type (Figure 3B). This was seen in both live imaging and anti-GFP antibody stains (Figure 3B). Interestingly, and in contrast to KEULE, KNOLLE was adequately recruited to the cell plate in *trs120-4* TRAPPII mutants (Figure 3C; Thellmann et al., 2010). In conclusion, the TRAPPII TRS120 component but not EXO84b was required for the proper sorting of KEULE-GFP throughout cytokinesis.

We monitored KEULE-GFP dynamics together with the exocyst subunit SEC6-mRFP (Fendrych et al., 2013) or with the TRAPPII marker TRS120-mCherry (Rybak et al., 2014). Contrary to KEULE-GFP, SEC6-mRFP behaved like all canonical exocyst subunits in being present at the onset of cytokinesis in anaphase,

Please cite this article in press as: Steiner et al., The Membrane-Associated Sec1/Munc18 KEULE is Required for Phragmoplast Microtubule Reorganization During Cytokinesis in *Arabidopsis*, Molecular Plant (2016), http://dx.doi.org/10.1016/j.molp.2015.12.005

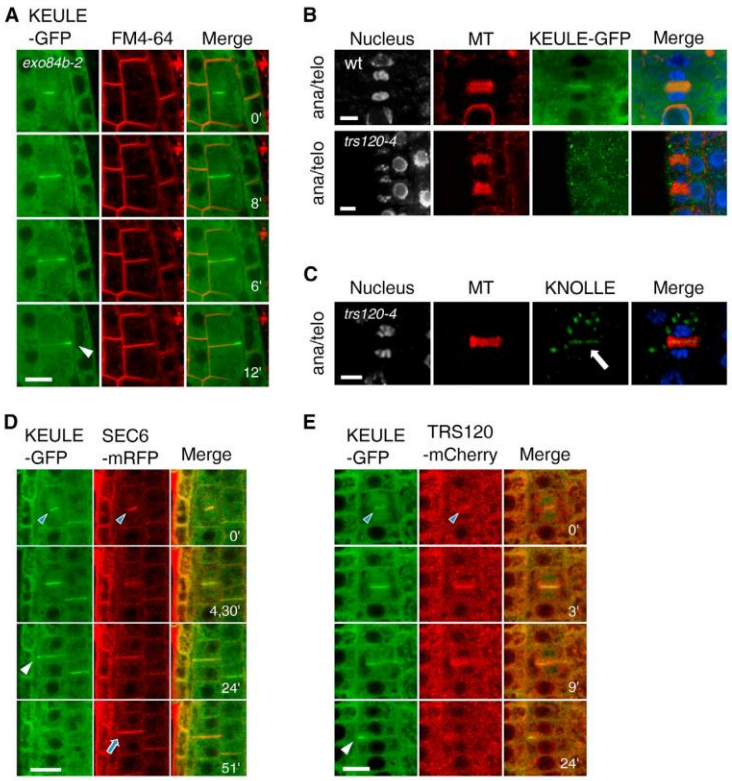

Figure 3. The Role of Tethering Factors in Recruiting KEULE to the Cell Plate.

(A, D, and E) Time lapses are shown, with minutes indicated in the right panel. Arrowheads point to the leading edges of the cell plate. Bars represent 10 μm.

(B and C) Antibody stains of root tips. DAPI/nucleus (white); microtubules (red); anti-KNOLLE/anti-GFP (green). MT, microtubule. Bars represent 5 μm.

(A) P_{KEU}::KEULE-GFP in *exo84b-2* exocyst mutant. Note the unimpaired localization dynamics.

(B) P_{KEU}::KEULE-GFP mis-localization in *trs120-4* TRAPPII mutant. Note the absence of a cytosolic or membrane-associated signal in the mutant (lower panel) compared with the wild-type (upper panel).

(C) Native KNOLLE in *trs120-4* TRAPPII mutant, impaired in cell plate biogenesis. Recruitment to the cell plate, however, does not appear to be impaired. Arrow points to the cell plate. See Figure 5A for wild-type control.

(D) P_{KEU}::KEULE-GFP with P_{35S}::SEC6-mRFP. See Supplemental Movie 1 for a full time lapse. White-rimmed blue arrowheads point to the first appearance of the markers at the cell equator and white-rimmed blue arrows to cross walls. The two markers differ in their localization dynamics.

(E) P_{KEU}::KEULE-GFP with P_{UBQ}::TRS120-mCherry. The two markers co-localize throughout cytokinesis.

diffuse during the anaphase/telophase transition, and then strongly staining the nascent cross wall after cytokinesis (Figure 3D, Supplemental Movie 1). Our analysis of SEC6 is discrepant with the findings of Wu et al. (2013), who describe a SEC6-GFP fusion as behaving like KEULE throughout cytokinesis in tobacco BY2 cells. The consensus in meristematic cells of root tips or embryos is that the exocyst signal is strong at the onset and end of cytokinesis and diffuse at the solid phragmoplast stage (this study; Fendrych et al., 2010; Zhang et al., 2013; Rybak et al., 2014). In contrast, TRS120-mCherry co-localized with KEULE-GFP throughout cytokinesis (Figure 3E). Thus, we conclude that KEULE localization dynamics differ from that of the exocyst but are identical to TRAPPII localization dynamics during and after cytokinesis.

KEULE-GFP Re-localization to the Leading Edges of the Cell Plate Lags Behind the Displacement of Microtubules to the Periphery of the Phragmoplast

How KEULE is recruited to the cell plate remains unclear. Although KEULE and KNOLLE physically interact at the cell plate, KEULE is still recruited to the cell plate in *knolle* null mutants (Park et al., 2012). A default model would postulate that KEULE might simply be delivered to the cell equator throughout cytokinesis by phragmoplast microtubules. However, little is known about the coordination between membrane and microtubule dynamics during cytokinesis. To see whether microtubule dynamics drive membrane dynamics or vice versa, we first simultaneously monitored microtubule and membrane dynamics throughout mitosis and cytokinesis with the help of a number of different markers. Microtubules at the phragmoplast midline were specifically labeled with a new GFP-MAP65-3/PLEIADE fusion. Membranes were labeled with a subunit of the TRAPPII tethering factor (TRS120; Rybak et al., 2014) and with KEULE-GFP. Both markers re-localize to the periphery of the cell plate at the ring-shaped phragmoplast stage. Thus, they are more informative than KNOLLE or SYP121 in monitoring cell plate membrane dynamics after the anaphase-telophase transition.

A GFP-PLEIADE N-terminal fusion, including genomic sequences spanning the native promoter region and all PLEIADE introns and exons, was shown to rescue the *pleiade* mutant phenotype (Supplemental Figure 2; Supplemental Experimental Procedures). This functional GFP-PLEIADE fusion sharply and specifically labeled the midzone of the phragmoplast (Supplemental Figure 2) as has been reported for other *MAP65-3/PLEIADE* gene fusions (Caillaud et al., 2008; Ho et al., 2012). Whereas KEULE-GFP appeared to lag behind phragmoplast microtubules, GFP-PLEIADE rapidly reorganized to the periphery of the phragmoplast midline in synchronization with microtubules (see 3D heat maps in Figure 4A). A quantitative analysis of time lapses of KEULE-GFP, TRS120-GFP, and GFP-PLEIADE together with the mCherry-TUA5 microtubule marker (Figure 4B; $p < 0.0005$ and $p = 0.001$ for a comparison between microtubule- and membrane-associated

Please cite this article in press as: Steiner et al., The Membrane-Associated Sec1/Munc18 KEULE is Required for Phragmoplast Microtubule Reorganization During Cytokinesis in *Arabidopsis*, Molecular Plant (2016), http://dx.doi.org/10.1016/j.molp.2015.12.005

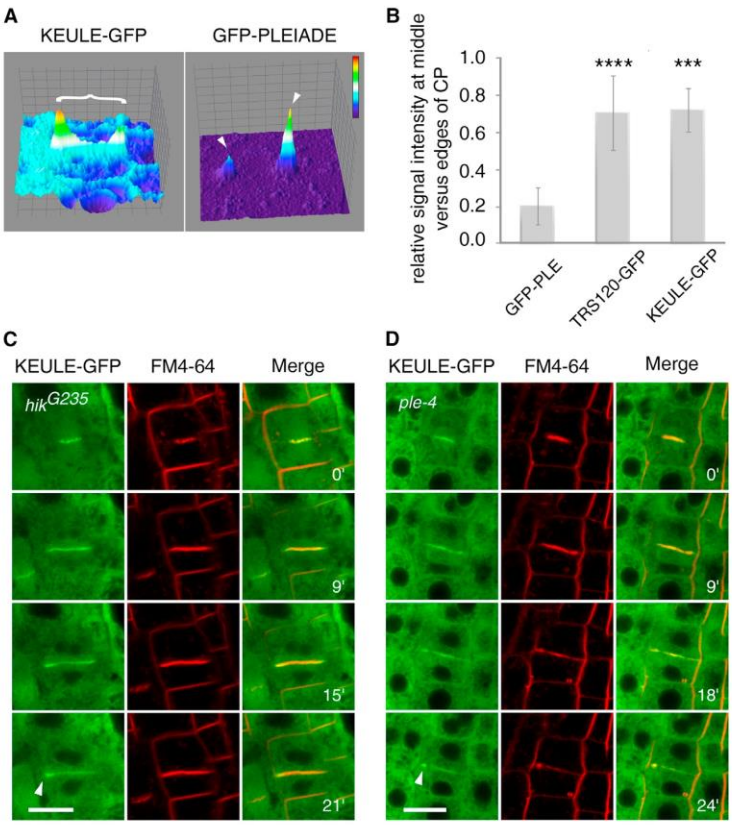

Figure 4. Localization Dynamics of P_{KEU}::KEULE-GFP During Cytokinesis, with Respect to Microtubule Markers and in Mutants with Defects in Microtubule Reorganization.

(A) 3D heatmaps of P_{KEU}::KEULE-GFP and P_{PLE}::GFP-PLEIADE depicting fluorescence intensity along the z axis with a scale ranging from blue (low) to red (high). Note that the P_{PLE}::GFP-PLEIADE signal is concentrated in sharp peaks at the leading edges of the cell plate (arrowhead), whereas P_{KEU}::KEULE-GFP is more evenly spread (bracket), suggesting that microtubule reorganization precedes membrane reorganization at the cell plate.

(B) Relative signal intensity at the middle compared with the leading edges of the cell plate (CP). Mean signal intensity was taken in line graphs of the earliest time points depicting phragmoplast microtubule reorganization from solid to ring-shaped in time lapses of the GFP markers in combination with mCherry-TUA5. Mean ± SEM. $^{****}p < 0.0005$; $^{***}p = 0.001$ for comparison with GFP-PLEIADE; $n \geq 4$.

(C and D) Time lapses are shown, with minutes indicated in the right panel. Arrowheads point to the leading edges of the cell plate. Bars represent 10 μm. **(C)** P_{KEU}::KEULE-GFP in *hik*^{G235}. **(D)** P_{KEU}::KEULE-GFP in *ple-4*. See Supplemental Figure 2 for the functionality and localization dynamics of P_{PLE}::GFP-PLEIADE gene fusion.

markers) shows that the membrane markers persist at the center of the cell plate after the phragmoplast microtubules have transitioned from the solid to the ring-shaped stages. This conclusion is entirely consistent with the widely accepted view that microtubule dynamics guide and drive membrane deposition at the cell plate.

Cell Plate Formation Is Largely Unaffected in Mutants Impaired in Phragmoplast Microtubule Organization

As microtubule movements precede membrane movements at the cell plate, we monitored KEULE-GFP dynamics in alleles of *MAP65-3/PLEIADE* and mitosis-specific kinesin *HINKEL/NACK1*, as these have been shown to affect phragmoplast microtubule array organization (Strompen et al., 2002; Söllner et al., 2002; Smertenko et al., 2004; Sasabe et al., 2015). We used *hinkel*^{G235} and *pleiade-4* alleles, initially identified in a collection of *keule*-like mutants (Mayer et al., 1991; Söllner et al., 2002; see scanning electron microscopy [SEM] panels in Figures 5 and 6). In the case of *pleiade*, this is because, even though other *pleiade* alleles are viable, the *ple-4* allele is seedling lethal, implying a strong defect in cytokinesis (Müller et al., 2002, 2004; Smertenko et al., 2004). KEULE-GFP recruitment to the cell plate at the anaphase to telophase transition, however, was not perturbed in these microtubule-associated mutants (Figure 4C and 4D).

Our live imaging results suggested that, even though sorting appears to take place, membrane dynamics might be driven by microtubule dynamics during cytokinesis. To explore this possibility genetically, we looked at cell plate formation in *hin*^{G235} and *ple-4*. Cell plate formation was monitored with an anti-KNOLLE antibody (Lauber et al., 1997) and microtubule organization from the solid to the ring-shaped phragmoplast stages was visualized with an anti-tubulin antibody via immunohistochemistry in root tips. In *ple-4*, the reorganization of microtubules from solid to ring-shaped phragmoplast stages occurred normally in 71.8% and partially in 23.1% of the telophase cells analyzed (n = 39; Figure 5B; compare with the wild-type in Figure 5A; Table 1). *hinkel* mutants have been reported to be impaired in phragmoplast reorganization during the transition from the solid to the ring-shaped phragmoplast, but only early cytokinetic events were shown and a quantitative analysis is lacking (Strompen et al., 2002). We quantified a phragmoplast reorganization defect in 35% of the telophase cells (29.2% solid and 6.2% partially reorganized phragmoplasts, n = 48; Figure 5C; Table 1). In summary, *pleiade* and *hinkel* mutants exhibited measurable defects in phragmoplast microtubule arrays but no clear impairment in cell plate assembly in dividing cells.

We found no cell plate formation defects in *clasp1-1* mutants (Table 1), which have been described as having a subtle decrease in the length of the phragmoplast (Ambrose et al., 2007). We then looked at *mor1-1* temperature-sensitive

Please cite this article in press as: Steiner et al., The Membrane-Associated Sec1/Munc18 KEULE is Required for Phragmoplast Microtubule Reorganization During Cytokinesis in *Arabidopsis*, Molecular Plant (2016), http://dx.doi.org/10.1016/j.molp.2015.12.005

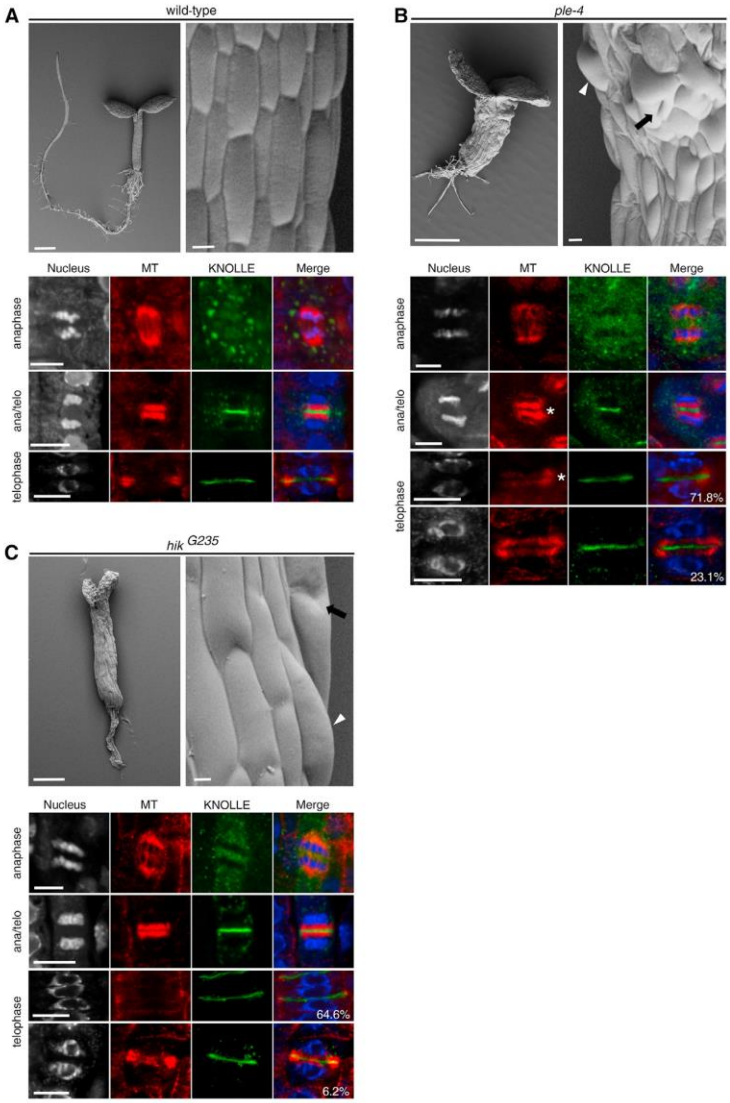

Figure 5. Microtubule Reorganization and Cell Plate Formation in Microtubule-Related Mutants.

Upper panels: Environmental scanning electron micrographs. Arrowheads point to bloated cells and arrows to cell wall stubs. Bars represent 0.5 mm overview; 20 μm close up. Lower panels: Antibody stains of root tips. DAPI/nucleus (white); microtubules (red); KNOLLE protein (green). Bars represent 10 μm.

(A) Wild-type.

(B) *ple-4*; note the enlarged microtubule (MT)-free phragmoplast midzone (asterisk), as has been described (Müller et al., 2004; Ho et al., 2012).

(C) *hik*^{G235}.

In both *ple-4* and *hik*^{G235} mutants, phragmoplast MT reorganization from solid to ring-shaped occurred in a majority of cases; in a minority of cases, partial reorganization of phragmoplast MTs was observed (% indicated in right panel). The overall appearance of the cell plate did not appear to differ from the wild-type. See Supplemental Figure 3 for *mor1-1* phenotypes.

mutants, as these have an interesting phragmoplast microtubule defect (Twell et al., 2002). We found anomalies in cell plate orientation and formation, including branching and discontinuous plates on different planes, in 28%–36% of telophase cells (Supplemental Figure 3; Table 1). Cell plate formation defects in *mor1-1* mutants have been reported (Whittington et al., 2001; Eleftheriou et al., 2005; Kawamura et al., 2006). Nonetheless, the severe defects we observe in the spatial organization of both the phragmoplast and cell plate in *mor1-1* mutants is a unique and defining feature that we have not seen in any other microtubule-related cytokinesis mutant. In conclusion, of the four microtubule-related mutants we tested, cell plate formation defects were only detected in *mor1-1* root tips (Table 1).

KEULE Is Required for the Efficient Reorganization of Phragmoplast Microtubules from the Solid to the Ring-Shaped Stage

We next set out to better understand the *keule* mutant phenotype, which has only been depicted by two-dimensional micrographs to date. For 3D reconstructions of high-resolution images of entire cells (Figure 6A and 6B), we applied focused ion beam (FIB)/SEM on cryofixed, freeze substituted root tips. FIB/SEM tomographic datasets showed that cell plates are at times completely absent in *keule* mutants (Figure 6B and Supplemental Figure 4). Indeed, the reconstructed *keule* cell in Figure 6B has four nuclei of unequal sizes, due presumably to nuclear fusion or aberrant ploidy in multinucleate cells (Assaad et al., 1996; Söllner et al., 2002), and no detectable cross walls. Given the laborious nature of FIB/SEM tomography, we were only able to reconstruct seven *keule* mutant root tip cells. All seven of these showed cell plate formation defects, consistent with our extensive confocal analysis of *keule* root tips. We then monitored microtubule reorganization in *keule* mutants via antibody stains in root tips (Figure 6D). As a control, we also included a mutant allele of the callose synthase *MASSUE/GSL8* (Figure 6C; Thiele et al., 2009). KNOLLE-positive plates were very rare in *keule* root tips. In the rare *keule* cells undergoing cytokinesis, phragmoplast microtubules had completely failed to reorganize from the solid to the ring-shaped arrays by late cytokinesis in 86% of telophase cells (Figure 6D; open arrowhead). This was in sharp contrast to the wild-type and to the more infrequent microtubule array defects observed in *hinkel*, *pleiade*, and *mor1-1* mutants (Table 1). These findings

Please cite this article in press as: Steiner et al., The Membrane-Associated Sec1/Munc18 KEULE is Required for Phragmoplast Microtubule Reorganization During Cytokinesis in *Arabidopsis*, Molecular Plant (2016), http://dx.doi.org/10.1016/j.molp.2015.12.005

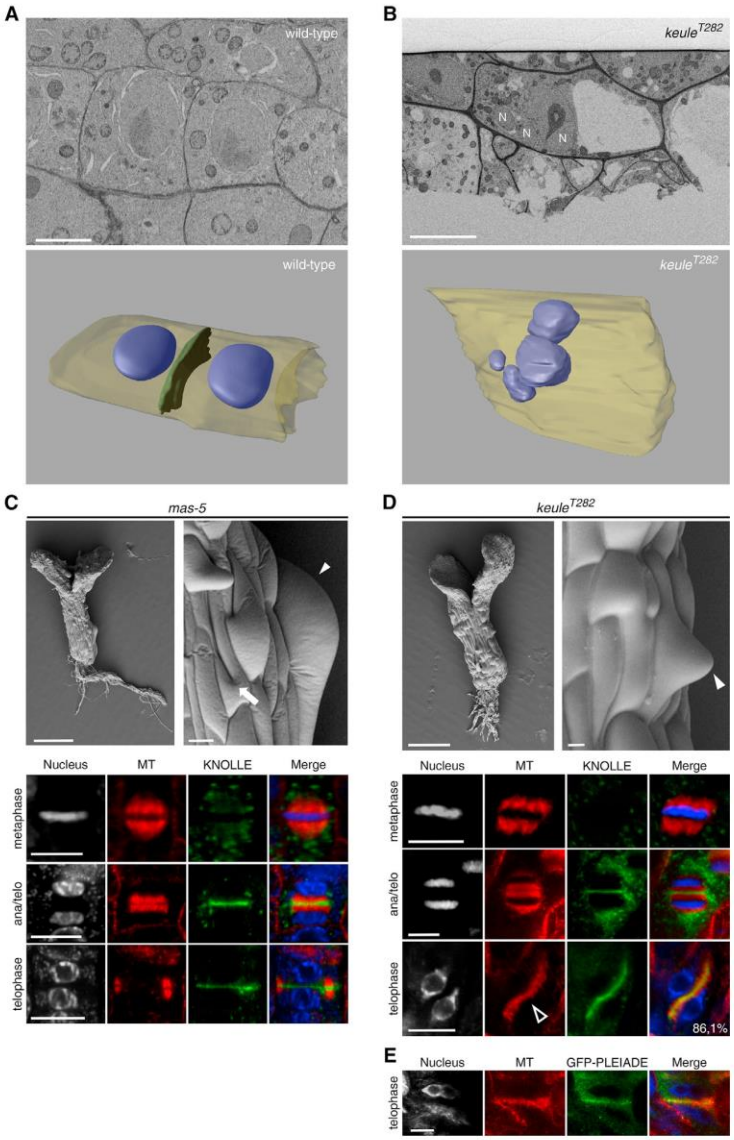

Figure 6. Characterization of *keule* Mutants: 3D Reconstructions and Phragmoplast Microtubule Array Organization.

(A and B) Focused ion beam/scanning electron micrographs of high-pressure frozen, freeze substituted 5-day-old root tips. Single slices are shown in the upper panel and 3D reconstructions of entire stacks in the lower panel. Nuclei, blue spherical structures; cross walls, green; cell outline, beige. Bars represent 2 μm.

(A) Wild-type. Note the regular shape of the cell and the complete cross wall.

(B) *keule*^{T282}. Note that there are four nuclei but no apparent cross walls in the 3D reconstruction (right panel). Three of these nuclei (N) can be seen in a single slice on the left. See Supplemental Figure 4 for a description of how the 3D reconstruction was carried out for **(B)**.

(C–E) Upper panels in **(C)** and **(D)**: environmental scanning electron micrographs of wild-type and mutant seedlings. Arrowheads point to bloated cells and arrows to cell wall stubs. Bars represent 0.5 mm overview; 20 μm close up. Lower panels and **(E)**: Antibody stains of root tips. DAPI/nucleus (white); microtubules (red); KNOLLE protein (green). Bars represent 10 μm. **(C)** *massue-5*. Note the complete cell plate and timely reorganization of phragmoplast microtubules, as in the wild-type (Figure 5A). **(D)** *keule*^{T282}. Note the unreorganized phragmoplast (open arrowhead). The cell plate appears to have assembled. It is clearly misoriented. **(E)** P_{PLE}::GFP-PLEIADE in *keule*^{T282}. MT, microtubules.

were corroborated with antibody stains of GFP-PLEIADE, which also failed to re-localize to the leading edges of the cell plate in a *keule* mutant background (Figure 6E). Note that in *keule* the cell plate, as monitored with the anti-KNOLLE antibody, appeared to have assembled in 78% of cases (Figure 6D and Table 1). As phragmoplast microtubule arrays were imaged in cells harboring KNOLLE-positive cell plates, their failure to reorganize by late telophase does not appear to be due to an absence of cell plate membranes in *keule* mutants. We therefore conclude that the Sec1/Munc18 protein KEULE is near-absolutely required for the reorganization of phragmoplast microtubules from the solid to the ring-shaped stages.

DISCUSSION

We have constructed functional KEULE-GFP and GFP-PLEAIDE fusions and used these to characterize cell plate formation and remodeling during cytokinesis. KEULE-GFP was cytosolic during interphase and not TGN-associated, contrary to what has been reported for KNOLLE (Chow et al., 2008). KEULE-GFP associated with the cell plate and GFP-PLEIADE sharply and specifically labeled the midzone of the phragmoplast throughout cytokinesis. We provide evidence for active sorting at the cell plate. In the case of KEULE, this sorting appears to require the TRAPPII tethering complex but not the EXO84b exocyst component. Our phenotypic analysis highlights the interdependence between membrane and microtubule phenotypes during cytokinesis, as mutants with a primary defect in microtubule organization had severe cell plate defects and vice versa.

One problem encountered with the phenotypic analysis of cytokinesis-defective mutants is that these tend to be severely impaired in their morphogenesis and to have pleiotropic phenotypes. It has thus been hard to assess which defects are merely a consequence of a primary defect in cytokinesis and which defects are truly specific for a given mutant. To characterize the unique primary defect in each mutant requires a direct

Please cite this article in press as: Steiner et al., The Membrane-Associated Sec1/Munc18 KEULE is Required for Phragmoplast Microtubule Reorganization During Cytokinesis in *Arabidopsis*, Molecular Plant (2016), http://dx.doi.org/10.1016/j.molp.2015.12.005

Mutant allele	Wild-type gene encodes	Cell plate formation	Reorganization of phragmoplast MT from solid to ring-shaped at telophase	Number of telophase cells[a]
Col-o wt		100% complete	100% ring-shaped; 0% solid	189
Ler 31°C[b]		100% complete	97% ring-shaped; 3% solid[c]	33
mas-5	CALLOSE SYNTHASE AtGSL8	100% complete	97.1% ring-shaped, 2.9% solid[c]	34
ple-4	MAP65-3	100% complete	71.8% ring-shaped, 23.1% partially reorganized, 5.1% solid	39
hik^{G235}	KINESIN	100% complete	64.6% ring-shaped, 6.2% partially reorganized, 29.2% solid	48
clasp-1	MAP215	100% complete	94% ring-shaped; 3% solid[c]	31
mor1-1 31°C[a]	MAP215	70.2% complete, **27.7% aberrant, discontinuous or branched**	61.7% ring-shaped, **36.2% partially reorganized**	47
keu^{T282}	SEC1/MUNC18	77.7% complete[d]	**86.1% solid (i.e., not reorganized)**	36

Table 1. Mutant Characterization.
The most pronounced differences between the mutant and wild-type are highlighted in bold type.
[a]The total number cells in telophase, as assessed by the appearance of the DAPI-stained nuclei.
[b]31°C is the restrictive temperature for *mor1-1*.
[c]Note that MT array defects can be detected at a basal rate of 3% in both the wild-type Ler and in *massue* mutants, which we used as controls, and in which we have documented an impairment in insertion into the lateral walls (Thiele et al., 2009).
[d]KNOLLE-positive structures were rare in *keule* mutants, but the cell plates that we detected appeared to be assembled.

comparison with a number of cytokinesis-defective mutants. In this study, we carried out a comparative, quantitative analysis of cell plate assembly and phragmoplast microtubule array organization in a sizable collection of mutants. Cell plate assembly did not appear to be disrupted in *hinkel* and *pleiade* mutants, impaired in phragmoplast microtubule organization. *clasp-1* mutants were similarly unaffected. In contrast, the spatial organization of both the cell plate and phragmoplast was severely impaired in *mor1-1* microtubule-related mutants. Conversely, *keule* mutants, impaired in membrane fusion events at the cell plate, were unprecedented in their near-absolute failure to reorganize phragmoplast microtubules from the solid to the ring-shaped stages.

The core mutants in our collection are all null alleles with strong seedling-lethal phenotypes. In contrast, *mor1-1* is a temperature-sensitive allele; while root tips in *mor1-1* after 2 days at the restrictive temperature cannot be compared with root tips in the other cytokinesis-defective mutants, they can be compared with mutant embryos whose cells have undergone a similar number of cell cycles. For this reason, we have carried out histological sections on embryos for all the mutants in our core collection (Söllner et al., 2002). It is interesting to note that, of the three microtubule-related mutants we analyzed and in spite of the difference in the nature of the alleles, *mor1-1* mutants were the most severely impaired in both phragmoplast organization and cell plate formation. Our failure to detect cell plate assembly defects in *hinkel* and *ple-4* mutants was surprising in light of the observation that, in their overall appearance, *hinkel* and *ple-4* mutants exhibit canonical *keule*-like cytokinesis-defective traits (Müller et al., 2002; Strompen et al., 2002; Söllner et al., 2002; Ho et al., 2012). It appears that, subsequent to cell plate assembly, cell plate expansion, stability, and/or insertion are impaired in *pleiade* and *hinkel* mutants. Analysis of *tetraspore/nack2 hinkel/nack1* double mutants in fact clearly demonstrates a role for these kinesins in phragmoplast expansion (Oh et al., 2008).

We have used a functional KEULE-GFP fusion to probe the default hypothesis that phragmoplast microtubules guide vesicle transport to the cell equator during the anaphase to telophase transition. Our time lapses are consistent with the general assumption that the cytoskeleton drives membrane deposition at the growing edges of the cell plate. However, we also show that active sorting takes place throughout cytokinesis, as closely related markers and interacting proteins differ. Thus, KEULE accumulated at the periphery of the cell plate during late telophase but KNOLLE and its close homolog SYP121 did not. Furthermore, KNOLLE was targeted to the vacuole for degradation at the end of cytokinesis, whereas SYP121 and KEULE-GFP were not (this study and Reichardt et al., 2011). KEULE-GFP sub-cellular localization and recruitment to the cell plate were unperturbed in *hinkel*, *pleiade*, and also in *exo84b-2* exocyst mutants. In contrast, the KEULE-GFP signal was reduced and aberrant in a TRAPPII mutant background. These observations provide evidence for active sorting at the cell plate throughout cytokinesis. This sorting appears to be mediated by the TRAPPII complex, a multi-subunit tethering complex that has been shown to be required for cell plate biogenesis (Thellmann et al., 2010; Qi et al., 2011; Rybak et al., 2014). Our observations do not necessarily challenge the default model that delivery routes are entirely dictated by the orientation and arrangement of phragmoplast microtubules in higher-order solid or ring-shaped arrays. Indeed, our spatiotemporal resolution of membrane and microtubule markers is compatible with the widely accepted hypothesis that microtubules drive membrane movements. It is likely that active sorting is simply superimposed upon the default transport routes.

Wu et al. (2013) have documented a physical interaction between KEULE and SEC6. In this study, KEULE-GFP dynamics was unperturbed in an exocyst mutant. It has to be noted, however, that we used *exo84b-2* and not *sec6* mutants. This is because

Please cite this article in press as: Steiner et al., The Membrane-Associated Sec1/Munc18 KEULE is Required for Phragmoplast Microtubule Reorganization During Cytokinesis in *Arabidopsis*, Molecular Plant (2016), http://dx.doi.org/10.1016/j.molp.2015.12.005

sec6 mutants are gametophytic lethal (Wu et al., 2013), whereas *exo84b-2* mutants are seedling lethal and have cytokinesis-related defects (Fendrych et al., 2010; Rybak et al., 2014). It is possible that SEC6 plays a different role in cytokinesis than EXO84b, even though they are two subunits of the same complex. Another possibility is that the exocyst and/or SEC6 do play an active role in recruiting KEULE and that looking at an *exo84b* allele could not detect this. Alternatively, we propose that the TGN-related TRAPPII tethering complex might mediate the sorting and recruitment of KEULE at the cell plate, while the exocyst would mediate the recruitment to the plasma membrane. Here, the root hair defects of *keule* mutants show that this Sec1/Munc18 protein is required not only for cytokinesis but also for tip growth, as is the exocyst (Hála et al., 2008). Furthermore, KEULE localization dynamics differ from that of the exocyst but are identical to TRAPPII localization dynamics throughout and after cytokinesis.

In addition to active sorting at the cell plate, we show a tissue-specific regulation of the KEULE-KNOLLE interaction; in light of the difference we observe between dividing (influorescences and root tips) and non-dividing (leaf) tissues, it is tempting to speculate that the KEULE-KNOLLE interaction may be cell-cycle regulated. Active sorting and the regulation of the Sec1/Munc18-syntaxin interaction would provide different layers of regulation for plant cytokinesis. Park et al. (2012) have postulated that KEULE's salient role is to stabilize the open form of KNOLLE, thereby enabling membrane fusion events at the cell plate. In this study, however, we document numerous differences between KEULE and KNOLLE. First, at the onset of cytokinesis, KNOLLE appears as TGN-associated puncta (Chow et al., 2008), whereas KEULE is cytosolic. Second, KEULE reorganizes to the leading edges of the cell plate to a considerably greater extent than KNOLLE. Third, KNOLLE is targeted to the vacuole for degradation at the end of cytokinesis (Reichardt et al., 2011), whereas KEULE is not. Fourth, KEULE-GFP requires the TRAPPII component TRS120 for recruitment to the cell plate and sorting but KNOLLE does not. Fifth, *keule* mutants have root hair tip growth phenotypes that have not been observed in *knolle* mutants (Assaad et al., 2001; Söllner et al., 2002). It thus appears that KEULE has properties that differ from and are independent of KNOLLE.

We have corroborated findings that microtubule-related mutants are impaired in cell plate formation. Surprisingly, *keule* mutants, with a primary defect in membrane traffic, are more severely impaired in phragmoplast microtubule reorganization than microtubule-related mutants. It has been postulated that the cell plate acts as an anchor to stabilize the plus ends of phragmoplast microtubules (Austin et al., 2005). This hypothesis is based on the observation that about one third of phragmoplast microtubules end roughly 30 nm from a cell plate membrane, suggesting that they might be connected via linker molecules (Austin et al., 2005). In this study, we identify KEULE as having a pivotal role in the reorganization of phragmoplast microtubules. As KEULE has been shown to interact with several trafficking components, including KNOLLE (Assaad et al., 2001; Park et al., 2012) and SEC6 (Wu et al., 2013), as yet unidentified links between KEULE and the cytoskeleton would comprise a central regulatory node in the coordination of membrane and microtubule dynamics throughout cytokinesis.

EXPERIMENTAL PROCEDURES

Lines and Growth Conditions

All the lines used in this study are listed in Supplemental Table 1. Seedling-lethal mutants were propagated as hetero- or hemi-zygotes. Insertion lines were selected via the TAIR and NASC web sites (Swarbreck et al., 2008). Plants were grown in the greenhouse throughout the year, under controlled temperature conditions and with supplemental light, or under controlled growth chamber conditions (16 h/8 h photoperiod at 250 μmol m^{-2} s^{-1}). Seedlings were surface sterilized, stratified at 4°C for 2 days and plated on MS medium supplemented with 1% sucrose and B5 vitamins (Sigma). The root tips or hypocotyls of 5-day-old plate-grown seedlings were used for light, confocal, and electron microscopy, with the exception of *mor1-1*, which was incubated for an additional 48 h at the restrictive temperature of 31°C in the light or in the dark prior to imaging.

Molecular Techniques

P_{KEU}::KEULE-GFP and P_{PLE}::GFP-PLEIADE gene fusions were constructed as follows.

For the P_{KEU}::KEULE-GFP construct, an Ala10-GFP insert was amplified from the pCambia2300 with the following primers: keuGFP_for: 5′-tatagctagc GCT GCT GCC GCT GCC GC-3′ and keuGFP_rev: 5′-tatagctagc TTA TTA CTT GTA CAG CTC GTC CAT GC-3′ and recombined into the NheI site of a KEULE rescue construct (Assaad et al., 2001) using DNA ligase. The construct was introduced into Ler plants heterozygous for the X-ray *keule* allele keu^{mm125} (Assaad et al., 2001). The T1 progeny was selfed to obtain rescued mutants.

For the P_{PLE}::GFP-PLEIADE construct, the genomic PLE fragment was amplified with the following primers: MAP65-3m-1496R AAC TGC AGT GAT TCA CAG TGA AAC AAG C and TCA TAC ATG GAG ACG AAA AAG TGG and cloned into pCR4-TOPO (Invitrogen). GFP was amplified from the pGREENII0029-35S-GFP-RL (Hellens et al., 2000) with primers GFP_FLGMAP65_3 + p3 (TTC GTT TTC CCT GTT AC**A TG**G TGA GCA AGG GCG A) and GFP_FLGMAP65_3 + p5 (ATG CTT AAG CCT GTA CTT GTA CAG CTC GTC CT) and recombined into the EcoNI site of the pCR4-TOPO-gPLE construct using the InFusion cloning (Clontech) technique. From the pCR4-TOPO-gPLE pmPLE:GFP-PLE was transferred using SpeI and NcoI into a modified pPZP211 vector with the multiple cloning site of pUC-SPYNE between the SmaI and XbaI sites. The construct was transformed into Col-0 and into homozygous *ple-3* backgrounds. We used the *ple-3* allele for complementation analysis (see Supplemental Figure 2) because it has the strongest phenotype among *pleiade* hypomorphic alleles. As null alleles such as *ple-4* are seedling lethal, they were not as readily amenable to transformation.

Antibody Stains and Confocal Microscopy

Root tips were fixed in paraformaldehyde, permeabilized, and stained according to Völker et al. (2001). Antibody stains were carried out as described by Völker et al. (2001), with anti-KNOLLE (rabbit, 1:2000; Lauber et al., 1997), anti-tubulin (mouse, 1:2500, Sigma), anti-rabbit monoclonal Alexa-m488 (goat, 1:600, Molecular Probes), as well as anti-mouse Cy3 (goat, 1:600, Dianova). Nuclei were stained with 1 mg/ml DAPI (Sigma). A Fluoview 1000 confocal laser scanning microscope (Olympus) was used. Images were acquired and processed with the Fluoview 1000 acquisition software (Olympus).

Electron Microscopy

For SEM of fresh material, samples were placed onto stubs and examined immediately in low vacuum with a Zeiss (LEO) VP 438 SEM operated at 15 kV. Electron micrographs were digitally recorded from the BSE signal. Cryofixation and freeze substitution protocols for FIB/SEM were as follows: root tips were placed in aluminum platelets, infiltrated with 20% bovine serum albumin in 80% isopropanol, and fixed by high-pressure

Please cite this article in press as: Steiner et al., The Membrane-Associated Sec1/Munc18 KEULE is Required for Phragmoplast Microtubule Reorganization During Cytokinesis in *Arabidopsis*, Molecular Plant (2016), http://dx.doi.org/10.1016/j.molp.2015.12.005

Molecular Plant

freezing using the Leica HPM100 high-pressure freezer. Freeze substitution was performed in acetone with 2% osmium tetroxide using the Leica ASF2 automatic freeze substitution system. Samples were incubated at −90°C for 20 h, the temperature was progressively lowered to −60°C over a period of 3 h, and then maintained at −60°C for 4 h. Uranyl acetate (0.2%) was added, including 5% water, and the samples were incubated at −60°C for a further 4 h. The temperature was progressively lowered to −30°C over a period of 3 h, samples were incubated at −30°C for 8 h, and the temperature was progressively lowered to 0°C over a period of 3 h. Samples were washed twice for 30 min in 100% acetone at 0°C. Samples were then infiltrated in resin, initially at 0°C but subsequently at room temperature, over a period of at least 2 days with 10 changes of resin/acetone solutions, starting with 1:20 and ending with 100% resin (see Assaad et al., 1996 for further details).

Ultrathin sections were cut with a diamond knife and mounted onto collodion-coated copper grids. The sections were post-stained with aqueous lead citrate (100 mM, pH 13.0). The FIB serial sectioning was performed on a Zeiss Auriga workstation. The FIB serial sectioning and tomographic datasets were obtained via the slice and view technique using a Zeiss Auriga 60 dual beam instrument (Carl Zeiss Microscopy). For further details, please see Supplemental Experimental Procedures.

KNOLLE Binding Assay

KNOLLE coding sequences lacking the membrane anchor were fused to the 11 amino acid T7 epitope tag and overexpressed in *Escherichia coli*, as described (Assaad et al., 2001). T7-KNOLLE from 2–10 ml of bacterial cultures was incubated with T7 antibody-agarose beads (Novagen). For each experiment, 0.5 g of plant tissue were homogenized, the debris pelleted by centrifugation at 1000 *g*, the supernatant supplemented with 1% Triton X-100, and the ensuing extract incubated with loaded beads in a batch for 1 h at room temperature, as described (Assaad et al., 2001).

Statistical Analysis and Image Processing

p Values were determined with the standard two-tailed Student's t test. Images were processed with Adobe Photoshop, analyzed with ImageJ, and assembled with Inkscape. 3D reconstructions were carried out with Imaris software (Bitplane).

SUPPLEMENTAL INFORMATION

Supplemental Information is available at *Molecular Plant Online*.

FUNDING

This research was funded by DFG grant AS110/5-1 to F.F.A. and G.W. and by the FWF grant P16410-B12 to M.T.H.

AUTHOR CONTRIBUTIONS

A.S. designed and performed experiments and assembled the figures; L.M., K.R., and G.W. designed and performed experiments; V.V., E.F., M.T., and R.R. performed experiments; M.T.H. and F.F.A. designed experiments and wrote the paper.

ACKNOWLEDGMENTS

We thank Prof. Grill and members of the Botany Department for their support. Silvia Dobler helped with sample preparation for imaging with electron microscopy. Carina Deli provided student help. Roland Baumgartner, Arnold Holik, and Juan Antonio Torres-Acosta helped generate GFP-PLE transgenics. We are grateful to David Ehrhardt, Geoff Wasteneys, Viktor Zársky, and Gerd Jürgens for sharing published resources. We thank Natasha Raikhel, Heather MacFarlane, and Staffan Persson for useful comments on the manuscript. No conflict of interest declared.

Received: August 28, 2015
Revised: October 28, 2015
Accepted: December 3, 2015
Published: December 14, 2015

REFERENCES

Ambrose, J.C., Shoji, T., Kotzer, A.M., Pighin, J.A., and Wasteneys, G.O. (2007). The *Arabidopsis* CLASP gene encodes a microtubule-associated protein is involved in cell expansion and division. Plant Cell **19**:2763–2775.

Assaad, F.F., Mayer, U., Wanner, G., and Jürgens, G. (1996). The KEULE gene is involved in cytokinesis in *Arabidopsis*. Mol. Gen. Genet. **253**:267–277.

Assaad, F.F., Huet, Y., Mayer, U., and Jürgens, G. (2001). The cytokinesis gene KEULE encodes a Sec1 protein that binds the syntaxin KNOLLE. J. Cell Biol. **152**:531–543.

Austin, J.R., Seguí-Simarro, J.M., and Staehelin, L.A. (2005). Quantitative analysis of changes in spatial distribution and plus-end geometry of microtubules involved in plant-cell cytokinesis. J. Cell Sci. **118**:3895–3903.

Binarová, P., Cenklová, V., Procházková, J., Doskocilová, A., Volc, J., Vrlík, M., and Bögre, L. (2006). Gamma-tubulin is essential for acentrosomal microtubule nucleation and coordination of late mitotic events in *Arabidopsis*. Plant Cell **18**:1199–1212.

Boruc, J., and Van Damme, D. (2015). Endomembrane trafficking overarching cell plate formation. Curr. Opin. Plant Biol. **28**:92–98.

Caillaud, M.-C., Lecomte, P., Jammes, F., Quentin, M., Pagnotta, S., Andrio, E., de Almeida Engler, J., Marfaing, N., Gounon, P., Abad, P., et al. (2008). MAP65-3 microtubule-associated protein is essential for nematode-induced giant cell ontogenesis in *Arabidopsis*. Plant Cell **20**:423–437.

Chow, C.-M., Neto, H., Foucart, C., and Moore, I. (2008). Rab-A2 and Rab-A3 GTPases define a trans-golgi endosomal membrane domain in *Arabidopsis* that contributes substantially to the cell plate. Plant Cell **20**:101–123.

Collins, N.C., Thordal-Christensen, H., Lipka, V., Bau, S., Kombrink, E., Qiu, J.-L., Hückelhoven, R., Stein, M., Freialdenhoven, A., Somerville, S.C., et al. (2003). SNARE-protein-mediated disease resistance at the plant cell wall. Nature **425**:973–977.

Dettmer, J., Hong-Hermesdorf, A., Stierhof, Y.-D., and Schumacher, K. (2006). Vacuolar H+-ATPase activity is required for endocytic and secretory trafficking in *Arabidopsis*. Plant Cell **18**:715–730.

Drakakaki, G., van de Ven, W., Pan, S., Miao, Y., Wang, J., Keinath, N.F., Weatherly, B., Jiang, L., Schumacher, K., Hicks, G., et al. (2012). Isolation and proteomic analysis of the SYP61 compartment reveal its role in exocytic trafficking in *Arabidopsis*. Cell Res. **22**:413–424.

Ehrhardt, D.W. (2008). Straighten up and fly right: microtubule dynamics and organization of non-centrosomal arrays in higher plants. Curr. Opin. Cell Biol. **20**:107–116.

Eleftheriou, E.P., Baskin, T.I., and Hepler, P.K. (2005). Aberrant cell plate formation in the *Arabidopsis thaliana* microtubule organization 1 mutant. Plant Cell Physiol. **46**:671–675.

Fendrych, M., Synek, L., Pecenková, T., Toupalová, H., Cole, R., Drdová, E., Nebesárová, J., Sedinová, M., Hála, M., Fowler, J.E., et al. (2010). The *Arabidopsis* exocyst complex is involved in cytokinesis and cell plate maturation. Plant Cell **22**:3053–3065.

Fendrych, M., Synek, L., Pecenková, T., Drdová, E.J., Sekeres, J., de Rycke, R., Nowack, M.K., and Zársky, V. (2013). Visualization of the exocyst complex dynamics at the plasma membrane of *Arabidopsis thaliana*. Mol. Biol. Cell. **24**:510–520.

Please cite this article in press as: Steiner et al., The Membrane-Associated Sec1/Munc18 KEULE is Required for Phragmoplast Microtubule Reorganization During Cytokinesis in *Arabidopsis*, Molecular Plant (2016), http://dx.doi.org/10.1016/j.molp.2015.12.005

Gutierrez, R., Lindeboom, J.J., Paredez, A.R., Emons, A.M.C., and Ehrhardt, D.W. (2009). *Arabidopsis* cortical microtubules position cellulose synthase delivery to the plasma membrane and interact with cellulose synthase trafficking compartments. Nat. Cell Biol. **11**:797–806.

Hála, M., Cole, R., Synek, L., Drdová, E., Pecenková, T., Nordheim, A., Lamkemeyer, T., Madlung, J., Hochholdinger, F., Fowler, J.E., et al. (2008). An exocyst complex functions in plant cell growth in *Arabidopsis* and tobacco. Plant Cell **20**:1330–1345.

Hellens, R.P., Edwards, E.A., Leyland, N.R., Bean, S., and Mullineaux, P.M. (2000). pGreen: a versatile and flexible binary Ti vector for Agrobacterium-mediated plant transformation. Plant Mol. Biol. **42**:819–832.

Ho, C.-M.K., Hotta, T., Kong, Z., Zeng, C.J.T., Sun, J., Lee, Y.-R.J., and Liu, B. (2011). Augmin plays a critical role in organizing the spindle and phragmoplast microtubule arrays in *Arabidopsis*. Plant Cell **23**:2606–2618.

Ho, C.-M.K., Lee, Y.-R.J., Kiyama, L.D., Dinesh-Kumar, S.P., and Liu, B. (2012). Arabidopsis microtubule-associated protein MAP65-3 cross-links antiparallel microtubules toward their plus ends in the phragmoplast via its distinct C-terminal microtubule binding domain. Plant Cell **24**:2071–2085.

Hotta, T., Kong, Z., Ho, C.-M.K., Zeng, C.J.T., Horio, T., Fong, S., Vuong, T., Lee, Y.-R.J., and Liu, B. (2012). Characterization of the *Arabidopsis* augmin complex uncovers its critical function in the assembly of the acentrosomal spindle and phragmoplast microtubule arrays. Plant Cell **24**:1494–1509.

Jaber, E., Thiele, K., Kindzierski, V., Loderer, C., Rybak, K., Jürgens, G., Mayer, U., Söllner, R., Wanner, G., and Assaad, F.F. (2010). A putative TRAPPII tethering factor is required for cell plate assembly during cytokinesis in *Arabidopsis*. New Phytol. **187**:751–763.

Karnik, R., Zhang, B., Waghmare, S., Aderhold, C., Grefen, C., and Blatt, M.R. (2015). Binding of SEC11 indicates its role in SNARE recycling after vesicle fusion and identifies two pathways for vesicular traffic to the plasma membrane. Plant Cell **27**:675–694.

Kawamura, E., Himmelspach, R., Rashbrooke, M.C., Whittington, A.T., Gale, K.R., Collings, D.A., and Wasteneys, G.O. (2006). MICROTUBULE ORGANIZATION 1 regulates structure and function of microtubule arrays during mitosis and cytokinesis in the *Arabidopsis* root. Plant Physiol. **140**:102–114.

Kim, S.J., and Brandizzi, F. (2014). The plant secretory pathway: an essential factory for building the plant cell wall. Plant Cell Physiol. **55**:687–693.

Kosetsu, K., de Keijzer, J., Janson, M.E., and Goshima, G. (2013). MICROTUBULE-ASSOCIATED PROTEIN65 is essential for maintenance of phragmoplast bipolarity and formation of the cell plate in *Physcomitrella patens*. Plant Cell **25**:4479–4492.

Lauber, M.H., Waizenegger, I., Steinmann, T., Schwarz, H., Mayer, U., Hwang, I., Lukowitz, W., and Jürgens, G. (1997). The *Arabidopsis* KNOLLE protein is a cytokinesis-specific syntaxin. J. Cell Biol. **139**:1485–1493.

Lee, Y.-R.J., and Liu, B. (2013). The rise and fall of the phragmoplast microtubule array. Curr. Opin. Plant Biol. **16**:757–763.

Lee, Y.-R.J., Li, Y., and Liu, B. (2007). Two *Arabidopsis* phragmoplast-associated kinesins play a critical role in cytokinesis during male gametogenesis. Plant Cell **19**:2595–2605.

Lukowitz, W., Mayer, U., and Jürgens, G. (1996). Cytokinesis in the *Arabidopsis* embryo involves the syntaxin-related KNOLLE gene product. Cell **84**:61–71.

Mayer, U., Ruiz, R.A.T., Berleth, T., Miseéra, S., and Juürgens, G. (1991). Mutations affecting body organization in the *Arabidopsis* embryo. Nature **353**:402–407.

McMichael, C.M., and Bednarek, S.Y. (2013). Cytoskeletal and membrane dynamics during higher plant cytokinesis. New Phytol. **197**:1039–1057.

Müller, S., Fuchs, E., Ovecka, M., Wysocka-Diller, J., Benfey, P.N., and Hauser, M.-T. (2002). Two new loci, PLEIADE and HYADE, implicate organ-specific regulation of cytokinesis in *Arabidopsis*. Plant Physiol. **130**:312–324.

Müller, S., Smertenko, A., Wagner, V., Heinrich, M., Hussey, P.J., and Hauser, M.-T. (2004). The plant microtubule-associated protein AtMAP65-3/PLE is essential for cytokinetic phragmoplast function. Curr. Biol. **14**:412–417.

Murata, T., Sonobe, S., Baskin, T.I., Hyodo, S., Hasezawa, S., Nagata, T., Horio, T., and Hasebe, M. (2005). Microtubule-dependent microtubule nucleation based on recruitment of gamma-tubulin in higher plants. Nat. Cell Biol. **7**:961–968.

Murata, T., Sano, T., Sasabe, M., Nonaka, S., Higashiyama, T., Hasezawa, S., Machida, Y., and Hasebe, M. (2013). Mechanism of microtubule array expansion in the cytokinetic phragmoplast. Nat. Commun. **4**:1967.

Nakamura, M., Ehrhardt, D.W., and Hashimoto, T. (2010). Microtubule and katanin-dependent dynamics of microtubule nucleation complexes in the acentrosomal *Arabidopsis* cortical array. Nat. Cell Biol. **12**:1064–1070.

Oh, S.A., Johnson, A., Smertenko, A., Rahman, D., Park, S.K., Hussey, P.J., and Twell, D. (2005). A divergent cellular role for the FUSED kinase family in the plant-specific cytokinetic phragmoplast. Curr. Biol. **15**:2107–2111.

Oh, S.-A., Bourdon, V., Das 'Pal, M., Dickinson, H., and Twell, D. (2008). *Arabidopsis* kinesins HINKEL and TETRASPORE act redundantly to control cell plate expansion during cytokinesis in the male gametophyte. Mol. Plant **1**:794–799.

Park, M., Touihri, S., Müller, I., Mayer, U., and Jürgens, G. (2012). Sec1/Munc18 protein stabilizes fusion-competent syntaxin for membrane fusion in *Arabidopsis* cytokinesis. Dev. Cell **22**:989–1000.

Pastuglia, M., Azimzadeh, J., Goussot, M., Camilleri, C., Belcram, K., Evrard, J.-L., Schmit, A.-C., Guerche, P., and Bouchez, D. (2006). Gamma-tubulin is essential for microtubule organization and development in *Arabidopsis*. Plant Cell **18**:1412–1425.

Qi, X., Kaneda, M., Chen, J., Geitmann, A., and Zheng, H. (2011). A specific role for *Arabidopsis* TRAPPII in post-Golgi trafficking that is crucial for cytokinesis and cell polarity. Plant J. **68**:234–248.

Reichardt, I., Stierhof, Y.-D., Mayer, U., Richter, S., Schwarz, H., Schumacher, K., and Jürgens, G. (2007). Plant cytokinesis requires de novo secretory trafficking but not endocytosis. Curr. Biol. **17**:2047–2053.

Reichardt, I., Slane, D., El Kasmi, F., Knöll, C., Fuchs, R., Mayer, U., Lipka, V., and Jürgens, G. (2011). Mechanisms of functional specificity among plasma-membrane syntaxins in *Arabidopsis*. Traffic **12**:1269–1280.

Rybak, K., Steiner, A., Synek, L., Klaeger, S., Kulich, I., Facher, E., Wanner, G., Kuster, B., Zarsky, V., Persson, S., et al. (2014). Plant cytokinesis is orchestrated by the sequential action of the TRAPPII and exocyst tethering complexes. Dev. Cell **29**:607–620.

Samuels, A.L., and Staehelin, L.A. (1996). Caffeine inhibits cell plate formation by disrupting membrane reorganization just after the vesicle fusion step. Protoplasma **195**:144–155.

Samuels, A.L., Giddings, T.H., and Staehelin, L.A. (1995). Cytokinesis in tobacco BY-2 and root tip cells: a new model of cell plate formation in higher plants. J. Cell Biol. **130**:1345–1357.

Sanderfoot, A.A., Assaad, F.F., and Raikhel, N.V. (2000). The *Arabidopsis* genome. An abundance of soluble n-ethylmaleimide-sensitive factor adaptor protein receptors. Plant Physiol. **124**:1558–1569.

Please cite this article in press as: Steiner et al., The Membrane-Associated Sec1/Munc18 KEULE is Required for Phragmoplast Microtubule Reorganization During Cytokinesis in *Arabidopsis*, Molecular Plant (2016), http://dx.doi.org/10.1016/j.molp.2015.12.005

Sasabe, M., Ishibashi, N., Haruta, T., Minami, A., Kurihara, D., Higashiyama, T., Nishihama, R., Ito, M., and Machida, Y. (2015). The carboxyl-terminal tail of the stalk of *Arabidopsis* NACK1/HINKEL kinesin is required for its localization to the cell plate formation site. J. Plant Res. **128**:327–336.

Seguí-Simarro, J.M., Austin, J.R., White, E.A., and Staehelin, L.A. (2004). Electron tomographic analysis of somatic cell plate formation in meristematic cells of *Arabidopsis* preserved by high-pressure freezing. Plant Cell **16**:836–856.

Shaw, S.L. (2013). Reorganization of the plant cortical microtubule array. Curr. Opin. Plant Biol. **16**:693–697.

Shaw, S.L., Kamyar, R., and Ehrhardt, D.W. (2003). Sustained microtubule treadmilling in *Arabidopsis* cortical arrays. Science **300**:1715–1718.

Smertenko, A.P., Chang, H.-Y., Wagner, V., Kaloriti, D., Fenyk, S., Sonobe, S., Lloyd, C., Hauser, M.-T., and Hussey, P.J. (2004). The *Arabidopsis* microtubule-associated protein AtMAP65-1: molecular analysis of its microtubule bundling activity. Plant Cell **16**:2035–2047.

Smertenko, A.P., Piette, B., and Hussey, P.J. (2011). The origin of phragmoplast asymmetry. Curr. Biol. **21**:1924–1930.

Söllner, R., Glässer, G., Wanner, G., Somerville, C.R., Jürgens, G., and Assaad, F.F. (2002). Cytokinesis-defective mutants of *Arabidopsis*. Plant Physiol. **129**:678–690.

Strompen, G., El Kasmi, F., Richter, S., Lukowitz, W., Assaad, F.F., Jürgens, G., and Mayer, U. (2002). The *Arabidopsis* HINKEL gene encodes a kinesin-related protein involved in cytokinesis and is expressed in a cell cycle-dependent manner. Curr. Biol. **12**:153–158.

Swarbreck, D., Wilks, C., Lamesch, P., Berardini, T.Z., Garcia-Hernandez, M., Foerster, H., Li, D., Meyer, T., Muller, R., Ploetz, L., et al. (2008). The Arabidopsis Information Resource (TAIR): gene structure and function annotation. Nucleic Acids Res. **36**:D1009–D1014.

Thellmann, M., Rybak, K., Thiele, K., Wanner, G., and Assaad, F.F. (2010). Tethering factors required for cytokinesis in *Arabidopsis*. Plant Physiol. **154**:720–732.

Thiele, K., Wanner, G., Kindzierski, V., Jürgens, G., Mayer, U., Pachl, F., and Assaad, F.F. (2009). The timely deposition of callose is essential for cytokinesis in *Arabidopsis*. Plant J. **58**:13–26.

Twell, D., Park, S.K., Hawkins, T.J., Schubert, D., Schmidt, R., Smertenko, A., and Hussey, P.J. (2002). MOR1/GEM1 has an essential role in the plant-specific cytokinetic phragmoplast. Nat. Cell Biol. **4**:711–714.

Vanstraelen, M., Inzé, D., and Geelen, D. (2006). Mitosis-specific kinesins in *Arabidopsis*. Trends Plant Sci. **11**:167–175.

Völker, A., Stierhof, Y.D., and Jürgens, G. (2001). Cell cycle-independent expression of the *Arabidopsis* cytokinesis-specific syntaxin KNOLLE results in mistargeting to the plasma membrane and is not sufficient for cytokinesis. J. Cell Sci. **114**:3001–3012.

Whittington, A.T., Vugrek, O., Wei, K.J., Hasenbein, N.G., Sugimoto, K., Rashbrooke, M.C., and Wasteneys, G.O. (2001). MOR1 is essential for organizing cortical microtubules in plants. Nature **411**:610–613.

Wu, J., Tan, X., Wu, C., Cao, K., Li, Y., and Bao, Y. (2013). Regulation of cytokinesis by exocyst subunit SEC6 and KEULE in *Arabidopsis thaliana*. Mol. Plant **6**:1863–1876.

Yasuhara, H., and Shibaoka, H. (2000). Inhibition of cell-plate formation by brefeldin A inhibited the depolymerization of microtubules in the central region of the phragmoplast. Plant Cell Physiol. **41**:300–310.

Yasuhara, H., Sonobe, S., and Shibaoka, H. (1995). Effects of brefeldin A on the formation of the cell plate in tobacco BY-2 cells. Eur. J. Cell Biol. **66**:274–281.

Zeng, C.J.T., Lee, Y.-R.J., and Liu, B. (2009). The WD40 repeat protein NEDD1 functions in microtubule organization during cell division in *Arabidopsis thaliana*. Plant Cell **21**:1129–1140.

Zhang, Y., Immink, R., Liu, C.-M., Emons, A.M., and Ketelaar, T. (2013). The Arabidopsis exocyst subunit SEC3A is essential for embryo development and accumulates in transient puncta at the plasma membrane. New Phytol. **199**:74–88.

Supplemental Information

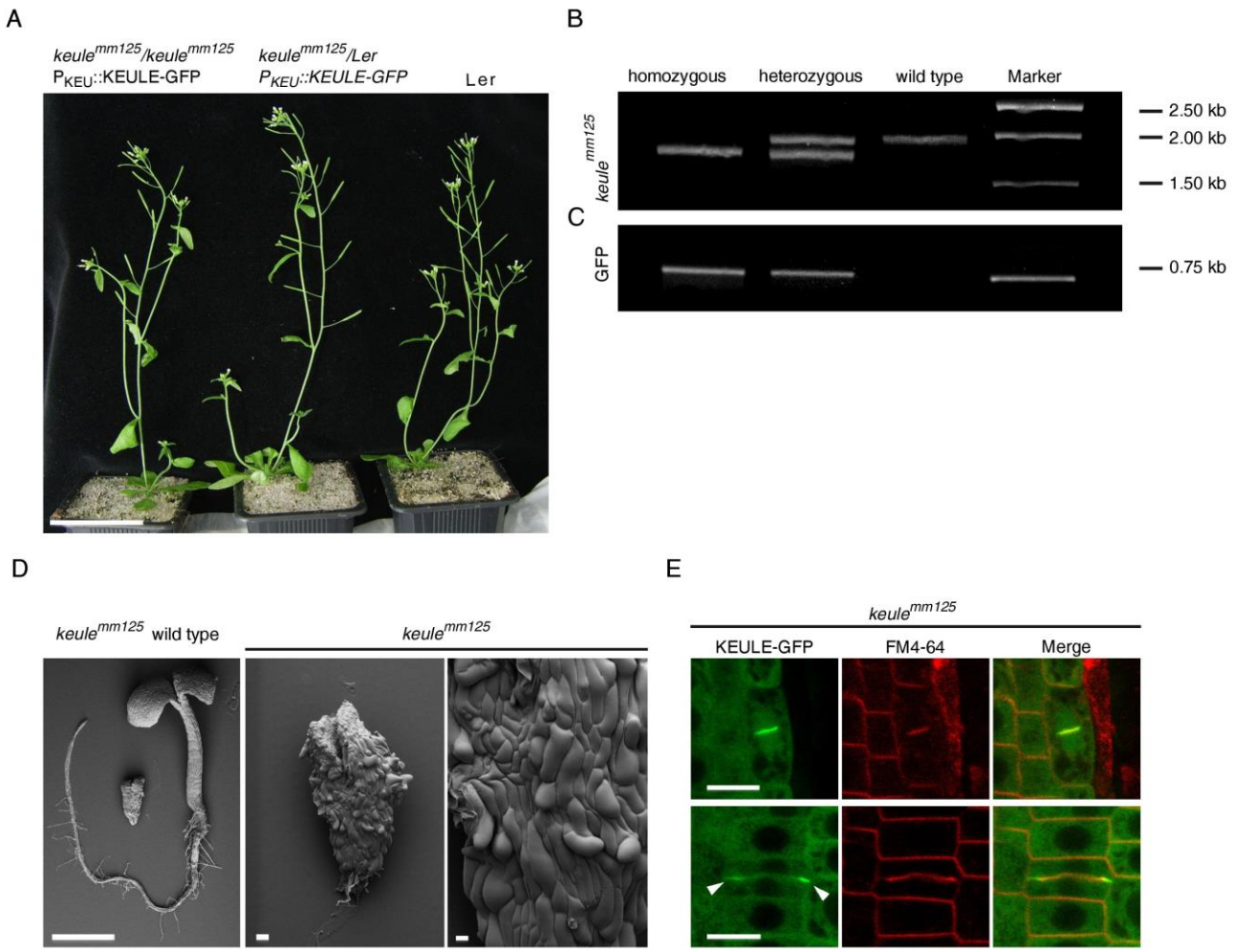

Figure S1. The P_{KEU}::KEULE-GFP fusion fully rescues the mutant phenotype. Related to Figure 1.
(A) Three plants are shown; a homozygous *keu*^{mm125} mutant line rescued by the GFP fusion (left), a heterozygous *keu*^{mm125} line (Assaad et al., 2001) and a wild-type Ler plant. The plants do not differ in their appearance. The canonical seedling-lethal *keule* null phenotype (Assaad et al., 1996) is shown in Fig. 3c, with a different null allele. Bar = 5 cm.
(B and C) Genotyping of lines shown in (A) via PCR analysis.
(B) A PCR fragment spanning the 156-bp deletion harbored by the X-ray keule allele *keu*^{mm125}.
(C) A GFP-specific fragment. The genotyping shows that the left-most line is homozygous for *keu*^{mm125}and that it harbors the transgene.
(D) Environmental Scanning Electron Micrographs of wild-type and *keu*^{mm125}seedlings. Bar = 1 mm overview comparison, Bar = 90 µm overview *keu*^{mm125} , Bar = 30 µm close up.
(E) P_{KEU}::KEULE-GFP with FM4-64 in dividing cells. Note cell plate (CP) localization and reorganization to the leading edges of the CP (arrowheads). Bars = 10 µm.

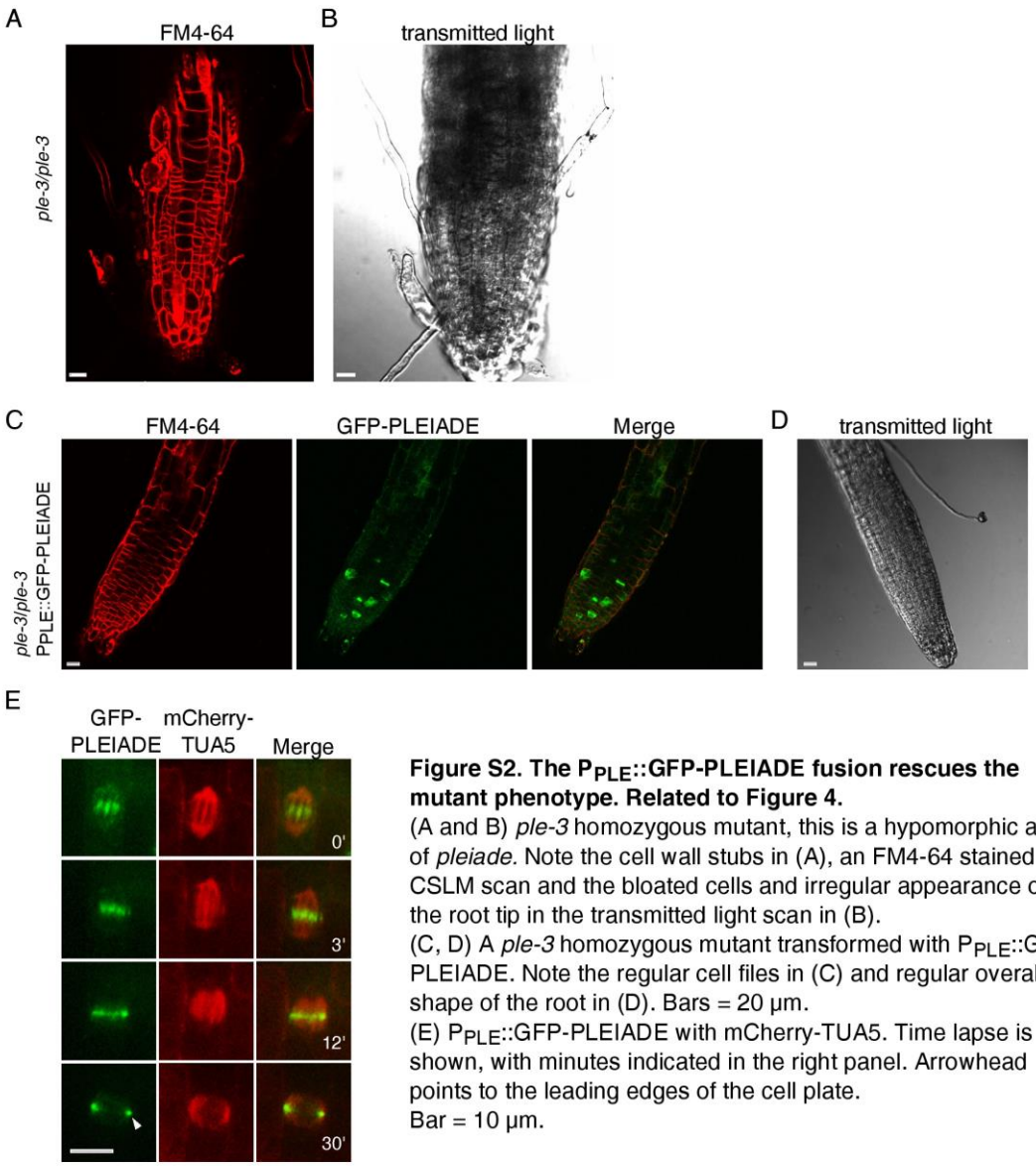

Figure S2. The P_{PLE}::GFP-PLEIADE fusion rescues the mutant phenotype. Related to Figure 4.
(A and B) *ple-3* homozygous mutant, this is a hypomorphic allele of *pleiade*. Note the cell wall stubs in (A), an FM4-64 stained CSLM scan and the bloated cells and irregular appearance of the root tip in the transmitted light scan in (B).
(C, D) A *ple-3* homozygous mutant transformed with P_{PLE}::GFP-PLEIADE. Note the regular cell files in (C) and regular overall shape of the root in (D). Bars = 20 µm.
(E) P_{PLE}::GFP-PLEIADE with mCherry-TUA5. Time lapse is shown, with minutes indicated in the right panel. Arrowhead points to the leading edges of the cell plate.
Bar = 10 µm.

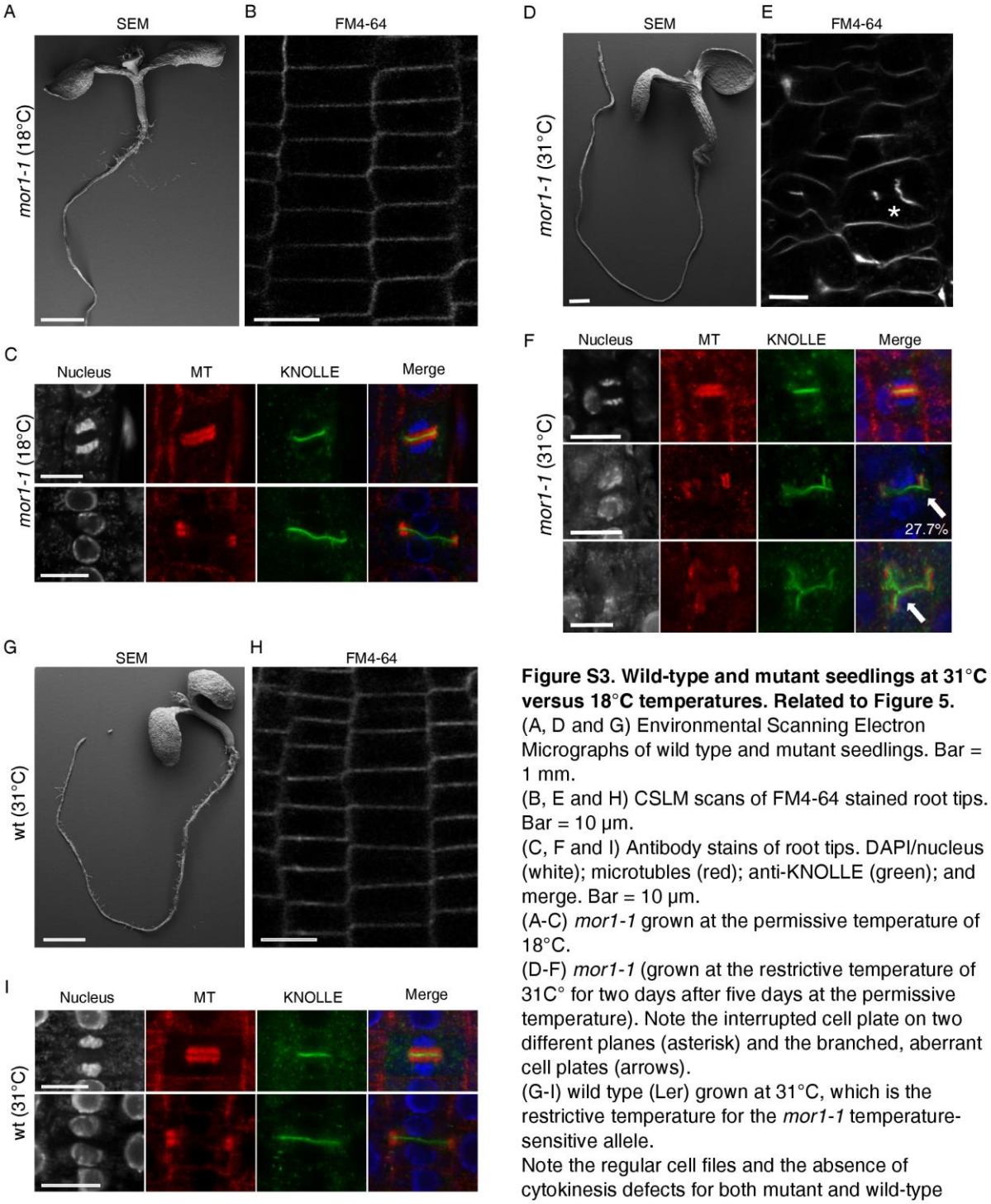

Figure S3. Wild-type and mutant seedlings at 31°C versus 18°C temperatures. Related to Figure 5.
(A, D and G) Environmental Scanning Electron Micrographs of wild type and mutant seedlings. Bar = 1 mm.
(B, E and H) CSLM scans of FM4-64 stained root tips. Bar = 10 µm.
(C, F and I) Antibody stains of root tips. DAPI/nucleus (white); microtubles (red); anti-KNOLLE (green); and merge. Bar = 10 µm.
(A-C) *mor1-1* grown at the permissive temperature of 18°C.
(D-F) *mor1-1* (grown at the restrictive temperature of 31C° for two days after five days at the permissive temperature). Note the interrupted cell plate on two different planes (asterisk) and the branched, aberrant cell plates (arrows).
(G-I) wild type (Ler) grown at 31°C, which is the restrictive temperature for the *mor1-1* temperature-sensitive allele.
Note the regular cell files and the absence of cytokinesis defects for both mutant and wild-type controls in (A-C and G-I).

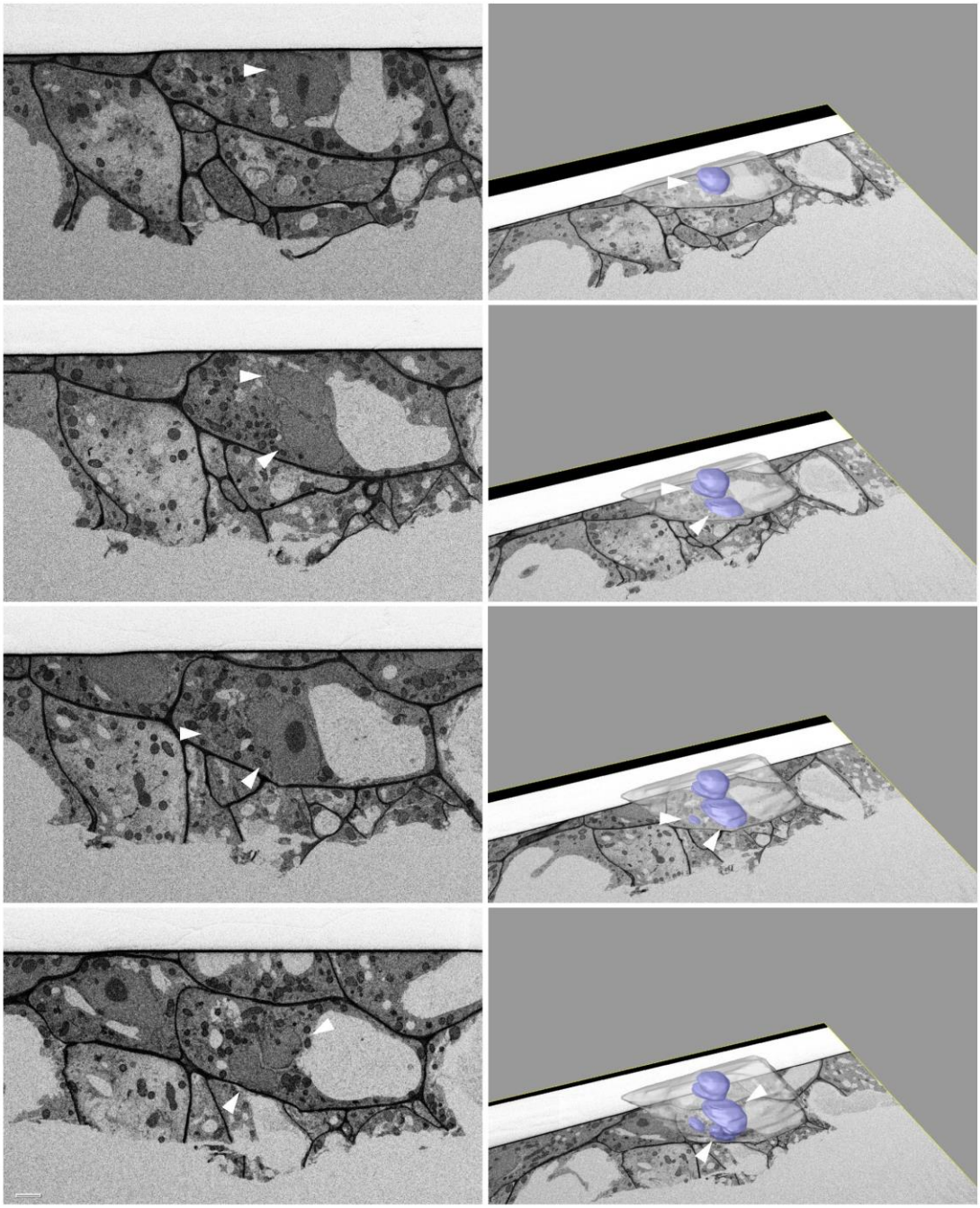

Figure S4. 3D reconstruction of *keule*^{T282}mutant via Focused Ion Beam/Scanning Electron Micrographs of high pressure frozen, freeze substituted five-day old root tips. Related to Figure 6. Single slices are shown on the left and 3D reconstructions of entire stacks on the right. Nuclei: blue spherical structures; cell outline transparent. Bar = 2 µm.

Allele	AGI gene identi-fication	Polymorphism	Intron/ exon	Nature of the allele	Reference
mas-5	At2g36850	SALK_015454	Intron	Null; sdlg[a] lethal	Thiele et al., 2009
ple-3	At5g51600	GCT to GAT substitution causing an A to D amino acid exchange at aa 414		Hypomorph, viable.	MT Hauser, unpublished
ple-4		EMS-induced null allele, A to V substitution at aa 421		Null; sdlg lethal	Söllner et al., 2002; Smertenko et al., 2004
hik^{G235}	At1g18370	EMS-induced null allele; not sequenced		Null; sdlg lethal	Söllner et al., 2002
clasp-1	At2g20190	SALK_120061	Exon	Null; viable	Ambrose et al., 2007
mor1-1	At2g36530	EMS-induced allele		Temperature-sensitive	Whittington et al., 2001
exo84b-2	At5g49830	SAIL_736_A04	Intron	Null; sdlg lethal	Fendrych et al., 2010
trs120-4	At5g11040	SAIL_1285_D07	Intron	Null; sdlg lethal	Thelmann et al., 2010
keu^{mm125}	At1g12360	X-ray induced 156bp deletion at 3' end of coding sequence			Assaad et al., 2001
keu^{T282}		EMS-induced point mutation at junction of 2nd exon/intron		Null; sdlg lethal	Assaad et al., 2001

Table S1. Mutant lines used in this study.
a: Seedling (abbreviated "sdlg")- lethal lines were propagated as hetero- or hemizygotes.

Supplemental Experimental Procedures

Molecular techniques

Standard molecular techniques were used for subcloning (Sambrook at al., 1989). DNA was isolated from rosette leaves or influorescences of soil-grown plants. CTAB minipreps were prepared as described by Assaad et al. (2001). PCR analysis was carried out with GoTaq (Promega) for standard purposes or with high fidelity PfuUltra II fusion HS DNA polymerase for gene fusions (Agilent Technology inc., Santa Clara, USA). Restriction enzymes were from Promega, NEB or Fermentas. All constructs were introduced into *Agrobacterium tumefaciens* strain GV3101 (Koncz and Shell, 1986) and plants were transformed using the simplified floral-dip method as described in Clough and Bent (1998). T1 plants were selected for transformants on Murashige and Skoog (MS) medium containing 50 µg/ml kanamycin.

Electron Microscopy

The FIB serial sectioning was performed by a Zeiss-Auriga workstation. The resin block was trimmed with a pyramitome (LKB) with glass knives so that vertical faces allowed lateral milling of the cells by the FIB. Tomographic datasets were obtained using the ‘‘slice and view’’ technique using a Zeiss Auriga 60 dual beam instrument (Carl Zeiss Microscopy, Oberkochen, Germany). For slicing with the focused ion beam, the conditions were as follows: 2 nA milling current of the Ga-emitter; with each step 30 to 60 nm of the Epon was removed with the FIB. SEM images were recorded with an aperture of 60 µm in the high current mode at 1.5 kV of the in-lens EsB detector with the EsB grid set to 1,350 - 1,400 V. Line averaging 4 was performed. The pixel size was 30 x 30 nm. The pixel dimensions of a recorded image were 2,048 x 1,536 pixel. The time to acquire one frame was 90 s. The slice and view process was repeated 130 to 1350 times to obtain the datasets. The contrast of the images was inversed, so that they appeared like a conventional bright field TEM image.

Supplemental References

Clough, S.J., and Bent, A.F. (1998). Floral dip: a simplified method for Agrobacterium-mediated transformation of Arabidopsis thaliana. Plant J. *16*, 735-743.

Koncz, C., and Schell, J. (1986). The promoter of TL-DNA gene 5 controls the tissue-specific expression of chimaeric genes carried by a novel type of Agrobacterium binary vector. Mol. Gen. Genet. *204*, 383-396.

Sambrook, J., Fritsch, E.F., and Maniatis, T. (1989). Molecular cloning: A laboratory Manual.
II ed^{n}. (New York: Cold Spring Harbourn Laboratory Press).

Cell cycle-regulated PLEIADE/AtMAP65-3 links membrane and microtubule dynamics during plant cytokinesis

Alexander Steiner[1], Katarzyna Rybak[1], Melina Altmann[2], Heather E. McFarlane[3,7], Susan Klaeger[4], Ngoc Nguyen[1], Eva Facher[5], Alexander Ivakov[3,7], Gerhard Wanner[5], Bernhard Kuster[4], Staffan Persson[3,6,7], Pascal Falter-Braun[2], Marie-Theres Hauser[8] and Farhah F. Assaad[1*]

[1] Botany, Technische Universität München, 85354 Freising, Germany

[2] Plant Systems Biology, Technische Universität München, 85354 Freising, Germany

[3] School of Biosciences, University of Melbourne, Parkville 3010, Victoria, Australia

[4] Chair of Proteomics and Bioanalytics, Technische Universität München, 85354 Freising, Germany

[5] Department Biologie I, Ludwig-Maximillians Universität, 82152 Planegg-Martinsried, Germany

[6] ARC Centre of Excellence in Plant Cell Walls, School of Biosciences, University of Melbourne, Parkville 3010, Victoria, Australia

[7] Max Planck Institute for Molecular Plant Physiology, 14476 Postdam, Germany

[8] Department of Applied Genetics and Cell Biology, University of Natural Resources and Life Sciences, 1190 Vienna, Austria

SUMMARY

Cytokinesis, the partitioning of the cytoplasm following nuclear division, requires extensive coordination between cell cycle cues, membrane trafficking and microtubule dynamics. Plant cytokinesis occurs within a transient membrane compartment known as the cell plate, to which vesicles are delivered by a plant-specific microtubule array, the phragmoplast. While membrane proteins required for cytokinesis are known, how these are coordinated with microtubule dynamics and regulated by cell cycle cues remains unclear. Here, we document physical and genetic interactions between Transport Protein Particle II (TRAPPII) tethering factors and microtubule-associated proteins of the PLEIADE/AtMAP65 family. These interactions do not specifically affect the recruitment of either TRAPPII or MAP65 proteins to the cell plate or midzone. Rather, and based on single versus double mutant phenotypes, it appears that they are required to coordinate cytokinesis with the nuclear division cycle. As MAP65 family members are known to be targets of cell cycle regulated kinases, our results provide a conceptual framework for how membrane and microtubule dynamics may be coordinated with each other and with the nuclear cycle during plant cytokinesis.

INTRODUCTION

In plants, the onset of cytokinesis is characterized by the assembly of a plant-specific microtubule array, the phragmoplast. Phragmoplast microtubules are initially organized in a solid array. As cells enter telophase, microtubules are translocated to the leading edges of the phragmoplast, giving rise to a ring-shaped phragmoplast (Müller and Jürgens, 2015). Recent studies have addressed the transition from the solid to the ring-shaped phragmoplast (for review see Lee and Liu, 2013). The centrifugal expansion that underlies this transition is a result of continuous microtubule assembly at the periphery of the phragmoplast concomitant with the disassembly of microtubules towards the center of the phragmoplast (Smertenko et al., 2011). New microtubules are nucleated on existing phragmoplast microtubules (Murata et al., 2013). Nucleation requires γ-tubulin, which is an essential and conserved component of plant and animal MTOCs. γ-tubulin is found at the phragmoplast, with a preference for microtubule minus ends at the distal edges facing the daughter nuclei; it is not found at the phragmoplast midzone (Kong et al., 2010). At the plus end, bundling of antiparallel microtubules coming from opposite sides of the division plane occurs selectively at the periphery of the phragmoplast. Bundling is mediated by the dimerization of microtubule cross-linking proteins of the MAP65 family, notably the cytokinesis-specific MAP65-3/PLEIADE member (Müller et al., 2002, 2004; Ho et al., 2012; Murata et al., 2013). The Arabidopsis MAP65 family encodes plant-specifc microtubule-associated proteins (MAPs) that have been shown to bind and bundle microtubules *in vitro* (Chan et al., 2003; Van Damme et al., 2004; Gaillard et al., 2008). The debundling of microtubules towards the center of the phragmoplast is mediated via phosphorylation of MAP65-3/PLEIADE by mitogen-activated protein MAP kinases (Takahashi et al., 2004). The MAP kinase cascade is, in turn, activated in a cell cycle dependent fashion by the Kinesin 7 member NACK1/HINKEL (Sasabe et al., 2006, 2011a; Vanstraelen et al., 2006). The NACK1/NACK2 kinesin-like proteins, together with the MAPK cascade, comprise the NACK-PQR pathway

(Lee and Liu, 2013). Debundled microtubules are thought to be severed and disassembled via the action of katanin (Panteris et al., 2011).

The organization of the phragmoplast microtubule array requires KINESIN 12A/12B motors, which specifically decorate the plus end of phragmoplast microtubules in a MAP65-3 dependent manner (Lee et al., 2007; Ho et al., 2011). Phragmoplast microtubules are organized in an antiparallel array with their plus ends facing the division plane, such that transport from both sides of a dividing cell delivers vesicles to the cell equator. At the equator, the nascent cross wall is assembled within the lumen of a transient membrane compartment referred to as the cell plate. The execution of plant cytokinesis requires a number of trafficking components involved in vesicle formation, tethering, docking and fusion (Ebine and Ueda, 2015; Müller and Jürgens, 2015). The BIG ARF-GEFs have recently been shown to regulate cytokinetic vesicle formation (Richter et al., 2014). The Transport Protein Particle II (TRAPPII) tethering complex and interacting Rab-GTPases are required for cell plate formation (Chow et al., 2008; Jaber et al., 2010; Qi and Zheng, 2011; Qi et al., 2011; Rybak et al., 2014; for review see Kim et al., 2016). Later in cytokinesis, the exocyst tethering complex is involved cell plate maturation (Fendrych et al., 2010; Rybak et al., 2014; reviewed by Boruc and Van Damme, 2015). Membrane fusion events at the cell plate are predominantly mediated by the t-SNARE KNOLLE and its interacting partner, the SM/Sec1 protein KEULE (Waizenegger et al., 2000; Assaad et al., 2001; Park et al., 2012; for review see Müller and Jürgens, 2015) . While membrane proteins required for cytokinesis are known, how these are coordinated with microtubule dynamics and regulated by cell cycle cues remains to be elucidated.

In this study, we document physical and genetic interactions between membrane and microtubule components of cytokinesis. We first identified membrane related cytokinesis components whose localization dynamics best follow phragmoplast microtubule array organization. We then used these membrane-related proteins as baits for immunoprecipitation experiments. Copurified proteins, identified by mass spectrometry, were

mined for proteins interacting with microtubule plus ends. We subsequently focused on the most interesting pair of membrane related proteins and MAPs: the TRAPPII - MAP65 interaction. The mass spectrometry data were validated with binary interaction assays, double mutant analyses and an analysis of co-localization. An appraisal of single versus double mutant phenotypes lead us to outline a conceptual framework for the coordination between membrane and cytoskeletal dynamics and their regulation by cell cycle cues during plant cytokinesis.

RESULTS and DISCUSSION

The TRAPPII tethering complex interacts with MAP65 family members

To identify interactions that govern the coordination between membrane and microtubule dynamics during cytokinesis, we performed immunoprecipitation experiments with mass spectrometry readout. We first monitored seven membrane-related markers (Table S1) for their localization dynamics at the cell plate, in conjunction with a microtubule marker (Gutierrez et al., 2009). Of these, the Sec1/Munc18 protein KEULE-GFP (Steiner et al., 2016) as well as the TRAPPII tethering factors TRS120-GFP and CLUB/AtTRS130-GFP (Rybak et al., 2014) best followed microtubule array reorganization from the solid to the ring-shaped phragmoplast stages. These three markers were subsequently used as baits and the mass spectrometry data were mined for potential microtubule-related hits.

An abundance of tubulin subunits and several proteins associated with microtubule plus-end tracking (+TIP; Bisgrove et al., 2004; Hamada, 2014) were enriched in TRAPPII but not in KEULE pulldowns (Table I; Table S2). Interestingly, six unique peptides corresponding to Arabidopsis Microtubule Associated Protein 65 (MAP65) proteins (Smertenko et al., 2004; Van Damme et al., 2004; Sasabe et al., 2011b; Ho et al., 2012)) co-purified with CLUB-GFP and five with AtTRS120-GFP; of these, four peptides were identified in both TRAPPII pull downs (Table I; Table S2; Figure S1). The signals showed strong intensity, a significant enrichment over the control (empty GFP-cassette) and a significant P value of 0.008 across three

biological replicates. Considering that genes that are co-expressed tend to be involved in related biological processes (Usadel et al., 2009), we evaluated co-expression coefficients using Genevestigator (Hruz et al., 2008; Table I). This identified positive correlations in a number of cases, with numbers in the 0.5 range that are similar to those found for known TRAPP components (see Table S2), which supports our proteomic data.

We focused on microtubule-associated proteins of the MAP65 family, which are known to bundle and stabilize the plus end of microtubules *in vitro* (Smertenko et al., 2004; Gaillard et al., 2008). The Arabidopsis MAP65 family consists of nine members of which three, AtMAP65-1, AtMAP65-2 and PLEIADE (also known as AtMAP65-3), have been shown to act redundantly during cytokinesis (Sasabe et al., 2011b). To test for binary interactions, we performed yeast two hybrid (Y2H) and bifluorescence complementation (BiFC) assays. The full-length CLUB/AtTRS130 and AtTRS120 TRAPPII proteins were poorly expressed in yeast and, in our hands, did not work for Y2H. We, therefore, constructed truncations. CLUB/AtTRS130 and AtTRS120 have conserved TRAPPII domain structures that span the entire length of the protein (Koumandou et al., 2007). Truncations were designed via phylogenetic analysis and the proteins accordingly split into highly conserved (C1, T1), intermediate or mixed (C2, T2) and plant-specific (C3, T3) moieties (Figure 1a). In yeast, the CLUB C3 plant-specific fragment yielded strong interactions with PLEIADE/AtMAP65-3 but the C1 and C2 fragments did not (Figure 1b). Bifluorescence complementation (BiFC) confirmed interactions between TRAPPII subunits and both AtMAP65-1 and PLEIADE/AtMAP65-3 (Figure 1c). While TRAPPII interactions were localized to membranes or to the cytosol, the TRAPPII – MAP65 interactions localized to an ordered, linear array that resembled cortical microtubules (Figure 1c).

Table I. Analysis of CLUB-GFP immunoprecipitates (IPs) via mass spectrometry. This table lists only microtubule-related proteins with a possible role in plus-end tracking or a microtubule stabilizing role detected in the IPs. The data are based on three biological replicates.

molecular function	AGI[a]	LOCUS NAME	p value in proteomic screen[b]	coexpression coefficient[c]	biological role (cellular phenotype)[d]	References
Stabilizing MAP	At5g55230	AtMAP65-1	0,008	0.53	binds and bundles MTs, stabilizes MTs, promotes nucleation. Is involved in mitotic cell cycle.	(Smertenko et al., 2004; Van Damme et al., 2004; Mao et al., 2005; Sasabe et al., 2011b)
+TIP	At4g27060	TOR1/SPR2	0,00003	0.48	plant-specific MAP that regulates the orientation of cortical MTs and organ growth. Is involved in mitotic cell cycle	(Yao et al., 2008; Wightman et al., 2013)
	At2g20190	AtCLASP	0,002	0.57	MAP215 member involved in cell division and cell expansion. Is thought to promote MT stability.	(Ambrose et al., 2007, 2011; Ambrose and Wasteneys, 2008; Kirik et al., 2007; Pietra et al., 2013)
	At2g35630	MOR1	0,00006	0.44	MAP215 member required for cortical MT organization. Required for cell division, cell expansion and root hair polarity.	(Eleftheriou et al., 2005; Kawamura et al., 2006; Lechner et al., 2012; Twell et al., 2002; Whittington et al., 2001)

a: (AGI) Arabidopsis genome initiative accessions (www.arabidopsis.org).

b: p values (< 0.002) were calculated using the t-test (two-sided). See Table S1 for the quality and specificity of the hits, which is comparable to that of known TRAPP interactors of CLUB/AtTRS130 (Table S1; Rybak et al., 2014).

c: Coexpression coefficients (Genevestigator (Hruz et al., 2008), perturbations), were similar to those found for other TRAPP components (see Table S1).

d: as seen by gene ontology annotation on www.arabidopsis.org (Swarbreck et al., 2007).

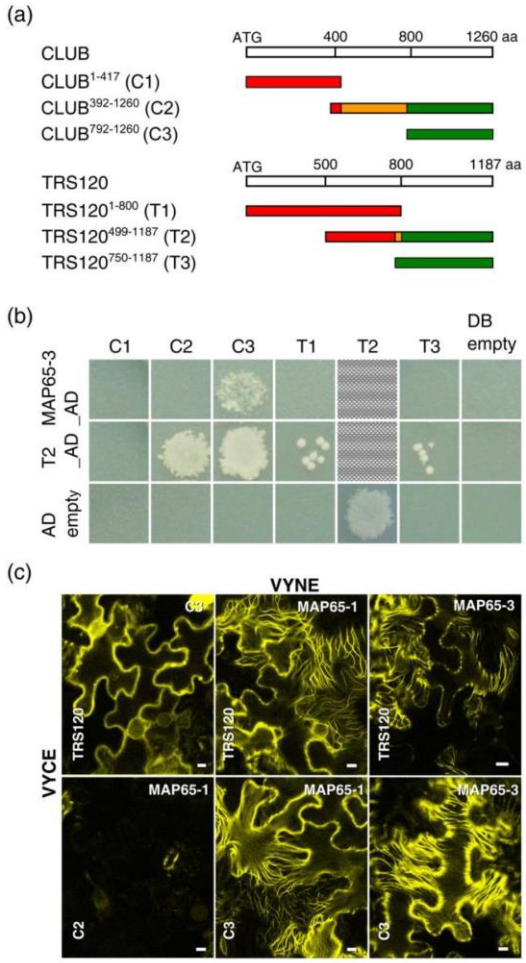

Figure 1. Physical interaction between the TRAPPII complex and MAP65 proteins. See also Figure S1.
(a) TRAPPII truncations used for binary interaction assays. Segments colored in red are conserved across kingdoms, while ones in green are plant-specific. The orange moiety of the C2 segment is poorly conserved across kingdoms. The T2 middle segment corresponds to sequences found to interact with the exocyst in a yeast two-hybrid screen (Rybak et al., 2014).
(b) Yeast two-hybrid experiments, the panels are spliced together from different plates. Note positive interactions between the plant specific C3_DB CLUB/AtTRS130 truncation and AtMAP65-3_AD, and between CLUB C2_DB or C3_DB and T2_AD. T2_DB is an auto activator, as evidenced by colony growth with the empty AD vector, and this precludes our ability to determine whether AtTRS120_T2 interacts with PLEIADE/ AtMAP65-3.
(c) BiFC experiments. VYNE and VYCE vectors represent fusions of the specified proteins or protein fragments to N- and C-terminal YFP moieties. The CLUB-C3 truncation and AtTRS120 full-length protein interact with AtMAP65-1 and AtMAP65-3. This interaction is localized to an ordered, linear array reminiscent of cortical microtubules. By contrast, TRAPPII complex interactions (here CLUB_C3 is shown to interact with TRS120) are localized to intracellular membranes and to the cytosol. As a negative control, AtMAP65-1 does not interact with the CLUB_C2 truncation. Bars = 10 μm.

For an assessment of genetic interaction, we focused on PLEIADE/AtMAP65-3 because it has a specific cytokinesis-defective phenotype reminiscent of *keule* and of TRAPPII mutants (Smertenko et al., 2004). Indeed, *pleiade* null mutants were identified in the same screens as *club* (Söllner et al., 2002) and *keule* (Gillmor et al., 2016). Double mutant analysis showed synergistic genetic interactions for *ple-2 trs120-*4 double mutants, in which we combined a hypomorphic, viable *ple-2* allele with a null seedling lethal allele of the TRAPPII-specific subunit TRS120 (Figure 2). An additional line of evidence for an interaction is the observation that the TRAPPII subunit TRS120-mCherry (Rybak et al., 2014), which co-localizes with CLUB-GFP at the cell plate (Figure S2), co-localizes with GFP-PLEIADE (Steiner et al., 2016) throughout cytokinesis (Figure 3; Figure S2).

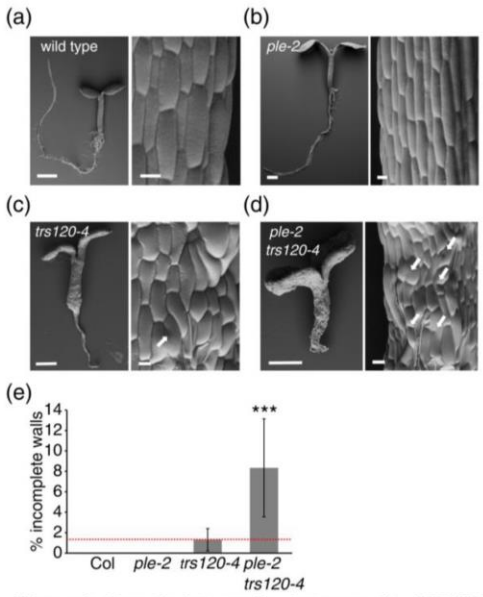

Figure 2. Genetic interaction between the TRAPPII complex and MAP65 proteins.
(a-d) Environmental Scanning Electron Micrographs of wild type and mutant seedlings. Arrows point to cell wall stubs.
Bars = 0.5 mm overview; 20 µm close-up.
(a) wild type.
(b) *ple-2*, a hypomorphic, viable allele of the *AtMAP65-3* locus.
(c) *trs120-4* , a *TRAPPII* null mutant.
(d) *ple-2 trs120-4* double mutant.
(e) % hypocotyl cells with incomplete cross walls in single and double mutants. The dotted red line depicts an additive phenotype; note the synthetically enhanced (i.e. larger than additive) number of incomplete walls. Mean ± S.E.M. ***$p = 3\ e^{-06}$ for a comparison between *trs120-4* and double mutants; Student's two-tailed t test. n = 20 wild type (Col-0), n = 3 *ple-2*, n = 18 *trs120-4* and n = 9 *ple-2 trs120-4* seedlings.

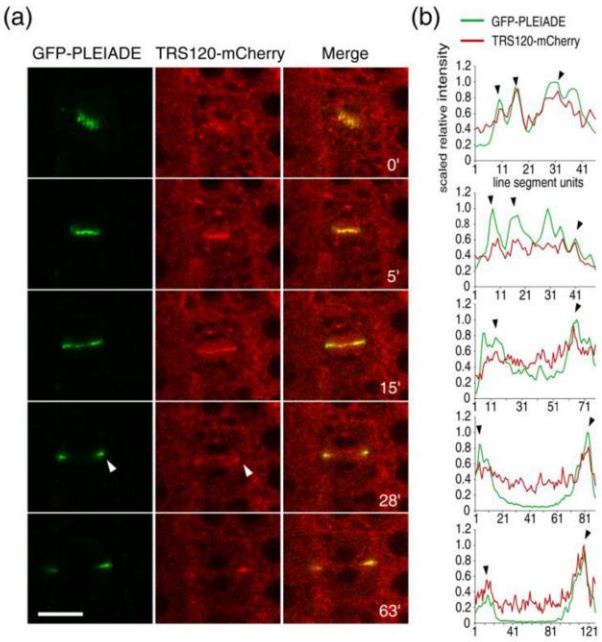

Figure 3. Colocalization between TRS120-mCherry and GFP-PLEIADE in meristematic arabidopsis root cells.
(a) Time lapse of P_{PLE}::GFP-PLEIADE with the P_{UBQ}::TRS120-mCherry TRAPPII subunit is shown, with minutes indicated in the right panel. The markers co-localize throughout cytokinesis. Arrowheads point to leading edges of the cell plate. Bars = 10 µm.
(b) The line graphs depict scaled relative intensity of GFP-PLEIADE and TRS120-mCherry at the cell plate. Note that throughout cytokinesis almost every peak of GFP-PLEIADE fluorescence coincides with a peak of TRS120-mCherry fluorescence (black arrowheads).

The TRAPPII complex does not appear to act as a membrane anchor for GFP-PLEIADE at the cell plate

To assess the biological relevance of the interactions between PLEIADE/AtMAP65-3 and TRAPPII in the specific context of plant cytokinesis, we first tested whether the TRAPPII membrane tether acts as an anchor for PLEIADE/AtMAP65-3 at the phragmoplast midzone by monitoring GFP-PLEIADE in *TRAPPII* mutants. GFP-PLEIADE was localized at the phragmoplast midzone in both wild-type and *TRAPPII* mutants, but the signal was sometimes discontinuous in *club-2* (Figure 4a). In *club-2* the phragmoplast microtubules were at times also discontinuous in their appearance (Figure 4b), reminiscent of patchy cell plates seen in this mutant line (Rybak et al., 2014). With antibody stains we observed 14%

patchy phragmoplasts in *club-2* mutants, as compared to 0.4 % in the wild type (n = 83 *club-2* or 228 wild-type telophase cells), and there was a 100 % correlation between patchy cell plates and patchy phragmoplasts (n = 12) in *club-2*. We conclude that the TRAPPII complex does not appear to act as a membrane anchor for GFP-PLEIADE at the cell plate.

PLEIADE/AtMAP65-3 is not essential for recruiting the TRAPPII complex to the cell plate

We next tested whether, conversely, PLEIADE/AtMAP65-3 may be required for the delivery of the TRAPPII complex to the cell plate. To this effect, we imaged TRS120-GFP in the *ple-4* mutant background. In 78% of cases, (n = 18), we found that the cell plate localization of TRS120-GFP was considerably more diffuse in the *ple-4* mutant background than in the wild-type (Figure 4c and 4d). PLEIADE/AtMAP65-3 is known to bundle antiparallel microtubules coming from opposite sides of the division plane, and as a consequence *pleiade* mutants are characterized by a larger midzone gap (Müller et al., 2004; Ho et al., 2012). The observed defect in TRS120-GFP localization in the *ple-4* background was also seen with the FM4-64 stain (Figure 4c and 4d) and may reflect the larger midzone characteristic of *pleiade* mutants rather than a specific defect resulting from a direct interaction between PLEIADE/AtMAP65-3 and the TRAPPII complex. Indeed, the increased cell plate thickness we observe (1.2 µm; Figure 4d) corresponds to the enlarged width of the midzone gap reported in *pleiade* null alleles (1.2 µm; Ho et al., 2012). Overall, in both the wild-type and *ple-4* mutant backgrounds, TRS120-GFP was recruited to the cell plate, reorganized to the leading edges as the cell plate expanded, and was removed from the cell plate at the end of cytokinesis (compare Figure 4c to Figure S2). These results imply that PLEIADE/AtMAP65-3 is not essential for recruiting the TRAPPII complex to the developing cell plate.

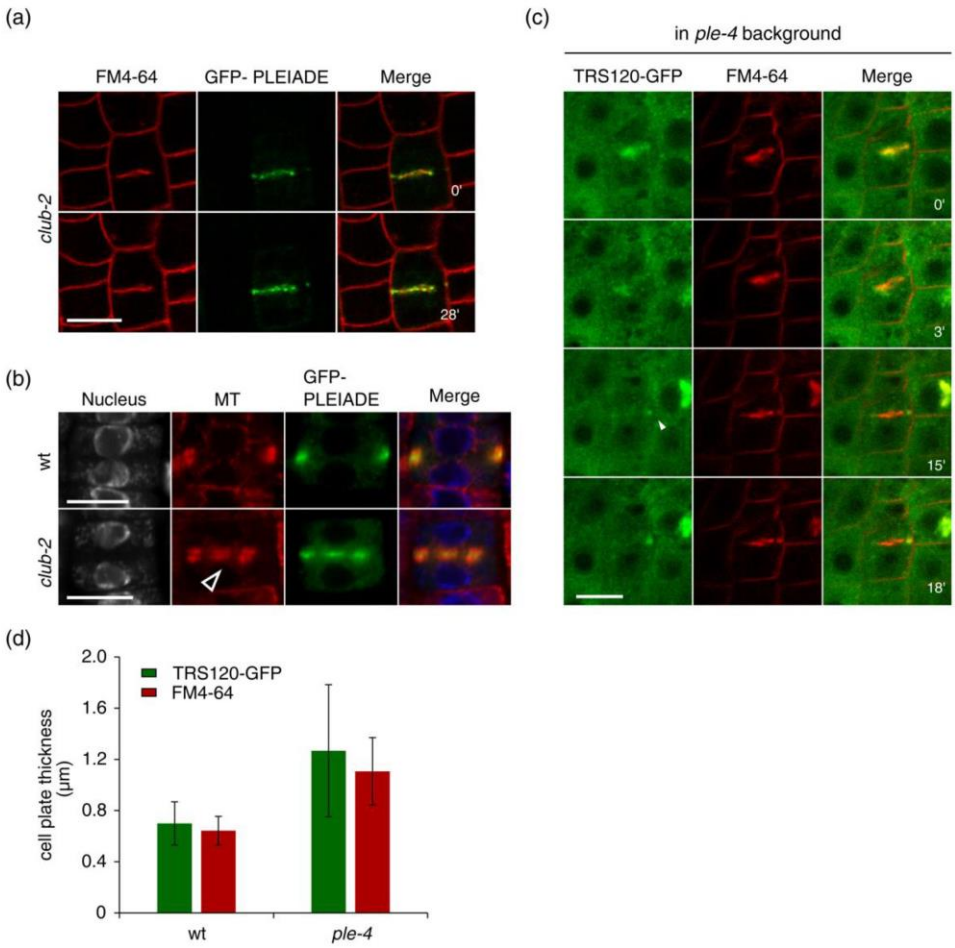

Figure 4. Localization of TRAPPII and PLEIADE/AtMAP65-3 gene fusions in mutant backgrounds.
(a-c) Time lapses are shown, with minutes indicated in the right panel. Arrowheads point to leading edges of the cell plate. Bars = 10 µm.
(a) P_{PLE}::GFP-PLEIADE time lapse in *club-2*, a *TRAPPII* null mutant. Note the punctate appearance of the cell plate. Also, within a 28 minute time lapse, GFP-PLEIADE has failed to reorganize to the leading edges of the cell plate, suggestive of an impairment in MT dynamics.
(b) Antibody stains in P_{PLE}:GFP-PLEIADE root tips. DAPI/nucleus (white); microtubules (red) anti-GFP; and merge. Note that in *club-2* mutants (lower panel), GFP-PLEIADE is found at the midzone of patchy phragmoplasts (open arrowhead). Bars = 10 µm.
(c) TRS120-GFP in *ple-4*, a null allele of the *AtMAP65-3* locus. Note the diffuse appearance of both TRS120-GFP and FM4-64.
(d) Thickness of cell plate in µm, as assessed with TRS120-GFP (green) or FM4-64 (red) in wild type and *ple-4* root tips. Mean ± S.E.M. Wild type n = 6 cell plates and 24 measurements; *ple-4* n = 18 cell plates and 70 measurements.

The nuclear cycle and cytokinesis appeared to be uncoupled in *pleiade/map65-3 trs120* double mutants

As TRAPPII or PLEIADE/AtMAP65-3 did not appear to specifically affect one another's localization dynamics during cytokinesis, we probed the significance of the interaction by carrying out a more thorough analysis of double mutant phenotypes. Immunofluorescence assays showed that *ple-2 trs120-4* double mutants had a synthetically enhanced number of cells in which four or more nuclei were clumped together in the apparent absence of even vestigial cross walls (Figure 5a-c). Cells with four or more nuclei were never observed in the wild-type or in *trs120-4* single mutants, occurred at a frequency of 0.6% in *ple-2* hypomorphs (n = 4136 cells), and of 12.1% in double mutant cells (n = 1185 cells; Figure 5c). This twenty-fold enhancement between *ple-2* and *ple-2 trs120-4* was highly significant ($p = 3.3\ e^{-05}$) and provided further evidence for a genetic interaction. In summary, in the double mutants the nuclear cycle and cytokinesis appeared to be uncoupled.

The interesting difference between *ple-2* hypomorphs and *trs120-4* null mutants with respect to the incidence of multinucleate cells prompted us to reevaluate the *ple-4* null phenotype. To this effect, we carried out histological sections (Figure 5d) and Focused Ion Beam/Scanning Electron Microscopy (FIB/SEM), which allows for 3D reconstructions at high resolution (Figure 5e). FIB/SEM tomographic datasets occasionally showed binucleate cells in which the cross wall was entirely absent in *ple-4* null mutants (Figure 5e). By contrast, FIB/SEM of *trs120-4* single mutants invariably revealed at least rudimentary cross walls between daughter nuclei (Rybak et al., 2014). Thus, in the double mutant, the *trs120-4* allele synthetically enhances a nuclear phenotype that it itself does not manifest on its own. The contrast between the single mutants further highlights the significance of the synergistic enhancement of the multinucleate phenotype in *ple-2 trs120-4* double mutants (Figure 5a-c).

Progression through the cell cycle involves four key transitions: entry into S-phase, entry into mitosis, exit from mitosis and fourth, the onset and execution of cytokinesis. The key regulators of the first three transitions, which include cyclin-dependent kinases and the

anaphase promoting complex, appear to be conserved across kingdoms (Assaad, 2001). The last stage of the cell cycle, however, appears to be different in plants as compared to both fungi and animals. Indeed, in plants a mitogen-activated protein (MAP) kinase cascade, rather than polo kinases, have been shown to regulate plant cytokinesis (Sasabe et al., 2006; Kosetsu et al., 2010). The MAP kinase cascade is activated in a cell cycle dependent fashion and, in turn, targets MAP65 proteins (Sasabe et al., 2006, 2011a; Kosetsu et al., 2010; Müller and Jürgens, 2015). It is interesting that the plant-specific moiety of CLUB/AtTRS130 interacts with PLEIADE/AtMAP65-3. This highlights the unique features of plant cytokinesis, which include the phragmoplast microtubule array and the nature of its cell cycle regulation.

The TRAPPII complex is required for cell plate biogenesis throughout cytokinesis, from cell plate initiation to insertion (Rybak et al., 2014), and it is possibly at this level that cell cycle regulation would be most effective. If the biological role of the TRAPPII-MAP65 interaction were to transmit cell cycle cues to cell plate membranes, we would predict that TRAPPII mutants should have additional phenotypes related to those of targeted MAP65 mutants insensitive to cell-cycle cues. In tobacco, such mutants are severely impaired in centrifugal phragmoplast expansion from the solid to the ring shaped phragmoplast stages (Sasabe et al., 2006). Phragmoplast expansion is also blocked in Arabidopsis Fused kinase TWO-IN-ONE (TIO) mutants; the TIO kinase interacts both with KINESIN 12 and with the NACK-PQR pathway that targets PLEAIDE/AtMAP65-3 (Oh et al., 2005, 2012, 2014). Thus, the NACK-PQR-MAP65 signal transduction pathway appears to act as a major node to regulate phragmoplast expansion. This consideration led us to monitor phragmoplast microtubule reorganization in TRAPPII *club-2* and *trs120-4* mutants. Both live cell imaging (Movies S1-S3; Figure S3) and antibody stains showed a pronounced defect in phragmoplast microtubule reorganization from the solid to the ring-shaped stages in both *club-2* and *trs120-4* (Figure S3). The live imaging shows that there is a delay but not an absolute block in the transition (Movies S1-S3). This is entirely consistent with our hypothesis.

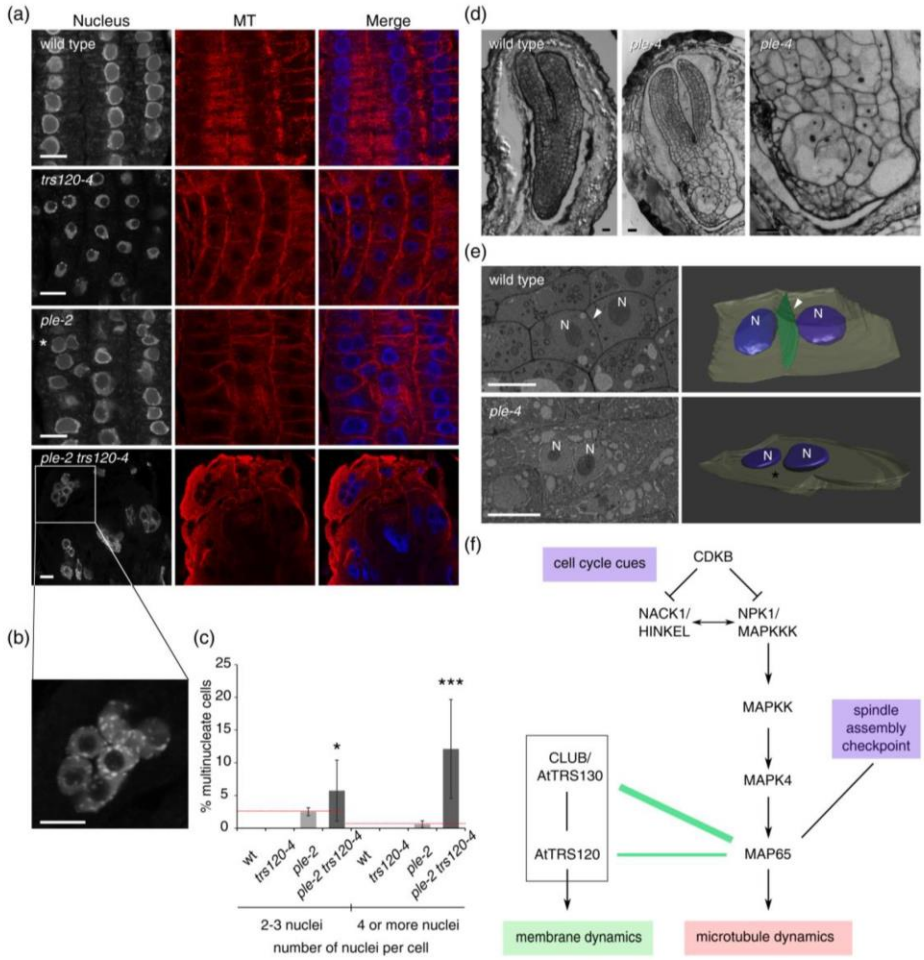

Figure 5. Characterization of TRAPPII and *pleiade* single and double mutants. See also Figure S3.
(a) Antibody stains of root tips. DAPI/nucleus (white); microtubules (red); and merge. Bars = 10 µm. Note the absence of multinucleate cells in wild type and *trs120-4*, but the binucleate cell in *ple-2* (asterisk) and the multinucleate cells in the *ple-2 trs120-4* double mutant.
(b) A multinucleate cell characteristic of the double mutant, in which seven nuclei are clumped together in the absence of even vestigial cross walls.
(c) % multinucleate cells lacking cross walls or stubs. Mean ± S.E.M. The horizontal dotted red line depicts an additive phenotype. *p = 0,03 for a comparison between *ple-2* and *ple-2 trs120-4* for 2-3 nuclei; ***p = 3 e^{-05} for a comparison between *ple-2* and *ple-2 trs120-4* for 4 or more nuclei; Student's two-tailed t test; wild type: n = 1798 cells; *trs120-4*: n = 1123 cells; *ple-2*: n = 4136 cells; *ple-2 trs120-4*: n = 1185 cells.
(d) Toluidine-blue stained histological sections of mutant embryos. Bars = 10 µm.
Wild-type embryo (left panel).
ple-4 embryo (middle and right panels); note that the cytokinesis defect is more pronounced in the radicle.
(e) Focused Ion Beam/Scanning Electron Micrographs of high pressure frozen, freeze substituted five-day old root tips. Single slices are shown in the left panel and 3D reconstructions of entire stacks in the right panel. Nuclei (N): blue spherical structures; cross walls: green; cell outline: beige. Bars = 10 µm. Wild type (upper panel); note the regular shape of the cell and the complete cross wall. *ple- 4* (lower panel); note that there are two nuclei but no apparent cross wall in the 3D reconstruction (lower right panel).
(f) A conceptual framework for the integration of cell cycle cues with membrane and microtubule dynamics during plant cytokinesis. MAP65 proteins are targets of cell cycle regulated kinases (Kosetsu et al., 2010; Sasabe et al. 2011a, 2011b) and PLEIADE/ AtMAP65-3 also interacts with spindle assembly checkpoint (SAC) proteins (Paganelli et al., 2015). The TRAPPII-MAP65 interaction would thereby transmit cues pertaining to cell cycle progression and chromosome attachment to the trafficking apparatus at the cell plate, while ensuring the coordination of membrane and microtubule dynamics throughout cytokinesis. The depicted interactions are published (black) or documented by multiple lines of evidence in this contribution (green). The thickness of the line is proportional to the number of lines of evidence that document the interaction.

CONCLUSION and PERSPECTIVE

On the basis of the molecular functions of the interacting partners and of single versus double mutant phenotypes, we outline a conceptual framework (Figure 5f) for the integration of membrane dynamics, phragmoplast microtubule dynamics and the nuclear division cycle throughout cytokinesis. PLEIADE/AtMAP65-3 has recently been shown to interact with spindle assembly checkpoint (SAC) proteins in Arabidopsis (Paganelli et al., 2015). The SAC ensures error-free chromosome segregation by preventing the onset of anaphase as long as any unattached or incorrectly attached chromosomes are present. Thus, PLEIADE/AtMAP65-3 ultimately transmits cues pertaining not only to cell cycle progression but also to chromosome attachment to phragmoplast microtubules. The confirmed TRAPPII-MAP65 interaction would enable these cues to be coordinated with membrane dynamics during cytokinesis. To avoid bisecting the nucleus, it is critical that cross wall deposition be coordinated with cell cycle cues. Our findings provide a conceptual framework for how this might be achieved. Knowledge of checkpoints acting after the spindle assembly checkpoint is lacking (Musacchio, 2015), yet the striking phenotype of the *pleiade trs120* double mutants, in which the nuclear cycle and cytokinesis appear to be uncoupled, tempts one to speculate as to the existence of a cytokinesis checkpoint. The unusual distribution of an Arabidopsis SAC protein at the phragmoplast midzone during cytokinesis has formerly led to similar speculation (Caillaud et al., 2009). The TRAPPII – MAP65 interaction might, in fact, comprise a safeguard mechanism that coordinates the completion of cytokinesis with cell cycle progression beyond anaphase.

EXPERIMENTAL PROCEDURES

Lines and growth conditions

Seedling lethal mutant lines (Table S3) were propagated as hetero- or hemi-zygotes. Plants were grown in the greenhouse under controlled temperature conditions and with supplemental light, or under controlled growth chamber conditions (16/8 hr photoperiod at 250 µmol $m^{-2}s^{-1}$). Seed were surface sterilized, stratified at 4°C for two days and plated on MS medium supplemented with 1% sucrose and B5 Vitamins (Sigma). The root tips or hypocotyls of five-day old plate grown seedlings were used for imaging.

Molecular methods

TRAPPII truncations were constructed via Gateway cloning as described in the Supporting Information Methods S1, using full length cDNA clones obtained from the RIKEN Bioresource Center (Seki et al., 2002).

Co-immunoprecipitation

Co-immunoprecipitation experiments were carried out on three grams of leaves, seedlings or inflorescences using GFP-trap beads (Chromotek) or anti-HA beads (Roche), as described (Park et al., 2012 with modifications described in Rybak et al., 2014). NanoflowLc-MS/MS was performed by coupling an EksigentnanoLC-Ultra 1D+ (Eksigent, Dublin, CA) to a Velos-LTQ-Orbitrap (Thermo Scientific, Bremen, Germany; see Supporting Information Methods S2).

Yeast two hybrid (Y2H)

Y2H screens were performed as described (Dreze et al., 2010). Briefly, open reading frames (ORFs) encoding fragments of CLUB/AtTRS130 (C1-C3) and TRS120 (T1, T2, T3) were transferred by Gateway cloning into the GAL4 DNA-binding domain (DB) encoding Y2H vector pDEST-pPC97, and subsequently transformed into the yeast strain Y8930. These

constructs were screened by yeast mating against a collection of 12,000 Arabidopsis ORFs fused to the Gal4 activation domain (AD) in the yeast strain Y8800 (Weßling et al., 2014). Screening was done as a binary mini-pool screen, *i.e.* each DB-ORF was screened against pools of 188 AD-ORFs. Interactions were assayed by growth on selective plates using the *HIS3* reporter, and using 1mM 3-Amino-1,2,4-triazole (3-AT) to suppress background growth. This primary screen was carried out once and interaction candidates were identified by Sanger sequencing. All candidate interactions were verified by pairwise one-on-one mating in three independent experiments. Only pairs scoring positives in all three assays were considered as *bona fide* interaction partners.

Bifluorescence complementation

Agrobacterium carrying individual vectors were co-infiltrated into young *Nicotiana benthamiana* leaves in a solution of 10mM MES, 10mM $MgCl_2$, and 100µm acetosyringone with each Agrobacterium vector strain (Gookin and Assmann, 2014) at OD_{600}=0.03. Combinations are indicated in figure panels. BiFC signal was visualized using a Leica SP2 confocal microscope with 514nm excitation and 525-600nm emission filter to detect YFP. See Supporting Information Methods S3.

Antibody stains and confocal microscopy. Root tips were fixed in paraformaldehyde, permeablized and stained according to (Völker et al., 2001), with anti-KNOLLE (Lauber et al., 1997) (rabbit, 1:2000), anti-tubulin (mouse, 1:2500, Sigma), anti-rabbit monoclonal Alexa-m488 (goat, 1:600, Molecular Probes) as well as anti-mouse Cy3 (goat, 1:600, Dianova). Nuclei were stained with 1µg/ml DAPI (Sigma). A Fluoview 1000 confocal laser scanning microscope (Olympus) was used for images acquisition and processing.

Light and Electron microscopy

Histological embryo sections were prepared and imaged as described (Assaad et al., 1996). Fresh seedlings were imaged in low vacuum with a Zeiss (LEO) VP 438 scanning electron microscope operated at 15 kV. For electron microscopy, root tips were fixed by high-pressure freezing and freeze substituted (Leica HPM100; Leica ASF2) and FIB/SEM tomographic datasets were acquired with a Zeiss-Auriga workstation (Carl Zeiss Microscopy) as described in the Supporting Information Methods S4.

Statistical and Image analyses

False discovery rates, determined with the standard two-tailed t-test, were set at a cutoff of 1%. Images were processed with Adobe photoshop, analyzed with Image J, and assembled with Adobe Illustrator. 3D reconstructions were carried out with Imaris software (Bitplane).

SUPPORTING INFORMATION

Figure S1. AtMAP65-1 peptides identified in TRAPPII immunoprecipitated complexes. Related to Figure1.
Figure S2. TRS120-mCherry co-localizes with CLUB-GFP at the cell plate. Related to Figure 3.
Figure S3. Impairment of microtubule reorganization in *club-2* and *trs120-4* mutants. Related to Figure 5.
Table S1. Marker lines used in this analysis.
Table S2. Analysis of CLUB-GFP immunoprecipitates via mass spectrometry.
Table S3. Mutant lines used in this study.
Movie S1. Microtubule reorganization in the wild-type. Related to Figures 5 and S3.
Movie S2. Delayed microtubule reorganization in *club-2*. Related to Figures 5 and S3.
Movie S3. Delayed microtubule reorganization in *trs120-4*. Related to Figures 5 and S3.

Acknowledgement

We thank Prof. Grill and members of the Botany department for their support. Silvia Dobler in the laboratory of Andreas Klingl (LMU) prepared samples for electron microscopy. Rosi Söllner performed histological sections. David Ehrhardt, Gerd Jürgens and the RIKEN Bioresource Center shared published or public resources. HEM is supported by an EMBO Long-Term Fellowship (EMBO ALTF 1246-2013) and an NSERC PDF (PDF-454454-2014); AI and SP were funded by the Max-Planck-Gesellschaft, and SP by a R@MAP Professorship at University of Melbourne. This research was funded by DFG grant AS110/5-1 to FFA and GW and by the FWF grant P16410-B12 to MTH. The authors declare no conflict of interest.

REFERENCES

Ambrose, J.C., and Wasteneys, G.O. (2008). CLASP Modulates Microtubule-Cortex Interaction during Self-Organization of Acentrosomal Microtubules. Mol. Biol. Cell *19*, 4730–4737.

Ambrose, C., Allard, J.F., Cytrynbaum, E.N., and Wasteneys, G.O. (2011). A CLASP-modulated cell edge barrier mechanism drives cell-wide cortical microtubule organization in Arabidopsis. Nat. Commun. *2*, 430.

Ambrose, J.C., Shoji, T., Kotzer, A.M., Pighin, J.A., and Wasteneys, G.O. (2007). The Arabidopsis CLASP Gene Encodes a Microtubule-Associated Protein Involved in Cell Expansion and Division. Plant Cell *19*, 2763–2775.

Assaad, F.F. (2001). Of weeds and men: what genomes teach us about plant cell biology. Curr. Opin. Plant Biol. *4*, 478–487.

Assaad, F.F., Mayer, U., Wanner, G., and Jürgens, G. (1996). The KEULE gene is involved in cytokinesis in Arabidopsis. Mol. Gen. Genet. MGG *253*, 267–277.

Assaad, F.F., Huet, Y., Mayer, U., and Jürgens, G. (2001). The Cytokinesis Gene KEULE Encodes a Sec1 Protein That Binds the Syntaxin Knolle. J. Cell Biol. *152*, 531–544.

Boruc, J., and Van Damme, D. (2015). Endomembrane trafficking overarching cell plate formation. Curr. Opin. Plant Biol. *28*, 92–98.

Caillaud, M.-C., Paganelli, L., Lecomte, P., Deslandes, L., Quentin, M., Pecrix, Y., Le Bris, M., Marfaing, N., Abad, P., and Favery, B. (2009). Spindle Assembly Checkpoint Protein Dynamics Reveal Conserved and Unsuspected Roles in Plant Cell Division. PLoS ONE *4*.

Chan, J., Mao, G., Smertenko, A., Hussey, P.J., Naldrett, M., Bottrill, A., and Lloyd, C.W. (2003). Identification of a MAP65 isoform involved in directional expansion of plant cells. FEBS Lett. *534*, 161–163.

Chow, C.-M., Neto, H., Foucart, C., and Moore, I. (2008). Rab-A2 and Rab-A3 GTPases Define a trans-Golgi Endosomal Membrane Domain in Arabidopsis That Contributes Substantially to the Cell Plate. Plant Cell *20*, 101–123.

Dreze, M., Monachello, D., Lurin, C., Cusick, M.E., Hill, D.E., Vidal, M., and Braun, P. (2010). Chapter 12 - High-Quality Binary Interactome Mapping. B.-M. in Enzymology, ed. (Academic Press), pp. 281–315.

Ebine, K., and Ueda, T. (2015). Roles of membrane trafficking in plant cell wall dynamics. Front. Plant Sci. *6*, 878.

Eleftheriou, E.P., Baskin, T.I., and Hepler, P.K. (2005). Aberrant cell plate formation in the Arabidopsis thaliana microtubule organization 1 mutant. Plant Cell Physiol. *46*, 671–675.

Fendrych, M., Synek, L., Pečenková, T., Toupalová, H., Cole, R., Drdová, E., Nebesářová, J., Šedinová, M., Hála, M., Fowler, J.E., et al. (2010). The Arabidopsis Exocyst Complex Is Involved in Cytokinesis and Cell Plate Maturation. Plant Cell *22*, 3053–3065.

Gaillard, J., Neumann, E., Van Damme, D., Stoppin-Mellet, V., Ebel, C., Barbier, E., Geelen, D., and Vantard, M. (2008). Two Microtubule-associated Proteins of Arabidopsis MAP65s Promote Antiparallel Microtubule Bundling. Mol. Biol. Cell *19*, 4534–4544.

Gillmor, C.S., Roeder, A.H.K., Sieber, P., Somerville, C., and Lukowitz, W. (2016). A Genetic Screen for Mutations Affecting Cell Division in the Arabidopsis thaliana Embryo Identifies Seven Loci Required for Cytokinesis. PLOS ONE *11*, e0146492.

Gookin, T.E., and Assmann, S.M. (2014). Significant reduction of BiFC non-specific assembly facilitates in planta assessment of heterotrimeric G-protein interactors. Plant J. *80*, 553–567.

Gutierrez, R., Lindeboom, J.J., Paredez, A.R., Emons, A.M.C., and Ehrhardt, D.W. (2009). Arabidopsis cortical microtubules position cellulose synthase delivery to the plasma membrane and interact with cellulose synthase trafficking compartments. Nat. Cell Biol. *11*, 797–806.

Ho, C.-M.K., Hotta, T., Guo, F., Roberson, R.W., Lee, Y.-R.J., and Liu, B. (2011). Interaction of Antiparallel Microtubules in the Phragmoplast Is Mediated by the Microtubule-Associated Protein MAP65-3 in Arabidopsis. Plant Cell *23*, 2909–2923.

Ho, C.-M.K., Lee, Y.-R.J., Kiyama, L.D., Dinesh-Kumar, S.P., and Liu, B. (2012). Arabidopsis Microtubule-Associated Protein MAP65-3 Cross-Links Antiparallel Microtubules toward Their Plus Ends in the Phragmoplast via Its Distinct C-Terminal Microtubule Binding Domain[W]. Plant Cell *24*, 2071–2085.

Hruz, T., Laule, O., Szabo, G., Wessendorp, F., Bleuler, S., Oertle, L., Widmayer, P., Gruissem, W., and Zimmermann, P. (2008). Genevestigator V3: A Reference Expression Database for the Meta-Analysis of Transcriptomes. Adv. Bioinforma. *2008*, e420747.

Jaber, E., Thiele, K., Kindzierski, V., Loderer, C., Rybak, K., Jürgens, G., Mayer, U., Söllner, R., Wanner, G., and Assaad, F.F. (2010). A putative TRAPPII tethering factor is required for cell plate assembly during cytokinesis in Arabidopsis. New Phytol. *187*, 751–763.

Kawamura, E., Himmelspach, R., Rashbrooke, M.C., Whittington, A.T., Gale, K.R., Collings, D.A., and Wasteneys, G.O. (2006). MICROTUBULE ORGANIZATION 1 regulates structure and function of microtubule arrays during mitosis and cytokinesis in the Arabidopsis root. Plant Physiol. *140*, 102–114.

Kim, J.J., Lipatova, Z., and Segev, N. (2016). TRAPP Complexes in Secretion and Autophagy. Front. Cell Dev. Biol. *4*, 20.

Kirik, V., Herrmann, U., Parupalli, C., Sedbrook, J.C., Ehrhardt, D.W., and Hülskamp, M. (2007). CLASP localizes in two discrete patterns on cortical microtubules and is required for cell morphogenesis and cell division in Arabidopsis. J. Cell Sci. *120*, 4416–4425.

Kong, Z., Hotta, T., Lee, Y.-R.J., Horio, T., and Liu, B. (2010). The {gamma}-tubulin complex protein GCP4 is required for organizing functional microtubule arrays in Arabidopsis thaliana. Plant Cell *22*, 191–204.

Kosetsu, K., Matsunaga, S., Nakagami, H., Colcombet, J., Sasabe, M., Soyano, T., Takahashi, Y., Hirt, H., and Machida, Y. (2010). The MAP kinase MPK4 is required for cytokinesis in Arabidopsis thaliana. Plant Cell *22*, 3778–3790.

Koumandou, V.L., Dacks, J.B., Coulson, R.M., and Field, M.C. (2007). Control systems for membrane fusion in the ancestral eukaryote; evolution of tethering complexes and SM proteins. BMC Evol. Biol. *7*, 29.

Lauber, M.H., Waizenegger, I., Steinmann, T., Schwarz, H., Mayer, U., Hwang, I., Lukowitz, W., and Jürgens, G. (1997). The Arabidopsis KNOLLE Protein Is a Cytokinesis-specific Syntaxin. J. Cell Biol. *139*, 1485–1493.

Lechner, B., Rashbrooke, M.C., Collings, D.A., Eng, R.C., Kawamura, E., Whittington, A.T., and Wasteneys, G.O. (2012). The N-terminal TOG domain of Arabidopsis MOR1 modulates affinity for microtubule polymers. J. Cell Sci. *125*, 4812–4821.

Lee, Y.-R.J., and Liu, B. (2013). The rise and fall of the phragmoplast microtubule array. Curr. Opin. Plant Biol. *16*, 757–763.

Lee, Y.-R.J., Li, Y., and Liu, B. (2007). Two Arabidopsis phragmoplast-associated kinesins play a critical role in cytokinesis during male gametogenesis. Plant Cell *19*, 2595–2605.

Mao, G., Chan, J., Calder, G., Doonan, J.H., and Lloyd, C.W. (2005). Modulated targeting of GFP-AtMAP65-1 to central spindle microtubules during division. Plant J. Cell Mol. Biol. *43*, 469–478.

Müller, S., and Jürgens, G. (2015). Plant cytokinesis-No ring, no constriction but centrifugal construction of the partitioning membrane. Semin. Cell Dev. Biol.

Müller, S., Fuchs, E., Ovecka, M., Wysocka-Diller, J., Benfey, P.N., and Hauser, M.-T. (2002). Two New Loci, PLEIADE and HYADE, Implicate Organ-Specific Regulation of Cytokinesis in Arabidopsis. Plant Physiol. *130*, 312–324.

Müller, S., Smertenko, A., Wagner, V., Heinrich, M., Hussey, P.J., and Hauser, M.-T. (2004). The Plant Microtubule-Associated Protein AtMAP65-3/PLE Is Essential for Cytokinetic Phragmoplast Function. Curr. Biol. CB *14*, 412–417.

Murata, T., Sano, T., Sasabe, M., Nonaka, S., Higashiyama, T., Hasezawa, S., Machida, Y., and Hasebe, M. (2013). Mechanism of microtubule array expansion in the cytokinetic phragmoplast. Nat. Commun. *4*.

Musacchio, A. (2015). The Molecular Biology of Spindle Assembly Checkpoint Signaling Dynamics. Curr. Biol. *25*, 3017.

Oh, S.A., Johnson, A., Smertenko, A., Rahman, D., Park, S.K., Hussey, P.J., and Twell, D. (2005). A divergent cellular role for the FUSED kinase family in the plant-specific cytokinetic phragmoplast. Curr. Biol. CB *15*, 2107–2111.

Oh, S.A., Allen, T., Kim, G.J., Sidorova, A., Borg, M., Park, S.K., and Twell, D. (2012). Arabidopsis Fused kinase and the Kinesin-12 subfamily constitute a signalling module required for phragmoplast expansion. Plant J. Cell Mol. Biol. *72*, 308–319.

Oh, S.A., Bourdon, V., Dickinson, H.G., Twell, D., and Park, S.K. (2014). Arabidopsis Fused kinase TWO-IN-ONE dominantly inhibits male meiotic cytokinesis. Plant Reprod. *27*, 7–17.

Paganelli, L., Caillaud, M.-C., Quentin, M., Damiani, I., Govetto, B., Lecomte, P., Karpov, P.A., Abad, P., Chabouté, M.-E., and Favery, B. (2015). Three BUB1 and BUBR1/MAD3-related spindle assembly checkpoint proteins are required for accurate mitosis in Arabidopsis. New Phytol. *205*, 202–215.

Panteris, E., Adamakis, I.-D.S., Voulgari, G., and Papadopoulou, G. (2011). A role for katanin in plant cell division: microtubule organization in dividing root cells of fra2 and lue1Arabidopsis thaliana mutants. Cytoskelet. Hoboken NJ *68*, 401–413.

Park, M., Touihri, S., Müller, I., Mayer, U., and Jürgens, G. (2012). Sec1/Munc18 protein stabilizes fusion-competent syntaxin for membrane fusion in Arabidopsis cytokinesis. Dev. Cell *22*, 989–1000.

Pietra, S., Gustavsson, A., Kiefer, C., Kalmbach, L., Hörstedt, P., Ikeda, Y., Stepanova, A.N., Alonso, J.M., and Grebe, M. (2013). Arabidopsis SABRE and CLASP interact to stabilize cell division plane orientation and planar polarity. Nat. Commun. *4*, 2779.

Qi, X., and Zheng, H. (2011). Arabidopsis TRAPPII is functionally linked to Rab-A, but not Rab-D in polar protein trafficking in trans-Golgi network. Plant Signal. Behav. *6*, 1679–1683.

Qi, X., Kaneda, M., Chen, J., Geitmann, A., and Zheng, H. (2011). A specific role for Arabidopsis TRAPPII in post-Golgi trafficking that is crucial for cytokinesis and cell polarity. Plant J. Cell Mol. Biol. *68*, 234–248.

Richter, S., Kientz, M., Brumm, S., Nielsen, M.E., Park, M., Gavidia, R., Krause, C., Voss, U., Beckmann, H., Mayer, U., et al. (2014). Delivery of endocytosed proteins to the cell–division plane requires change of pathway from recycling to secretion. eLife *3*.

Rybak, K., Steiner, A., Synek, L., Klaeger, S., Kulich, I., Facher, E., Wanner, G., Kuster, B., Zarsky, V., Persson, S., et al. (2014). Plant cytokinesis is orchestrated by the sequential action of the TRAPPII and exocyst tethering complexes. Dev. Cell *29*, 607–620.

Sasabe, M., Soyano, T., Takahashi, Y., Sonobe, S., Igarashi, H., Itoh, T.J., Hidaka, M., and Machida, Y. (2006). Phosphorylation of NtMAP65-1 by a MAP kinase down-regulates its activity of microtubule bundling and stimulates progression of cytokinesis of tobacco cells. Genes Dev. *20*, 1004–1014.

Sasabe, M., Boudolf, V., Veylder, L.D., Inzé, D., Genschik, P., and Machida, Y. (2011a). Phosphorylation of a mitotic kinesin-like protein and a MAPKKK by cyclin-dependent kinases (CDKs) is involved in the transition to cytokinesis in plants. Proc. Natl. Acad. Sci. *108*, 17844–17849.

Sasabe, M., Kosetsu, K., Hidaka, M., Murase, A., and Machida, Y. (2011b). Arabidopsis thaliana MAP65-1 and MAP65-2 function redundantly with MAP65-3/PLEIADE in cytokinesis downstream of MPK4. Plant Signal. Behav. *6*, 743–747.

Seki, M., Narusaka, M., Kamiya, A., Ishida, J., Satou, M., Sakurai, T., Nakajima, M., Enju, A., Akiyama, K., Oono, Y., et al. (2002). Functional annotation of a full-length Arabidopsis cDNA collection. Science *296*, 141–145.

Smertenko, A.P., Chang, H.-Y., Wagner, V., Kaloriti, D., Fenyk, S., Sonobe, S., Lloyd, C., Hauser, M.-T., and Hussey, P.J. (2004). The Arabidopsis microtubule-associated protein AtMAP65-1: molecular analysis of its microtubule bundling activity. Plant Cell *16*, 2035–2047.

Smertenko, A.P., Piette, B., and Hussey, P.J. (2011). The origin of phragmoplast asymmetry. Curr. Biol. CB *21*, 1924–1930.

Söllner, R., Glässer, G., Wanner, G., Somerville, C.R., Jürgens, G., and Assaad, F.F. (2002). Cytokinesis-Defective Mutants of Arabidopsis. Plant Physiol. *129*, 678–690.

Steiner, A., Müller, L., Rybak, K., Vodermaier, V., Facher, E., Thellmann, M., Ravikumar, R., Wanner, G., Hauser, M.-T., and Assaad, F.F. (2016). The Membrane-Associated Sec1/Munc18 KEULE is Required for Phragmoplast Microtubule Reorganization During Cytokinesis in Arabidopsis. Mol. Plant *9*, 528–540.

Takahashi, Y., Soyano, T., Sasabe, M., and Machida, Y. (2004). A MAP kinase cascade that controls plant cytokinesis. J. Biochem. (Tokyo) *136*, 127–132.

Twell, D., Park, S.K., Hawkins, T.J., Schubert, D., Schmidt, R., Smertenko, A., and Hussey, P.J. (2002). MOR1/GEM1 has an essential role in the plant-specific cytokinetic phragmoplast. Nat. Cell Biol. *4*, 711–714.

Usadel, B., Obayashi, T., Mutwil, M., Giorgi, F.M., Bassel, G.W., Tanimoto, M., Chow, A., Steinhauser, D., Persson, S., and Provart, N.J. (2009). Co-expression tools for plant biology: opportunities for hypothesis generation and caveats. Plant Cell Environ. *32*, 1633–1651.

Van Damme, D., Van Poucke, K., Boutant, E., Ritzenthaler, C., Inzé, D., and Geelen, D. (2004). In vivo dynamics and differential microtubule-binding activities of MAP65 proteins. Plant Physiol. *136*, 3956–3967.

Vanstraelen, M., Inzé, D., and Geelen, D. (2006). Mitosis-specific kinesins in Arabidopsis. Trends Plant Sci. *11*, 167–175.

Völker, A., Stierhof, Y.D., and Jürgens, G. (2001). Cell cycle-independent expression of the Arabidopsis cytokinesis-specific syntaxin KNOLLE results in mistargeting to the plasma membrane and is not sufficient for cytokinesis. J. Cell Sci. *114*, 3001–3012.

Waizenegger, I., Lukowitz, W., Assaad, F., Schwarz, H., Jürgens, G., and Mayer, U. (2000). The Arabidopsis KNOLLE and KEULE genes interact to promote vesicle fusion during cytokinesis. Curr. Biol. *10*, 1371–1374.

Weßling, R., Epple, P., Altmann, S., He, Y., Yang, L., Henz, S.R., McDonald, N., Wiley, K., Bader, K.C., Glaesser, C., et al. (2014). Convergent Targeting of a Common Host Protein-Network by Pathogen Effectors from Three Kingdoms of Life. CELL HOST MICROBE *16*, 364–375.

Whittington, A.T., Vugrek, O., Wei, K.J., Hasenbein, N.G., Sugimoto, K., Rashbrooke, M.C., and Wasteneys, G.O. (2001). MOR1 is essential for organizing cortical microtubules in plants. Nature *411*, 610–613.

Wightman, R., Chomicki, G., Kumar, M., Carr, P., and Turner, S.R. (2013). SPIRAL2 determines plant microtubule organization by modulating microtubule severing. Curr. Biol. CB *23*, 1902–1907.

Yao, M., Wakamatsu, Y., Itoh, T.J., Shoji, T., and Hashimoto, T. (2008). Arabidopsis SPIRAL2 promotes uninterrupted microtubule growth by suppressing the pause state of microtubule dynamics. J. Cell Sci. *121*, 2372–2381.

Cell cycle-regulated PLEIADE/AtMAP65-3 coordinates membrane and microtubule dynamics during plant cytokinesis

Alexander Steiner[1], Katarzyna Rybak[1], Melina Altmann[2], Heather E. McFarlane[3,7], Susan Klaeger[4], Ngoc Nguyen[1], Eva Facher[5], Alexander Ivakov[3,7], Gerhard Wanner[5], Bernhard Kuster[4], Staffan Persson[3,6,7], Pascal Falter-Braun[2], Marie-Theres Hauser[8] and Farhah F. Assaad[1*]

Supporting Information

Figure S1. MAP65-1 Sequence (FASTA from NCBI Reference Sequence Database, version 28.02.2013). Related to Figure 1.

Figure S2. Colocalization between TRS120-mCherry and CLUB-GFP in meristematic Arabidopsis root cells. Related to Figure 3.

Figure S3. Microtubule reorganization is impaired in *TRAPPII* mutants. Related to Figure 5.

Table S1. Membrane-related marker lines used in this study.

Table S2. Analysis of CLUB-GFP immunoprecipitates via mass spectrometry.

Table S3. Mutant lines used in this study.

Movie S1. Showing microtubule reorganization in wild type. Related to Figure 5.

Movie S2. Showing delay in microtubule reorganization in *trs120-4* mutant.
Related to Figure 5.

Movie S3. Showing delay in microtubule reorganization in *club-2* mutant.
Related to Figure 5.

Supporting Information Methods

Supporting Information References

MAVTDTESPHLGEITCGTLLEKLQEIWDEVGESDDERDKLLLQIEQECLDVYKRKVEQAAKSRAELL
QTLSDANAELSSLTMSLGDKSLVGIPDKSSGTIKEQLAAIAPALEQLWQQKEERVREFSDVQSQIQK
ICGDIAGGLSNEVPIVDESDLSLKKLDDFQSQLQELQKEKSDRLRKVLEFVSTVHDLCAVLGLDFLST
VTEVHPSLDEDTSVQSKSISNETLSRLAKTVLTLKDDKKQRLQKLQELATQLIDLWNLMDTPDEER
ELFDHVTCNISSSVDEVTVPGALARDLIEQAEVEVDRLDQLKASRMKEIAFKKQSELEEIYAR
AHVEVNPESARERIMSLIDSGNVEPTELLADMDSQISKAKEEAFSRKDILDRVEKWMSACEEESW
LEDYNRDQNRYSASRGAHLNLKRAEKARILVSKIPAMVDTLVAKTRAWEEEHSMSFAYDGVPLLA
MLDEYGMLRQEREEEKRRLREQKKVQEQPHVEQESAFSTRPSPARPVSAKKTVGPRANNGGAN
GTHNRRLSLNANQNGSRSTAKEAGRRETLNRPAAPTNYVAISKEEAASSPVSGAADHQVPASP

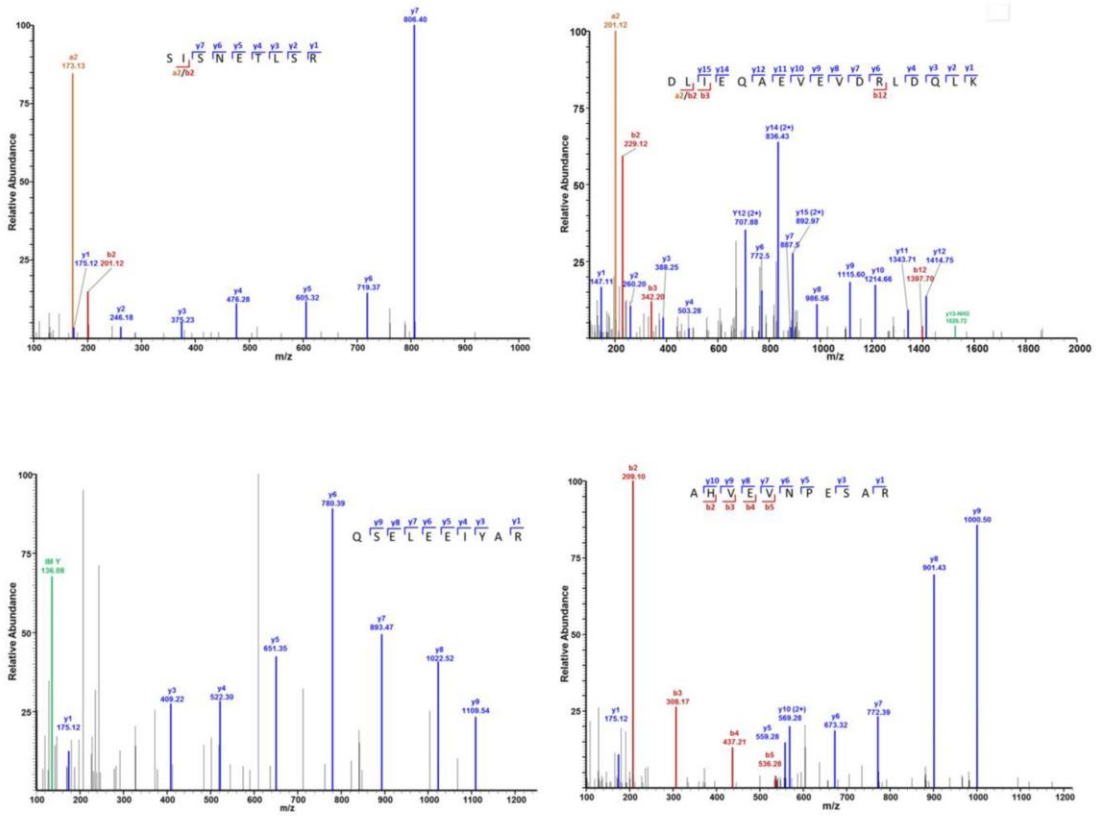

Figure S1. MAP65-1 Sequence (FASTA from NCBI Reference Sequence Database, version 28.02.2013). Related to Figure 1.
Peptides leading to identification are underlined. Peptides only identified in the CLUB-IP are highlighted in yellow, a peptide only identified in the TRS120-IP is marked in violet and peptides highlighted in blue were identified in both IPs. The four annotated MS/MS spectra are printed bold. The y ion series (containing the C terminus) and some complementary b-ions (respective N Terminal part of the fragmented peptide) are shown.
AtMAP65-1 expression is more than one order of magnitude stronger than that of PLEIADE/AtMAP65-3 in inflorescences (Van Damme et al., 2004). As our CLUB-GFP pull downs were with inflorescences, this could explain why we saw AtMAP65-1 but not AtMAP65-3 in the immunoprecipitated complexes.

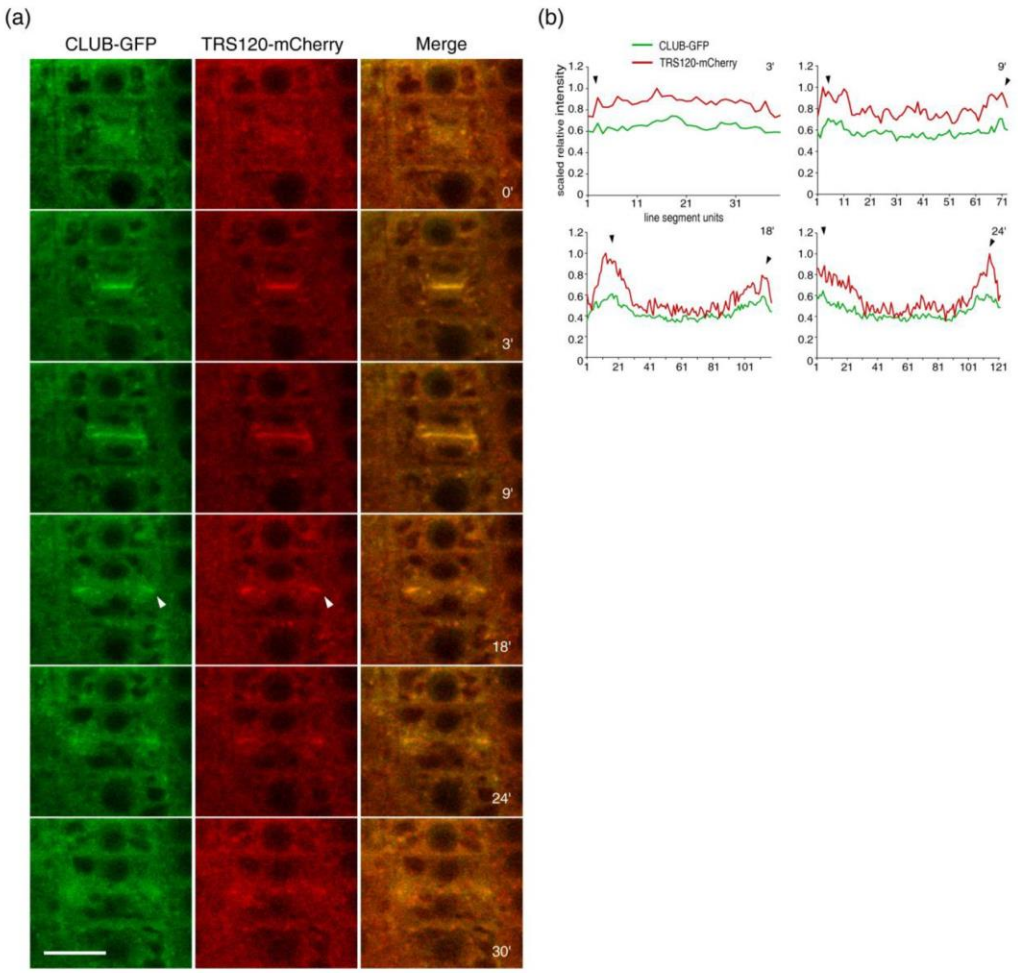

Figure S2. Colocalization between TRS120-mCherry and CLUB-GFP in meristematic arabidopsis root cells. Related to Figure 3.

(a)Time lapse of P_{UBQ}::CLUB-GFP with P_{UBQ}::TRS120-mCherry is shown, with minutes indicated in the right panel. Arrowheads point to leading edges of the cell plate. The markers co-localize throughout cytokinesis. Bars = 10 µm.

(b) The line graphs depict scaled relative intensity of GFP-CLUB and TRS120-mCherry at the cell plate. Note that throughout cytokinesis almost every peak of GFP-CLUB fluorescence coincides with a peak of TRS120-mCherry fluorescence (black arrowheads).

(a)

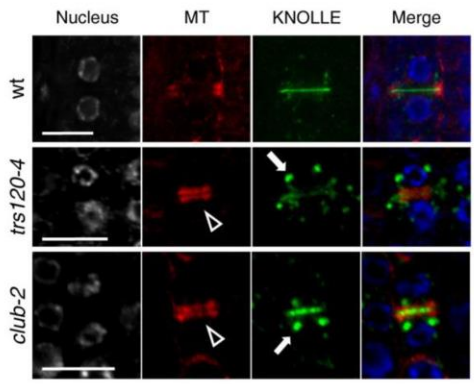

(b)

mutant allele	reorganization of phragmoplast MT from solid to ring-shaped at telophase			number of telophase cells n =
	ring-shaped	partially reorg.	solid	
Col-o wt	100%	0%	0%	189
trs120-4	31.3%	21.9%	46.9%	32
club-2	44%	27.2%	28.8%	111

(c)

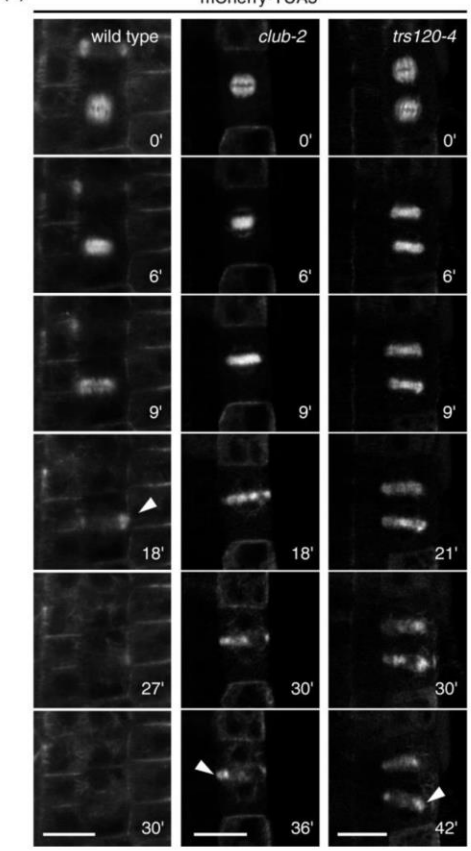

Figure S3. Microtubule reorganization is impaired in TRAPPII mutants. Related to Figure 5.
(a) Antibody stains of root tips. DAPI/nucleus (white); microtubules (red); anti-KNOLLE (green); and merge. Bars = 10 µm.
Upper panel, wild type telophase cell.
Middle panel, *trs120-4* telophase cell.
Lower panel, *club-2* telophase cell. Note the large endomembrane compartments around the cell plate (arrow). Furthermore, the phragmoplast is solid (meaning not reorganized; open arrowhead) even though the nuclei are decondensed (indicative of telophase) as is characteristic for the ring-shaped phragmoplast stage.
(b) We saw solid (as opposed to ring-shaped) phragmoplasts in 28.8% *club-2* (n = 111) and 46.9% *trs120-4* (n = 32) telophase cells. By contrast, this was never seen in Col-0 wild-type telophase cells.
(c) Live imaging with mCherry-TUA5 in wild-type and mutant root tips. In wild-type cytokinetic cells, a timely reorganization of phragmoplast microtubules was observed (arrowhead). By contrast, in both TRAPPII mutant backgrounds, solid phragmoplasts persisted longer after spindle assembly and the translocation of phragmoplast microtubules was delayed (arrowheads).

Construct	Promotor	Reference
KNOLLE-YFP	native	(Völker et al., 2001)
SYP121-GFP	native	(Collins et al., 2003)
SYP122-CFP	P35S	(Assaad et al., 2004)
KEULE-GFP	native	(Steiner et al., 2016)
TRS120-GFP	native	(Rybak et al., 2014)
CLUB/AtTRS130-GFP	native	(Rybak et al., 2014)
EXO84b2-GFP	native	(Fendrych et al., 2010)

Table S1: Membrane-related markers monitored in this study.

Supporting Information Tables

Description	Accession number (AGI)	Gene description	CLUB-GFP IP inflorescences				Co-expression coefficient[c]
			Average number of unique peptides	Average Log2 (ratio)[a]	Standard deviation	p-value[b]	
TRAPP complexes							
TRAPPII-specific	At5g54440	CLUB/ AtTRS130	121	12,5	1,6	0,0001	
	At5g11040	TRS120	40	10,0	2,2	2,5E-03	0.56
common to TRAPPI, II and III	At3g05000	TRS33	9	12,8	1,3	2,54E-05	
	At2g20930	Trs20/Tca17	8	14,29/0	0,0	8,91E-06	0.51
	At5g54750	Bet3	10	13,4	1,6	0,00015	
	At5g58030	TRS31	6	9,2	4,4	0,012	
MICROTUBULE-related hits							
α-tubulin	At1g64740	TUA1	5	14,29/0	0,0	0,0000005	
	At5g19770, At5g19780	TUA3/TUA5	5	6,2	0,5	0,001	0.46
β-tubulin	At1g75780	TUB1	3	12,1	3,7	0,006	
	At5g62690, At5g62700	TUB2/TUB3	4	7,2	1,3	0,0002	0.45
	At5g44340	TUB4	4	7,2	0,8	0,00002	
	At1g20010	TUB5	7	7,0	0,9	0,00007	
	At5g12250	TUB6	6	7,9	1,8	0,0006	
	At2g29550	TUB7	4	6,4	0,5	0,0001	
	At5g23860	TUB8	2	6,6	0,6	0,00002	
	At4g20890	TUB9	3	6,8	1,6	0,0018	
Stabilizing MAP	At5g55230	AtMAP65-1	4	11,6	4,6	0,008	0.53
+TIP	At4g27060	TOR1/SPR2	7	14,29/0	0,0	0,00003	0.48
	At2g20190	AtCLASP	3	5,6	1,1	0,002	0.57
	At2g35630	MOR1	1	14,29/0	0,00	0,00006	0.44

Table S2. Analysis of CLUB-GFP immunoprecipitates (IPs) via mass spectrometry.
The data are based on three biological replicates. AGI: Arabidopsis genome initiative accessions (www.arabidopsis.org). a: The log2 intensity ratio for each protein was calculated from its signal intensity in the experiment divided by its intensity in the control, which was an empty soluble GFP vector. If there was no signal in the control, we write "/0" and give an artificial value of 14.29 so as not to be at infinity. Note that the log2 ratios for a number of the cytoskeletal hits are larger than or comparable to those of the TRAPPII subunits, supporting their identification as true positives. b: p values (< 0.02) were calculated using the t-test (two-sided). c: Co-expression coefficients were looked up in Genevestigator (perturbations; Hruz et al., 2008). This table lists only TRAPP components (described in Thellmann et al., 2010) and MT +TIP or plus end stabilizing proteins detected in the IPs.

Allele	AGI gene identification	Polymorphism	Intron/ Exon	Nature of the allele	Reference
ple-2	At5g51600	EMS-induced splice site variant affecting 2nd intron		Hypomorph, viable.	MT Hauser, unpublised; this study
ple-4		EMS-induced null allele, A to V substitution at a.a. 421		Null; sdlg lethal	(Söllner et al., 2002; Smertenko et al., 2004)
club-2	At5g54440	SALK_039353	Intron	Null; sdlg lethal	(Jaber et al., 2010)
trs120-4	At5g11040	SAIL_1285_D07	Intron	Null; sdlg lethal	(Thellmann et al., 2010)

Table S3. Mutant lines used in this study. a: Seedling (abbreviated "sdlg)- lethal lines were propagated as hetero- or hemizygotes.

Supporting Information Methods

LC-MS/MS analysis

The rationale for the proteomics approach is described in (Cox and Mann, 2008). NanoflowLc-MS/MS was performed by coupling an EksigentnanoLC-Ultra 1D+ (Eksigent, Dublin, CA) to a Velos-LTQ-Orbitrap (Thermo Scientific, Bremen, Germany). Peptides were first delivered to a trap column (100 µm inner diameter (i.d.) x 2 cm, packed with 5 µm C18 resin, Reprosil PUR AQ, Dr. Maisch, Ammerbuch, Germany) at a flow rate of 5 µl/min in 100% solvent A (0.1% FA in HPLC grade water). After 10 min of loading and washing, peptides were transferred to an analytical column (75 µm i.d. x 40 cm C18 column Reprosil GOLD, 3 µm, Dr. Maisch, Ammerbuch, Germany) and separated using a 210 min gradient from 4% to 32% solvent B (0.1% FA in acetonitrile) at 300 nL/min flowrate. Data acquisition occurred in data dependent mode, automatically switching between MS and MS^2. Full scan MS spectra were acquired in the Orbitrap at 30,000 resolution. Tandem mass spectra were generated for up to 10 peptide precursors by using higher energy collisional dissociation (HCD) and analyzed in the Orbitrap.

Peptide and Protein Identification/ Data analysis

Raw MS files were loaded into the MaxQuant software (version 1.3.0.3) and microtubule-related components searched against an Arabidopsis thaliana RefSeq database (003702_RefSeq.fasta) using carbamidomethyl cysteine as fixed modification, oxidation of Methionin and acetylation of protein N-terminus as variable modifications. Trypsin was specified as proteolytic enzyme and up

to 2 missed cleavages were allowed. Mass tolerance of precursor ion was set to 6 ppm and for fragment ions to 20 ppm. Protein identifications were filtered to 0.01 % peptide and protein false discovery rates (FDR). Label free quantification and match between runs was enabled, using a retention time window of 2 min. For data evaluation, Max Quant data were loaded into Perseus Software (1.4.0.11) and filtered for reverse identifications (false positives) and contaminants. Intensity values were used to calculate protein ratios between sample and control experiment.

Bifluorescence complementation

Each vector was individually electorporated into Agrobacterium strain C58pGV3101::pPM90 (Gookin and Assmann, 2014) and grown on LB supplemented with the appropriate antibiotics. Single colonies were picked and grown for 2 days in 10mL LB with antibiotics. Cells were pelleted and resuspended in 10mM MES, 10mM MgCl2, and 100µm acetosyringone (pH 5.7) to a final concentration of OD_{600}=0.03, and incubated for 1-2 hours. Vectors were combined (as indicated in figure panels) at equal concentrations and infiltrated into leaves of young *Nicotiana benthamiana* plants. Infiltrations were performed in duplicate and each experiment was performed at least three times. After 60 hours, infiltrated regions of the leaves were excised, mounted in water, and viewed with an inverted Leica SP2 microscope. YFP was detected using 514nm excitation and 525-600nm emission filter using an average of 8 line scans. Identical imaging conditions (e.g. pinhole, laser power, detector gain and offset) were used to collect data from all vector combinations.

Electron Microscopy

For electron microscopy, root tips were placed in aluminum platelets, infiltrated with 20% bovine serum albumin in 80% isopropanol and fixed by high-pressure freezing using the Leica HPM100 high pressure freezer. Freeze substitution was performed in acetone with 2% osmium tetroxide and 0.2% uranyl acetate, including 5% water, using the Leica ASF2 automatic freeze substitution system as described (Steiner et al., 2016). Samples were then infiltrated in resin, initially at 0°C but subsequently at room temperature, over a period of at least two days with ten changes of resin:acetone solutions, starting with 1:20 and ending with 100% resin (for further details see(Assaad et al., 1996)).

Ultrathin sections were cut with a diamond knife and mounted onto collodion coated copper grids. The sections were post-stained with aqueous lead citrate (100 mM, pH 13.0).The FIB serial sectioning was performed by a Zeiss-Auriga workstation. The resin block was trimmed with a pyramitome (LKB) with glass knives so that vertical faces allowed lateral milling of the cells by the FIB. Tomographic datasets were obtained using the ‘‘slice and view’’ technique using a Zeiss Auriga 60 dual beam instrument (Carl Zeiss Microscopy, Oberkochen, Germany) as described (Rybak et al., 2014). Electron micrographs were digitally recorded from the BSE-signal. The

contrast of the images was inversed, so that they appeared like a conventional bright field TEM image.

Molecular techniques

Standard molecular techniques were used for subcloning (Sambrook at al., 1989). DNA was isolated from rosette leaves or influorescences of soil-grown plants. Full length cDNA clones obtained from the RIKEN Bioresource Center (Seki et al., 2002) were used as templates for all clones used in binary interaction assays. PCR analysis was carried out with GoTaq (Promega) for standard purposes or with high fidelity PfuUltra II fusion HS DNA polymerase for gene fusions (Agilent Technology inc., Santa Clara, USA). The E.Coli strain DH5α was used for all cloning experiments. Restriction enzymes were from Promega, NEB or Fermentas.

Construct	vector	template	Primer sequence (5' to 3')	
P_{35S}:: nVenus MAP65-1	pDEST-VYNE(R) GW	cDNA from Col-0	Fwd	GGGGACAAGTTTGTACAAAAAAGCAGGCTCCATGGCAGTTACA GATACTGAAAG
			Rev	GGGGACCACTTTGTACAAGAAAGCTGGGTCTCATGGTGAAGC TGGAACTTGATG
P_{35S}:: cVenus MAP65-1	pDEST-VYCE(R) GW	cDNA from Col-0	Fwd	GGGGACAAGTTTGTACAAAAAAGCAGGCTCCATGGCAGTTACA GATACTGAAAG
			Rev	GGGGACCACTTTGTACAAGAAAGCTGGGTCTCATGGTGAAGC TGGAACTTGATG
P_{35S}:: nVenus MAP65-3	pDEST-VYNE(R) GW	cDNA from Col-0	Fwd	GGGGACAAGTTTGTACAAAAAAGCAGGCTCCATGGCAAGTGTT CAAAAAGATCCG
			Rev	GGGGACCACTTTGTACAAGAA AGCTGGGTCTCACTGTAGCAT GAAGGCGAG
P_{35S}:: cVenus MAP65-3	pDEST-VYCE(R) GW	cDNA from Col-0	Fwd	GGGGACAAGTTTGTACAAAAAA GCAGGCTCCATGGCAAGTGTTCAAAAAGATCCG[c]
			Rev	GGGGACCACTTTGTACAAGAA AGCTGGGTCTCACTGTAGCAT GAAGGCGAG[c]
P_{35S}:: nVenus TRS120	pDEST-VYNE(R) GW	RAFL19-61-L11[a]	Fwd	GGGGACAAGTTTGTACAAAAAAGCAGGCTTCATGGAACCTGAC GTCAGTATCGAGA
			Rev	GGGGACCACTTTGTACAAGAAAGCTGGGTCTCACAGTGCACCT CCAGCTACACAG
P_{35S}:: cVenus TRS120	pDEST-VYCE(R) GW	RAFL19-61-L11	Fwd	GGGGACAAGTTTGTACAAAAAAGCAGGCTTCATGGAACCTGAC GTCAGTATCGAGA
			Rev	GGGGACCACTTTGTACAAGAAAGCTGGGTCTCACAGTGCACCT CCAGCTACACAG
P_{35S}:: nVenus CLUB	pDEST-VYNE(R) GW	pET24 (+) CLUB[b]	Fwd	GGGGACAAGTTTGTACAAAAAAGCAGGCTTCATGGCGAACTAC TTGGCTCAGTTCC
			Rev	GGGGACCACTTTGTACAAGAAAGCTGGGTCTTACTTGACAGGT AAGCAGTAGGAA
P_{35S}:: cVenus CLUB	pDEST-VYCE(R) GW	pET24a (+) CLUB	Fwd	GGGGACAAGTTTGTACAAAAAAGCAGGCTTCATGGCGAACTAC TTGGCTCAGTTCC
			Rev	GGGGACCACTTTGTACAAGAAAGCTGGGTCTTACTTGACAGGT AAGCAGTAGGAA
P35S:: nVenus CLUB C2	pDEST-VYNE(R) GW	pET24a (+) CLUB	Fwd	GGGGACAAGTTTGTACAAAAAAGCAGGCTCCATGGGATATCTG ATAGGATATGG
			Rev	GGGGACCACTTTGTACAAGAAAGCTGGGTCTTACTTGACAGGT AAGCAGTAGGAA
P_{35S}:: cVenus CLUB C2	pDEST-VYCE(R) GW	pET24a (+) CLUB	Fwd	GGGGACAAGTTTGTACAAAAAAGCAGGCTCCATGGGATATCTG ATAGGATATGG
			Rev	GGGGACCACTTTGTACAAGAAAGCTGGGTCTTACTTGACAGGT AAGCAGTAGGAA
P_{35S}:: nVenus CLUB C3	pDEST-VYNE(R) GW	pET24a (+) CLUB	Fwd	GGGGACAAGTTTGTACAAAAAAGCAGGCTCCATGCATAGCTTT TCGAAGGGTGG
			Rev	GGGGACCACTTTGTACAAGAAAGCTGGGTCTTACTTGACAGGT AAGCAGTAGGAA
P_{35S}:: cVenus CLUB C3	pDEST-VYCE(R) GW	pET24a (+) CLUB	Fwd	GGGGACAAGTTTGTACAAAAAAGCAGGCTCCATGCATAGCTTT TCGAAGGGTGG
			Rev	GGGGACCACTTTGTACAAGAAAGCTGGGTCTTACTTGACAGGT AAGCAGTAGGAA
P_{35S}:: nVenus TRS120 T2	pDEST-VYNE(R) GW	RAFL19-61-L11	Fwd	GGGGACAAGTTTGTACAAAAAAGCAGGCTCCATGGATAGATTA CCTTCTGGAACT
			Rev	GGGGACCACTTTGTACAAGAAAGCTGGGTCTCACAGTGCACCT CCAGCTACACAG
P_{35S}:: cVenus TRS120 T2	pDEST-VYCE(R) GW	RAFL19-61-L11	Fwd	GGGGACAAGTTTGTACAAAAAAGCAGGCTCCATGGATAGATTA CCTTCTGGAACT
			Rev	GGGGACCACTTTGTACAAGAAAGCTGGGTCTCACAGTGCACCT CCAGCTACACAG
P_{ADH1}:: TRS120-GAL4 AD	pDEST_AD-pPC86	RAFL19-61-L11	Fwd	GGGGACAAGTTTGTACAAAAAAGCAGGCTTCATGGAACCTGAC GTCAGTATCGAGA
			Rev	GGGGACCACTTTGTACAAGAAAGCTGGGTCTCACAGTGCACCT CCAGCTACACAG
P_{ADH1}:: TRS120-GAL4 DB	pDEST-pPC97	RAFL19-61-L11	Fwd	GGGGACAAGTTTGTACAAAAAAGCAGGCTTCATGGAACCTGAC GTCAGTATCGAGA
			Rev	GGGGACCACTTTGTACAAGAAAGCTGGGTCTCACAGTGCACCT

				CCAGCTACACAG
P_{ADH1}:: CLUB-GAL4 AD	pDEST_AD-pPC86	pET24a (+) CLUB	Fwd	GGGGACAAGTTTGTACAAAAAAGCAGGCTTCATGGCGAACTACTTGGCTCAGTTCC
			Rev	GGGGACCACTTTGTACAAGAAAGCTGGGTCTTACTTGACAGGTAAGCAGTAGGAA
P_{ADH1}:: CLUB-GAL4 DB	pDEST-pPC97	pET24a (+) CLUB	Fwd	GGGGACAAGTTTGTACAAAAAAGCAGGCTTCATGGCGAACTACTTGGCTCAGTTCC
			Rev	GGGGACCACTTTGTACAAGAAAGCTGGGTCTTACTTGACAGGTAAGCAGTAGGAA
P_{ADH1}:: CLUB C1-GAL4 AD	pDEST_AD-pPC86	pET24a (+) CLUB	Fwd	GGGGACAAGTTTGTACAAAAAAGCAGGCTTCATGGCGAACTACTTGGCTCAGTTCC
			Rev	GGGGACCACTTTGTACAAGAAAGCTGGGTCTTACCAAGGCAGCATACTGAGAC
P_{ADH1}:: CLUB C1-GAL4 DB	pDEST-pPC97	pET24a (+) CLUB	Fwd	GGGGACAAGTTTGTACAAAAAAGCAGGCTTCATGGCGAACTACTTGGCTCAGTTCC
			Rev	GGGGACCACTTTGTACAAGAAAGCTGGGTCTTACCAAGGCAGCATACTGAGAC
P_{ADH1}:: CLUB C2-GAL4 AD	pDEST_AD-pPC86	pET24a (+) CLUB	Fwd	GGGGACAAGTTTGTACAAAAAAGCAGGCTCCATGGGATATCTGATAGGATATGG
			Rev	GGGGACCACTTTGTACAAGAAAGCTGGGTCTTACTTGACAGGTAAGCAGTAGGAA
P_{ADH1}:: CLUB C2-GAL4 DB	pDEST-pPC97	pET24a (+) CLUB	Fwd	GGGGACAAGTTTGTACAAAAAAGCAGGCTCCATGGGATATCTGATAGGATATGG
			Rev	GGGGACCACTTTGTACAAGAAAGCTGGGTCTTACTTGACAGGTAAGCAGTAGGAA
P_{ADH1}:: CLUB C3-GAL4 AD	pDEST_AD-pPC86	pET24a (+) CLUB	Fwd	GGGGACAAGTTTGTACAAAAAAGCAGGCTCCATGCATAGCTTTTCGAAGGGTGG
			Rev	GGGGACCACTTTGTACAAGAAAGCTGGGTCTTACTTGACAGGTAAGCAGTAGGAA
P_{ADH1}:: CLUB C3-GAL4 DB	pDEST-pPC97	pET24a (+) CLUB	Fwd	GGGGACAAGTTTGTACAAAAAAGCAGGCTCCATGCATAGCTTTTCGAAGGGTGG
			Rev	GGGGACCACTTTGTACAAGAAAGCTGGGTCTTACTTGACAGGTAAGCAGTAGGAA
P_{ADH1}:: TRS120 T1-GAL4 AD	pDEST_AD-pPC86	RAFL19-61-L11	Fwd	GGGGACAAGTTTGTACAAAAAAGCAGGCTTCATGGAACCTGACGTCAGTATCGAGA
			Rev	GGGGACCACTTTGTACAAGAAAGCTGGGTCTTATCCGTCTTTTGGTCTTCCTG
P_{ADH1}:: TRS120 T1-GAL4 DB	pDEST-pPC97	RAFL19-61-L11	Fwd	GGGGACAAGTTTGTACAAAAAAGCAGGCTTCATGGAACCTGACGTCAGTATCGAGA
			Rev	GGGGACCACTTTGTACAAGAAAGCTGGGTCTTATCCGTCTTTTGGTCTTCCTG
P_{ADH1}:: TRS120 T2-GAL4 AD	pDEST_AD-pPC86	RAFL19-61-L11	Fwd	GGGGACAAGTTTGTACAAAAAAGCAGGCTCCATGGATAGATTACCTTCTGGAACT
			Rev	GGGGACCACTTTGTACAAGAAAGCTGGGTCTCACAGTGCACCTCCAGCTACACAG
P_{ADH1}:: TRS120 T2-GAL4 DB	pDEST-pPC97	RAFL19-61-L11	Fwd	GGGGACAAGTTTGTACAAAAAAGCAGGCTCCATGGATAGATTACCTTCTGGAACT
			Rev	GGGGACCACTTTGTACAAGAAAGCTGGGTCTCACAGTGCACCTCCAGCTACACAG
P_{ADH1}:: TRS120 T3-GAL4 AD	pDEST_AD-pPC86	RAFL19-61-L11	Fwd	GGGGACAAGTTTGTACAAAAAAGCAGGCTCCATGGCTTTACAGTCTGCTCTTCC
			Rev	GGGGACCACTTTGTACAAGAAAGCTGGGTCTCACAGTGCACCTCCAGCTACACAG
P_{ADH1}:: TRS120 T3-GAL4 DB	pDEST-pPC97	RAFL19-61-L11	Fwd	GGGGACAAGTTTGTACAAAAAAGCAGGCTCCATGGCTTTACAGTCTGCTCTTCC
			Rev	GGGGACCACTTTGTACAAGAAAGCTGGGTCTCACAGTGCACCTCCAGCTACACAG

Vectors, Templates and Primers used for Subcloning.

a: The TRS120 full length cDNA (RAFL19-61-L11) from Riken had some deletions, which were corrected by further subcloning, as in b. b: A full length CLUB cDNA (Riken clone RAFL09-39-B05) was cloned into pET24a(+) (Novagen). Due to a 5-bp deletion (1602-1606) in the Riken clone, a 1892 bp fragment obtained by RT-PCR on Col-0 was subsequently subcloned into the vector. c: the last 6 a.a. of the AtMAP65-3 coding sequences were missing.

Supporting Information References

Assaad, F.F., Qiu, J.-L., Youngs, H., Ehrhardt, D., Zimmerli, L., Kalde, M., Wanner, G., Peck, S.C., Edwards, H., Ramonell, K., et al. (2004). The PEN1 Syntaxin Defines a Novel Cellular Compartment upon Fungal Attack and Is Required for the Timely Assembly of Papillae. Mol. Biol. Cell *15*, 5118–5129.

Collins, N.C., Thordal-Christensen, H., Lipka, V., Bau, S., Kombrink, E., Qiu, J.-L., Hückelhoven, R., Stein, M., Freialdenhoven, A., Somerville, S.C., et al. (2003). SNARE-protein-mediated disease resistance at the plant cell wall. Nature *425*, 973–977.

Cox, J., and Mann, M. (2008). MaxQuant enables high peptide identification rates, individualized p.p.b.-range mass accuracies and proteome-wide protein quantification. Nat. Biotechnol. *26*, 1367–1372.

Sambrook, J., Fritsch, E. F., Maniatis, T. and Cold Spring Harbor Laboratory (1989). Molecular cloning: a laboratory manual (2nd ed). Cold Spring Harbor Laboratory Press, New York.

Thellmann, M., Rybak, K., Thiele, K., Wanner, G., and Assaad, F.F. (2010). Tethering Factors Required for Cytokinesis in Arabidopsis. Plant Physiol. *154*, 720–732.